Physical Oceanography of the Gulf of Aden

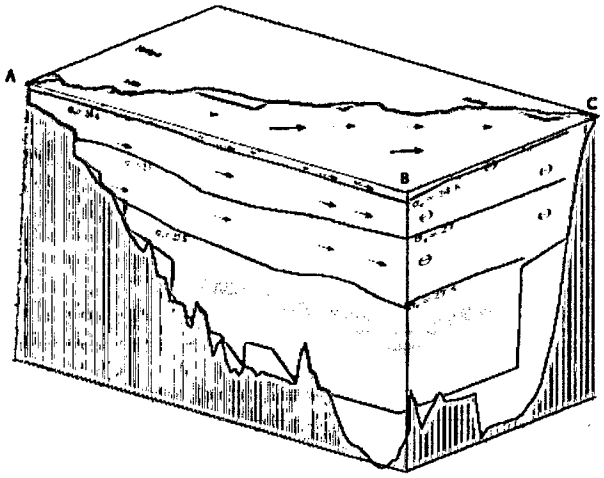

Mohammed Ali Yahya Al Saafani

Physical Oceanography of the Gulf of Aden

Thesis

submitted to

Goa University

for the Degree of

Doctor of Philosophy

in

Marine Sciences

Mohammed Ali Yahya Al Saafani

National Institute of Oceanography

Dona Paula, Goa 403004

July 2008

بسم الله الرحمن الرحيم

"وقل ربي زدني علما"

to *my parents*

my wife

Hagar and Ebrahim

Statement

As required under the University ordinance 0.19.8.(vi), I state that this thesis entitled *Physical Oceanography of the Gulf of Aden* is my original contribution and it has not been submitted on any previous occasion.

The literature related to the problem investigated has been cited. Due acknowledgements have been made wherever facilities and suggestions have been availed of.

Mohammed Ali Yahya Al Saafani

National Institute of Oceanography, Goa

July 2008

Certificate

This is to certify that the thesis entitled *Physical Oceanography of the Gulf of Aden*, submitted by Mohammed Ali Yahya Al Saafani to Goa University for the degree of Doctor of Philosophy, is based on his original studies carried out under my supervision. The thesis or any part thereof has not been previously submitted for any other degree or diploma in any university or institution.

SATHEESH SHENOI

National Institute of Oceanography, Goa

July 2008

The suggested modifications are incorporated.

31 July, 08

Vita

Name Mohammed Ali Yahya Al Saafani

Born 21 July 1970, Sana'a, Republic of Yemen.

Education

B.S.c. Physical Oceanography. King Abdul-Aziz
King Abdul-Aziz University.Jeddah, Saudi Arabia.
1995

M.Sc. Marine Sciences
Department of Marine Science
and Biotechnology, Goa University, India.
April 2002

Work

1995 to date
Demonstrator in physical oceanography, Oceanography Department (Earth Science), Faculty of Science, Sana'a University.

May 1997 to June 1999
GEF/UNDP (Global Environment Facilities/United Nations Development Programme) Environmental Monitoring and Public Awareness Advisor.

2000 to date
On study leave to do MSc. and Ph.D. in India.

Address for communication

Mailing adress	Physical Oceanography Division, National Institute of Oceanography, Dona Paula, Goa 403 004, India.
By e-mail	alsafany@yahoo.co.uk, alsafany@nio.org.
Permanent address	Department of Earth Science and Environment Faculty of Science, Sana'a University P . O . Box :- 13356 Sana'a, Republic of Yemen. Tel. : +967-1-607184.

Publications

- **Al Saafani, M. A.** and S. S. C. Shenoi, D. Shankar, M. Aparna, J. Kurian, F. Durand, and P. Vinayachandran. Westward movement of eddies into the Gulf of Aden from the Arabian Sea. *Journal of Geophysical Research*,112, C11004, doi:10.1029/2006JC004020, 2007.

- **Al Saafani, M. A.** and S. S. C. Shenoi. Water masses in the Gulf of Aden. *J. Oceanogr.*, 63, 1, 1-14, 2007.

- **Al Saafani M. A.** and S. S. C. Shenoi. Seasonal cycle of hydrography in the Bab el Mandab region, Southern Red Sea. *Proceedings Earth and Planetary Sciences* Vol 113,3, 269–280, 2004.

- **Al Saafani M. A.** *Hydrography of the Bab-El-Mandab Region, Southern Red Sea.* M.Sc. Thesis, Department of marine Science and Biotechnology, Goa University. 2002

- Tony Rouphael, Oliver J. and **Al Saafani M. A.** A monitoring program for Yemen's Red Sea. In A DauAbul and T. Rouphael: *Protection of marine ecosystems of the Red Sea coast of Yemen.* UN publications, 1999.

- **Al Saafani M. A.** Preliminary analysis of sea water temperature data from Yemen's Red Sea. In A DauAbul and T. Rouphael: *Protection of marine ecosystems of the Red Sea coast of Yemen*. UN publications, 1999.

Conferences

- **Al Saafani, M. A.** and S. S. C. Shenoi. Seasonal and Interannual Variability of eddy field and surface circulation in the Gulf of Aden. *Presented at 15 years of Progress in Radar Altimetry Symposium* 13-18 March 2006, Venice, Italy, 2006.
- **Al Saafani, M. A.** and S. S. C. Shenoi. Seasonal circulation in the Gulf of Aden. *Presented at First Prof. Ananthakrishnan Memorial Conference*, IITM, Pune on 18th - 19th January 2005, 2005.
- Murray S. P., W. Johns, A. Fisseha, A. DouAbul and **M. Al Saafani**. Seasonal variation of transport between the Red Sea and the Indian Ocean. *Proceedings of IAMAS/IAPSO 97 joint assemblies*, Melbourne Convention Centre, 1-9 July 1997.

Acknowledgements

Working at NIO for this thesis has been very pleasurable on account of a creative and helpful atmosphere in the research group. Needless to say, it has been a tremendous learning experience for me, and I would like to thank all the people who were close to me all this time.

First, I would like to express my deep sense of gratitude and sincere thanks to my supervisor Dr. S. S. C. Shenoi, Scientist F, NIO, Goa, for providing me incredible support, encouragement, and guidance in the development of my Ph.D. work. Without his help, it would have been practically impossible for me to make the thesis as it is.

I express my special thanks to Dr. S. R. Shetye, the Director, NIO, for granting me permission to carry out the work at NIO and for his support, encouragement and guidance throughout my Ph.D. from selecting the topic to the final submission.

I am particularly grateful to Dr. D. Shankar for his invaluable help during my PhD, sharing his great expertise and inexhaustible ideas concerning oceanography with me and for his detailed and stimulating commentaries on the work at every stage of its development.

The financial support from Sana'a University, Republic of Yemen is gratefully acknowledged. I would like to thank the Cultural attache, Embassy of the Republic of Yemen, New Delhi, for their support and smoothening the processes for releasing the fund from Sana'a University.

I would like to express my deep sense of gratitude and sincere thanks to Dr.

Mohammed Abubakr, Department of Earth Sciences and Environment, Sana'a University, for his continuous support and encouragement.

I express my special thanks to the co-guide Dr. Ramesh Pai, Department of Physics, Goa University, for his support and encouragement during the course of the Ph.D. work.

I express my sincere gratitude to Prof. G. N. Nayak, Head, Marine Science Department, Dr. H. B. Menon and Dr. Aftab Can for their kind advices, encouragement and help.

I express my special thanks to Professor P. Vinayachandran and Dr. Jaison Kurian for providing the output of the MOM4 simulations. I express my special thanks to Dr. Fabien Durand, IRD/LEGOS, and Dr. M. Aparna, NIO, for their support and help.

During the process of gathering the publicly available data and information about the Gulf of Aden, several institutions and scientists have supported me and provided the requested information. In this regard, I would like to especially thank Dr. Piechura, Institute of Oceanology, Polish Academy of Sciences, Dr. Baars, Royal Netherlands Institute for Sea Research, Netherlands, Director of Marine Science Research and Resource Center (MSRRC), Aden, Canadian Nexen Petroleum, Yemen, Dr. Abdu Al Maqalih, Civil Aviation and Meteorology Authority, Yemen and Capt. Roy Facey, Port of Aden Authority.

I express my special thanks to Dr. Unnikrishnan, Dr. Rameshkumar, Mr. Michael, Mr. Sundar, Mr. Almieda, Mr. Albert, Mr. Arun Mahale and Mr. Tapaswi.

Special thanks goes to all of my friends in NIO including Sreejith, Nuncio, Suprit, Syam, Manoj, Sindhu, Aneesh, Shantanu, Rabindra, Ricky, Sini, Vijay, Kaushik, Dattaram and Nagesh.

Throughout these years I spent in India, my Yemeni colleagues, specially Ammar, Hisham, Mondher and Abdul Salam were always around me, we shared moments of happiness and sadness, special thanks to all of them.

I would like to express my special thanks to Mrs. Marie Mendonica, who considered me and my family as a part of her family during our stay in Goa. I express my thanks to

Mr. Bob Godfrey and Mrs. Charmian Godfrey for their encouragement and help.

This thesis has been typed using LaTeX 2_ε[1]. The "style file", `guthesis.sty` is the Goa University style written by Shankar. FERRET, GMT, and Latex are used extensively in this thesis

It is absolutely impossible to remember everyone who helped me during my time in India. Here, I want to apologize to those I have left behind and thank them all.

I wish to express my profound thanks to my parents for their constant encouragement. My father extended his own creativity and love of learning to me while I was young, and my mother has been a constant source of support. I thank my brothers, Adnan, Khalid, Abdulghani and Muamar, my wife, my children Hagar and Ebrahim and my nephew Ahmed for their inspiration and moral supports. My wife has made life more than easy during her stay in Goa. I wish to share this moment of happiness with them.

MOHAMMED ALI YAHYA AL SAAFANI

National Institute of Oceanography, Goa

July 2008

[1] LaTeX 2_ε is an extension of LaTeX, a collection of macros for TeX. TeX is a trademark of the American Mathematical Society.

Synopsis

The Gulf of Aden presents a unique ecosystem that deserves scientific attention. In addition to its extraordinary biotic richness, the Gulf of Aden also serves as a highway for international trade between east and west. At present, approximately 3 million barrels of oil are being transported daily through the gulf. Traditionally, the Gulf of Aden has provided considerable amounts of sea food for the inhabitants of the surrounding arid lands. It will continue to do so in future if the fisheries are developed using modern scientific knowledge and techniques. In spite of the importance of the Gulf of Aden, very little information is available on its physical oceanography. Most of the investigations in this area were either aimed at understanding the exchanges between the Red Sea and the Gulf of Aden [Maillard and Soliman, 1986; Murray and Johns, 1997; Aiki et al., 2006], or at the spreading of Red Sea outflow into the Gulf of Aden [Fedorov and Meshchanov, 1988; Bower et al., 2000, 2002, 2005; Ozgokman et al., 2003; Peters and Johns, 2005; Peters et al., 2005] and its pathway into the Arabian Sea [Beal et al., 2000]. A few studies have used the available hydrographic data to describe the water masses in the Gulf of Aden [Rochford, 1964; Khimitsa, 1968; Piechura and Sobaih, 1986; Nasser, 1992; Mohamed et al., 1996; Mohammed, 1997]. All these studies, however, are either localized in space and time or have devoted themselves to describing the Red Sea outflow. Hence, they fall short of providing a comprehensive picture of the structure of water masses in the Gulf of Aden as they evolve round the year. These studies have also not succeeded in providing quantitative estimates of the different types of water masses that occupy the Gulf of Aden.

Often, the definition of water masses (the temperature–salinity–σ_θ ranges) vary drastically depending on the limited data used for the study. Similarly, the earlier studies did not deal in detail with the circulation and eddies in the Gulf of Aden.

This thesis aims at the synthesis of various data sets (hydrography, sea levels, winds, and model outputs) to describe the circulation and water masses in the Gulf of Aden more precisely than before. The main objectives of the study are: (i) to describe the seasonal cycle of circulation and hydrography in the Gulf of Aden, (ii) to describe the interannual variability of circulation in the Gulf of Aden, and (iii) to identify the possible mechanisms that control the circulation.

After presenting an introduction to the thesis in Chapter 1, Chapter 2 deals with the data used in this thesis. A new climatology of hydrography was prepared by assembling the data available from the National Oceanographic Data Center (NODC), USA, Japanese Oceanographic Data Center (JODC), and a few other data centres and individuals because the existing climatology [Stephens et al., 2002; Boyer et al., 2002] was found to be insufficient for deciphering the fine features in the Gulf of Aden.

The satellite altimeter derived sea level data used in this thesis were obtained from CLS Space Oceanography Division. The merged gridded TOPEX/Poseidon, Jason, and ERS-1/2 sea level anomaly (SLA) data for January 1993 to December 2003 were available for every 7 days on a 1/3 degree Mercator grid projection. These data have low mapping errors and better spatial coverage than the TOPEX/Poseidon data alone [Ducet et al., 2000; Volkov, 2005].

Chapter 3 describes the hydrography and water masses in the Gulf of Aden. The newly prepared climatology of hydrography was used to identify and describe the water masses in the Gulf of Aden and their variability in space and time. Four water masses have been identified based on their θ–S characteristics. The Red Sea Water (RSW) that flows from the Red Sea is the most prominent water mass in the Gulf of Aden; it occupies about 37% of the total volume of the Gulf of Aden. The Gulf of Aden Surface Water ($\sim$

3%) forms as a mixture of local water and the water from western Arabian Sea during winter and Red Sea Surface Water during summer. The intermediate water, identified as Gulf of Aden Intermediate Water (GAIW), occupies about 9% of the total volume of Gulf of Aden; a characteristic salinity minimum is associated with it at σ_θ = 26.50 kg m^{-3}. The northward spread of Sub–tropical Subsurface Water from the south appears to be the major source of GAIW. The bottom water, named Gulf of Aden Bottom Water (GABW), showed the least variability. It was formed by mixing of Red Sea Water and water of southern origin. Mixing triangles have been used to analyze the composition of water in the Gulf of Aden.

Chapter 4 deals with the seasonal and interannual variability of circulation in the Gulf of Aden. Mean monthly variability of circulation in the Gulf of Aden is described using several data sets: hydrography, ship drifts, and satellite–derived sea levels. All data sets showed the dominance of eddies in the seasonal cycle. During winter (November–March), the net flow is westward all over the gulf, with a host of cyclonic and anticyclonic eddies embedded in it. The flow inside the gulf during the transition periods, April and October, is similar to that during the winter months. During May, the flow inside the gulf is dominantly geostrophic because the Ekman drift is weak. During June, when the summer monsoon establishes over the gulf and the northwestern Arabian sea, the flow is eastward along the northern side of the gulf and is towards west along the southern side. Later in July–September, an eastward flow establishes all over the gulf. An anticyclonic eddy is seen at the centre of the gulf during June-September.

The vertical structure of circulation is described using the geostrophic currents derived from hydrographic data. The circulation pattern at 300 and 600 m during November to March is similar to that at the surface. The cyclonic and anticyclonic eddies seen at the surface extend up to $\sim$ 600–800 m. During summer, the eastward flow extends till 600–700 m during June, July and September, but only till 200 m in August. In August, the flow below 200 m is westward.

Merged altimeter SLA for 11 years is used to describe the interannual variability of surface circulation. Several techniques are available to resolve the signals at different periodicities hidden in the time series; wavelet analysis is one among them. To determine the dominant modes of variability in the SLA time series we have used the Morlet wavelet. This method allowed us to estimate the wavelet power due to the variability in SLA at different periods ranging from high–frequency (2 weeks) to interannual (5 years) periods. The annual and high–frequency signals dominate the sea level variability in the Gulf of Aden. The SLA variability in the gulf at interannual frequency is minimum and insignificant at 99% confidence level. It is significant at 95% confidence level only over a patchy area inside gulf. Since the variability in SLA is prudential to the geostrophic currents at the surface, the interannual variability in the surface geostrophic currents inside the gulf also are insignificant at 95 and 99% confidence levels.

Chapter 5 describes the mesoscale eddies that influence the circulation in the gulf and their origin. Inside the gulf, the eddies move at a speed of $\sim$ 6.0–8.5 cm s^{-1}, comparable to the first–mode baroclinic Rossby wave speed of 7.2 cm s^{-1}. The eddies, which enter the gulf from the Arabian Sea, owe their existence to more than one mechanism. Local Ekman pumping in the western Arabian Sea is important during the summer monsoon (June–September). During the winter monsoon (November–March), the dominant mechanism involves the westward propagating Rossby waves generated either in the Arabian Sea by Ekman pumping or along the west coast of India by poleward propagating Kelvin waves. These Rossby waves from the Arabian Sea propagate slower on entering the gulf because of a shallower thermocline in the gulf. Analysis shows that the SLA signal consists of low (annual and inter–annual) and high ($\sim$ 100–180 days) frequencies. The low–frequency signal (mainly annual) shows a discontinuity between 52° E and 60° E. Though the high–frequency signal is seen at all longitudes, a wavelet analysis shows that it is significant only west of 60° E. An energy analysis, based on model simulations, suggests that barotropic instabilities are important during the entire year and that baroclinic

instabilities are also important during the summer monsoon.

The results described above are summarized in Chapter 6.

Contents

List of Tables

List of Figures

Chapter 1

Introduction

The Gulf of Aden presents a unique ecosystem that deserves scientific attention. In addition to it's extraordinary biotic richness, the Gulf of Aden also serves as the highway for international trade between east and west. At present, approximately 3 million barrels of oil is being transported daily through the Gulf of Aden. Traditionally, the Gulf of Aden had provided considerable amount of sea food for the inhabitants of the surrounding arid lands. It will continue to do so in future also if the fisheries are developed using modern scientific knowledge and techniques.

The Gulf of Aden is an elongated stretch of water separating the African continent from the Asian continent (Figure 1.1). It is located approximately between the latitudes 10–15° N and longitudes 43–52° E. On its western end it joins the Red Sea, that produces one of the most saline water masses in the world oceans, and in the east it joins with the Arabian Sea (the Indian Ocean). In effect, the Gulf of Aden acts as the passage for the Red Sea water before it enters the Indian Ocean. The physical boundaries of the Gulf of Aden can be fixed approximately at the narrow Strait of Bab el Mandab in the west upto a line connecting Ras Fartak (east of Mukalla, Yemen) in the north and Ras Asir (northern corner of the Somali Peninsula) in the south. The northern and southern boundaries are well constrained with the land masses of Yemen and Djibouti-Somalia respectively.

The Gulf of Aden is a young ocean basin formed by the rifting of Asia (Arabia) from Africa (Somalia) [Girdler et al., 1980]. It has a well-defined continental margin, small oceanic basin, and an active mid-ocean ridge (Sheba Ridge) in the center characterized by a rift valley and fracture zones [Matthews et al., 1967; Bosworth et al., 2005]. The only other modern continental margin at a similar stage in its development is the Gulf of California [Cochran, 1981]. The Gulf of Aden is approximately 900 km in length and varies in width from 26 km at Bab el Mandab to about 320 km at Ras Asir. It is deepest in the middle $\sim$ 2000–2500 m and shallowest ($<$ 1000 m) in the west (west of 45° E). The average depth of Gulf of Aden is $\sim$ 1800 m. In general, the depth increases from west to east. Some studies consider the eastern end of the Gulf of Aden as the north-south line connecting Socotra Island in the south and Ras Fartak along the Yemen coast.The southeastern part of the Al-Surat mountain range (of about 1800 m height) surrounds the Gulf of Aden on the northern side while the Karkaar mountains of approximately the same height surround the coastal plain on the south. The major ports on the coasts of the Gulf of Aden include Aden, Djibouti and Berbera.

1.1 Weather and climate

The Gulf of Aden and the adjoining north Indian Ocean come under the influence of seasonally reversing monsoon winds, a feature unique to the north Indian Ocean region. The monsoon winds over the north Indian Ocean, in general, reverse twice a year, blowing generally from the southwest during summer monsoon (June-September) and from the northeast during winter monsoon (November-February). March-May and October are the months of transition between the two monsoons. This temporal reversal of the winds arise due to the changes in atmospheric pressure patterns associated with the deferential heating and cooling of the Asian land mass, especially the Indian sub-continent, with respect to the neighboring ocean. Earlier authors have followed different criteria in combining

Figure 1.1 Map of the Gulf of Aden and parts of the western Arabian Sea.

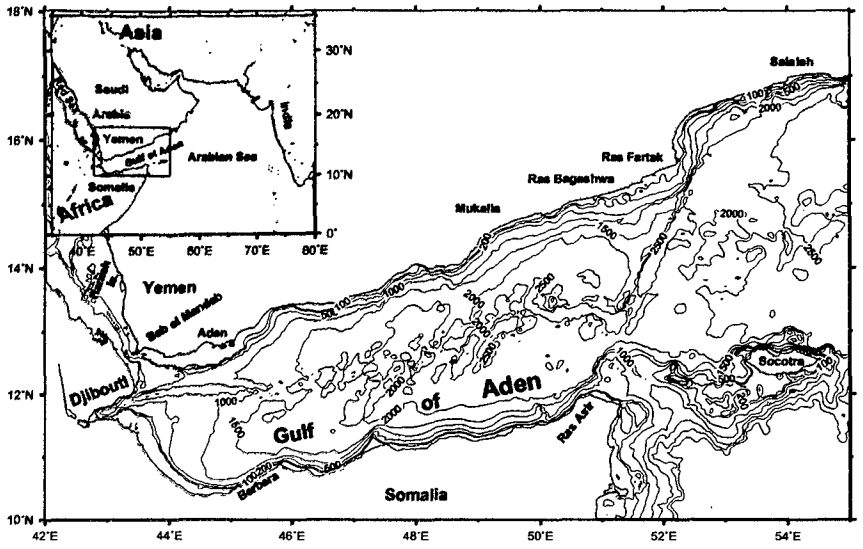

the months to represent the seasons. Anonymous [1982] stated that the Gulf of Aden experiences two distinct monsoon seasons, the southwest monsoon during the months of May to September and a northeast monsoon during the months of October to April. The months of April–May, and September–October are transitional months. Piechura and Sobaih [1986] considered the months of July–August as the period of southwest monsoon. However, they point out that sometimes the southwest monsoon starts in the west in June and in the east in May. They considered that the northeast monsoon was restricted to the months of November–February. Other months were considered as periods of weak variable winds. To study the seasonal variation of dissolved oxygen Al Sayed and Kolli [1992] described four seasons in the Gulf of Aden. Northeast monsoon during December–February, premonsoon during March–May, southwest monsoon during June–September and postmonsoon during October–November. Sobaih [1986] also made use of the same seasons while describing the data collected from the coastal stations of Yemen.

The description of wind patterns, over the Gulf of Aden, available in the literature also

do not suggest a uniform definition for the seasons. Hence, to avoid the arbitrariness in defining the prevailing seasons over the Gulf of Aden, it is necessary to propose a uniform definition based on the prevailing winds. In the present study, the pattern of climatological winds from satellite derived (QuikSCAT) data are used to categorise the months under different seasons. Figure 1.2 shows the climatological monthly mean winds over the Gulf of Aden and northwestern Arabian Sea. Over the Gulf of Aden, the southwesterly winds set in June, heralding the arrival of summer monsoon. They strengthen further during July and August (~ 8 m s^{-1} west of 51 °E). In September, the winds are weak (< 2 m s^{-1}) and blow from different directions inside the gulf. While over the northwestern Arabian Sea, the summer monsoon sets in May and persists till September. The easterly/northeasterly winds start inside the gulf in October (~ 4 m s^{-1}) and persists till April. In the northwestern Arabian Sea, the winter monsoon appears in November rather than in October and continues till March. In May, the magnitude of the winds weakens considerably to less than 2 m s^{-1} though the direction remains more or less the same (easterly) except in the eastern gulf (east of 50° E) where they blow from south. The summer monsoon appears to last only for 3 months (June-August) over the gulf as against the 5 months duration (May–September) in the western Arabian Sea. Similarly, the east/northeasterly winds prevail over the Gulf of Aden for 7 months (October–April) compared to the 5 months duration (November–March) over the western Arabian Sea. In essence, the Gulf of Aden experiences a shorter summer monsoon (June–August) and a longer winter monsoon (October–April). Since the Gulf of Aden and northwestern Arabian Sea are strongly linked with each other in their circulation and dynamics, it is proposed to consider the months of June–September as summer monsoon months and the months of November–March as winter monsoon months. The months of April–May and October will be considered as the months of transition or inter-seasonal months (Table 1.1). The pattern is similar in the wind climatology provided in Comprehensive Ocean-Atmosphere Data Set (COADS) [Woodruff et al., 1993].

Occasionally, a tropical cyclone originating in the north Arabian Sea reaches the entrance to the Gulf of Aden. The greatest chance of encountering a cyclone in the gulf is in November [Anonymous, 1982]. In addition, three extreme weather conditions also occur in the Gulf of Aden. These are locally known as (i) *Belat*, a strong sand storm, during the winter monsoon in mid-December (it generally persists for one to three days), (ii) *Khamsin* hot dry north wind that blows across the Gulf of Aden during the summer monsoon that occurs for three to four times a year lasting for 3–4 hours, and (iii) *Shamal*, also occuring during the summer monsoon, blows mostly from the north for a few successive days [Anonymous, 1993].

Precipitation in the region is sparse, hence no study has been conducted on the rainfall over the Gulf of Aden. The data available from the raingauge stations in Yemen (Aden and Mukalla) indicates that most of the precipitation occurs during the winter monsoon. However, at Salalah, a station to the east of the gulf along the southern coast of Oman, most of the rainfall occurs during the summer monsoon [Anonymous, 1993]. The rainfall information for the years 2001, 2002 and 2003 at Aden and Mukalla are shown in Table 1.2. The annual rainfall varies drastically from year to year, as do the rainy months during the three years. The annual rainfall was maximum during 2002 ($\sim$85 mm) at Mukalla and at Aden ($\sim$58 mm). Most of the rain in 2002 was during April at Mukalla ($\sim$63 mm) and Aden ($\sim$42 mm); rest of the rain was received during December–March. In contrast to 2002, the annual rainfall during 2001 was < 15 mm both at Aden and Mukalla. Similarly the rainfall in 2003 was also low at Aden (< 30 mm) and Mukalla (< 4 mm).

Table 1.1 The four seasons over the Gulf of Aden based on the patterns in winds

Season	*Period*
Summer (southwest) monsoon	**June–September**
Fall inter-season	**October**
Winter (northeast) monsoon	**November–March**
Spring inter-season	**April–May**

Figure 1.2 Monthly climatology of surface winds over the Gulf of Aden derived from QuikSCAT data.

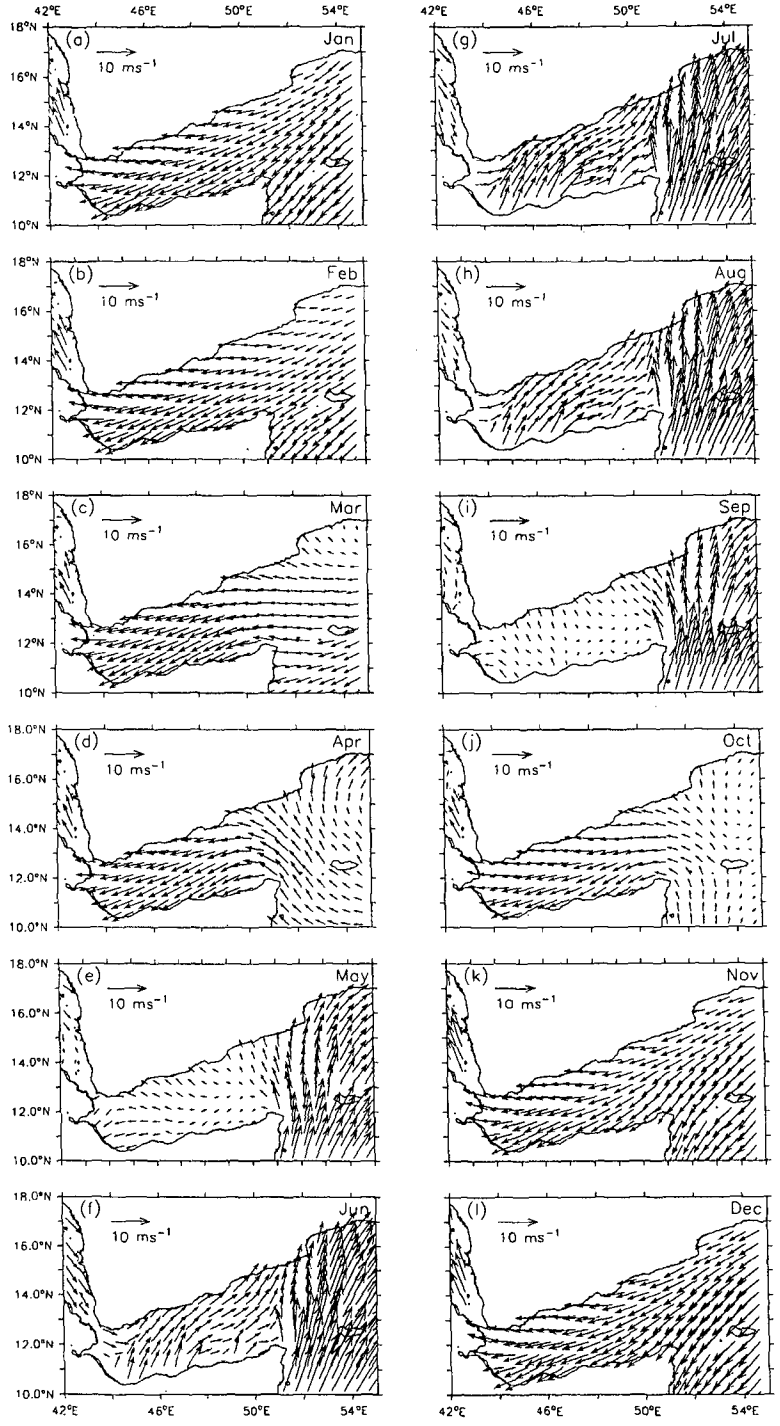

Table 1.2 Monthly mean rainfall (mm) at Aden and Mukalla (stations located on the northern coast of the Gulf of Aden) for the years 2001, 2002 and 2003. Data source - Civil Aviation & Meteorology Authority of Yemen.

Month	Aden			Mukalla		
	2001	2002	2003	2001	2002	2003
January	3.1	1.1	0.0	0.0	1.0	0.0
February	0.0	2.0	0.0	0.0	4.1	1.0
March	0.0	9.5	0.0	0.0	7.8	0.0
April	0.0	42.4	5.2	0.0	63.0	0.0
May	4.5	0.0	0.0	0.0	0.0	0.0
June	0.0	0.0	0.0	0.0	0.0	0.0
July	0.0	0.0	0.0	0.0	0.2	1.2
August	6.3	0.0	11.0	0.0	0.1	0.0
September	0.0	0.0	0.0	4.2	0.0	0.0
October	0.0	0.0	0.0	0.0	0.0	0.0
November	0.0	0.0	0.0	0.0	0.0	0.2
December	0.0	2.1	13.7	8.3	9.0	1.1
Annual	13.9	57.1	29.9	12.5	85.2	3.5

1.2 Hydrography and water masses

After the conclusion of the International Indian Ocean Expedition (IIOE) a few Soviet research vessels and Food and Agriculture Organization (FAO), through Norway fisheries research, collected hydrographic data from this region. Most of the data was collected for fishery research and not for the study of physical oceanography of the Gulf of Aden. Details of one such survey conducted by the Marine Science Research and Resource Center (MSRRC) of Yemen for the northern Gulf of Aden is available in Stirn et al. [1985], Piechura and Sobaih [1986] and Nasser [1992]. Subsequent investigations carried out in this area concentrated mostly on the study of the exchange of water between the Red Sea and the Gulf of Aden [Maillard and Soliman, 1986; Murray and Johns, 1997; Siddall et al., 2002; Aiki et al., 2006] and on the spreading of Red Sea water in the Gulf of Aden [Fedorov and Meshchanov, 1988; Bower et al., 2000, 2002; Ozgokman et al., 2003; Peters and Johns, 2005; Peters et al., 2005]. Beal et al. [2000] dealt with the spreading of the Red Sea Water out of the Gulf of Aden.

The extensive exchange of water between the Red Sea, the Gulf of Aden and the Arabian Sea, the strong evaporation and the monsoonal winds that blow over the region, all assist in the formation of complex vertical structures in the water column of the Gulf of Aden [Khimitsa, 1968; Stirn et al., 1985]. The earlier studies that used the available hydrographic data to describe the water masses in the Gulf of Aden include Rochford [1964], Khimitsa [1968], Piechura and Sobaih [1986], Nasser [1992], Maiyza and Mohamed [1993], Mohamed et al. [1996] and Mohammed [1997]. Since Chapter 3 is exclusively dedicated to deal with the water masses in the Gulf of Aden, the summary of the findings of these studies will be presented there.

Seasonal changes of the surface layer water characteristics described by Piechura and Sobaih [1986]; Nasser [1992]; Maiyza and Mohamed [1993] gives an account of the variability in the surface temperature of Gulf of Aden. Most of the variability in the sea surface temperature (SST) is seasonal. SST is highest (31–32 °C) during end May and

beginning of June. In July–August, it cools down to 29–30 °C, the degree of cooling depends on the strength of the summer monsoon. During the summer monsoon, the SST along the Arabian coast, the region adjacent to the Gulf of Aden, reaches a minimum of 17 °C. The heating of the surface takes place in September soon after the weakening of summer monsoon winds over the gulf and the SST bounces back to ~30 °C within a month. It cools again in October–January, ~ 24–25 °C, in response to the winter monsoonal winds and warms again during February–May in response to the spring warming that dominates the region during this period. The cycle is apparent in the satellite derived SST too. Figure 1.3, shows the annual cycle of SST derived from Tropical Rainfall Measuring Mission/TRMM Microwave Imager (TRMM/TMI) satellite over the Gulf of Aden. It reaches the maximum in May-June, falls in July–August, rises again in September and falls again in October–January before warming steadily in February–May. In essence, the SST over the Gulf of Aden exhibits strong seasonality.

Similar to the changes in SST, the surface mixed layer also shows strong seasonality. In summer, the mixed layer depth (MLD) decreases to less than 20 m and increases to over 100 m in winter. Accordingly, the depth of thermocline also shoals and deepens in summer and winter respectively; about 20–120 m in summer and 150–250 m in winter [Piechura and Sobaih, 1986].

Seasonal changes in the subsurface water, though much smaller than in the surface water, are still distinguishable. The lowest temperature and highest salinity is observed during the summer months and the highest temperature and lowest salinity during the winter months [Piechura and Sobaih, 1986].

1.3 Surface circulation

Very little information is available on the surface circulation in the Gulf of Aden. Most of the information on surface currents come from the ship drift observations [Kolli et al.,

Figure 1.3 Annual cycle of sea surface temperature (°C) over the Gulf of Aden. The SST was derived from Tropical Rainfall Measuring Mission/TRMM Microwave Imager (TRMM/TMI) satellite data for the period from January 1998 to December 2005

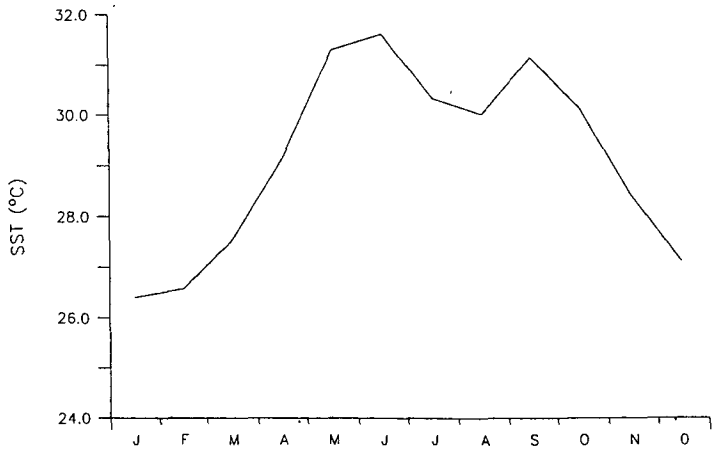

1992]. The general understanding of the surface currents in the gulf from the previous studies indicate that the flow during the winter monsoon months (November–February) is from east to west along the northern coast of the gulf and from west to east along the southern coast of the gulf. During the summer monsoon (June–August) and in September the flows are in the opposite direction; westward along the southern coast and eastward along the northern coast. In between these two seasons, the currents are weak and varying. In fact the flow in the Gulf of Aden is not regular suggesting any large scale currents along the coast, but is broken down to various closed circulation cells during the two prominent monsoon periods [Kolli et al., 1992]. Wooster et al. [1967] stated that the winter pattern starts in October with a weak flow of water into the gulf, which is fully developed in November through April. During summer, the direction reverses but with increased strength. An anticyclonic eddy is also seen in the central gulf during July–August (see charts CA1–CA4 in Wooster et al. [1967]). Though this analysis provided a fair picture of surface currents in the Gulf of Aden it used very little data from the southern part of the gulf.

The dynamic topography maps prepared by [Wyrtki, 1971] indicate a weak flow during January–February with a northeastward flow along the northeastern part of the Gulf of Aden. During the summer monsoon months, July–August, an anticyclonic cell forms in the center of the gulf and shifts eastward towards the mouth of the gulf during September–October. The dynamic topography maps of Seriy and Khimitsa [1963] indicate two eddies, one cyclonic in the gulf (east of 50° E) and the other, an anticyclonic eddy, to the east of the gulf off Ras Fartak. The geostrophic current derived from the hydrographic data collected by *R. V. F. Nansen* in the upper 500 m [Sandven, 1979] also indicated numerous eddies at different locations.

The recent attempts that described the circulation in the Gulf of Aden or along its segments include Mohammed and Kolli [1992] and Johns et al. [2001]. The details of their findings will be presented in Chapter 4 dedicated exclusively to describe the currents in the Gulf of Aden.

1.4 Upwelling

Numerous investigators have reported the occurrence of upwelling along the Gulf of Aden and Arabian coasts [Bruce, 1974; Swallow, 1984; Piechura and Sobaih, 1986; Savidge et al., 1990]. Understanding the process of upwelling is important since the Gulf of Aden has been regarded as one of the most productive areas [Kabanova, 1968; Currie et al., 1973; Krey and Babenard, 1976]. Piechura and Sobaih [1986] showed that the upwelling develops first in the far eastern parts of the Yemeni coastal waters in May and subsequently, progresses further towards the west. Mostly, the upwelling appears in separated patches similar to those appear in the coastal waters elsewhere [Boje and Tomczak, 1978]. Awad and Kolli [1992] studied the upwelling process in the Gulf of Aden by analyzing the hydrographic data collected during 1984–85. They described the distribution of hydrographic properties and estimated the strength of upwelling. The most conspicuous

feature is the cooling of near surface layer by more than 8 °C. Figure 1.4 reproduces the figure from Awad and Kolli [1992]. The temperature and salinity sections along 49° E during July extends from the central region of the gulf (station 173) to the northern coast (station 179). The isotherms shallow towards north within a short distance; the isotherm of 20 °C rises from $\sim$ 100 m depth at station 173 to 20 m at station 179 in the north. Similarly the isohalines shallow towards the north. They attributed the upwelling during summer monsoon and downwelling during winter along the northern part of the gulf to the dominant wind over the gulf. However they could not describe the upwelling along the southern coast of the gulf due to insufficient data. Al Sayed and Ghaddaf [1993] attributed the frequent occurrence of fish mortality in the Gulf of Aden during the southwest monsoon to the presence of very cold, low oxygen water near the surface. Morcos and Piechura [1990], using the data in the archives of the British Museum, stated that very strong upwelling takes place along the Yemen coast in the west.

1.5 Sea level

The attempts made to understand the sea level variations in the Gulf of Aden are very limited [Morcos, 1990]. Patzert [1974] presented the sea level changes at Aden and Perim (Myuun) Island and concluded that these changes resulted from the reversal of circulation, which is closely associated with the reversals in the monsoon winds acting on the sea surface. Figure 1.5 shows the monthly climatology of mean sea level at Aden, based on PSMSL data for the periods 1879–1893, 1916–1933 and 1937–1969. The sea level at Aden rises between September and May and falls during June–July to reach the minimum in August. The seasonal oscillations in the mean sea level can arise due to astronomical effects, effects of evaporation, precipitation and river discharge, atmospheric pressure, and steric sea-level effects. The effects of purely astronomical conditions (long-period tides) are not significant; they do not exceed 12 mm at these latitudes [Pattullo et al.,

Figure 1.4 Vertical distribution of temperature and salinity along 49° E during July in the Gulf of Aden. After Awad and Kolli [1992]

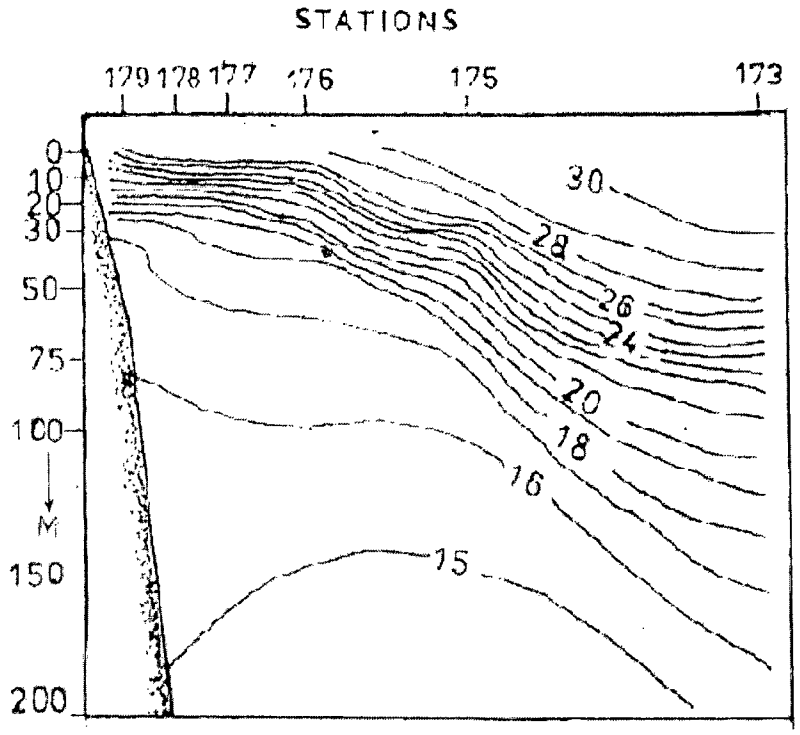

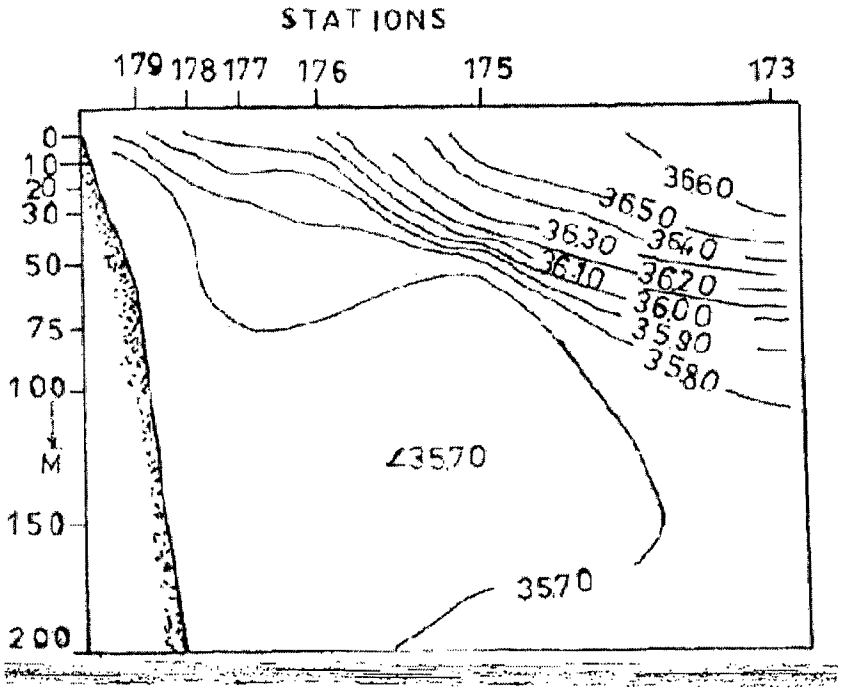

1955]. Because rainfall is very low and no large rivers are discharging into the Gulf of Aden, these two factors can be ignored. Maximum evaporation over the gulf occurs during winter when the sea level is highest [Privett, 1959]. Since the sea level variations are completely out of phase with the variations in evaporation, evaporation also does not appear to control the oscillations of mean sea level.

The isostatic adjustment of the ocean surface to changing atmospheric pressure requires that the sea surface rise (fall) by 1 cm for every 1 mbar decrease (increase) in pressure. Patzert [1974] noted that the atmospheric pressure at mean sea-level is highest during January and lowest during July at Aden with a range of $\sim$ 10 mbar. Corrections to the monthly mean sea-level curves for the pressure variations results in an increase in the range of mean sea level. Thus the observed variations in mean sea level does not appear to be due to the effect of atmospheric pressure change.

Variations of the density within a water column, from which the steric sea level is calculated, depends on the thermohaline variations within the column. It is high when water is warm and/or less saline and low when water is cold and/or more saline. In the upper 300 m of the water column near Aden, the steric variations have the same phase and similar range as the sea level at Aden, though the range of the steric variations is larger by approximately 8 cm [Patzert, 1974]. This variation in density of the upper 300 m of the water column is due to the upwelling of cool, low-salinity water that occurs in the northwestern Gulf of Aden during the southwest monsoon.

1.6 Objectives

From this brief summary of the previous studies it is clear that the information available on the hydrography and circulation of the Gulf of Aden is meagre. For example, the literature is incomplete on the description of the annual cycle of hydrography, the water masses, their origin, the annual cycle of circulation at different depth levels, the meso-

Figure 1.5 Annual cycle of sea level (cm) at Aden.

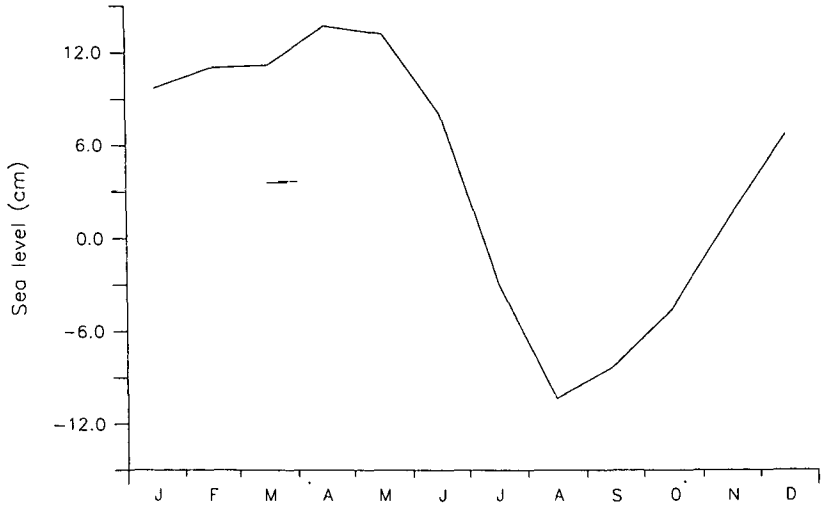

scale features like eddies that occur in the gulf and their origin. The data sets used by the earlier researchers were either specific to a smaller region within the gulf or were confined to specific timings. With the recent developments in satellite techniques in measuring various oceanographic parameters and due to the advancement in numerical modeling skills, larger reliable data sets are now available for further research in this area.

In this thesis, we have synthesized various data sets, hydrography, satellite derived sea levels, satellite derived winds and some model outputs to describe the circulation and water masses in the Gulf of Aden more precisely than before. The major objective of this study is to describe the seasonal cycle of circulation and hydrography in the Gulf of Aden and to identify the possible mechanisms that control the circulation. Towards this, we have first described the variability in hydrography and water masses in the Gulf of Aden quantitatively on a monthly scale and identified their origins. Next, we have described the mean monthly picture of circulation in the Gulf of Aden using different data sets like hydrography, ship drifts and satellite derived sea levels and last, we have examined the mesoscale features that influence the circulation in the Gulf of Aden and identified their

forcing mechanisms using various data sets and model outputs.

Chapter 2 describes the data sets, specifically, the hydrographic data used in the thesis and the procedures followed for quality control and objective analysis. Chapter 3 is devoted to describe the hydrography and water masses in the Gulf of Aden. In Chapter 4, we describe the circulation in the Gulf of Aden using ship drift, hydrography, satellite altimetry and winds derived from satellite scatterometers. Chapter 5 describes the mesoscale eddies that influence the circulation in the gulf and their origin. Using satellite derived sea levels, we argue that the westward propagating eddies in the gulf are linked to the westward propagating Rossby waves in the Arabian Sea. Chapter 6 summarizes and concludes the thesis.

Chapter 2

Data

2.1 Introduction

As mentioned in the earlier chapter, the Gulf of Aden is a data sparse region from an oceanographic point of view. As per the available records, the first measurements of hydrographic parameters (temperature and salinity) in the Gulf of Aden were made during the research cruises of Vityaz during 1886–1889. During this cruise, about 209 profiles were collected from the Indian and Pacific Oceans; of which only 4 were from the Gulf of Aden. The second Expedition in the region was the Italian Expedition during 1923 on board Ammiraglio Magnani. During this cruise, about 144 profiles of temperature–salinity were collected mostly from the Red Sea and Bab el Mandab region. The second Italian cruise during 1924 extended to the western part of the Gulf of Aden. In 1929 the Netherlands Expedition on board Willebrod Snelluis collected about 311 profiles, of which 17 profiles were from the Gulf of Aden during their navigation through the gulf in April 1929. One of the famous expeditions in the Indian Ocean and the Gulf of Aden was the United Kingdom Expedition on board the Mabahiss during 1933–1934. During this cruise, about 119 profiles were collected, of which 19 were from the gulf. After a gap of 15 years, during 1947–1949, Swedish researchers on board the Albatross collected

about 86 profiles including 3 from the Gulf of Aden. Since then, several expeditions in the Indian Ocean have included stations in the Gulf of Aden; especially the International Indian Ocean Expedition (IIOE) during 1960–65. Making use of the hydrographic measurements from the world oceans, Levitus [1982] published a climatological atlas of world oceans. The first atlas published by Levitus [1982] provided the annual oxygen, seasonal salinity and monthly temperature climatologies at 19 standard depth levels (0/1000) at a spatial resolution of $1° \times 1°$ longitude–latitude grid for the world oceans. Though this atlas included areas of the Gulf of Aden, its reliability for this region remained low due to scart data which went into the analysis. The improved versions of this atlas published in 1994 [Levitus and Boyer, 1994; Levitus et al., 1994] and in 1998 [Antonov et al., 1998; Boyer et al., 1998] at $1° \times 1°$ longitude–latitude grid also suffered similar problems due to the low data density in the Gulf of Aden. Moreover, the large interpolation scales (4, 6, and 8 degree in the case of 1998 atlas) used by them while interpolating and mapping the data on to equal sized grids might introduce large errors in a region like Gulf of Aden where the temperature-salinity varies drastically over shorter spatial scales.

To overcome the difficulties in data sparseness, it is prudent to use a variety of data sets available from all sources. This chapter describes the data sets used in this thesis, their source, quality controlling and the processing. The in situ data set, the hydrographic measurements consisting of temperature–salinity and oxygen profiles, were obtained from several sources as described in the next section. Also the measurements made by the sensors mounted on board satellites are used, specially, the sea level heights measured by the satellite based altimeters and the sea winds measured by the sactterometer.

2.2 Hydrographic data

2.2.1 Data source

The available climatology of temperature and salinity for the Gulf of Aden prepared globally appeared to be inadequate to represent several known features, like the inversions in salinity and temperature profiles associated with the Red Sea Water (RSW) in the intermediate levels and the upwelling along the northern coast during summer (see section 2.2.4). Hence, to generate a reliable hydrographic data set, attempts have been made to obtain as many temperature–salinity profiles from the Gulf of Aden from all possible sources. The publicly available data were downloaded from different data centers, and also through personal contacts. The main sources of hydrographic data are:

- The archives of the National Oceanographic Data Center (NODC). NODC data are considered as the main source of data since most of the data (60%) were downloaded from NODC web site. The downloaded data consisted of data obtained using the profiling instrument 'Conductivity–Temperature–Depth (CTD)', 'Expendable Bathythermograph (XBT)' and 'Mechanical Bathythermograph (MBT)' and the 'Ocean Station Data (OSD)', obtained using reversing bottles attached with reversing thermometers. NOCD05 data released in May 2006 [Boyer et al., 2006], as an update to NOCD01 data, was obtained through internet downloads (http://www.nodc.noaa.gov/OC5/WOD05/pr_wod05.html) for the Gulf of Aden region (between 43 and 55° longitudes and 10 and 18° latitudes). The details of the number of temperature–salinity–oxygen profiles are listed in (Table 2.1). Altogether, 23766 profiles consisting of 23705 temperature profiles, 3993 salinity profiles and 2474 oxygen profiles were obtained from NODC.

- The archives of the Japan Oceanographic Data Center (JODC). A total of 15470 profiles was obtained from JODC, consisting 2142 salinity profiles and 15458 tem-

perature profiles.

- The temperature–salinity–oxygen profiles collected, using CTD, during the Bab el Mandab Experiment (BAM) [Murray and Johns, 1997; Al Saafani and Shenoi, 2004]. These profiles collected during 1995–1997 from the western Gulf of Aden and Bab el Mandab region contained 42 profiles of temperature–salinity–oxygen from the western Gulf of Aden.

- The CTD profiles available from the Netherlands Indian Ocean Programme (NIOP) [Baars, 1994]. 74 profiles of temperature, salinity and oxygen were obtained from this source.

- The data collected during 1984–85 through a survey under the auspices of the Marine Science and Resources Research Center (MSRRC) of Yemen [Stirn et al., 1985]. This data were obtained personally from Dr. Peichura. It consisted of 100 profiles of temperature, salinity and oxygen.

The total number of profiles obtained from the aforementioned sources was 39452; of which 39379 profiles contained temperature, 6351 profiles contained salinity and 2690 profiles contained oxygen (Tables 2.2, 2.3 and 2.4).

Table 2.1 The temperature–salinity–oxygen profiles obtained from National Oceanographic Data Center (NODC05 data sets).

Data type	Total	Temperature	Salinity	Oxygen
CTD	469	469	469	469
OSD	4609	4548	3524	2005
XBT	9655	9655	-	-
MBT	9033	9033	-	-
Total	23766	23705	3993	2474

2.2.2 Quality Control

Since, the profiles were spot measurements in time and space, their distributions were not even either in space or time. Hence, to map them over regular spatial and temporal intervals it is necessary to interpolate them following robust techniques. But before the data are interpolated, it is necessary to subject them to various quality checks. Boyer and Levitus [1994] described a set of quality checks used by them to check the quality of temperature–salinity profiles before subjecting them for interpolation and mapping. Various steps followed to ensure the quality of profiles and the procedure followed to map them on equally spaced spatial grids during each month are described in the following sections.

Position Check

A few profiles appeared in the data sets with wrong positions, say on land. Obviously, these errors occurred due to the wrong entry of station locations. In this step, 31 profiles of temperature, 12 profiles of salinity, and 5 profiles of oxygen having wrong positions were identified and removed (Tables 2.2, 2.3 and 2.4).

Duplicate profile check

Since we have obtained the data from different data centers, it is possible to have the same profile in more than one data source. Thus the second step in the quality check was the removal of duplicate profiles. A duplicate profile is one that contains the identical information to another profile, including position, date, and the data values. The NODC data were used as the reference data set. The profiles found to be repeated in other data sets were then removed. This process removed 16618 profiles of temperature and 2150 profiles of salinity, mostly, from JODC data, and 144 profiles of oxygen (Tables 2.2, 2.3 and 2.4). After the removal of duplicate profiles, 22730 profiles of temperature, 4189 profiles of salinity and 2541 profiles of oxygen were retained. Obviously, the availability

of temperature profiles is larger than (at least 5 times) the availability of salinity profiles in the Gulf of Aden.

Table 2.2 The number of temperature profiles discarded at various stages of quality checks and the number of accepted profiles. See section 2.2.1 for the details on data sources.

Data source	Before quality control	Bad position	Duplicate profiles	Temperature inversion	Accepted
NODC-CTD	469	-	62	-	407
NODC-OSD	4548	5	296	10	4237
NODC-XBT	9655	12	5	22	9616
NODC-MBT	9033	7	958	30	8038
JODC-CTD	328	-	328	-	-
JODC-OSD	3947	7	3780	2	158
JODC-XBT	7223	-	7223	-	-
JODC-MBT	3960	-	3960	-	-
BAM-EXP.-CTD	42	-	-	-	42
NIOP-CTD	74	-	6	-	68
MSRRC-Yem.-CTD	100	-	-	-	100
Total	39379	31	16618	64	22666

Depth inversion and depth duplication checks

After the removal of duplicate profiles, individual profiles of each parameter were checked for duplicate depths and depth inversions. Depth inversion occurs when an observation has a shallower depth than the observation directly preceding it. Depth duplication occurred due to reporting of the same data more than once. In such cases the second observation was flagged and eliminated.

Temperature inversions

Unnecessary temperature inversions can occur due to erroneous recordings or measurements. However, the temperature inversions in the upper layers and locations of a large influx of totally different water masses are not unnatural. For example, in the western Gulf of Aden where a large influx of RSW occurs. Hence, it is necessary to apply this check cautiously. For this reason, the profiles from western Gulf of Aden (west of 47° E) were not subjected to this check. For the profiles from other regions of Gulf of Aden, the temperature inversions were considered unacceptable when the increase in temperature exceeded 0.3 °C per meter between adjacent observations. Boyer and Levitus [1994] had used a similar value to identify the temperature inversions. These checks resulted in the loss of 64 temperature profiles.

Table 2.3 The number of salinity profiles discarded at various stages of quality checks and the number of accepted salinity profiles. See section 2.2.1 for the details on data sources.

Data source	Before quality control	Bad position	Duplicate profiles	Accepted
NODC-CTD	469	-	62	407
NODC-OSD	3524	5	105	3414
JODC-CTD	328	-	328	-
JODC-OSD	1814	7	1649	158
BAM-EXP.-CTD	42	-	-	42
NIOP-CTD	74	-	6	68
MSRRC-Yem.-CTD	100	-	-	100
Total	6351	12	2150	4189

A common approach to identify the inversions in salinity profiles is not possible because of the presence of different water mases. However, any errors that can arise due to erroneous salinities can be checked, though indirectly, through the checks for stability (monotonic increase in density with depth) described later.

Table 2.4 The number of oxygen profiles discarded at various stages of quality checks and the number of accepted oxygen profiles. See section 2.2.1 for the details on data sources.

Data source	Before quality control	Position check	Duplicate profiles	Accepted
NODC-CTD	469	-	62	407
NODC-OSD	2005	5	76	1924
BAM-EXP.-CTD	42	-	-	42
NIOP-CTD	74	-	6	68
MSRRC-Yem.-CTD	100	-	-	100
Total	2690	5	144	2541

Vertical Interpolation

Before checking the temperature–salinity profiles for stability of a water column, they were first interpolated to standard levels. The interpolation of the data to standard levels is necessary because the observed levels differ from one profile to another. The interpolation to 26 standard levels (0, 10, 20, 30, 50, 75,100, 125, 150, 200, 250, 300, 400, 500, 600, 700, 800, 900, 1000, 1100, 1200, 1300, 1400, 1500, 1750 and 2000 m) was done using a three point Lagrangian interpolation method based on Scarborough [1966]. This interpolation scheme used one value above and two values below or two values above and one value below the interpolation level. If the observed level reported a value within 5 meters of the surface, then that value is used as the surface value (at 0 m).

Stability check

The station data containing both temperature and salinity were then used to check for the stability of the water column. Spurious inversions in the density values indicate the instability of the water column that is unnatural in most cases. However, minor instability or inversion in density in the upper layers and in the intermediate layers is natural because

of the measurement, made at the time of mixing and stabilization of the water column.

Hence, up to a depth of 30 m, the inversions in excess of 3×10^{-5} g cm^{-3} in density only were rejected, below this depth, down to 400 m level, inversions in excess of 2×10^{-5} g cm^{-3} were rejected . No inversions were allowed below 400 m. If the number of unacceptable inversions in each profile is more than two, then the entire profile was eliminated. This check rejected about 950 levels.

Standard deviation check

As a final check, the data retained at each standard level have been subjected to a 'standard deviation check' by grouping the profiles during a month in one–degree spatial grids in the case of temperature and two–degree spatial grids in the case of salinity. This check is expected to discard non–representative data. The monthly mean and standard deviations of temperature (salinity) at each standard level were calculated in each one–degree (two–degree) grid and the individual values were checked against them. When the value at any standard level of the profile exceeded 3 standard deviations, then that was flagged and discarded. This check was performed only when there were enough profiles available within the one–degree (two–degree) grids, say a minimum of three profiles. Hence, the check was not performed when the one–degree (two–degree) grids contained fewer than three profiles. Only 4 one–degree grids in the case of temperature (along the southern side of the gulf) and 3 two–degree grids in the case of salinity had less than 3 profiles (mostly in the eastern gulf). Boyer and Levitus [1994] had used 5 standard deviations in a five–degree latitude by a five–degree longitude grid. Considering the high variability in the temperature–salinity structure in the Gulf of Aden, we have used the smaller grids (two–degree in case of salinity and one–degree in case of temperature) but smaller standard deviation values (3 standard deviations rather than 5). This criteria helped us to retain the small scale features within the Gulf of Aden like the upwelling along the northern side of the gulf. The five-degree grid practiced by Boyer and Levitus [1994] ought to have

smoothed these features unnecessarily.

At the end of the series of quality checks described above, 22666 profiles of temperature, 4189 profiles of salinity and 2541 profiles of oxygen were retained (Tables 2.2, 2.3 and 2.4). The number of oxygen profiles is low compared to the temperature and salinity profiles. hence the oxygen profiles were not subjected to the objective analysis described in the following subsection. The earlier climatologies included 13229 temperature profiles [Stephens et al., 2002] and 1917 salinity profiles [Boyer et al., 2002] for this region. The one–degree spatial grid used for the mapping of temperature by Antonov et al. [1998] and for salinity by Boyer et al. [1998] appears to be inadequate to describe the features in the coastal waters (see for example Figure 2.4). Hence, to describe the observed features in the Gulf of Aden, it is necessary to carry out a similar analysis on 0.5° grids. The number of temperature and salinity profiles available in each 0.5° grid during every month is shown in Figures 2.1 and 2.2. Among the 86 half degree grids, covering the Gulf of Aden, between the longitudes 43° E and 51° E, 2 grids did not have temperature profiles in April and July, 3 grids in May and one grid in September. The number of grids which did not have salinity profiles are more than that of temperature profiles. Nevertheless, considering the distribution of profiles, it is possible to map them over 0.5° grids following the procedures described in Antonov et al. [1998].

2.2.3 Objective Analysis

After the quality control, the data are ready for interpolation and mapping on to equally spaced grids. Since the final numbers of temperature and salinity profiles are sufficiently high in the Gulf of Aden region, we have decided to map them on to 0.5 × 0.5 grids. An interpolation technique called 'Objective Analysis' is often adopted for the mapping of such data sets [Antonov et al., 1998]. Antonov et al. [1998] used the objective analysis scheme described in Barnes [1964] to prepare the atlas of temperature for the Indian Ocean. The analysis scheme used the data values at standard levels and first–guess values

Figure 2.1 The number of temperature profiles available in 0.5° × 0.5° grids during a month after applying the series of quality checks described in section 2.2.

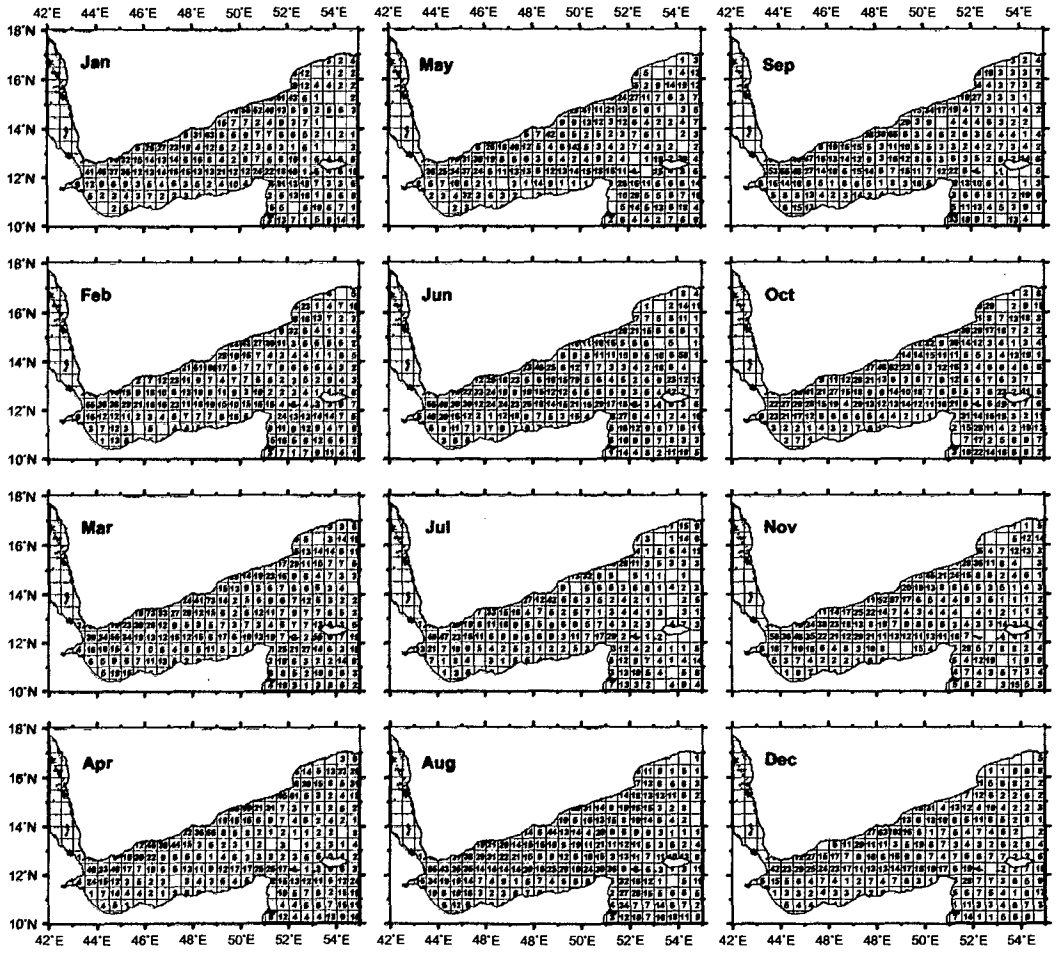

Figure 2.2 The number of salinity profiles available in 0.5° × 0.5° grids during a month after applying series of quality checks described in section 2.2.

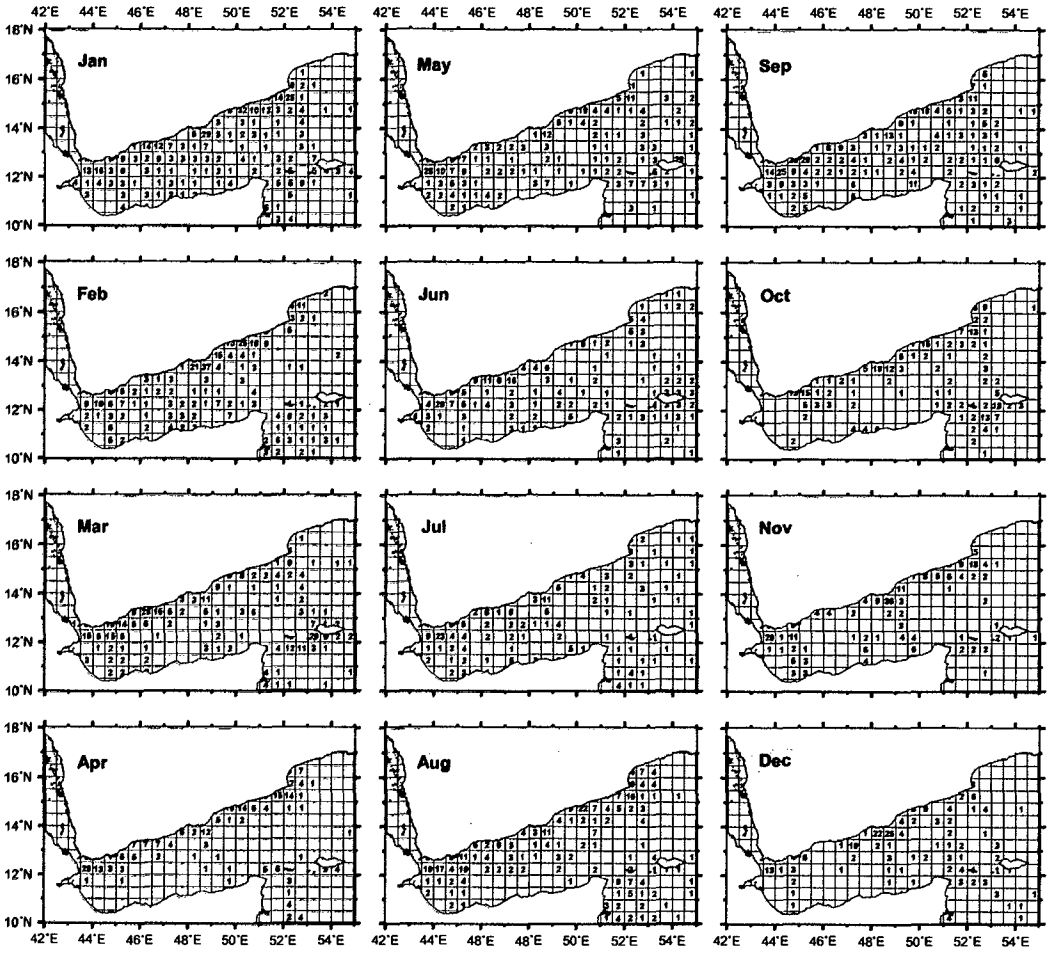

for each grid. Antonov et al. [1998] defined the first–guess using the annual 'zonal mean' of the parameter under consideration. For the Gulf of Aden region, this approach caused large errors due to the large variability in the values of temperature and salinity from the western end to the eastern end. The influx of high saline RSW at the western end of the gulf generates sharp zonal gradients rendering the use of zonal means as first–guess values meaningless. On the contrary, the meridional gradients of temperature and salinity in the Gulf of Aden are low. Hence, we have used the meridional means (of each 0.5° longitude bands) as the first–guess values rather than the zonal means.

Together with the first–guess values, the other required inputs for the scheme are the observed values at standard levels regardless of when they were observed. The next input required for the scheme is the 'radius of influence' specifying the distance up to which the interpolation scheme should consider the influence of a particular value. Using these three inputs, the first–guess values, the observed values at standard levels and the radius of influence, the scheme first computes the difference between the observed value and the first–guess value. Later the scheme, corrects the first–guess values at all grid points by applying a distance–weighted mean of all values that lie within the area around the grid point defined by the radius of influence. Mathematically, the correction factor suggested by Barnes [1964] can be written as

$$C_{i,j} = \frac{\sum_{s=1}^{n} W_s Q_s}{\sum_{s=1}^{n} W_s} \tag{2.1}$$

where (i,j) are the coordinates of a grid point in the longitude–latitude directions, $C_{i,j}$ is the correction factor at grid point denoted by (i,j), n is the number of observations that fall within the area around the point i,j defined by the radius of influence, Q_s is the difference between the observed value and the first–guess at the s^{th} point in the influence area, W_s is the weighting function given as $\exp(-Er^2R^{-2})$ for $r < R$ and zero for $r > R$, r is the distance of the observation from the grid point (i,j), R the radius of influence set

to be 1° for this analysis. E is set to a value 4. Antonov et al. [1998] used a value of R = 4, 6 and 8 degrees for the global analysis. For a region like the Gulf of Aden, such a large value of R would introduce undesirable errors because it forces the analysis to use values from the west (where the RSW influx occurs) to obtain a value in the east and vice versa.

At each grid point the analysis computes the analyzed value $G_{i,j}$ as the sum of the first–guess, $F_{i,j}$, and the correction $C_{i,j}$. ie.

$$G_{i,j} = F_{i,j} + C_{i,j} \tag{2.2}$$

The working of the objective analysis scheme based on the radius of influence is shown in the schematic in Figure 2.3. For the analysis at a particular time for a 0.5 × 0.5 grid centered at 'c', the procedure includes all observations that fall within the radius of influence R; in this case, the values at locations 1 to 6. According to the scheme, to compute C_{ij} at location 'c', the value at 5 will be accorded the maximum weightage and the value at 6 will be accorded with minimum weightage. The values at locations outside the radius of influence 'R' (locations 7,8, 9) will have no effect on the C_{ij} at 'c'. If there are no data points within the area defined by the influence radius, then the correction, C_{ij}, will be set to zero leaving the first–guess field unchanged. In such cases, the analyzed value will be the first–guess value itself. This correction procedure is applied at all grid points to produce an 'annual analyzed field'.

The 'annual analysed values' obtained at every grid point were then used as first–guess values for a bi-monthly analysis, again following the same procedure as described above. For the bi–monthly analysis, the mean values in the grids were computed using the data in bi–monthly durations (Jan–Feb, Mar–Apr, May–Jun, Jul–Aug, Sep–Oct, and Nov–Dec). The 'bi–monthly analysed values' thus obtained were then used as the first–guess values and the same procedure was repeated to generate monthly analysed values of temperature and salinity in each half degree grid point in the Gulf of Aden and its vicinity.

Figure 2.3 A schematic showing the grid size and the radius of influence (R) used for the objective analysis scheme. Location 'c' represents the center of 0.5° × 0.5° grid where the interpolated value needs to be assigned. The numbers from 1 to 9 represent the locations where the data are available. According to the scheme, profiles 1-6 located within the radius of influence (R) of 'c' will be considered for interpolation. Maximum weightage will be accorded for Station 5 and minimum for Station 6.

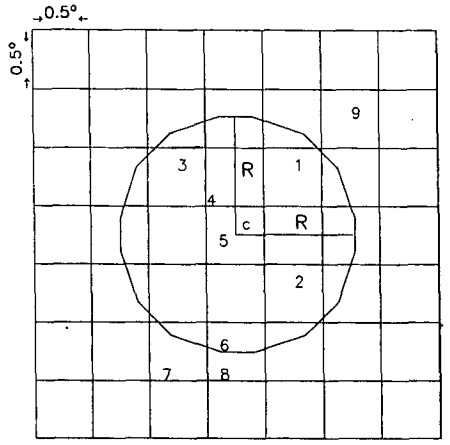

2.2.4 Post objective analysis

After the initial objective analysis, additional checks were performed to identify and rectify the unrealistic features occasionally seen, mostly, in data sparse areas. To eliminate these features, all the data in an area were examined to find the anomalous behaviour, if any, in the profiles. Any suspicious data were then eliminated and the whole procedure of objective analysis was repeated again using the rectified inputs.

The objectively analysed temperature and salinity fields on half degree grids were compared with the previous World Ocean Atlas–1998 (WOA98) of temperature [Antonov et al., 1998] and salinity [Boyer et al., 1998] and also with the new World Ocean Atlas data–2001 (WOA01) of temperature [Stephens et al., 2002] and salinity [Boyer et al., 2002] (Figures 2.4 and 2.5). WOA01 has a spatial resolution of 0.25° × 0.25°. Figure 2.4a (panels to the left) shows the horizontal distribution of temperature from three data sets during July. The intense upwelling that occured along the northern part of the

gulf is not seen in WOA98 (upper panel) due to the coarse spatial resolution (1° × 1° grid), but is seen clearly in the new climatology (lower panel). It is seen in WOA01, but with lesser intensity (middle panel). The new climatology clearly shows three pockets (marked 1, 2 and 3) of upwelling along the northern coast. These three pockets of upwelling seen along the northern coast of the Gulf of Aden are similar to those reported in Piechura and Sobaih [1986]. Figure 2.4a (panels to the right) shows the same for the month of March where the WOA98 does not show any variations inside the gulf, while the new climatology shows better distribution inside and outside the gulf. Similary horizontal distribution of surface salinity (Figure 2.4b) shows the three pockets of upwelling along the northern coast from the new climatology and the WOA01 and not seen from WOA98. The eastern part (location 3) of WOA01 shows salinity < 34.5 psu, which is very low for the region like Gulf of Aden as compared with 35.7 psu from new climatology. During March (right panels) the new climatology shows also similar distribution of salinity to that of temperature. Figure 2.5a, b and c shows the vertical distribution of salinity, along an east–west section in the Gulf of Aden, during July from the three data sets. The high saline RSW is seen in all data sets in the intermediate layer. The new climatology (Figure 2.5c) shows high salinity RSW in the western end of the gulf with $\sim$ 37 psu, while it is 36.2 psu in WOA98 and 36.4 psu in WOA01. The other advantage of this new climatology is that, it captures the core of RSW at two depth levels in the western part of the Gulf of Aden similar to that reported earlier [Maillard and Soliman, 1986; Bower et al., 2000] using in situ observations. The third advantage of this climatology is that it produces the data to a 2000 m depth (Figure 2.5 panel d) compared to 1500 m in WOA98 and WOA01. The data to 2000 m is useful to describe the bottom water in the Gulf of Aden.

Having shown the advantages of new climatology over the previous climatologies, data sets were also compared with the average values of in situ temperature and salinity in the grids where they existed in the data during a month. Figure 2.6a shows the difference between the temperature in each climatology and the average temperature estimated

from the observed profiles falling in the corresponding grids. The mean of the differences and the standard deviations are lowest for the new climatology. Some of the differences are as high as 6.1 °C for WOA98 and 6.4 °C for WOA01. On the contrary, in the new climatology, very few differences showed higher values (Figure 2.6a, right column). Similarly, higher differences are evident in the salinity fields of WOA98 and WOA01. The differences in excess of 0.5 psu are too many in WOA98 and WOA01 climatologies (Figure 2.6b, left and central columns). On the contrary, the differences, between the analysed value and mean were low for the new climatology (Figure 2.6b, right column).

2.3 Sea level data from satellite based altimeters

The altimeter data, used in this thesis, have been obtained from AVISO (Archiving, Validation, and Interpretation of Satellite Oceanography Data) operations centre. AVISO archives and distributes the satellite altimeter data processed by CLS Space Oceanography Division as part of the European Union Environment and Climate (EU ENACT) project (EVK2–CT2001–00117) with support from CNES (Centre National d'Études Spatiales). AVISO distributes sea surface heights (SSH) and sea level anomalies (SLA) measured by TOPEX/Poseidon (T/P), Jason and ERS–1/2 satellites separately and as a merged product by merging all of them. The T/P was launched in August 1992, and had a repeat cycle of 10 days. ERS–1 was launched in July 1991 with a repeat cycle of 35 days; later ERS–2 replaced ERS–1 in April 1995. As a replacement to T/P, Jason–1 was launched on 7 December 2001 with same repeat cycle of 10 days. Jason–1 was designed to follow the T/P orbit and provide same quality data, if not better. In August 2002, Jason replaced T/P. Although the T/P and Jason satellites have the same repeat cycle (10 days) their ground tracks were separated by a distance of 315 km at the equator; more than the average span of an ocean eddy. On the other hand, the ground tracks of ERS–1 and ERS–2 satellites were separated by a maximum distance of about 80 km. Therefore, merging the T/P–

Figure 2.4 (a) Horizontal distribution of temperature (°C) for the months of July and March form the new climatology (lower panels) compared with the temperature of the same months of WOA98 (upper panels) and WOA01 (middle panels).

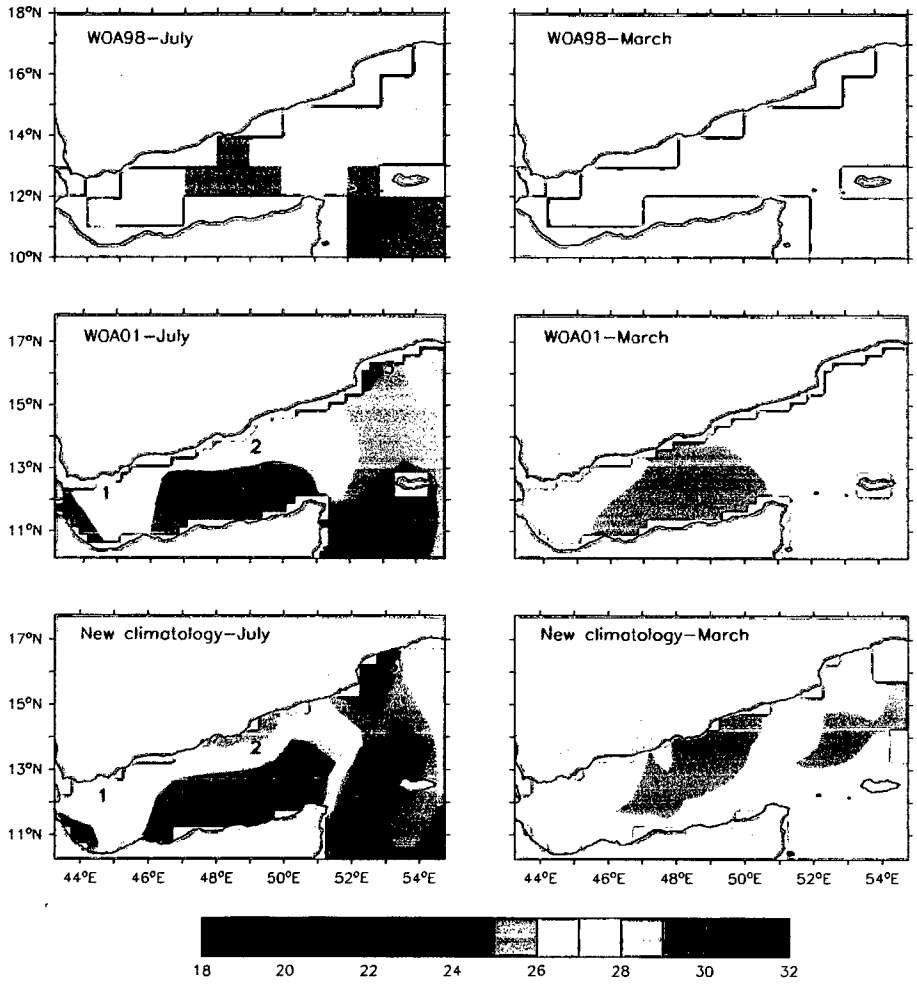

Figure 2.4 (b) Same as Figure 2.4(a) for salinity (psu).

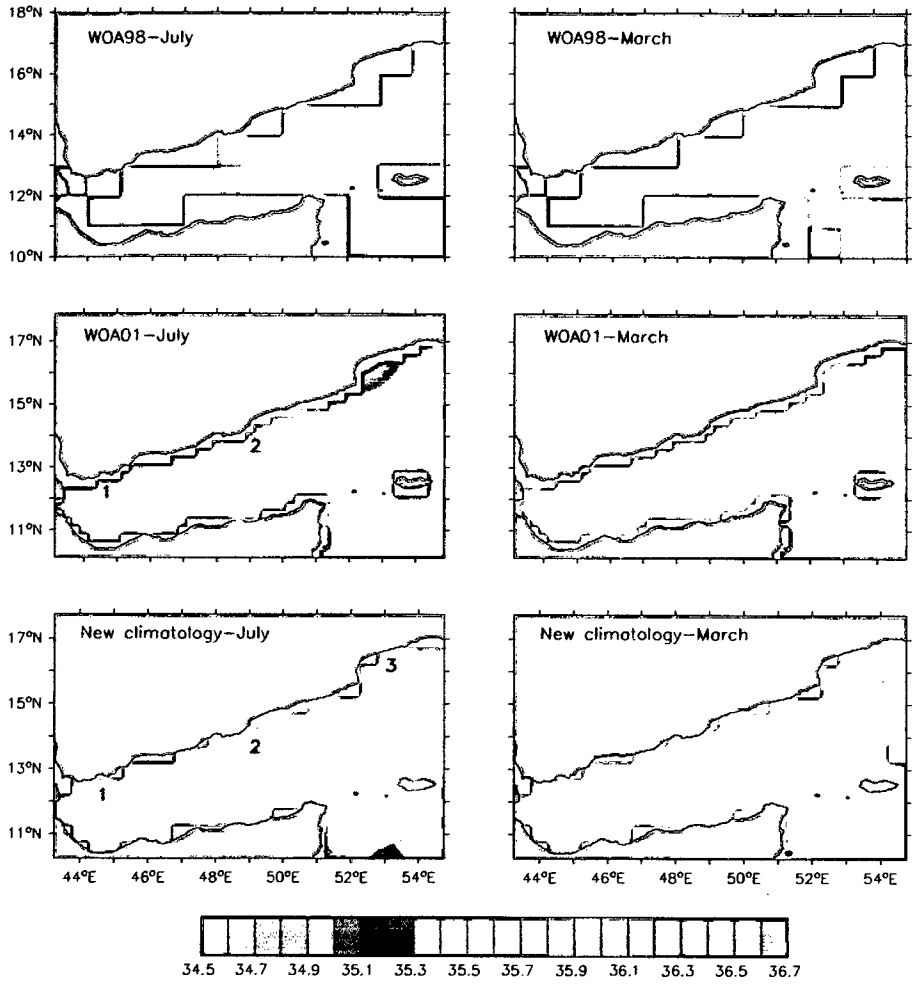

Figure 2.5 A comparison between the vertical distribution of salinity (psu) for the month of July of (a) WOA98, (b) WOA01 and (c) new climatology. The vertical distruibution is restricted up to 1500 m because of the maximum coverage of WOA98 and WOA01. The lower panel (d) shows the vertical distribution of salinity from the new climatology extending up to 2000 m. The extention up to 2000 m includes bottom water.

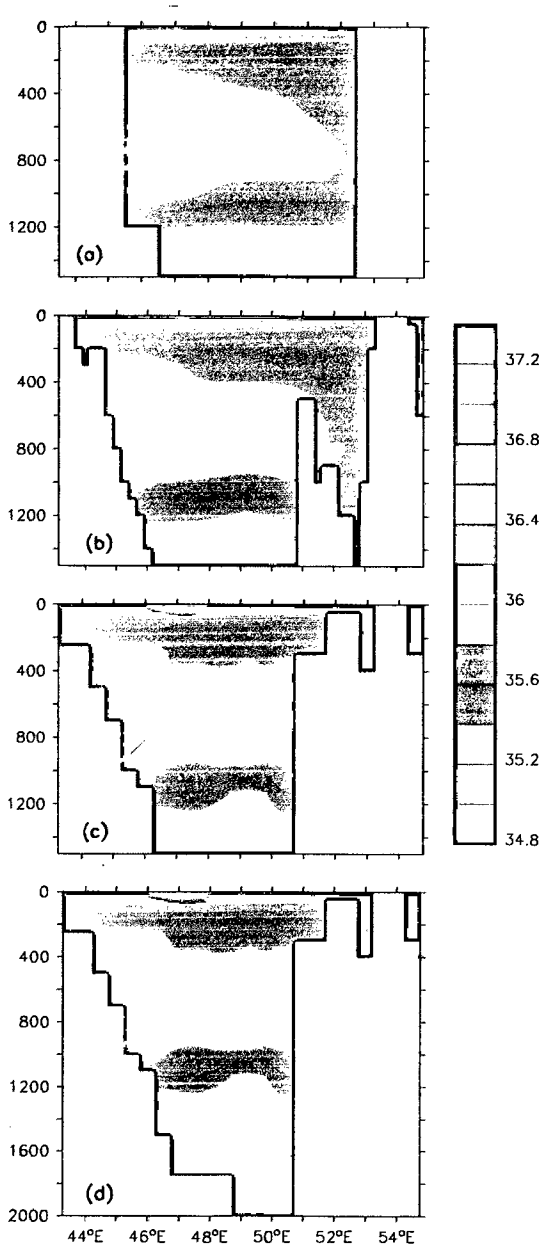

Figure 2.6 (a) The differences between the mean temperature from the observations in a grid and the analysed temperature in the same grid for each data set. The mean, maximum, and standard deviation of the differences are also shown.

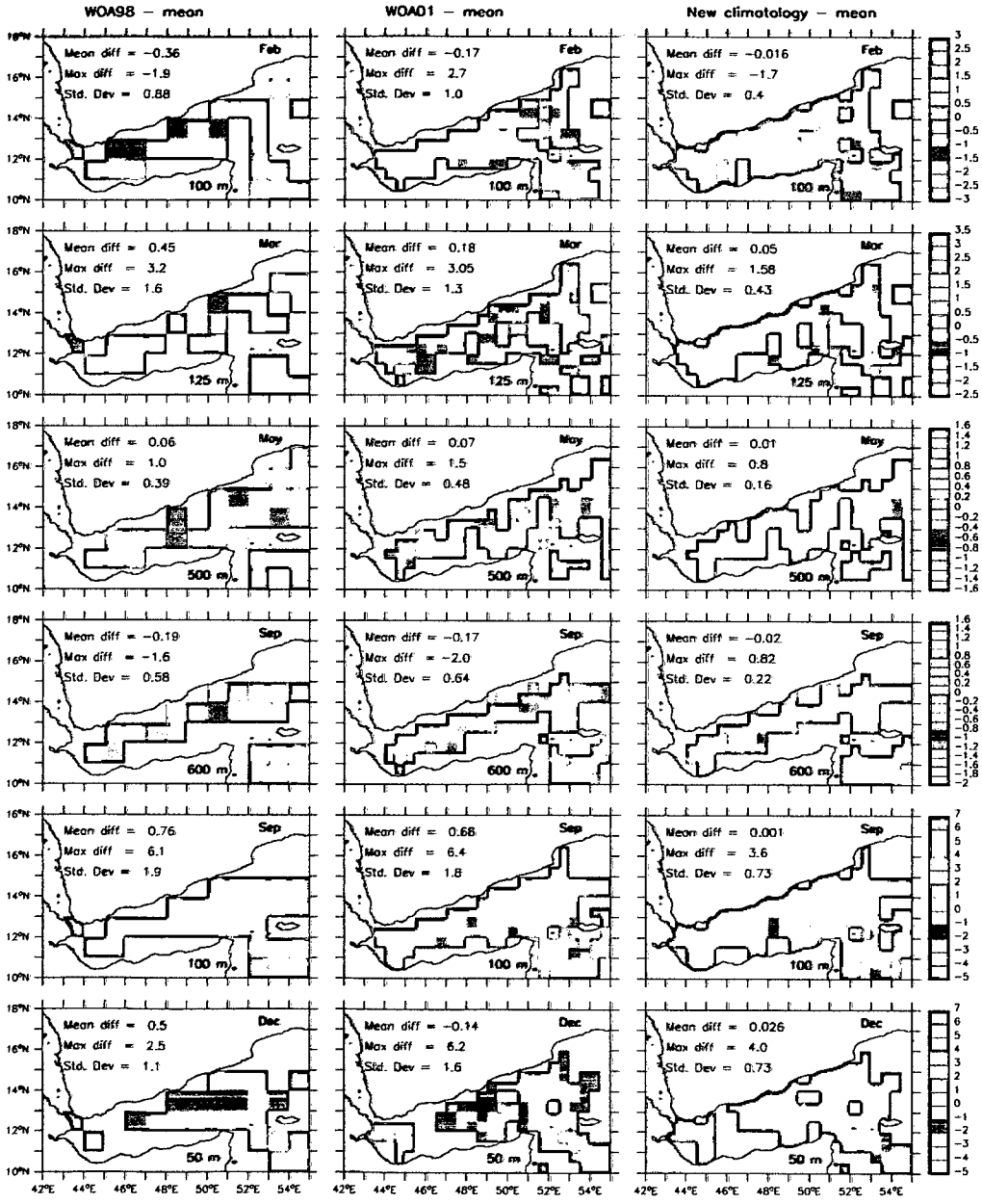

Figure 2.6 (b) Same as 2.6a but for salinity.

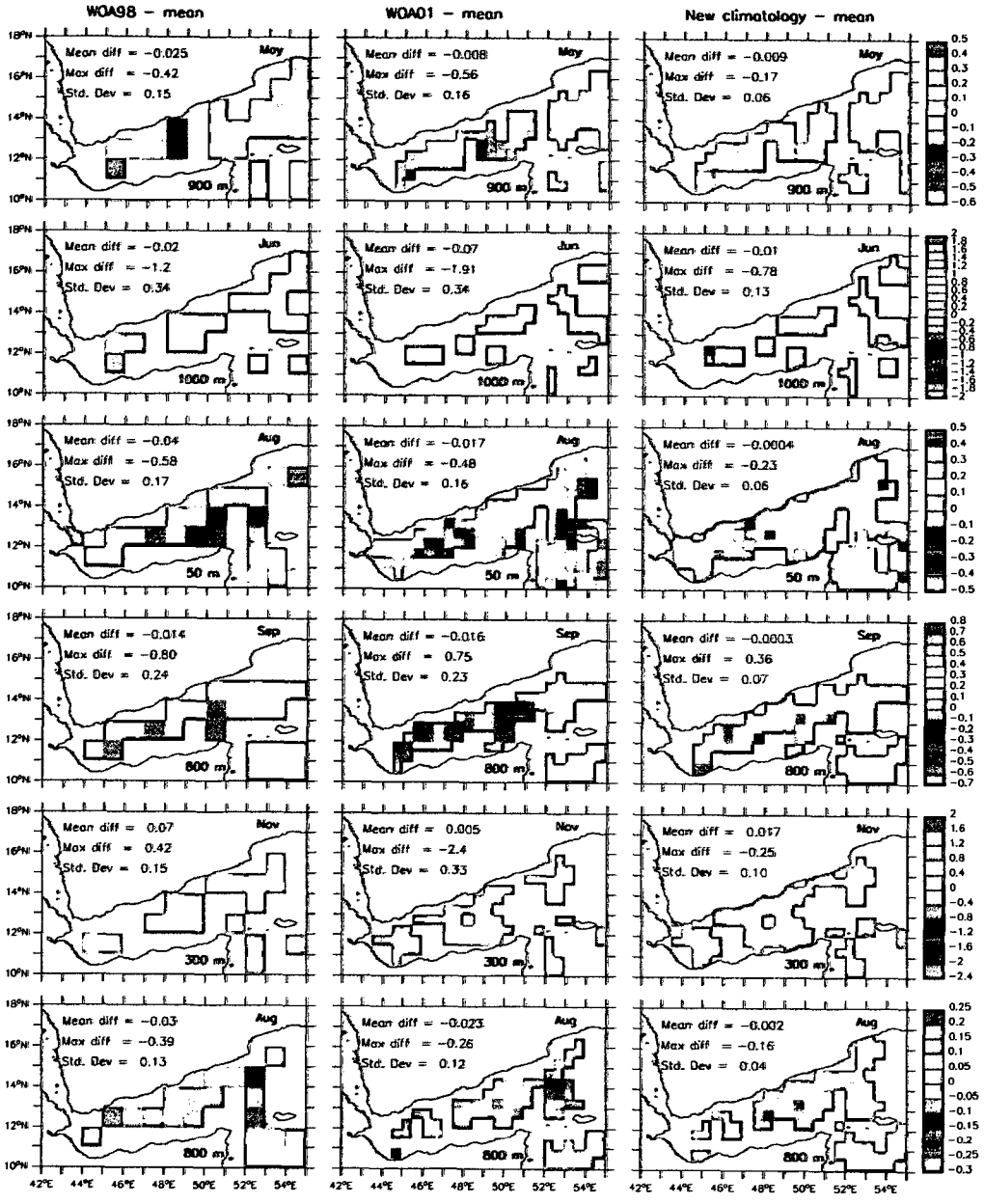

Jason and ERS–1/2 altimeter data helped in better resolving the mesoscale variability.

The merged T/P–Jason+ERS data provide more homogeneous and reduced mapping errors than the individual data set [Ducet et al., 2000]. The weekly (7 days) data set of sea level anomaly (SLA) obtained from AVISO spanning over a period of 11 years from 1 January 1993 to 31 December 2003 on a 1/3° Mercator projection spatial grid are used in this study. The anomalies of sea level heights (SLA) were obtained relative to a 7–year mean (January 1993 to December 1999). Specific processing was also performed to obtain ERS–1/2 mean consistent with a T/P mean [Anonymous, 2001a].

The data were corrected for instrumental errors, environmental perturbations (wet tropospheric, dry tropospheric and ionospheric effects), ocean wave influence (sea state bias), tidal influence (most recent GOT99 tidal correction [Ray, 1999]), and inverse barometer effect corrected with a variable mean pressure [Dorandeu and Le Traon, 1999]. Tidal and inverse barometer corrections for ERS–1/2 were made to be homogeneous with T/P; the ERS–1/2 orbit was globally adjusted to the more precise T/P orbit [Le Traon and Ogor, 1998].

2.4 Sea surface winds from QuikSCAT scatterometer

QuikSCAT was launched from California, USA on 19 June 1999 with the SeaWinds instrument, a specialized microwave radar, to measure the near–surface wind speed and direction under all weather conditions over the oceans globally. The SeaWinds instrument on QuikSCAT is an active microwave radar designed to measure electromagnetic backscatter from wind roughened ocean surface. QuikSCAT/SeaWinds is a conically scanning pencil–beam scatterometer. See Dunbar et al. [2001] for further details on QuikSCAT scatterometry.

The processed QuikSCAT data is freely distributed by Physical Oceanography Distributed Active Archive Center (PO.DAAC) at NASA Jet Propulsion Laboratory (JPL)

and is available at http://podaac.jpl.nasa.gov/quikscat/. For this study, we have obtained the Level 3 data set that consisted of gridded values of scalar wind speed, meridional and zonal components of wind velocity, wind speed squared and time in a fraction of a day [Anonymous, 2001b]. The data used in this research, the Level 3 daily winds, have a spatial resolution of 0.25° × 0.25° for the period from July 1999 till December 2006. The daily data were used to create a monthly climatology of meridional and zonal components of wind velocity. The climatology was then compared with COADS (Comprehensive Ocean–Atmosphere Data Set) climatology available on a spatial grid of 2° × 2° [Woodruff et al., 1993]. COADS was prepared by gathering all possible in situ measurements of winds spanning over a period of 30 years during 1950 to 1979 (Figure 2.7). In general, the magnitude and directions of the wind vectors during each month compare well.

2.5 Ship drift Data

Before the days of satellite–tracked floats and buoys and satellite–based altimeters and scatterometers, scientists relied on ship drift data to map the surface currents in the oceans. In the mid 1800s, Matthew Fontaine Maury of the U.S. Naval Oceanographic Office initiated an effort to assemble navigation charts that included information on currents. He estimated the current speeds based on the ship logs maintained by Naval and merchant ships. In this method, the difference between a ship's dead–reckoned position (determined from its previous position determined from a navigational fix) is ascribed solely to the effect of surface currents. The U.S. Naval Oceanographic Office continued to record these ship drifts until the mid 1970s. Maximum data on ship drift is available for the period between 1920 and 1940. Most of our knowledge about large–scale ocean circulation patterns and the velocity, kinematics, and seasonal variability of surface currents and eddies are from the ship drift data. One of the earlier compilations of Indian Ocean surface

Figure 2.7 Monthly climatology of surface wind derived from QuikSCAT data (left panels) compared with the 2° × 2° grid COADS climatology (right panels).

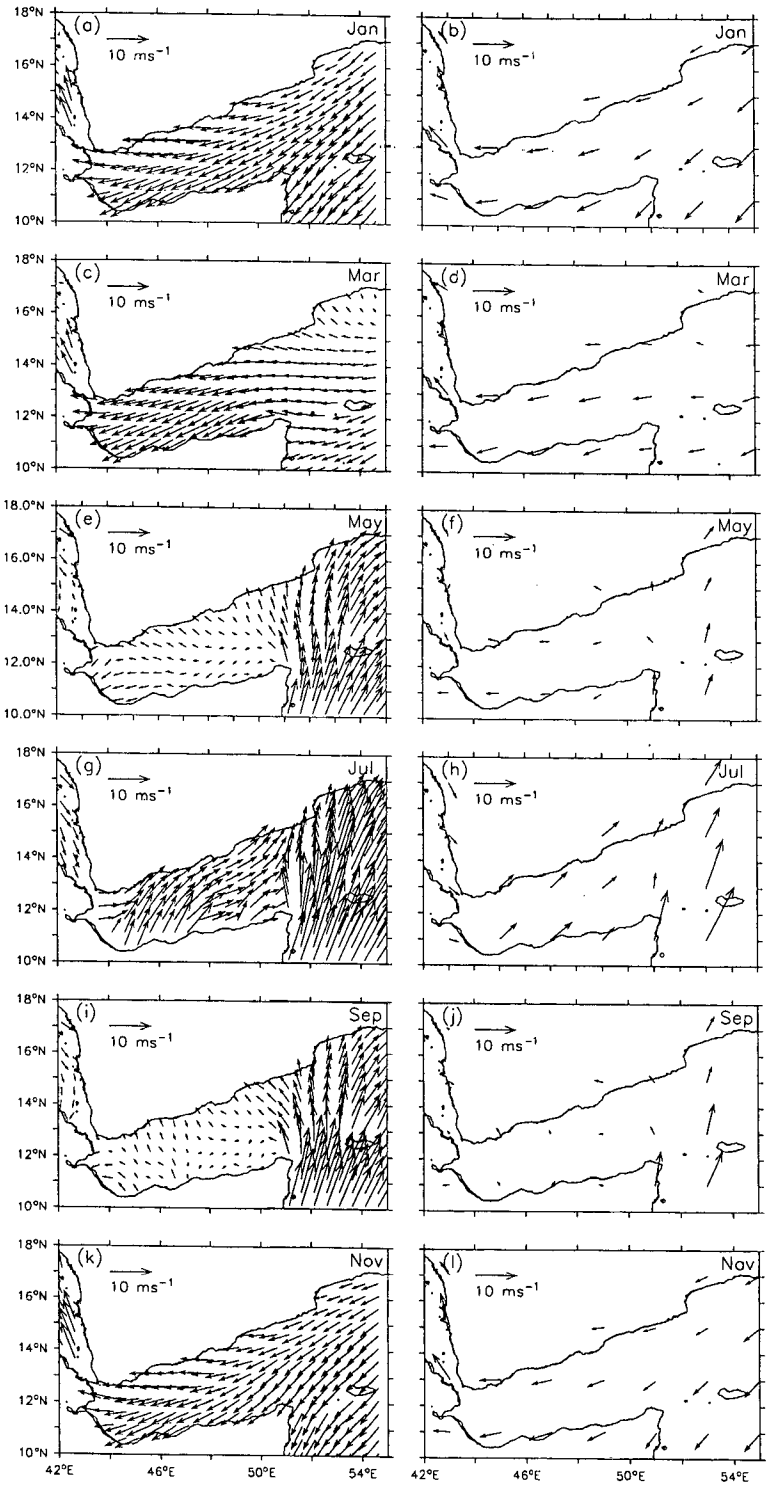

currents is contained in the Koninklijk Netherlands Meteorologisch Institut (KNMI) atlas [Anonymous, 1952], which contains a series of monthly charts at a spatial resolution of $2° \times 2°$ grids. Cutler and Swallow [1984] also produced the surface currents using the ship drift observations from 1854 to 1974 for the Indian Ocean region from 50° E (eastern side of the Gulf of Aden) to 100° E, for every ten days.

In this study, to describe the surface circulation in the Gulf of Aden, we have used the monthly climatology of ship drifts available from National Oceanographic Data Center (NODC), NOAA, on a spatial resolution of 1° longitude $\times$ 1° latitude.

Chapter 3

Hydrography and water masses in the Gulf of Aden

3.1 Introduction

As mentioned in Chapterl, the Gulf of Aden is the only passage for Red Sea Water (RSW), one of the most saline water masses in the world oceans, into the Indian Ocean. We have also seen in Chapter 2 that very little information is available on the hydrography of the Gulf of Aden. The extensive exchange of water between the Red Sea, the Gulf of Aden and the Arabian Sea, the strong evaporation and the monsoonal winds that blow over the region, all assist in the formation of a complex vertical structure in the water column of the Gulf of Aden [Khimitsa, 1968; Stirn et al., 1985].

Seasonal changes of the surface layer water characteristics described by Piechura and Sobaih [1986]; Nasser [1992]; Maiyza and Mohamed [1993] give an account of the variability in the surface temperature of the Gulf of Aden. Most of the variability in the sea surface temperature (SST) is seasonal. SST is highest (31–32 °C) during end of May and beginning of June. In July–August it cools down to 29–30 °C, the degree of cooling depends on the strength of summer monsoon. During the summer monsoon, the SST along

the Arabian coast, the region adjacent to the Gulf of Aden, reaches a minimum of 17 °C. The heating of the surface takes place in September soon after the weakening of the summer monsoon winds over the gulf and the SST bounces back to 30 °C within a month. It cools again in October-January (24–25 °C) in response to the winter monsoonal winds and warms again during February–May in response to the spring warming that dominates the region during this period.

Similar to the variability in SST the surface mixed layer also shows strong seasonality. In summer, the mixed layer depth (MLD) decreases to less than 20 m and increases to over 100 m in winter. Accordingly, the depth of thermocline also shoals and deepens in summer and winter respectively; about 20–120 m in summer and 150–250 m in winter [Piechura and Sobaih, 1986]. Seasonal changes in the subsurface water, though much lower than in the surface water, are still distinguishable. The lowest temperature and highest salinity of the subsurface layer were observed during the summer months and the highest temperature and lowest salinity were observed during winter months [Piechura and Sobaih, 1986].

A few studies have used the available hydrographic data to describe the water masses in the Gulf of Aden. Rochford [1964] identified two water masses in the eastern Gulf of Aden, namely, high salinity Arabian Sea Water (ASW at σ_t levels 23.5–24.0) and RSW (at σ_t levels 27.0–27.4). Khimitsa [1968] identified four layers of water in the gulf based on their physical and chemical properties. A top layer (50–100 m) of high salinity (($\sim$ 36.0–36.5 psu) and high oxygen content, an intermediate layer, between 100–500 m, of lower salinity ($\sim$ 35.3 psu) and low oxygen content, another intermediate layer, between 500–1000 m, of high salinity RSW ($\sim$ 36.5–38.0 psu), and a layer near the bottom containing the bottom water of low salinity ($\sim$ 34.9–35.5 psu) and temperature. He suggested that the water in the upper intermediate level enters the gulf from the south as a strong jet between Cape Gvardafui and Socotra at depths $\sim$ 150 to 200 m. He attributed its origin to the Southern Ocean bottom water. Piechura and Sobaih [1986] described three water

masses in the upper 1000 m of the gulf. They named them Surface Water, Subsurface Water, and RSW. They suggested that the local heating and evaporation are the causative factors for the formation of surface water, which is deeper in winter (200–300 m) and shallower in summer (70–80 m). For the subsurface water, the highest temperature and lowest salinity were found in winter. They suggested the subtropical front as the origin of Subsurface Water. Nasser [1992] also identified three water masses in the upper 1000 m of the northern Gulf of Aden, namely: Surface High Salinity Water, Subsurface Low Salinity Water and RSW. He concluded that the Subsurface Low Salinity Water is transported in the Gulf of Aden from the Somali basin during the summer monsoon. More recently, Mohamed et al. [1996] and Mohammed [1997] identified four salinity maxima in the gulf. They identified the first maximum between the σ_t levels 24.0 and 25.0, the second between 25.0 and 26.0, the third between 26.0 and 27.0 and the fourth between 27.0 and 28.0. They identified the third maximum as a mixture of waters originating from the Persian Gulf, the Timor Sea and Subtropical Subsurface and the fourth maximum as a mixture of Red Sea Water, Antarctic Intermediate Water and Timor Sea Water. Most of the other studies of the GA [Maillard and Soliman, 1986; Fedorov and Meshchanov, 1988; Bower et al., 2000, 2002] dealt only with the outflow and spreading of RSW. Ozgokman et al. [2003]; Peters and Johns [2005]; Peters et al. [2005] described the structure and dynamics of the Red Sea outflow plume in the western Gulf of Aden.

All these studies were either localized in space or time or focused on the Red Sea outflow. None of them provided a comprehensive picture of the hydrographic structure and the water masses in the Gulf of Aden as they evolved during the year nor provided a quantitative estimate. Furthermore, the temperature–salinity–σ_θ range of the water masses defined by various authors often varied drastically depending on the limited data they had used in their studies. As discussed in Chapter 2, the Gulf of Aden is a data sparse region and hence a new climatology of hydrographic parameters was compiled. In this chapter[1]

[1] A major part of this chapter is based on the paper by **Al Saafani, M. A.** and S. S. C. Shenoi. Water masses in the Gulf of Aden. *J. Oceanogr.*, 63, 1, 1-14, 2007.

we have used this newly compiled temperature–salinity climatology to define the θ–S–σ_θ (potential temperature-salinity-potential density) ranges of water masses rather than the limited data used in the previous studies. Based on well demarcated boundaries of the water masses, we have also calculated the volumes occupied by the water masses and their changes during a year. Before we describe the water masses in the Gulf of Aden, first we describe the hydrographic structure of the Gulf of Aden in the following section.

3.2 Hydrographic structure

In this section we will describe the horizontal and vertical distribution of temperature, salinity and density in the Gulf of Aden on a month to month basis. Besides the distribution of properties at the horizontal surfaces, two vertical sections were also used for this description; one along the east–west axis of the gulf and the other across the gulf along 48° E meridian.

During January, the distribution of temperature at the surface is uniform with $\sim$ 0.5–1.0 °C difference between west and east; it is 25.5–26.0 °C in the west and about 25.0 °C in the east (Figure 3.1a). Along the southern coast, from 47 to 51° E, the temperature is cooler than that along the northern coast ($\sim$ 1 °C) indicating upwelling along the southern coast. Similarly, the distribution of salinity at the surface shows almost uniform salinity of 36.0 psu over the entire gulf (Figure 3.1a). The horizontal distribution of density at the surface follows the distribution of temperature with lower density in the west and higher density in the eastern part of the gulf (Figure 3.1a).

Section 1 shows a mixed layer extending to about 80–100 m with temperature 25 to 26 °C decreasing from west to east, salinity 36.0 psu and σ_t 24.5 (Figure 3.1a). The thermocline extends to about 200 m where temperature decreases from 25 °C to about 16 °C, whereas the halocline extends to about 120 m only. A layer of fresher water was occupying the depths from 100–400 m with salinity of $\sim$ 35.6 psu (Figure 3.1a). In the

west, this layer was limited to 300 m due to the presence of high salinity RSW. The RSW occupies a 700 m (400–1100 m) thick water column in the Gulf of Aden. In this layer, the salinity increases with depth from about 35.8 psu at 400 m to $\sim$ 36.8 psu at 800 m in the western part of the gulf. The salinity of this layer decreases towards the east. Deeper than 1000 m, the temperature and salinity decreases gradually with depth.

Along Section 2, at 48° E, the mixed layer extends to about 80 m, with the southern side cooler than the northern side (Figure 3.1a). The thermocline extends to about 200 m where the temperature decreases from 25 to 16 °C and salinity decreases from 36.0 at the surface to 35.8 psu. The low salinity layer (< 35.6 psu) is seen along the southern side between 100 and 300 m. The RSW extends to about 1000 m, with its core at about 700 m where the salinity exceeds 36.2 psu. Deeper than that the temperature and salinity decrease with depth.

During February, the distribution of temperature at the surface is similar to that of January; the northern coast of the gulf warmer than the southern coast by about 1 °C. The SST along the southern coast is 24.5–25.0 °C and that along the northern coast is 25.5–26.0 °C (Figure 3.1b). The cooler patch of temperature seen to the east of the gulf during January has cooled further during this month. The surface distribution of salinity is almost uniform (36.0 psu) over the entire gulf (Figure 3.1b). To the east of the gulf, the salinity along the eastern coast of Somali is less than that inside the gulf.

The vertical distribution of temperature and salinity along Section 1 shows that the mixed layer extends to about 80–100 m with temperature between 25 and 26 °C, salinity 36.0 psu and σ_t 24.5 (Figure 3.1b). Along the eastern part of the section, the isotherms and isohalines lift upward indicating the presence of cyclonic eddy. Similar to that during January the thermocline extends to about 200 m where temperature decreases to about 16 °C. Whereas, the halocline extends to about 160 m only in the west and about 200 m in the east. The intermediate low saline layer is seen between 160 m and 400 m, where it extends in the east to about 600 m with salinity of $\sim$ 35.4 psu (Figure 3.1b). Also similar

Figure 3.1 (b) Same as 3.1a, but for February.

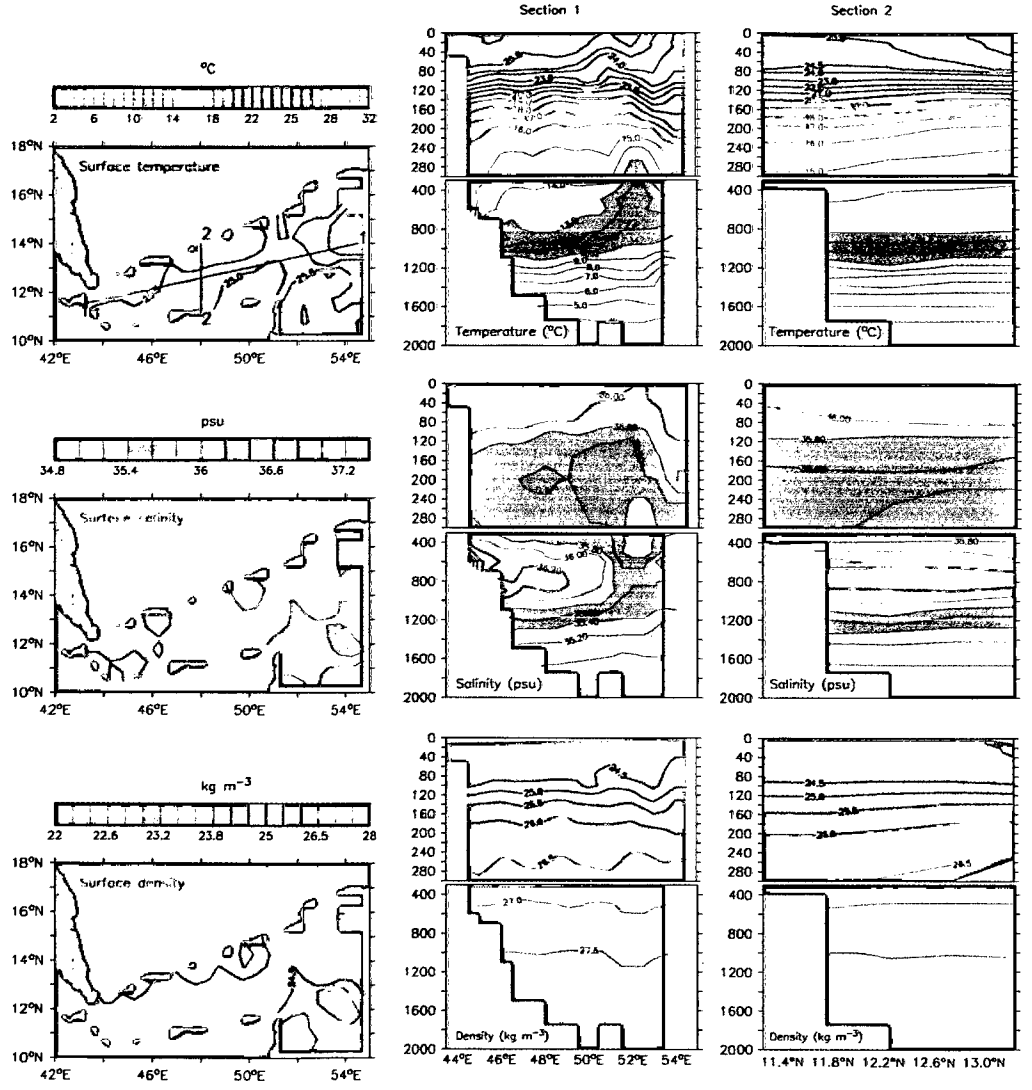

Figure 3.1 (c) Same as 3.1a, but for March.

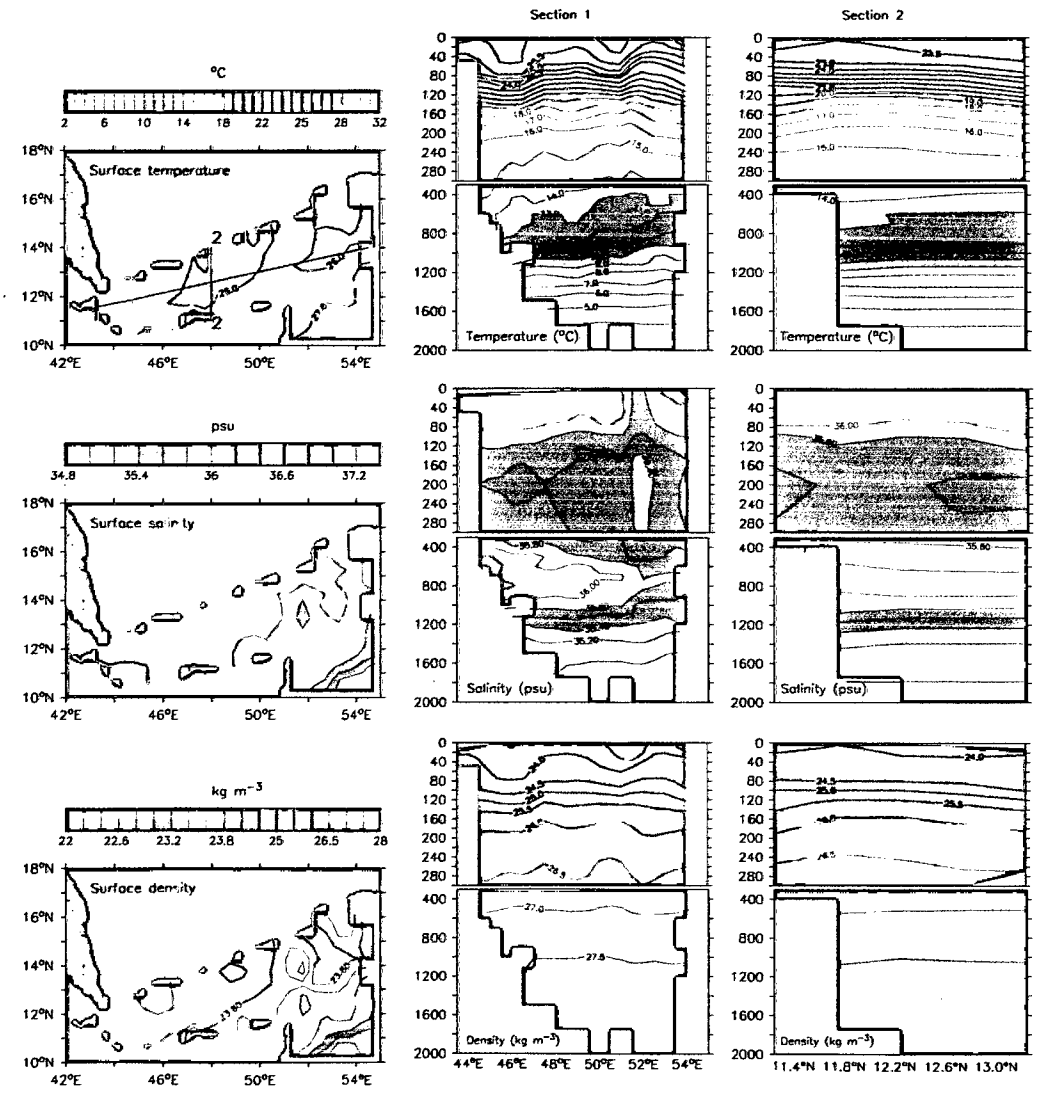

to that during January, the RSW occupies about 700 m (400–1100 m) of the water column in the Gulf of Aden. The salinity of this layer decreases towards the east. Deeper than 1000 m, the temperature and salinity decreases with depth gradually.

Section 2 shows a mixed layer shallower along the southern side, with cooler and fresher water, than that in the north indicating the effect of the upwelling along the southern coast (Figure 3.1b). Below the mixed layer, the thermocline extends to about 200 m with the temperature decreasing from 25 to 16 °C and salinity decreasing from 36.0 at the surface to 35.6 psu with a fresher patch in the southern side (< 35.6 psu occupying depths from 140 to 300 m). This layer of fresher water extends to about 400 m. The RSW is seen deeper, extending to about 1000 m, with its core between 600 and 800 m. Deeper than that the temperature and salinity decrease with depth in the bottom layer.

During March, the surface layer temperature increases to 26 °C all over the gulf with a uniform salinity of 36 psu. Salinity decreases in the eastern side especially along the eastern Somali coast (Figure 3.1c); the density also decreases following the decrease in salinity. The low salinity patch extends northward towards the mouth of the gulf.

The vertical distribution of temperature and salinity along Section 1 shows a shallower mixed layer than that in January–February, the average depth is $\sim$ 60 m. The mixed layer depth in the eastern side of the section is shallower than that in the west (Figure 3.1c). The low saline layer extends from $\sim$ 200 m till $\sim$ 500 m in the east and $\sim$ 400 m in the west; the salinity of this layer is $\sim$ 35.4 psu. Deeper than that, the RSW is seen between 400 and 1100 m (Figure 3.1c).

The shallower mixed layer is also seen in Section 2, where it extends only to about 60 m, with temperature $\sim$ 25–26 °C, and salinity $\sim$ 36.0 psu. The low saline layer extends below the thermocline from about 180 m to 300 m with salinity < 35.6 psu along the northern and southern sides.

During April–May, the mixed layer continues to shallow and warm up, where it is about 40 m with temperature $\sim$ 27–28 °C, and salinity $\sim$ 36–36.4 psu during April (Fig-

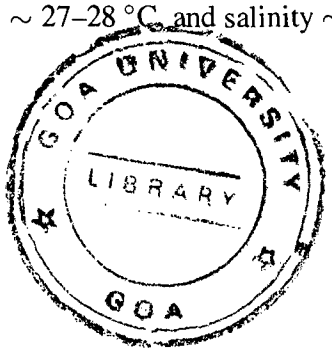

ure 3.1d). It shallows further to 30 m with an increase in temperature to 29-30 °C during May (Figure 3.1e). During both months, the salinity in the north and in the west is more than that in the east (Figure 3.1d and e).

The shallowing of the mixed layer is seen more clearly from section 1 (Figure 3.1d and e) with temperature decreasing by about 1–2 °C within the upper 40 m. The vertical structure of salinity also shows the east–west variation of the mixed layer. The isotherms, isohalines and isopycnals deepens in the eastern part of the section during May indicating the presence of an anticyclonic eddy (see Chapter 4 for the details of circulation during this month). Below the mixed layer, the low salinity layer extends from 200 m to about 500 m in the eastern part of the section, while in the west, due to the presence of the RSW, it extends from 150 m to 300 m only. Similarly the RSW (salinity 36.6 psu) is seen extending from 300 m to 1200 m in the western part of the section. In the eastern part, it is seen between 400 m and 1000 m.

Section 2 also shows a vertical structure similar to Section 1, with the low saline layer occupying a deeper water column along the southern side of the section during April (Figure 3.1d).

During June, the surface layer temperature and salinity show more variations due to the onset of the summer monsoon, with maximum temperature (31 °C) and salinity (36.6 psu) in the western and southern parts of the gulf (Figure 3.1f). Along the northern coast, weak upwelling is seen as indicated by the decrease in temperature (27 °C) and salinity (~ 36.0 psu). The temperature and salinity also decrease towards the east along the Somali coast (23 °C and 35.6 psu). This horizontal variation of the temperature and salinity causes the horizontal variation in density.

The vertical structure along Section1 also shows a four layer structure similar to that in May, with the surface layer shallowing further to about 20 m. The intermediate, low saline layer is seen between 150 m and 400 m in the east and between 120 m and 220 m in the west (with salinity of 35.6 psu) (Figure 3.1f). Below that, the RSW extends to ~ 1100

Figure 3.1 (d) Same as 3.1a, but for April.

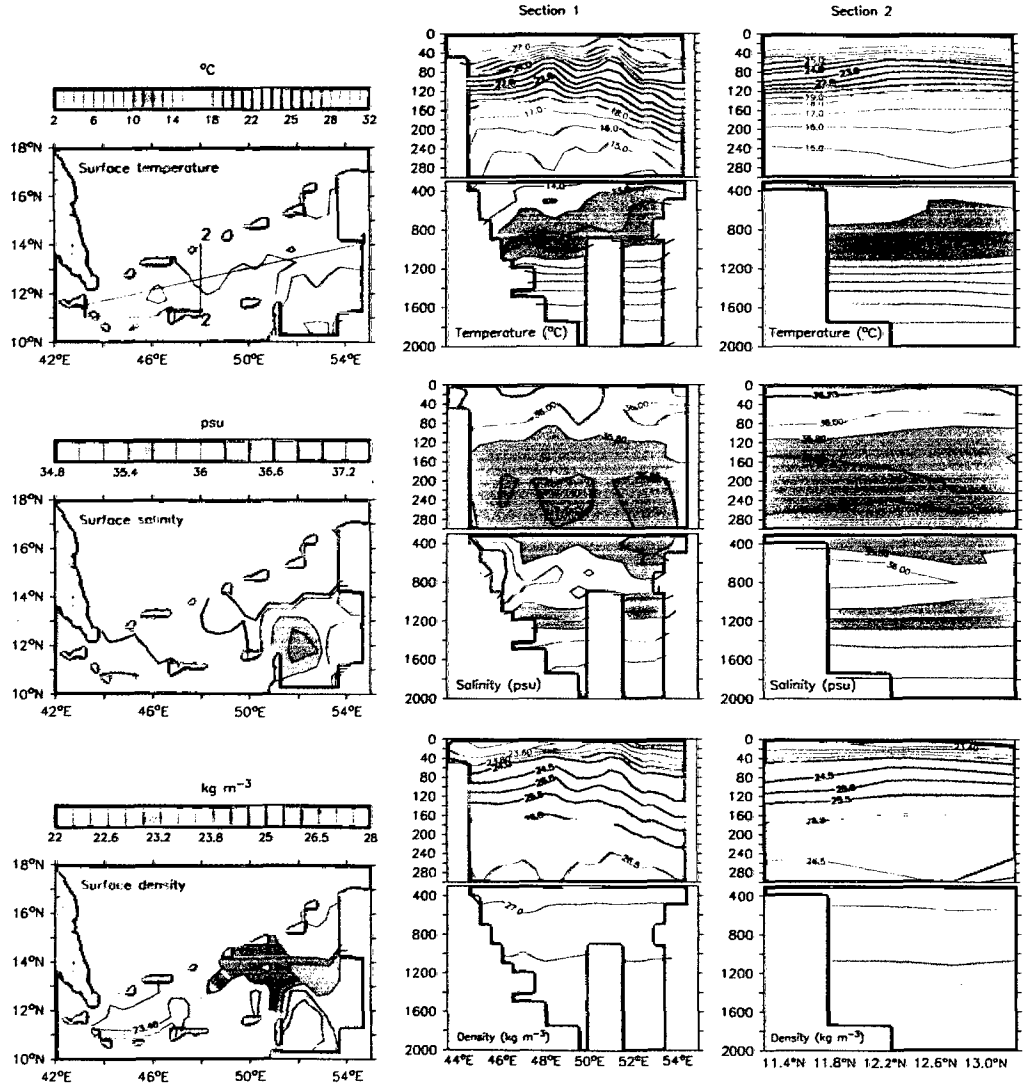

Figure 3.1 (e) Same as 3.1a, but for May.

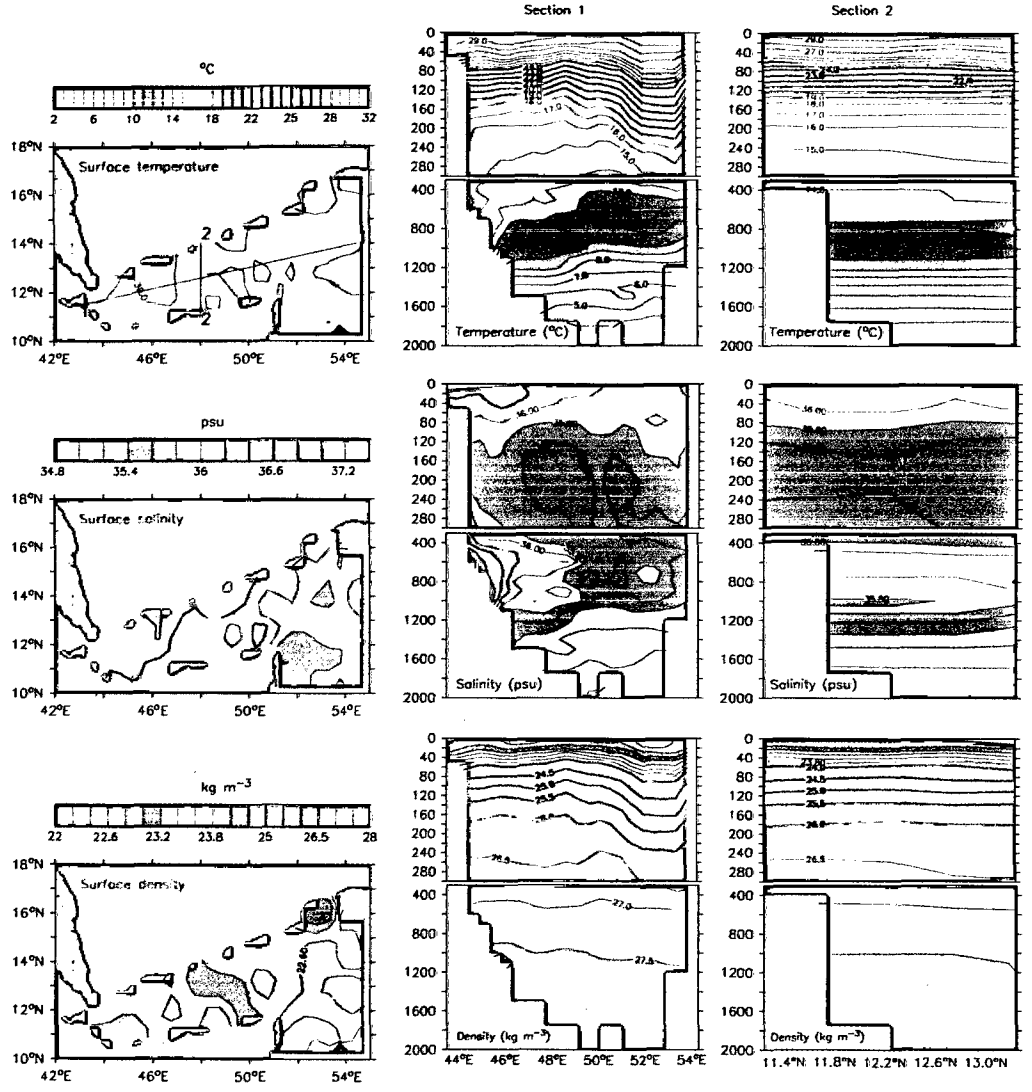

Figure 3.1 (f) Same as 3.1a, but for June.

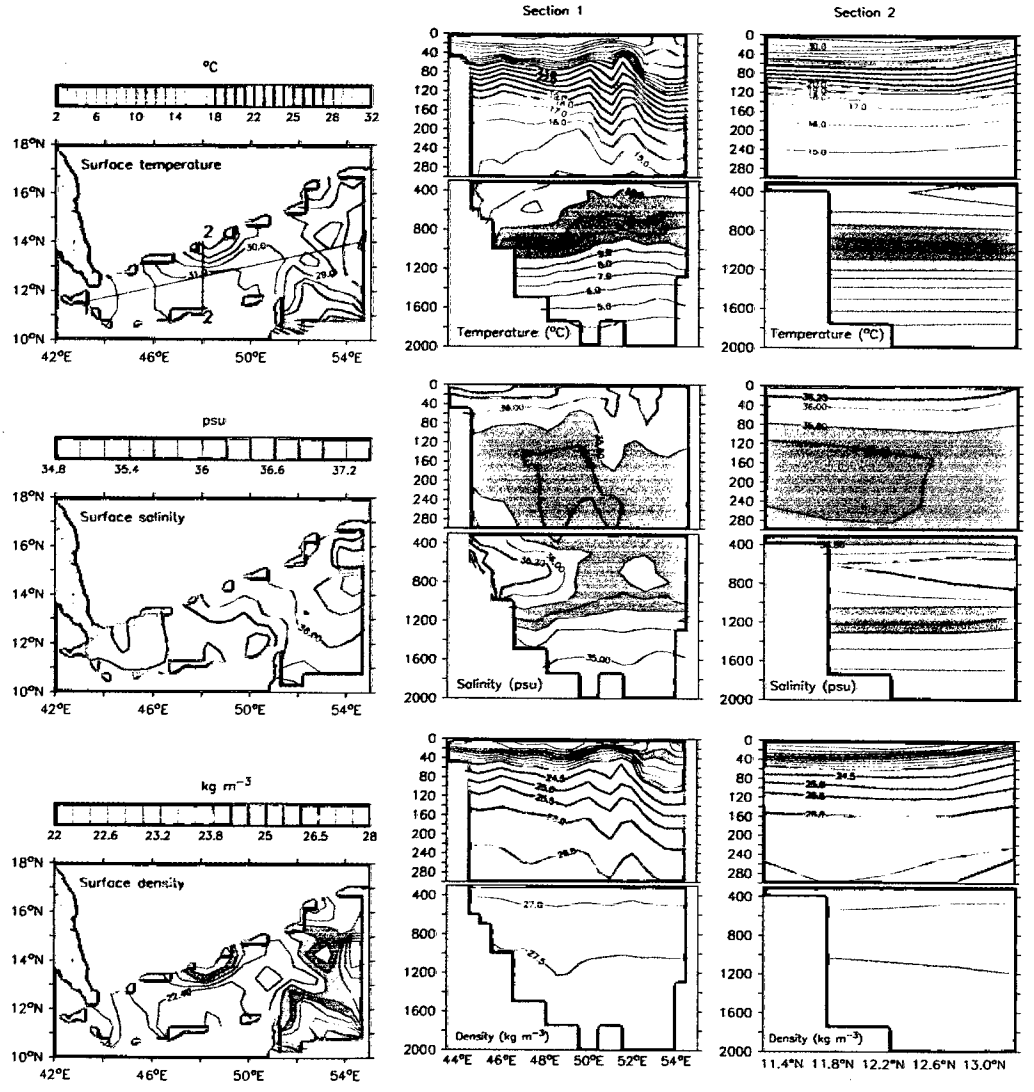

m. Deeper than that, the temperature and salinity decreases gradually in the bottom layer. Section 2 shows the uplifting of isotherms, isohalines and isopycnals along the northern side indicating upwelling (Figure 3.1f).

During July–August, the summer monsoon strengthens the upwelling along the northern coast of the gulf and along the Somali region (Figure 3.1g and h). The upwelling along the northern coast of the gulf extends towards the west, where it is seen in three smaller patches as reported by Piechura and Sobaih [1986]. The horizontal gradient of the temperature at the surface is about 8 °C between north and south (Figure 3.1g and h). In the western part of the gulf, the high salinity Red Sea Surface Water is seen along the southern side with salinity > 36.6 psu.

The vertical structure of temperature and salinity is similar to that in June. The surface mixed layer extends to about 20 m, with the uplifted thermocline extending to 160 m. The temperature in the thermocline decreases from 29 °C at the surface to about 16 °C at 160 m (Figure 3.1g, section 1). The thermocline further shallows during August, where its lower extent is seen at 140 m (Figure 3.1h). The low saline layer is also shallower than that during June; it extends between 120 m and 400 m. Below that layer, the RSW is seen between 400 and 1000 m. Section 2 also shows the upwelling along the northern side of gulf.

During September, the strength of the summer monsoon is reduced inside the gulf, but the region of low SST along the northern side still exists (Figure 3.1i). The surface temperature over the gulf is about 30 °C all over the gulf except in the upwelling regions along the northern coast. The high salinity region seen in the southern part of the western gulf during August is still seen during this month indicating the continuation of the surface Red Sea outflow (Figure 3.1i). The density inside the gulf is less than that to the east of it due to the high temperature inside the gulf. The vertical structure is similar to that in August except for the shallower low saline layer extending from $\sim$ 80 m to 300 m (Figure 3.1i, Section 1 and 2).

Figure 3.1 (g) Same as 3.1a, but for July.

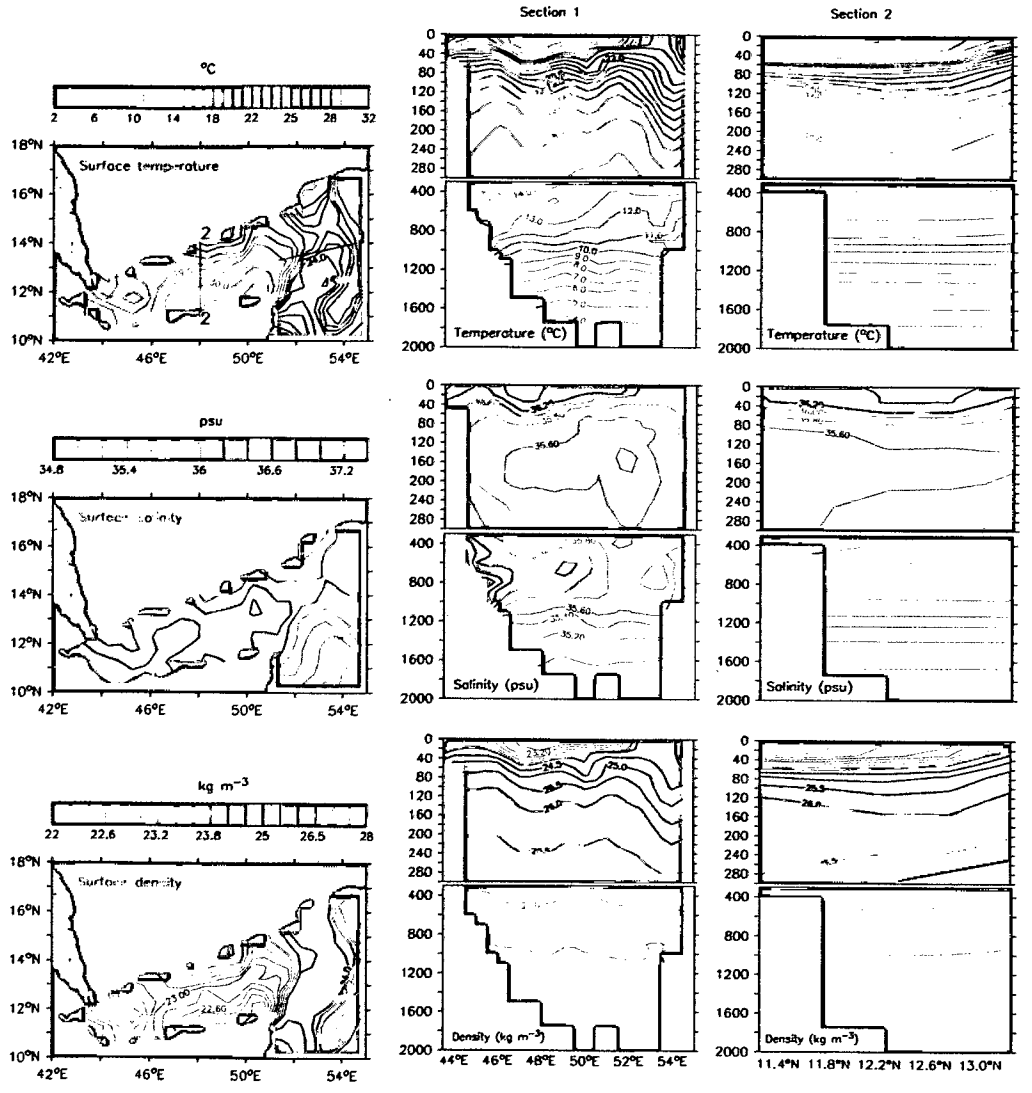

Figure 3.1 (h) Same as 3.1a, but for August.

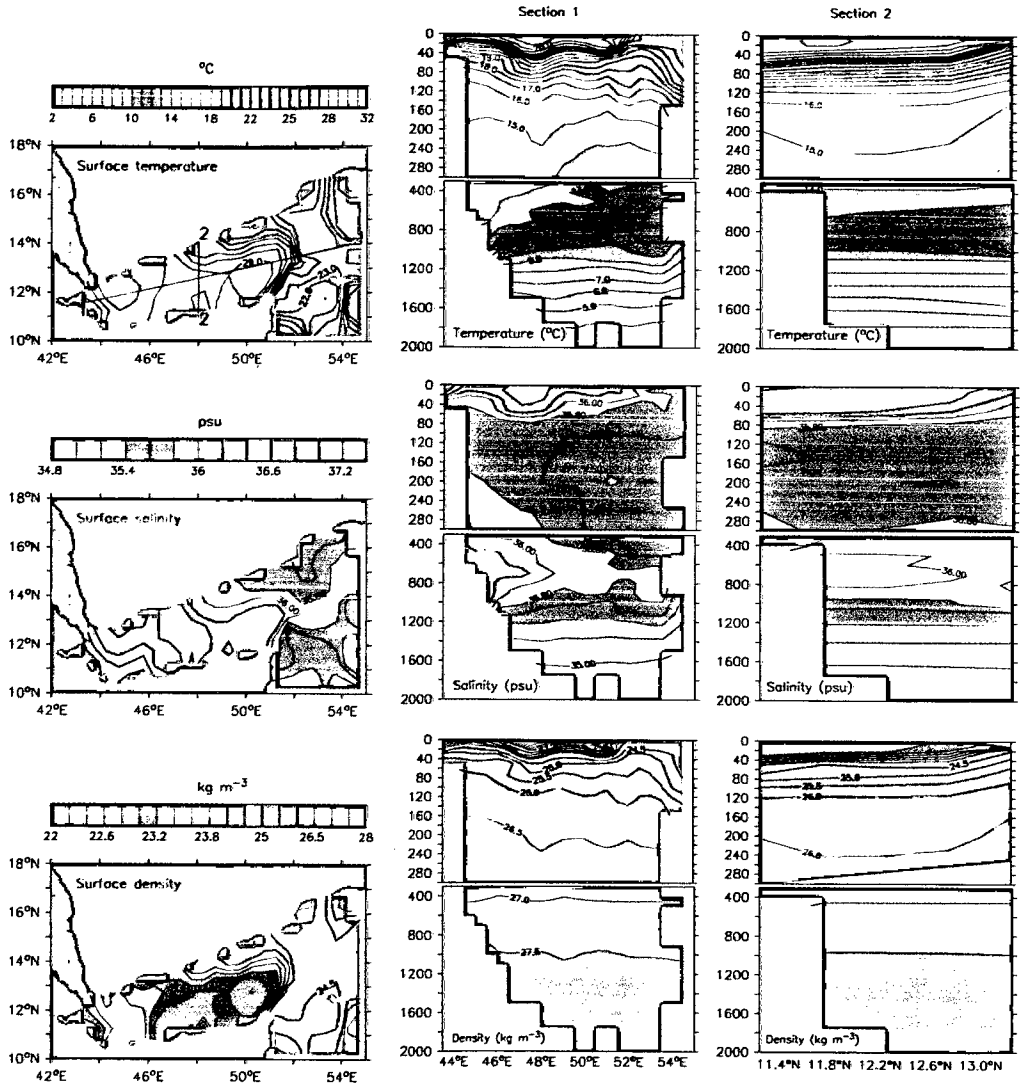

Figure 3.1 (i) Same as 3.1a, but for September.

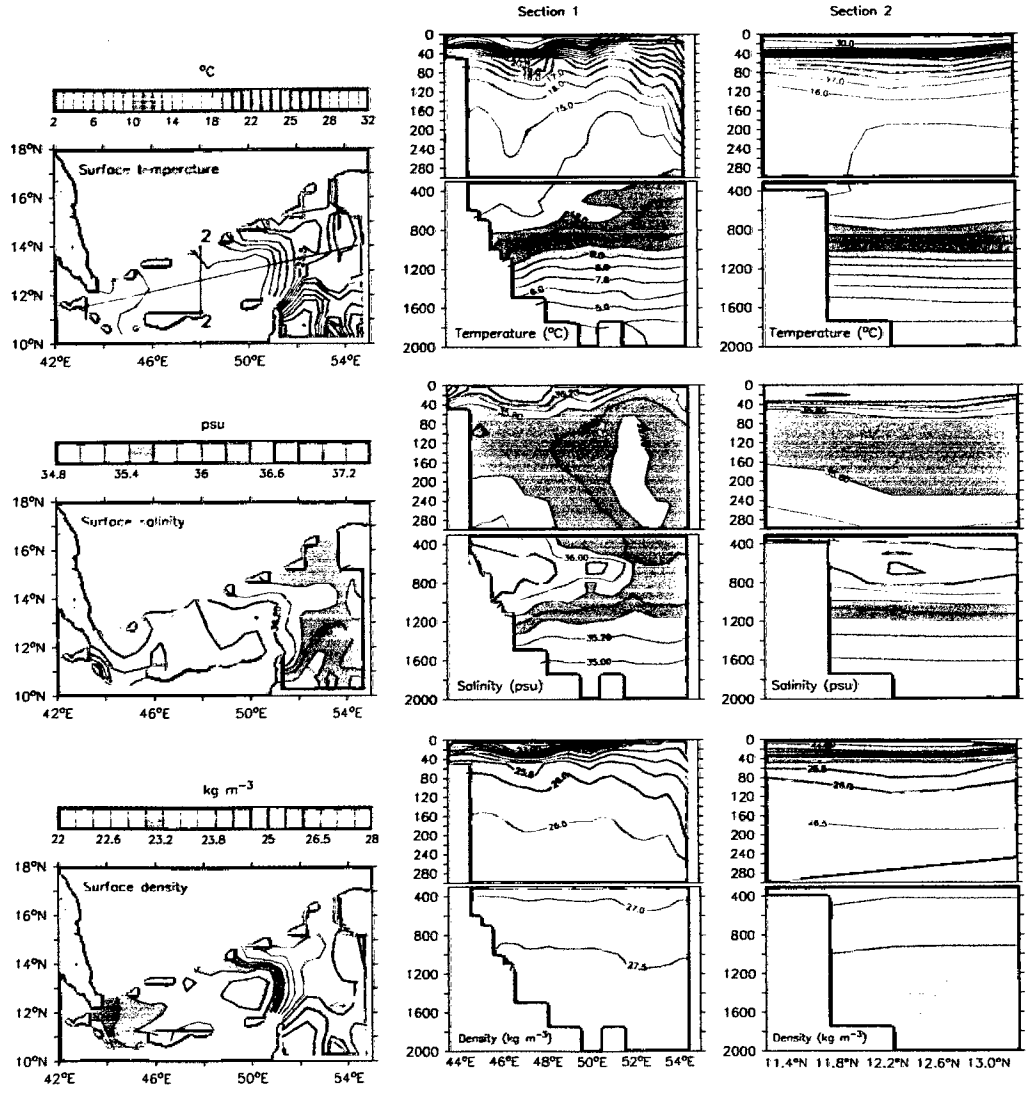

Figure 3.1 (j) Same as 3.1a, but for October.

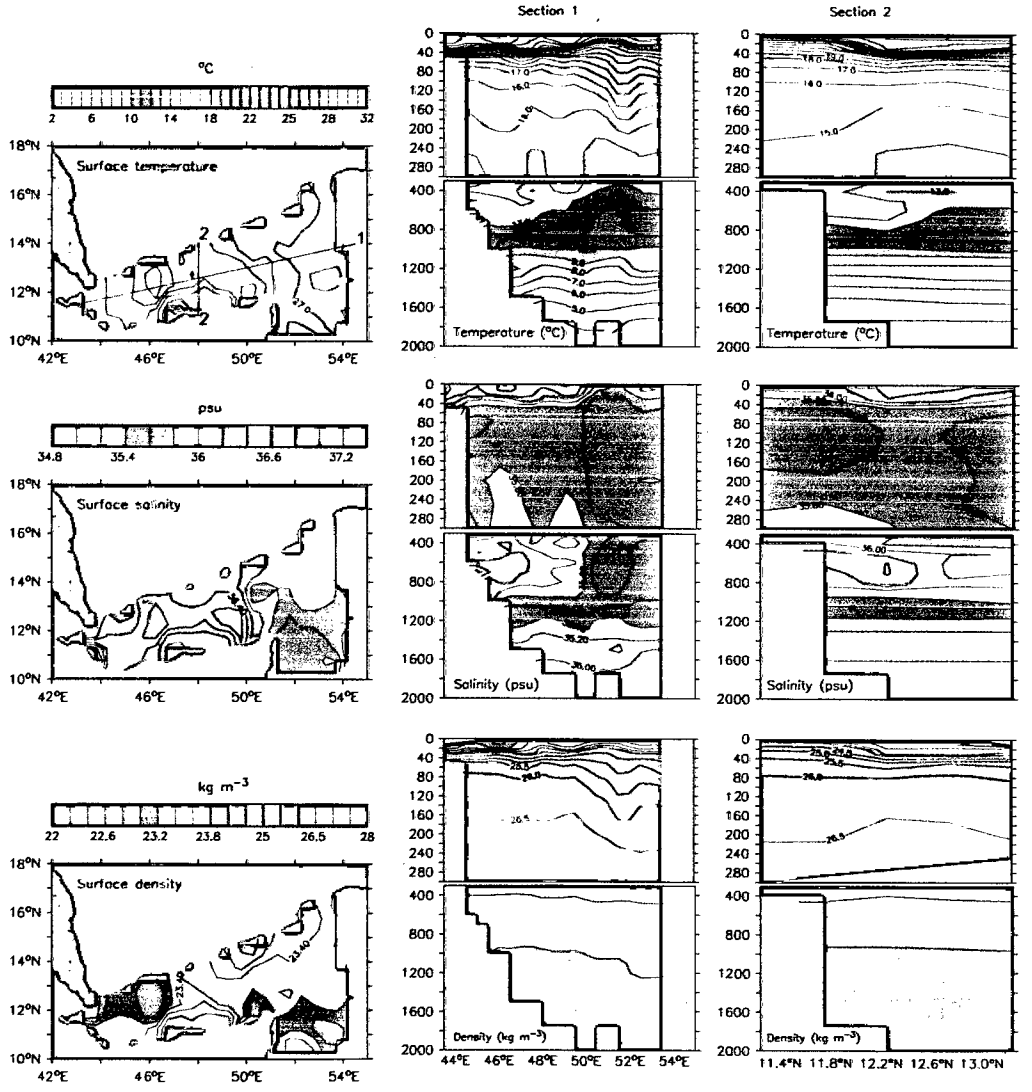

Figure 3.1 (k) Same as 3.1a, but for November.

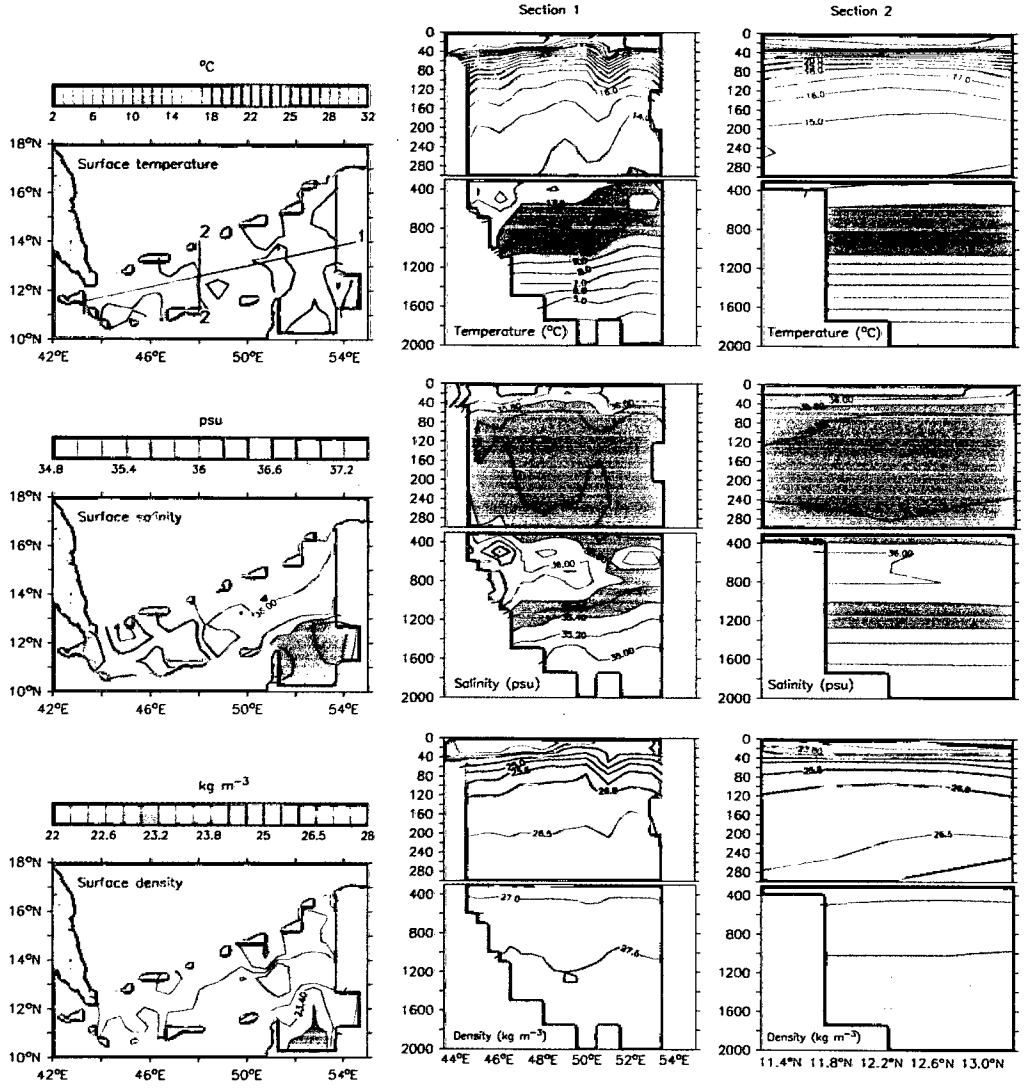

Figure 3.1 (l) Same as 3.1a, but for December.

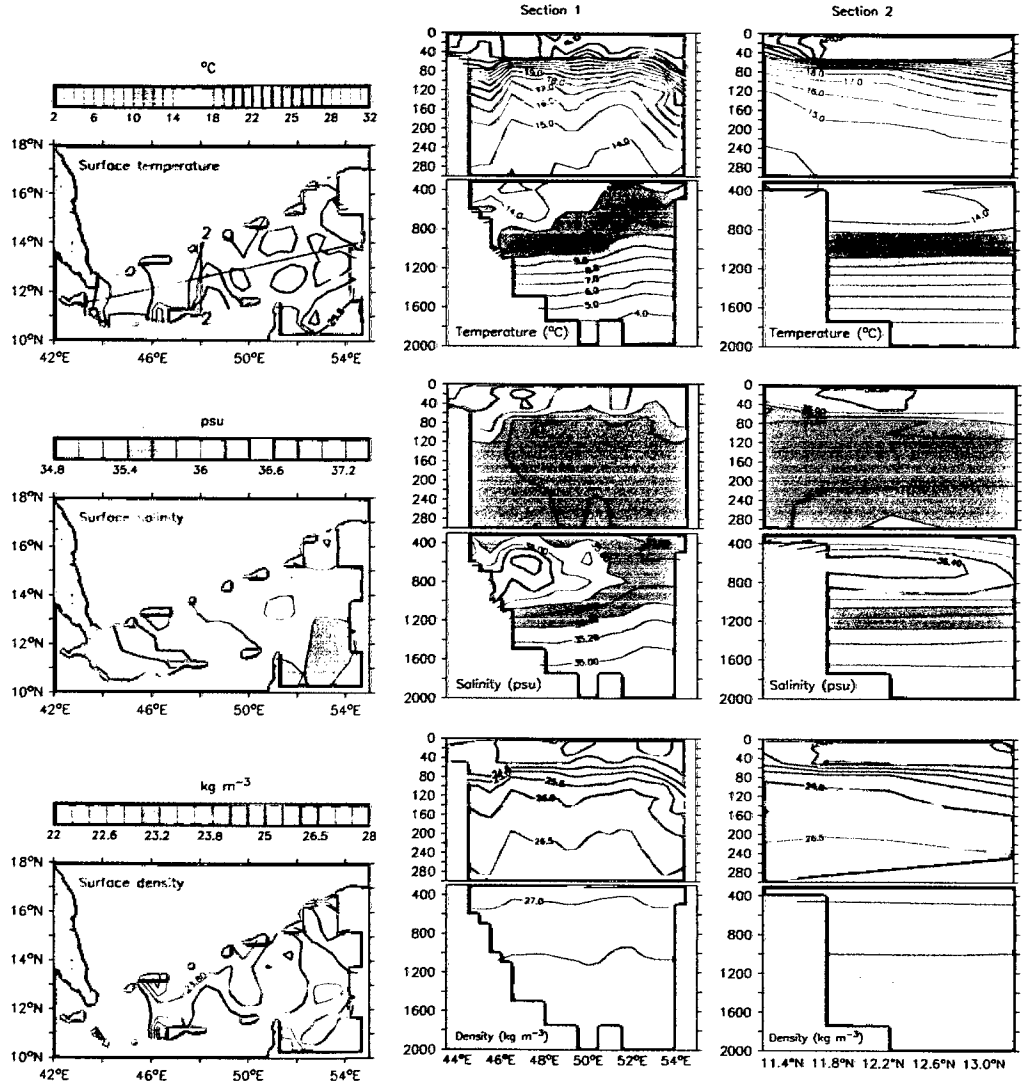

During October, the surface layer is cooler than that during September by $\sim$ 1 °C, where it is about 29 °C all over the gulf except for the cooler patch along the southern coast (25 °C) between 46° E and 49° E and the warmer patch along the northern side (30 °C) between 45° E and 47° E (Figure 3.1j). Similarly, the surface salinity along the southern side is about 35.8 psu compared to 36.4 over the rest of the gulf (Figure 3.1j).

The vertical structure along Section 1 shows that the surface mixed layer deepened compared to that during September (Figure 3.1j). The low salinity layer is seen between 80 and 400 m (Figure 3.1j). The RSW in the deeper layer extends to $\sim$1000 m. Section 2 shows the uplifting of isotherms and isohalines along the southern side indicating upwelling (Figure 3.1j).

During November, the surface mixed layer extends to $\sim$ 40 m with a temperature of $\sim$ 27 °C all over the gulf and salinity decreases from 36.4 psu in the west to $<$ 36.0 psu in the east (Figure 3.1k). Below the surface mixed layer, the thermocline extends to about 140 m, where the temperature decreases to $\sim$ 16 °C and salinity decreases to $\sim$ 35.6 psu. This low salinity layer extends to about 400 m (Figure 3.1k). The RSW is seen extending from $\sim$ 400 m to 1100 m with the core at $\sim$ 500 m in the west.

During December, the surface temperature cools down to $\sim$ 25 °C and the mixed layer deepens to about 60 m due to the strengthening of winter. Along the southern coast, the temperature is about 2 °C cooler than that along the northern coast due to the upwelling along the southern coast. Similar to that in November, the salinity decreases from west towards east. The low saline layer with salinity $<$ 35.6 psu is seen extending from $\sim$ 120 m to about 400 m. Also the RSW extends till about 1100 m with its core seen between 600–800 m (Figure 3.1l, Section 1).

In general, the hydrographic structure in the Gulf of Aden shows a four layer structure. The surface layer experiences strong seasonality in its characteristics and depth. The SST is about 24–25 °C during winter (November–February) increasing to its maximum in March to May. During summer (June–August), the SST decreases along the northern side

due to upwelling. In September, SST starts to rise again to $\sim$ 30 °C. Similarly, the mixed layer depth decreases from $\sim$ 80 m during winter to about $\sim$ 20 m during summer. The upwelling along the northern side during summer starts at the eastern side during June and extends towards the west during July–August. The seasonal variation is also seen in the intermediate low saline layer. It is cooler and more saline during summer than in winter. The RSW layer extends from 400 m to $\sim$ 1100 m during most of the months.

3.3 Water masses

As described above, the Gulf of Aden hydrographic structure comprises four layers with specific characteristics for each layer. In this section, we will describe the characteristic of the four water masses associated with each of these layers and identify their origins.

A typical θ–S (potential temperature–salinity) curve for the Gulf of Aden (Figure 3.2) clearly shows four distinct water masses similar to those reported by Khimitsa [1968]. The upper three water masses also show similarities to those reported by Piechura and Sobaih [1986] and Nasser [1992]. Mohamed et al. [1996] reported five water masses in the Gulf of Aden, but the temperature–salinity–density ranges they used to define the water masses varied drastically from those shown in Figure 3.2. The θ–S curve in Figure 3.2 shows high saline surface water followed by low saline water in the intermediate levels and high saline water below that. The bottom water is comparatively fresher than that in the upper water column. Such θ–S curves constructed individually and collectively were then used for further analysis.

3.3.1 T-S Characteristics

Figure 3.3 shows the θ–S diagrams constructed using temperature–salinity profiles available from the Gulf of Aden west of 51° E. The number of profiles available during a month varied from 146 in December to 313 in January. Since the Gulf of Aden receives

Figure 3.2 Typical θ–S curve for the Gulf of Aden. Four water masses are identified from the profiles. The contour lines represent the σ_θ surfaces.

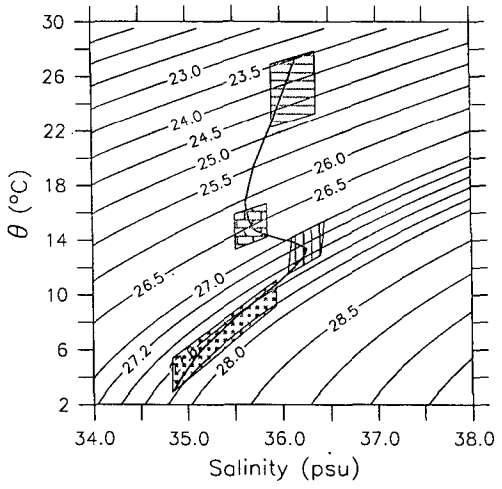

high saline Red Sea water in the west and moderately saline Arabian Sea water in the east, we have divided the region into three sub–regions, namely: the western region (between 43.5° E and 45.0° E), the central region (between 45.0° E and 49.0° E), and the eastern region (between 49.0° E and 51.0° E).

Four water masses are identifiable from the θ–S diagrams in Figure 3.3. They are: (i) a salinity maximum near the surface between the σ_θ levels 22.20 kg m^{-3} and 24.80 kg m^{-3}; we call this water Gulf of Aden Surface Water (GASW); Khimitsa [1968] called it Surface Aden Water. (ii) A salinity minimum between the σ_θ levels 26.20 and 26.90 kg m^{-3}; we call this water Gulf of Aden Intermediate Water (GAIW); Khimitsa [1968] called it Low Salinity Layer or Subsurface Salinity Minimum. (iii) A salinity maximum between the σ_θ levels 26.90 and 27.50, which is easily identifiable as Red Sea Water (RSW). Finally, (iv) a distinct water between the σ_θ levels 27.50 and 27.80; we call this Gulf of Aden Bottom Water (GABW); Khimitsa [1968] called this Bottom Water. Among the four water masses, the θ–S relationship is tightest for the bottom water mass, but the potential temperature and salinity varies over a wider range (3 to 9 °C and 34.70 to 35.60

psu). The ranges of potential temperature and salinity for the four water masses are given in Table 3.1. The histograms (Figure 3.4) show the distribution of potential temperature and salinity within the four water masses. Histograms are useful for the identification of potential temperature and salinity at the core of water mass. For example, the potential temperature and salinity of the GASW core is 25.5 °C and 36.0 psu. Similarly, the potential temperature and salinity of the RSW core is 12.5 °C and 35.8 psu respectively.

Gulf of Aden Surface Water

The spatio–temporal variability of the salinity of the GASW that occupies the surface layer is not more than 1.00 psu (Figures 3.1 and 3.3), but the potential temperature ranges between 21.0 °C and 32.0 °C during summer and 22.0 °C and 26.0 °C during winter. The cooler surface temperature during winter is due to the cool dry northeasterlies that blow over the northern Arabian Sea and adjoining areas [Piechura and Sobaih, 1986]. Accordingly, the lower limit of its σ_θ range also undergoes wide variations from 23.50 kg m^{-3} in January–February to 22.20 kg m^{-3} in June–July. GASW is seen in all three regions of the gulf: western, central and eastern. The profile–to–profile variation in salinity is maximum in the western region and minimum in the central region. Few profiles in the western region showed salinities as high as 37.00 psu during August–September due to high saline surface water outflow from the Red Sea during summer (Figure 3.1g, h and i). Similarly, a few profiles in the eastern region showed lower salinities (35.5 psu) than expected (Figure 3.3). Since the profiles observed over several years are included for this analysis, inter–annual variability is also a reason for the large variations.

Gulf of Aden Intermediate Water

This water, identifiable by a salinity minimum, shows very little variability from month to month compared to GASW (Figures 3.1 and 3.3). Its core, situated at σ_θ level 26.50, is well defined throughout the year. On an average, the spatio–temporal variability in the

range of salinity and potential temperature is less than 0.75 psu and 3.0 °C. The salinity in the eastern region is comparatively lower than that in the central one. The salinity profiles in the western region show large variations (> 2 psu). Some of them must have occurred due to the high salinity water that outflows from Bab el Mandab into the Gulf of Aden [Maillard and Soliman, 1986; Murray and Johns, 1997; Al Saafani and Shenoi, 2004].

Table 3.1 Potential temperature-salinity-σ_θ and depth ranges of the water masses in the Gulf of Aden.

$Watermass$	$\theta(°C)$	$S(psu)$	$\sigma_\theta(kgm^{-3})$	$Depth(m)$
GASW	21.0–32.0	35.4–36.8	22.20–24.80	0–100
GAIW	12.0–17.0	35.1–36.4	26.20–26.90	120–420
RSW	7.0–20.0	35.2–38.2	26.90–27.50	350–1050
GABW	3.0–9.0	34.7–35.6	27.50–27.80	1200–1600

Red Sea Water

This is the most prominent water mass in the Gulf of Aden and there is no ambiguity about its origin. It outflows into the Gulf of Aden from the Red Sea through Bab el Mandab strait; its core exists at σ_θ level 27.20. 68% of the observations showed salinities in the range 35.30 to 36.00 psu and 32% of them showed salinity greater than 36.00 psu. The profiles from the western region show salinities as high as 38.00 psu (see Figure 3.3 for January and May–July). In the central region, both potential temperature and salinity showed large variability, especially during the summer months (May–September). The outflow of RSW from the Red Sea undergoes a seasonal cycle in response to the monsoon winds [Murray and Johns, 1997; Aiki et al., 2006]; the outflow is minimum at the end of the summer monsoon season and maximum during the peak of winter. Hence, in addition to the interannual variability, the seasonal variability in the θ–S could be associated with the variability in the outflow of RSW from the Red Sea.

Figure 3.3 θ–S diagram for Gulf of Aden for all months. All available profiles from the Gulf of Aden (west of 51° E) are included. Profiles from the region west of 45° E are in red (western region), those in the region between 45–49° E are in black (central region) and those from the region between 49° E and 51° E are in blue (eastern region). Number of θ–S profiles available during each month is also indicated.

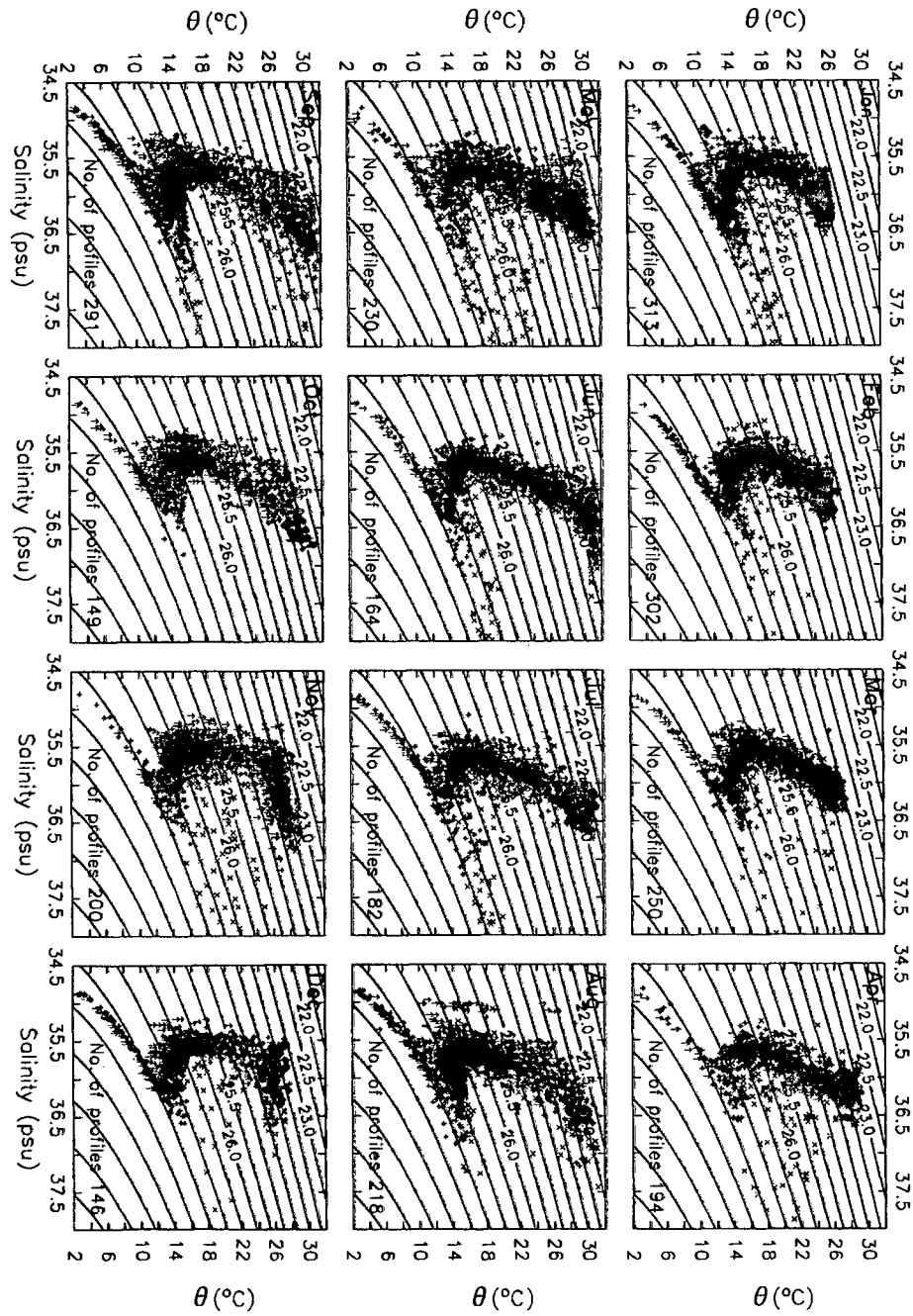

Figure 3.4 Histograms of potential density, potential temperature and salinity for GASW, GAIW, RSW and GABW. The histograms were constructed by counting the data values constrained within the θ–S–σ_θ ranges given in Table 3.1

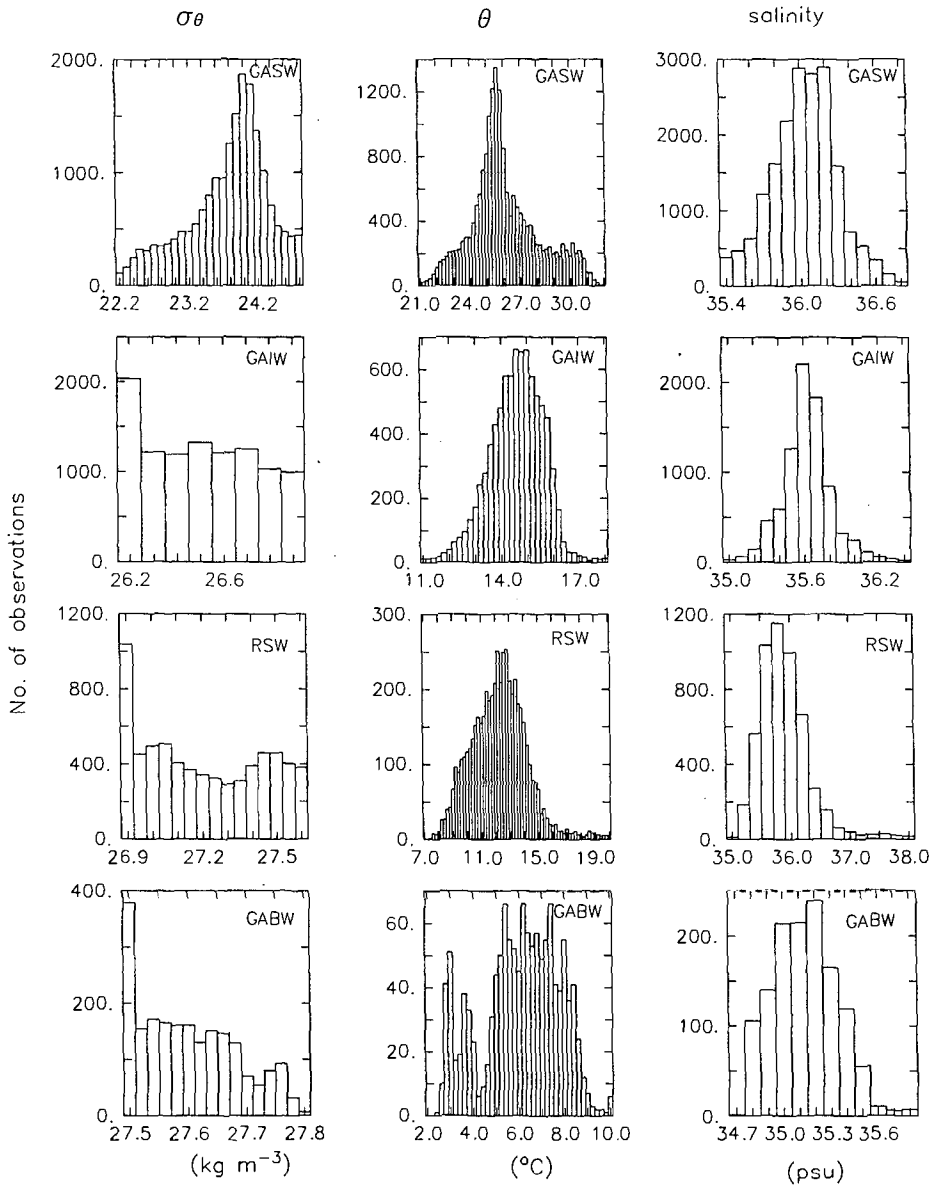

Gulf of Aden Bottom Water

The GABW is easily identifiable in the σ_θ range 27.50 to 27.80. Though this water mass has a narrow σ_θ range, its potential temperature and salinity has wider ranges; the potential temperature ranges between 3.0 and 9.0 °C and salinity between 34.70 and 35.60 psu (Figure 3.4). Being the bottom water, the temporal variability of the θ–S structure is very low.

3.3.2 Horizontal distribution

The spatial distribution of θ–S profiles alone is insufficient to describe the variations in the horizontal distribution of the water masses. Hence, maps of horizontal distribution of water masses were prepared for two major seasons: the summer (August–September) and the winter (January–February). Here we chose the last two months of the seasons because the circulation effects on the water mass are best seen towards the end of the season. The salinity at the core of the water mass is used as a tracer to describe the horizontal distribution (Figure 3.5). The core is defined using the maximum/minimum salinities. For example, for RSW we picked the maximum salinity between the σ_θ levels 26.90 and 27.50 and for GAIW we picked the minimum salinity between the σ_θ levels 26.20 and 26.90. As expected, the salinity of the core of RSW is higher in the west due to the discharge from the Red Sea. The core of RSW flows within the depth range 600–650 m except in a few pockets where it deepens to 700–800 m. This is consistent with the description of Bower et al. [2000, 2005]. On an average, the core of RSW shallows during summer, in the east, by about 50–100 m. The lowest salinity in the core is seen near the Somali coast at around 49.0° E in both seasons. Low salinities are also seen near the coast of Yemen in summer.

The salinity in the core of GAIW water increases towards the west. The salinity in the core is considerably higher in the west due to mixing with high saline outflow from

the Red Sea [Khimitsa, 1968; Piechura and Sobaih, 1986]. The core shallows by at least 50 m during summer from its winter position, as described in the previous section. From the pattern of salinity contours it appears that the GAIW spreads from east to west. The salinity distribution in the core of GASW is very different from that for RSW and GAIW. The core salinities are highest in the central region and lowest in the eastern region. In summer, a large patch of high salinity, exceeding 36.10 psu, occupies the central region between 45° E and 48° E. The large patch of high salinity is due to the anticyclonic eddy that occupied the center of the Gulf of Aden during summer [Piechura and Sobaih, 1986] (see Chapter 5 for details of the eddies in the gulf).

The structure of these water masses is also clearly seen in the vertical salinity section running through the middle of the gulf (Figure 3.6). The GAIW and the GABW spread from the east while the RSW spreads from the west.

3.3.3 Volumetric analysis

The volumes occupied by the water masses were estimated following Montgomery [1958] for an average θ–S profile in the Gulf of Aden. For this calculation the volume of the Gulf of Aden was considered as $\sim 4840 \times 10^{11}$ m^3; this includes twenty 1° × 1° grids covering a surface area of 242×10^9 m^2 and average depth of 2000 m. All profiles of temperature and salinity within 20 grids were averaged to generate one θ–S profile representing the annual average profile. This average θ–S curve was then sliced in to 0.5 °C temperature × 0.1 psu salinity grids (see Figure 3.7). The volume of each grid was then estimated by multiplying their respective thicknesses by the surface area. The volumes of 0.5 °C temperature × 0.1 psu salinity grids falling within the pre-defined bounds of the water masses (based on θ–S–σ_θ ranges) were then added together to determine the total volume of each water mass. As per the estimate, the volume of RSW in the gulf is about 1769.0×10^{11} m^3 while the volumes of GAIW and GABW are about 418.7×10^{11} m^3 and 1851.3×10^{11} m^3 respectively. The volume of GASW is about 138.0×10^{11} m^3 only. In terms

Figure 3.5 Horizontal distribution of the water masses during winter (January–February) and summer (August–September). The salinity (psu) in the core layer of the water mass is used to trace the spread of the water mass. The contours represent the depth of core layer.

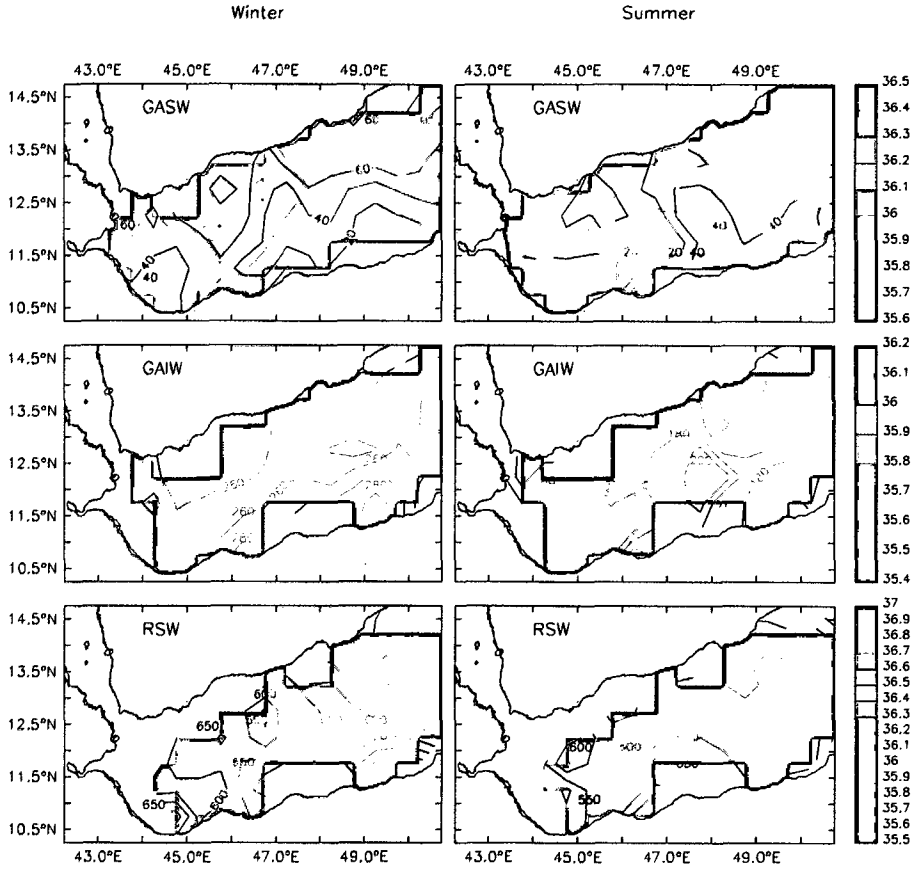

Figure 3.6 Vertical section of salinity (psu) along the east-west axis of the Gulf of Aden (along 12.5° N) (a) for winter (January–February) and (b) for summer (August–September). σ_θ contours are also shown.

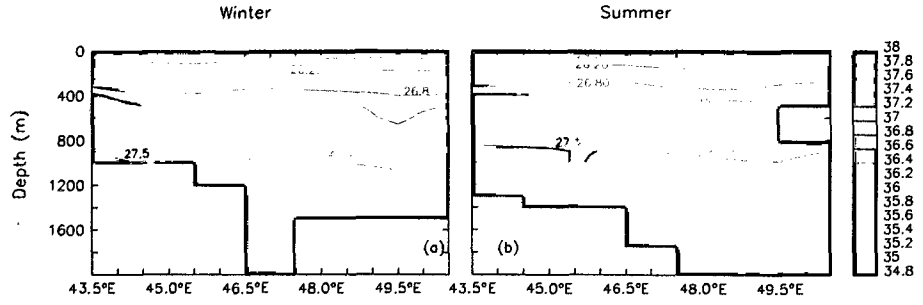

of percentages, the RSW occupies ~ 37% of the total volume of the Gulf of Aden while GAIW and GABW occupy ~ 9% and 38% respectively.

While the estimates based on the mean θ–S profile for the Gulf of Aden provided the approximate volumes of water masses, they are inadequate to describe the temporal and spatial variability. Estimates based on monthly mean θ–S profiles within 1° grids spread over the Gulf of Aden would have been ideal to describe the spatial and temporal variability. The data sparseness, however, prevents such estimates. Hence, mean θ–S profiles were constructed for two seasons (summer and winter). Similarly, due to the paucity of data in some of the 1° × 1° grids, the volume computations were carried out over a 1° longitude band. A mean θ–S curve for a 1° longitude band was computed first and then sliced in to 0.5 °C temperature × 0.1 psu salinity grids . Since the mean θ–S profiles in several grids do not extend beyond 1200 m, it was not be possible to estimate the volume of GABW. The volumes thus estimated for 1200 m deep water column along the east–west axis of the Gulf of Aden are shown in Figure 3.8. During winter, the volume of RSW is 100 × 10^{11} m^3 in the western grid and it is 72 × 10^{11} m^3 in the eastern grid. In the center, it is ~ 88 × 10^{11} m^3; the sharp decrease (~ 72 × 10^{11} m^3) occurs only in the grids east of 49° E. During summer, though the volume of RSW remains more or less the same (~ 100 × 10^{11} m^3) in the west, it decreases gradually towards the east (Figure 3.8).

Figure 3.7 θ–S–V diagram constructed for an annual mean profile from the Gulf of Aden. The volumes ($\times 10^{11}$ m^3) occupied by GASW, GAIW, RSW and GABW are marked in different shades. Thin lines represent the 0.5 °C × 0.1 psu θ–S grid. The θ–S grids used to estimate volumes of water masses are shown in different shades. The σ_θ lines are also shown. Assuming an average depth of 2000 m, the total volume of Gulf of Aden is ~ 4840 × 10^{11} m^3.

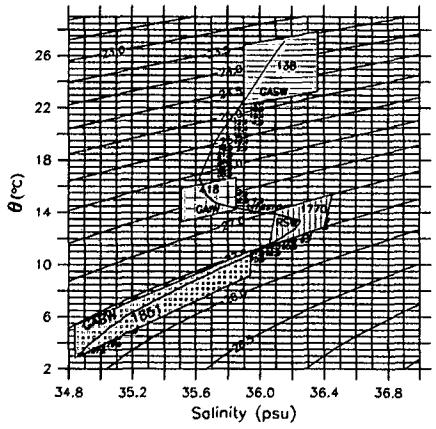

GAIW is present more in the east (25 × 10^{11} m^3) than that in the west (~ 12 × 10^{11} m^3) during winter. In summer, however, the east-west variation as well as its variability in volume are low (~ 18–20 × 10^{11} m^3). The volume of GASW is about 10 × 10^{11} m^3 in winter and about 6 × 10^{11} m^3 in summer. The east–west variability in the volume of GASW during both seasons is negligible.

The volumes of all three water masses, the RSW, the GAIW and the GASW, are higher during winter than in summer. The increase in volumes results in increased sea level during winter. The seasonal cycle of sea level recorded by the tide gauge at Aden show an increase of ~ 35 cm during winter (see Figure 1.5 on page 15).

3.3.4 Percentage composition of Gulf of Aden water

TS–diagram continued to be a useful tool for the analysis of a variety of oceanographic situations, many of which involved more than three water masses. When four or more

Figure 3.8 East–west variations in the volumes of water masses in the Gulf of Aden ($\times 10^{11}$ m^3). Meridonally (1° wide longitude bands) averaged θ–S profiles were used to estimate the volumes following the θ–S–V diagrams.

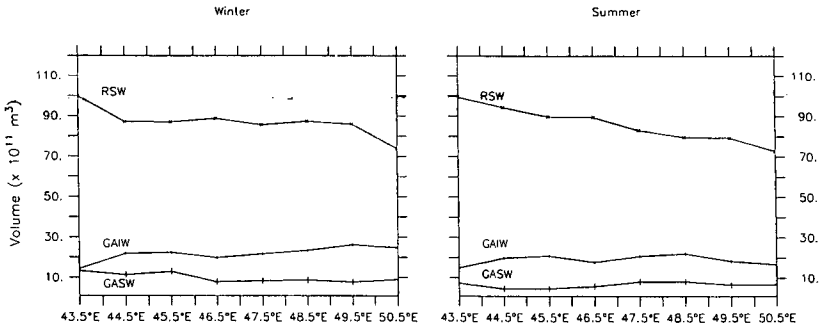

water masses are involved, the role of the assumption of vertical layering becomes more crucial. In the case of the mixing of three water masses, there exists a unique solution to any combination of temperature and salinity within the mixing triangle for the percentage contribution of the three water masses involved. In the case of four or more water masses, there exists a whole range of solutions, and the assumption of vertical layering is necessary to select a particular solution [Tomczak, 1981a]. This vertical layering forms the basis for a TS–diagram analysis which divides the TS–range, spanned over the four water masses, into two triangles (Figure 3.9). The method of breaking down a given area on the TS–diagram into a set of mixing triangles can be extended to any number of water types if only three of them can have simultaneous contact at any point in space [Mamayev, 1975]. In most oceanic situations these conditions are met because the corresponding water masses are layered vertically, and mixing between them is predominantly vertical.

The percentage composition of water masses in a water sample in the Gulf of Aden was estimated following Tomczak [1981a,b]. The method is an extension of the set of equations which forms the basis of the mixing triangle. Consider a situation where 'n' water masses are contributing to the mixture of water at an oceanographic station. Then a minimum of n-1 characteristics, the independent parameters, of the water masses are

necessary to describe them using the theory of a mixing triangle. Conserving the mass, the relative contribution of any water mass to the water sample at a location can be determined from the linear system of equations given as

$$AX = B \tag{3.1}$$

where A is an n $\times$ n matrix of the parameter values for the n water masses, B is a vector of n elements which contains n-1 observations, and X is a vector of n elements which gives the relative contributions of the water masses. The elements of the last row in A and the last element of B are identically 1, to express the condition that all contributions must add up to 100% of the observed volume of water. Since four water masses are to be considered to describe the composition of water samples in the Gulf of Aden, three parameters were considered, namely: potential temperature, salinity and oxygen. Consideration of oxygen as one of the parameters might introduce an element of uncertainty in the estimate because it is not a conservative tracer, especially in the shallow depths (depths $<$ 200–300 m). Nevertheless, we have used oxygen as one of the parameter in the absence of other suitable information. Hence, the equation (3.1) becomes

$$\begin{aligned} x_1T_1 + x_2T_2 + x_3T_3 + x_4T_4 &= T_{obs} \\ x_1S_1 + x_2S_2 + x_3S_3 + x_4S_4 &= S_{obs} \\ x_1O_1 + x_2O_2 + x_3O_3 + x_4O_4 &= O_{obs} \\ x_1 + x_2 + x_3 + x_4 &= 1 \end{aligned} \tag{3.2}$$

Matrix A was defined using the thermohaline indices (T_i, S_i, O_i) of the water mass i ($i = 1,2,3,4$) before they entered and mixed in the Gulf of Aden (Table 3.2); ie., the θ–S–O_2 of the water mass when it was outside the Gulf of Aden. Mixing triangles were used to determine the thermohaline indices (see for example Figure 3.9). GAIW and GABW enter the gulf from the east, hence the profiles from the eastern region were used to determine their thermohaline indices. Similarly, the profiles from the western region

were used to determine the thermohaline index for RSW before it entered the gulf. A similar definition of thermohaline index for GASW could be ambiguous because that does not have a definite source region. Part of the GASW forms inside the gulf due to air–sea fluxes and part is advected into the Gulf of Aden either from the western Arabian Sea and/or from the Red Sea. The surface flow in the Gulf of Aden inferred from the climatology of sea level height anomalies estimated from the satellite altimetry is towards the west during the winter and towards the east during the summer [Al Saafani and Shenoi, 2006] (also see the description of circulation in Chapter 4). Hence, the profiles from the eastern (western) Gulf of Aden were used to determine the thermohaline index during winter (summer).

Table 3.2 Thermohaline indices for the four water masses in the Gulf of Aden.

$Watermass$	$\theta(°C)$	$Salinity(psu)$	$Oxygen(ml L^{-1})$
GASW	27.00	36.10	5.00
GAIW	14.50	35.25	0.70
RSW	18.50	37.90	0.50
GABW	3.10	34.80	2.00

The percentage composition of water in the Gulf of Aden along the east–west axis of the gulf is shown in Figure 3.10. As expected, the percentage of water of Red Sea origin reduces from 90% in the west (near Bab el Mandab) to less than 40% in the east (Figure 3.10e and f). The water in the bottom (deeper than 1100 m) as well as the surface and intermediate (less than 400 m) levels also contains about 10–20% water of Red Sea origin. Similarly, the water that is responsible for the GAIW is maximum in the intermediate levels; it also contributes to the water that is found in the deeper layers (deeper than 1200 m) and surface layers (less than 100 m). The presence of more of this water in the east than in the west suggests that the water responsible for GAIW enters the Gulf from the east. The water that is responsible for the GASW does not contribute much to the water

Figure 3.9 Typical mixing triangles for the western and eastern Gulf of Aden. They were used to identify the thermohaline indices of water masses (see Table 3.2).

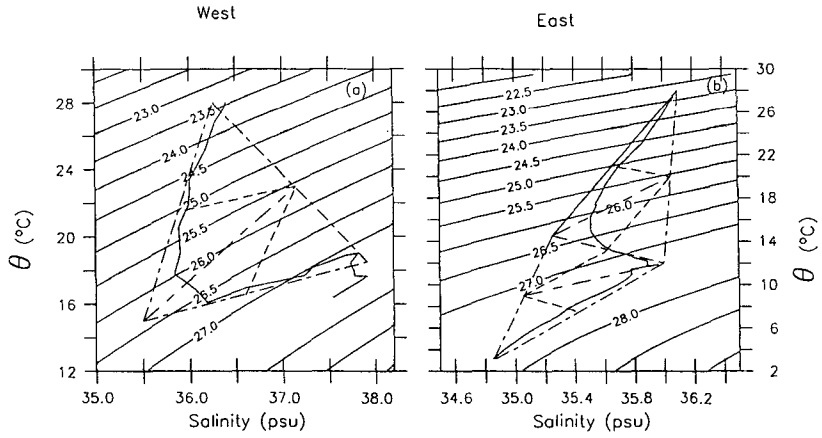

below 150 m. It is maximum (> 90%) in the surface layers (< 40 m), decreasing rapidly towards the deeper layers. Most of this water also appears to enter the Gulf of Aden from the east. The water that is responsible for the formation of GABW shows highest concentrations (~ 90%) in the bottom layers and dilutes rapidly towards the upper layers (< 1200 m).

3.4 Discussion

Previous reports [Khimitsa, 1968; Piechura and Sobaih, 1986; Nasser, 1992; Mohamed et al., 1996] used limited data sets to describe the hydrography and water mass in the Gulf of Aden. Though they succeeded in identifying the water masses, they failed to give an integrated picture of the presence of distinct water masses in the gulf. Moreover, the definitions and nomenclature of the water masses varied among themselves, except for the RSW.

As expected, the vertical hydrographic structure of the Gulf of Aden shows four layers, surface layer, intermediate low saline layer, high saline RSW and bottom layer. The sur-

Figure 3.10 Percentage composition of the Gulf of Aden water. The water in the Gulf of Aden is presumed to be constituted due to the four water masses, namely, GASW, GAIW, RSW, and GABW.

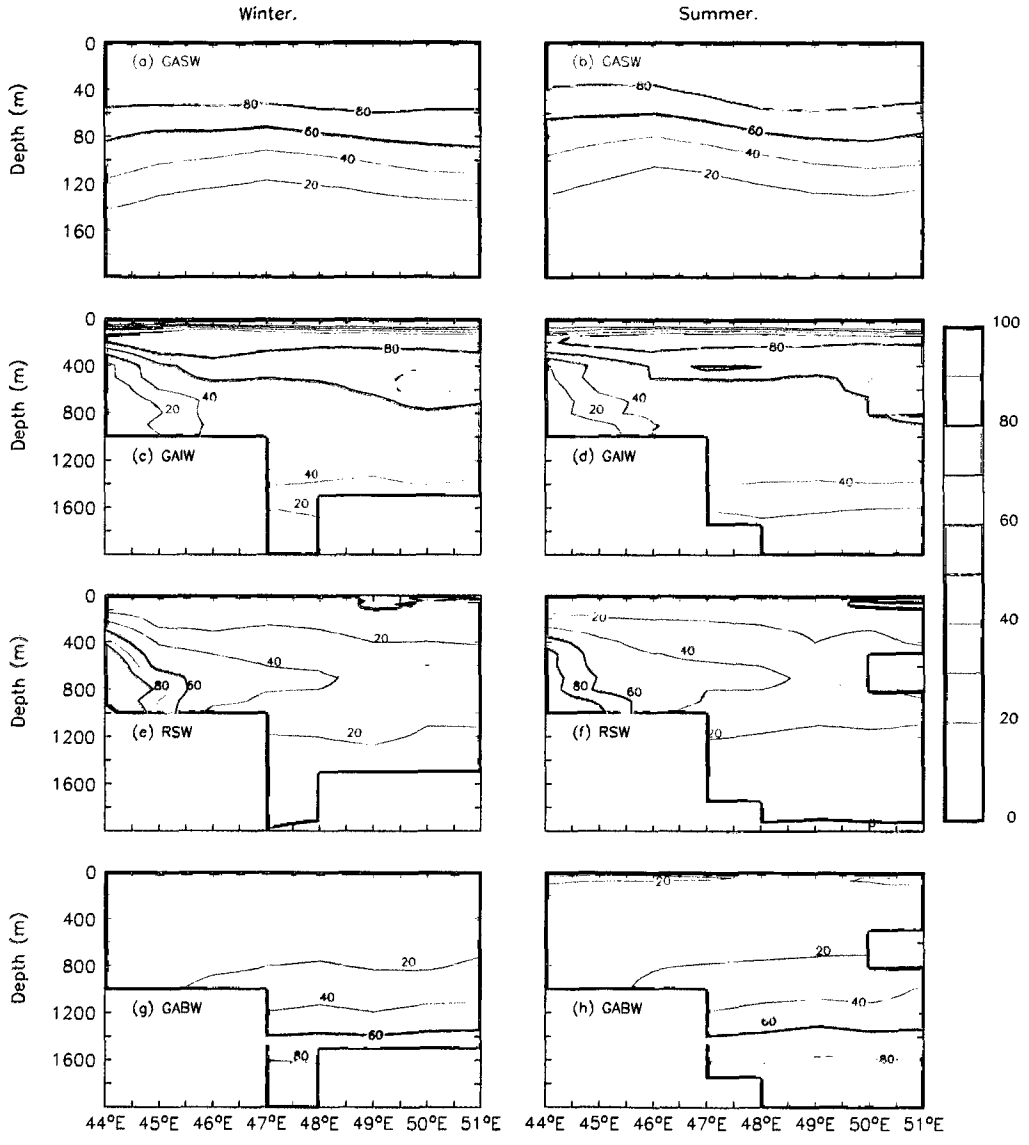

face layer showed strong seasonal variations in its characteristics and depth. The SST was about 24–25 °C during winter (November–February). It increased to reach a maximum in May (31 °C). During summer (June–August) the SST decreased along the northern side due to upwelling. In September, the SST started to rise again to $\sim$ 30 °C. Similarly, the mixed layer depth decreased from $\sim$ 80 m during winter to $\sim$ 20 m during summer. The seasonal variation was lesser in the intermediate low saline layer. It was cooler and more saline during summer compared to that in winter. The upwelling along the northern side during summer started in the eastern side during June and extended towards the west during July–August as reported earlier [Piechura and Sobaih, 1986].

Similar to earlier studies (for example Khimitsa [1968]), four water masses were identified using the newly compiled hydrographic data set. Among them, the origin of RSW is well known. Hence, we will focus on identifying the origins of the other three water masses, the GASW, GAIW and GABW.

Being the surface water, seasonal as well as the monthly variabilities were highest for the GASW. Though the core density is $\sim$ 1024.10 kg m^{-3}, the lower limit of density varied from 1023.50 kg m^{-3} in winter to 1022.20 kg m^{-3} in summer due to the increase in temperature. The salinity of the core increased towards west (Figure 3.5 and Figure 3.6). The θ–S–σ_θ structure of this water mass (core θ–S 26.0 °C–36.0 psu and σ_θ 24.1) is similar to the salinity maximum D of Rochford [1964] and ASHSW described in Shenoi et al. [1993]. The salinity maximum D or ASHSW forms in the surface of Arabian Sea and spreads along the σ_θ level 23.8 (θ–S range 24.0–26.5 °C and 35.1–36.5 psu). The θ–S range of GASW is 21.0–32.0 °C and 35.4–36.8 psu and the core σ_θ is $\sim$ 24.1 kg m^{-3}. In summer, the temperature of this surface water increases to 32 °C, while in winter, it decreases to 26.0 °C. The θ–S profiles [Antonov et al., 1998; Boyer et al., 1998] for 4° $\times$ 4° region in the northwestern Arabian Sea (54–58° E, 10–14° N) for summer (July) and winter (January) is shown in Figure 3.11. During winter, the characteristics of water in the surface layers of northwestern Arabian Sea are similar to that of GASW, while

Figure 3.11 θ–S–Diagram during summer (July) solid–line and winter (January) dashed–line for 4° × 4° averaged profile (54–58° E, 10–14° N) in the western Arabian Sea.Climatologies of Antonov et al. [1998] and Boyer et al. [1998] are used.

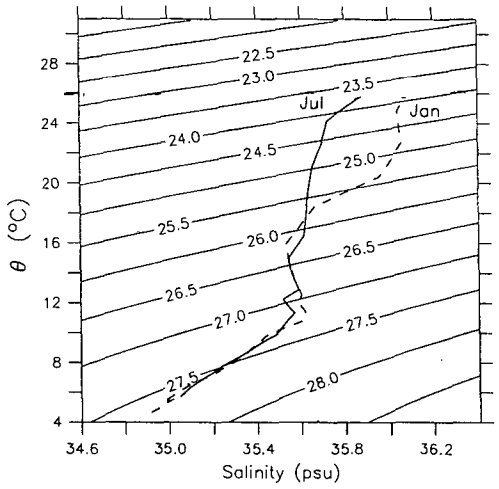

during summer the surface layer in the northwestern Arabian Sea was cooler than GASW (Figure 3.11). The surface current is towards the west during winter and towards the east during summer ([Khimitsa, 1968; Piechura and Sobaih, 1986]; also see Chapter 4 for details on circulation). Hence, during winter, a sizable amount of ASHSW enters the Gulf of Aden from the east. Similarly, during summer, a sizable amount of surface water from the Red Sea enters the gulf from the west. In addition, during both seasons, some water forms locally due to precipitation and evaporation. Hence, during winter the GASW forms as a mixture of locally formed water and ASHSW, while during summer it is a mixture of locally formed water and Red Sea Surface Water.

In the intermediate layers (200–300 m), the GAIW, appears as a minimum in the θ–S diagram at σ_θ level 26.5. Usually, a minimum occurs between two maxima and it is unnecessary to trace its origin or determine the processes that actively depress the salinity. However, this particular minimum does not appear to be the typical minimum found between two maxima because (i) in the θ–S structure it appears as a distinct water

mass (Figure 3.3) and (ii) it is seen only at a particular σ_θ level and not spread over the entire water column between the two maxima. Hence it is necessary to identify the source of this minimum. Khimitsa [1968] suggested that the water in the intermediate level (150–200 m) enters the gulf as a strong jet between Cape Gvardafui and Socotra. Mohamed et al. [1996] identified the water between σ_θ levels 26.0 and 27.0 as a mixture of PGW, Arabian Sea Water and Timor Sea water.

To identify the pathways of GAIW, a series of θ–S diagrams were constructed using data from Antonov et al. [1998] and Boyer et al. [1998] for selected locations along three paths: (i) from Gulf of Oman to Gulf of Aden (Figure 3.12a); (ii) from the western Arabian Sea to the Gulf of Aden (Figure 3.12b); and (iii) from the equator to the Gulf of Aden (Figure 3.12c). The θ–S profiles constructed along the path from the Gulf of Oman to the Gulf of Aden show maxima at σ_θ = 26.5, corresponding to Persian Gulf Water (PGW), up to station 3, which is situated outside the Gulf of Aden. From station 4 onwards, the station situated just outside the Gulf of Aden, the maximum is replaced by a minimum at σ_θ = 26.5 and its salinity decreases further at station 5, the entrance to the Gulf of Aden (Figure 3.12a). The minimum is well marked at stations 6 and 7, inside the gulf. Thus, PGW cannot be the source of GAIW. The sections made normal to the coast of Oman [Morrison, 1997] also suggest very little flow of PGW towards the south along the coast of Oman. Most of the PGW flows towards the east and later spreads towards south following the eastern boundary of the Arabian Sea basin [Shenoi et al., 1993].

The θ–S curves at locations along the paths from the western Arabian Sea (west of 60° E) to the Gulf of Aden as well as that along the path from the equator to the Gulf of Aden show the presence of salinity minima at around σ_θ= 26.5 (Figure 3.12b and c). Hence, it is likely that the GAIW enters the gulf either from the south or from the east. During summer, a well developed northward flow (Somali current) penetrates far deeper with velocities above 50 cm s^{-1} at 300 m depth; it transports about 37±5 Sv of water off the coast of Somalia [Beal and Chereskin, 2003]. Part of the Somali current system enters

the Gulf of Aden through the passage between Socotra and the Horn of Africa [Schott and McCreary, 2001]. Fischer et al. [1996] estimated the total transport, west of Socotra, into the Gulf of Aden during summer as 13–14 Sv. Figures 3.5, 3.6, and 3.10 also indicate the east–to–west spread of GAIW. If the GAIW, which has a characteristic salinity minimum, enters the gulf from the western Arabian Sea, especially through the Socotra passage, then what is the source of low salinity water in the western Arabian Sea?

Three sources have been identified for the low salinity water in the western Arabian Sea, the Somali basin. First, the low salinity water brought into the Somali basin by the northern branch of the South Equatorial Current (SEC) [Swallow et al., 1983]; this brings the water from the eastern equatorial Indian Ocean. Warren et al. [1966] recognized Bay of Bengal as a likely source of fresh water for the Somali basin. Morrison [1997] reported the presence of low saline Indian Central Water in the western Arabian Sea at σ_θ= 26.6. However, Wyrtki [1971] suggested that the water of SEC in the lower thermocline (18.0–19.0 °C) originates near the Indonesian archipelago and not from the Bay of Bengal. This water flows at the density surface σ_θ= 25.0.

The second possibility is the low salinity Subtropical Subsurface Water (SSW), which originates at the Subtropical Convergence in the southern hemisphere near 40° S [Quadfasel and Schott, 1982]. Warren et al. [1966] and Wyrtki [1971] showed that this water penetrates as far as 10° N off East Africa and is partially responsible for the low salinity in the intermediate layer of the northern Somali basin. In the Somali basin, in the density range from σ_θ = 26.5 to 27.0, its core layer lies between 300 and 400 m. The temperature varies between 8.0 and 15.0 °C and salinity between 34.8 and 35.5 psu [Quadfasel and Schott, 1982]. This description of SSW matches well with the salinity minimum associated with GAIW. The salinity minimum that lies on the σ_θ level 26.5 in the Gulf of Aden has a potential temperature range between 11.0 and 18.0 °C and salinity between 35.0 and 36.4 psu; its core layer lies between 200 and 300 m. The corresponding thermohaline index (Table 3.2) was θ = 14.5 °C and S = 35.25 psu.

Figure 3.12 θ–S curves at selected locations in the western Arabian Sea (see the corresponding map on the right side for the location of profiles) during winter and summer. Climatologies of Antonov et al. [1998] and Boyer et al. [1998] were used. The location of θ–S profiles were selected along the three probable pathways of the water that might contribute to the GAIW. (a) from Gulf of Oman to Gulf of Aden, (b) from the western Arabian sea to Gulf of Aden and (c) from the western equatorial Indian Ocean to Gulf of Aden.

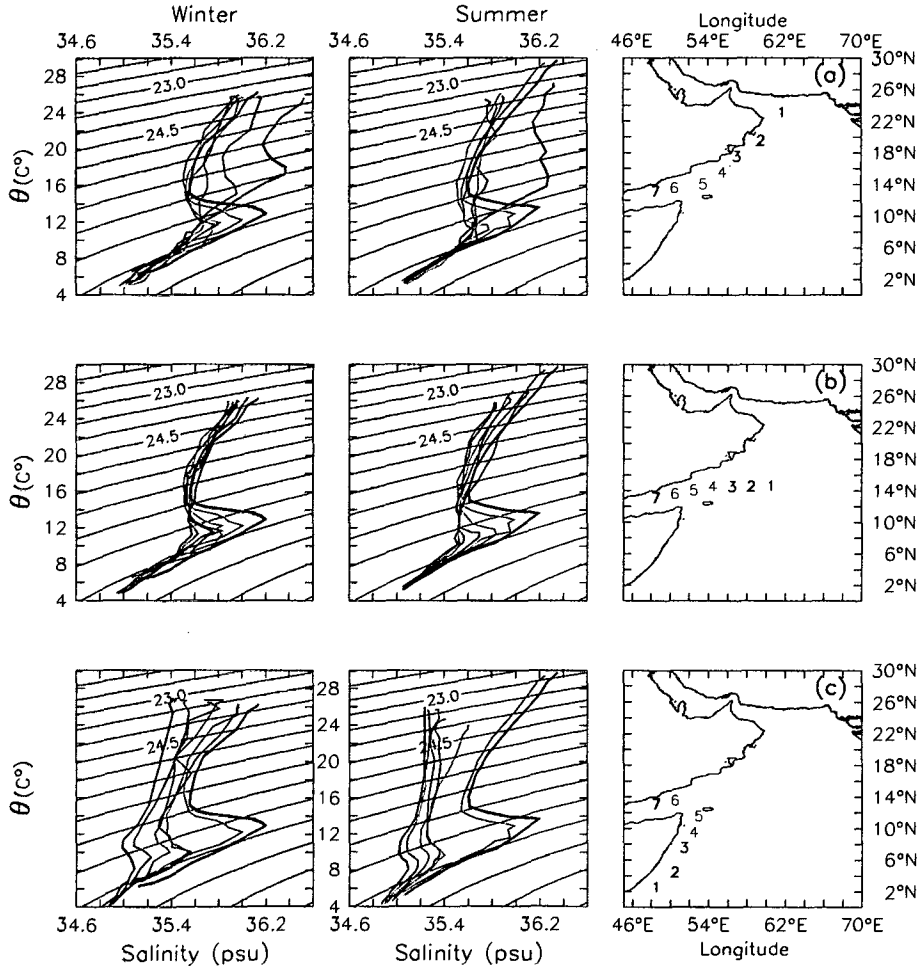

The third possibility is the Antarctic Intermediate Water (AIW), which forms at the Antarctic Convergence Zone at around 40–50° S, sinks and flows north. This water is characterized by low salinity (< 34.3 psu) and high oxygen content (> 5.0 ml L^{-1}); at its source the core layer σ_θ is 27.4. Wyrtki [1971] reported its existence at 5° S and Quadfasel and Schott [1982] at 4° S at the depth rage 700–800 m. Tchernia [1980] suggested that AIW could extend to the extreme northwest Indian Ocean at the Gulf of Aden and Gulf of Oman, where it rises up to depths as shallow as 200–300 m in order to override the relatively saline water spreading southwestward from the Arabian Sea. Hence, it is possible that both SSW and AIW contribute to the existence of the salinity minimum in the Gulf of Aden at intermediate levels.

The Socotra passage seems to be the main connection between the Gulf of Aden and the Somali Basin. The passage also acts as the pathway for the southward migration of RSW. A southward under–current below the northward Somali current in the latitude band 8–12° N [Quadfasel and Schott, 1983; Schott and Fischer, 2000] transports the RSW southward at depths $\sim$ 600–1000 m.

The GABW identified in the σ_θ range 27.5 to 27.8 occupies about 38% of the total volume of the Gulf of Aden. Khimitsa [1968] identified this water with the water originating from the Southern Ocean. Since there is no production of bottom water in the Arabian basin [Quadfasel et al., 1997] it is necessary to transport the bottom water from elsewhere. Johnson et al. [1998] showed that approximately 1–1.7 Sv of Circumpolar Deep Water (CDW) enters the Somali basin through Aminrante Passage at 8° S. The potential density of this water is much higher (σ_θ > 28.5) than the GABW, and its representative θ–S characteristic is 1.0–1.1 °C and 34.72–34.75 psu. Hence it is not possible to identify the GABW with CDW. Another possibility is the water of southern origin, as noted in the θ–S and θ–O_2 curves of Johnson et al. [1998]. This water having $\theta \sim 3$ °C has low salinity (34.70–34.72 psu) and a higher oxygen content (see figure 3 of Johnson et al. [1998]). Although Johnson et al. [1998] do not specify the southern source of this water

it is possible that the AIW could be one among them because that also is characterized by low salinity and high oxygen content. From Figures 3.12 and 3.13 it appears that this water of southern origin spreads further north into the Gulf of Aden (between the σ_θ levels 27.5 and 27.8). The θ–S (Figure 3.12) and the σ_θ–O_2 curves (Figure 3.13) show lower salinity and higher oxygen for this water ($\sim$ 2.0 ml L^{-1} near the equator). The water of southern origin that enters the Gulf of Aden from the south, through the Somali Basin, ultimately mixes with the high saline RSW to produce the GABW with salinity more than 34.80 psu. The mixing of warm RSW with cooler water from the south leaves a wide range of potential temperature (2–11 °C). The percentage compositions estimated based on the mixing theory of water masses (Figure 3.10) suggest the presence of $\sim$ 10–20% RSW in the GABW. Fedorov and Meshchanov [1988] and Mecking and Warner [1999] have shown that some RSW remains relatively undiluted (at $\sigma_\theta > 27.5$) as it flows out of the Red Sea and descends in the western Gulf of Aden. Hence, the bottom water in the western most Gulf of Aden could be the RSW itself.

Figure 3.13 As Figure 3.12, except that curves are for O_2 vs σ_θ. This figure is also used to trace the pathway of GABW.

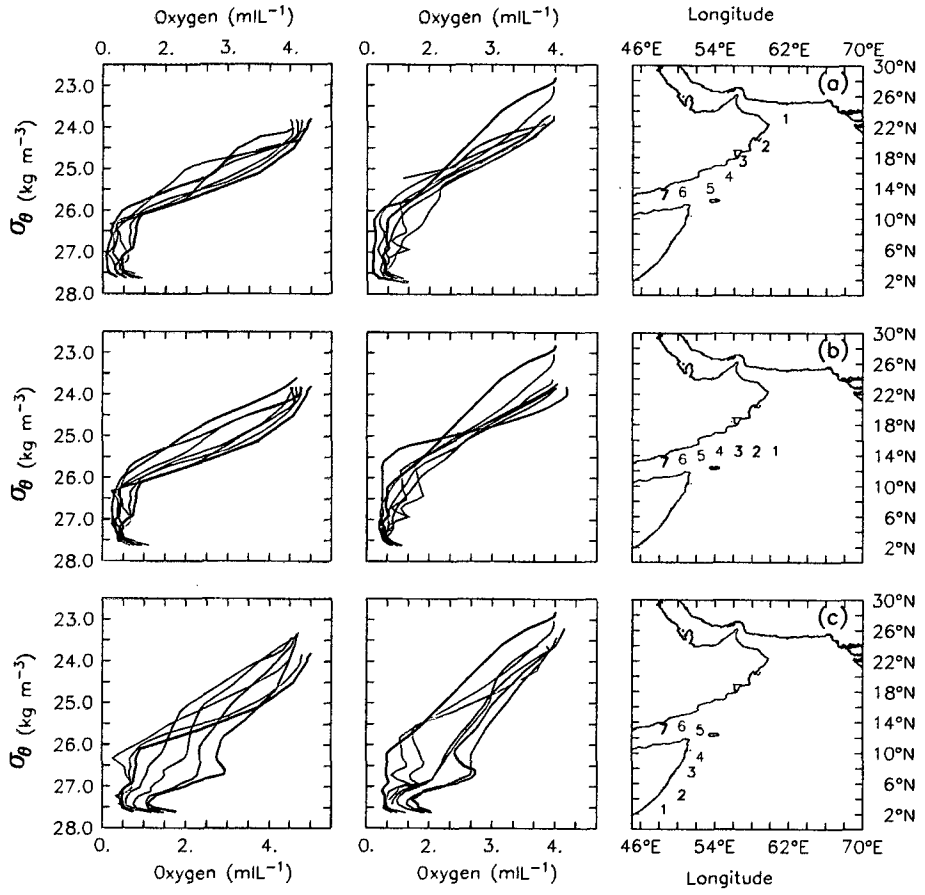

Chapter 4

Circulation in the Gulf of Aden

4.1 Introduction

As described in Chapter 1 the winds over the north Indian Ocean and Gulf of Aden reverse their direction from summer to winter owing to monsoons. Over the Gulf of Aden and the northwestern Arabian Sea, the winter monsoon sets in from November and persists till March (Figure 1.2). The summer monsoon sets in towards the end of May over the Gulf of Aden, shortly after it is established over the western Arabian Sea (Figure 1.2). During this season, over the gulf, the wind speed increases rapidly from ~ 6 m s^{-1} in the west to $\sim$17 m s^{-1} in the east and adjoining northwestern Arabian Sea. October represents the transition between the summer to winter monsoons and April–May (first half of May) represents the transition between winter to summer. The winds are much stronger during the summer monsoon than those during the winter monsoon. These seasonally reversing monsoonal winds over the Arabian Sea and Gulf of Aden force a seasonally reversing circulation in the surface layer. The best studied seasonally reversing current in the northwestern Arabian Sea, the Somali Current, flows poleward (equator ward) along the coast of Somalia during the summer (winter) monsoon (see the reviews by Schott [1983]; Shetye and Gouveia [1998]; Schott and McCreary [2001]). Owing to the reversal

of winds, the surface currents in the Gulf of Aden also reverse seasonally.

From the available literature, it appears that very few attempts have been made to study the circulation in the Gulf of Aden. Due to the lack of published literature, in peer reviewed journals, we have to depend, mainly, on the unpublished articles. In one such article, Kolli et al. [1992] presented a preliminary analysis of the surface currents in the Gulf of Aden based on ship drifts and limited hydrographic observations. Wooster et al. [1967] stated that the winter pattern starts in October with a weak westward flow into the gulf. It developed fully in November and persisted till April . During summer, the direction of the surface current reversed with an increased strength. An anticyclonic eddy also appeared in the center during July–August (see charts no. CA1-CA4 of Wooster et al. [1967]).

The dynamic topography maps prepared by Wyrtki [1971] indicated weak northeasterly flows along the northeastern part of Gulf of Aden during January–February. During the summer monsoon period (July–August), an anticyclonic eddy formed in the center of the gulf, and shifted eastward towards the mouth of the gulf during September–October. The dynamic topography maps of Seriy and Khimitsa [1963] indicated two eddies in the Gulf of Aden during the winter monsoon, one cyclonic in the gulf, east of 50° E, and the other anticyclonic to the east of the gulf off Ras Fartak.

Mohammed and Kolli [1992] used the hydrographic data from three cruises to describe the circulation in the northern Gulf of Aden. During January, one cyclonic eddy developed between 46° E and 50° E. West of the cyclonic eddy, the flow was towards Bab el Mandab. During May, the flow was generally weak with an anticyclonic eddy in the eastern gulf. During August, an anticyclonic eddy appeared in the center of the gulf and another near the eastern end of the gulf between 50° E and 52° E.

Murray and Johns [1997] studied the exchange between the Red Sea and the Gulf of Aden and found that it is strongly seasonal due to the influence of monsoon winds and due to the variations in buoyancy fluxes; the maximum outflow of RSW (0.6 Sv) occurred

during winter and the minimum (0.05 Sv) during summer. Recent observations of Bower et al. [2002, 2005] revealed the spreading of RSW influenced by a chain of deep–reaching mesoscale eddies. The exchange between the Gulf of Aden and the Somali current system occurs mainly through the Socotra Passage [Schott and Fischer, 2000].

Though the aforementioned studies gave a preliminary description of the seasonal behaviour of surface currents in the Gulf of Aden, they could not provide a detailed description of the monthly evolution of circulation in the Gulf of Aden. Similarly, most of these studies covered only the northern part of the gulf due to the paucity of data along the southern part. Thus there is a controversy among them on the characteristics of eddies and their role in the circulation. For example, the dynamic topography maps of Wyrtki [1971] during January–February indicated a northeasterly flow along the northeastern part of the gulf; while Mohammed and Kolli [1992] showed a cyclonic cell between 46 and 50° E indicating a westward flow along the northern side of the gulf. Also they could not establish the influence of eddies on the circulation at the surface or in the deeper layers.

To describe the surface circulation in the Gulf of Aden, we have used four different datasets: (i) ship drift data to get an overall idea of the circulation in the gulf, (ii) the QuikSCAT winds (described in Chapter 2) to estimate the surface Ekman drift, (iii) the hydrographic data (described in Chapter 2) and satellite altimeter derived sea level anomaly (SLA) (also described in Chapter 2) to estimate the geostrophic currents. The net surface currents resulting from Ekman drifts and geostrophic currents were then used to describe the surface circulation. The geostrophic current derived from hydrographic data was first compared with the geostrophic currents derived from altimeter and then used to describe the circulation in the deeper region of the Gulf of Aden.

Figure 4.1 The surface currents derived from ship drifts (cm s^{-1}). The source for the ship drifts is the Ocean Current Drifter Data CDROMs NODC-53 and NODC-54 (NODC, Department of Commerce, NOAA).

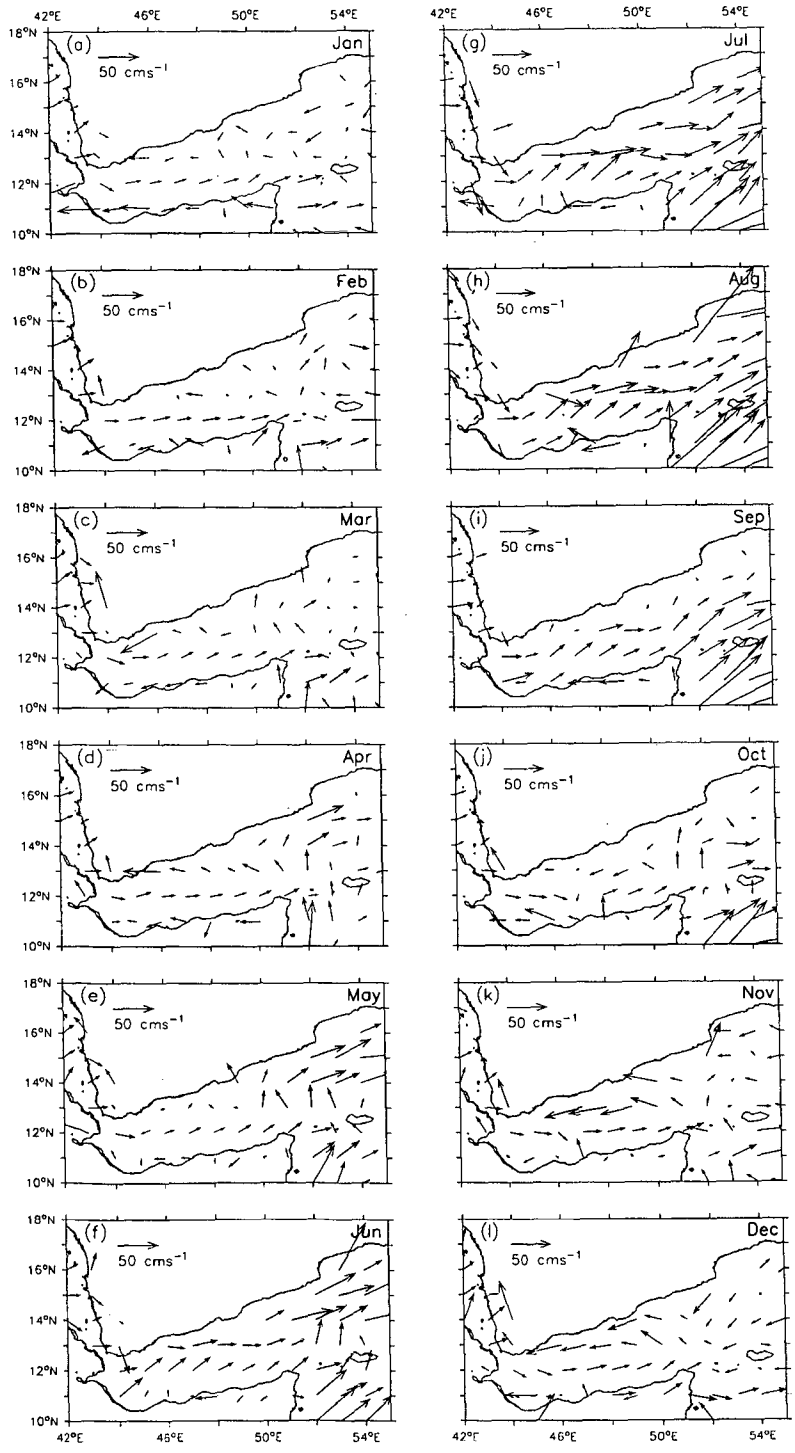

4.2 Surface currents

4.2.1 Ship drifts

Before the days of satellite–tracked floats and buoys and satellite-based altimeters and scatterometers, scientists relied on ship drift data to map the surface currents in the oceans. Here we have used the monthly climatology of ship drifts available from the National Oceanographic Data Center (NODC), NOAA on a spatial resolution of 1° longitude x 1° latitude to describe the surface circulation in the Gulf of Aden. Figure 4.1 shows the monthly climatology of ship drifts over the Gulf of Aden.

In November, a typical winter month, westward flows are observed in the northern gulf and eastward flows are observed in the mid and southern gulf. The flows along the southern coast are weak; eastward in the east (east of 48° E) and westward in the west (west of 45° E). The westward flow in the northern gulf appears to be stronger than the eastward flow. Similar patterns continue in December. The magnitude of the westward flow in December is $\sim$ 30 cm s^{-1} whereas the eastward flow in the south is about 20 cm s^{-1} (Figure 4.1l). During January–March the flows continue to follow the same pattern with a westward flow along the northern side and an eastward flow in the middle. However, during these months, the traces of weak westward flow seen in November–December along the southern coast extend all along the coast. In April–May, the pattern continues but with weaker magnitudes (Figure 4.1d, and e).

In June when the summer monsoon establishes over the gulf, flows along the northern and southern boundaries undergo a complete reversal. The eastward flows get established all over the gulf during June–September. Their magnitude peaks in July–August to 40–50 cm s^{-1} (Figure 4.1g and h). During this period, the flows outside the gulf, in the adjacent northwestern Arabian Sea, are stronger than that inside the gulf. In October, the period of transition from summer to winter, the flows diminish and reverse direction along the northern and southern coasts (Figure 4.1j).

In summary, the ship drifts clearly capture the annual cycle of reversing surface currents in the Gulf of Aden. During the summer monsoon, a strong eastward current is established all over the gulf. Whereas during the winter monsoon the westward currents are seen along the northern and southern coasts with eastward flows in the middle.

4.2.2 Ekman Drift

Wind stress is communicated to the ocean surface layer through viscous (frictional) processes that extend several tens of meters into the ocean. For time scales longer than inertial periods, the response is strongly affected by Coriolis acceleration. This wind–driven frictional layer is called the "Ekman layer". The wind drag acting on the Ekman layer tries to push the water in the direction of the wind, but the Coriolis force, which is the only other force involved, must balance the wind drag therefore must be equal in magnitude but opposite to the wind drag. The net effect of these two forces deflects the surface currents at 45° to the right (left) of the wind in the northern (southern) hemisphere. Such currents arising due to the direct effect of winds at the surface are called Ekman drifts.

The surface Ekman drift was computed using the Ekman spiral method described in Pond and Pickard [1983]. Following this method, the zonal (u) and meridional (v) velocities were estimated as:

$$u = \frac{\tau_x}{\rho_0\sqrt{A|f|}}\sin(45) + \frac{\tau_y}{\rho_0\sqrt{A|f|}}\cos(45) \tag{4.1}$$

$$v = -\frac{\tau_x}{\rho_0\sqrt{A|f|}}\cos(45) + \frac{\tau_y}{\rho_0\sqrt{A|f|}}\sin(45) \tag{4.2}$$

where τ_x, τ_y are the magnitudes of the wind stress in zonal and meridional directions respectively, A is the vertical eddy diffusivity, ρ_0 is the average density of seawater, and $|f|$ is the magnitude of the Coriolis parameter. We used $A = 10^{-2}m^2s^{-1}$ [Hastenrath and Greischar, 1991].

Figure 4.2 Climatology of surface Ekman drifts (cm s^{-1}) in the Gulf of Aden and northwestern Arabian Sea. The Ekman drift was estimated using the QuikSCAT wind climatology for the period 1999-2006.

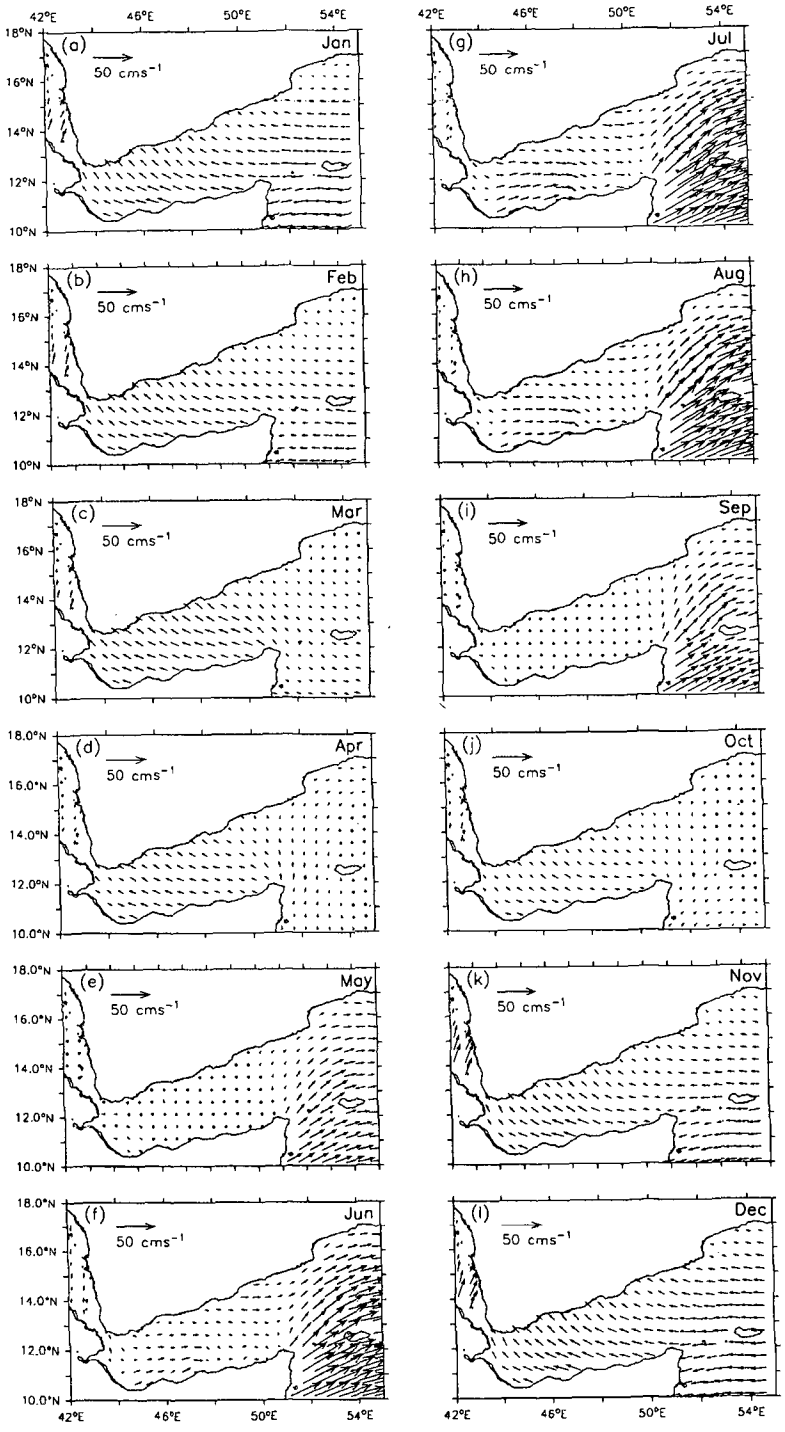

Figure 4.2 shows the climatology of surface Ekman drift over the Gulf of Aden and adjoining northwestern Arabian Sea estimated using the QuikSCAT wind climatology for the period 1999–2006. In November, when the winter monsoon establishes over the gulf, the Ekman drift in the Gulf of Aden and the adjacent northwestern Arabian Sea is towards the west. The winter monsoon peaks in December–January with northeasterly winds over the Arabian Sea and Gulf of Aden. The associated westward Ekman drift also strengthens ($\sim$ 20 cm s^{-1}). It is westward over the eastern gulf (east of 48° E) and the adjacent northwestern Arabian Sea but veers towards the northwest over the western gulf (west of 48° E). This winter monsoon pattern continues till February–March over the northwestern Arabian Sea and till April over the gulf but with weaker magnitude. In fact, the westward drift, though weaker ($<$ 10 cm s^{-1}) , starts in October (Figure 4.2j) before the establishment of winter monsoon winds over the gulf and adjacent Arabian Sea. Hence, in general, the winter pattern of Ekman drift (westward drift) sets over the gulf in October and continues till April.

The summer monsoon sets over the northwestern Arabian Sea towards the end of May with southwesterly winds and strong Ekman drifts towards the northeast (20 cm s^{-1}). But the Ekman drifts over the gulf remain weak ($<$ 5 cm s^{-1}) due to weak winds (Figure 4.2e). The summer monsoon pattern strengthens during June over the Arabian Sea as well as over the gulf (Figure 4.2f). Over the gulf, the eastward drift has a magnitude $\sim$ 15 cm s^{-1} , when the northeastward drift is much stronger ($\sim$ 40 cm s^{-1}) over the northwestern Arabian Sea. In July–August, the peak of the summer monsoon, eastward Ekman drifts reach $\sim$ 20 cm s^{-1} over the gulf and $\sim$ 80 cm s^{-1} over the adjacent northwestern Arabian Sea. Similar drift magnitudes were observed earlier [Shankar et al., 2002] using Hellerman and Rosenstein [1983] wind stress also. The summer monsoon pattern vanishes over the gulf in September though it continues to prevail over the northwestern Arabian Sea (Figure 4.2i).

During the summer monsoon, Ekman drift over the Gulf of Aden is weaker than that

over the northwestern Arabian sea. The Ekman drift over the gulf is favourable for upwelling along the northern coast during summer monsoon and it is favourable for upwelling along the southern coast during the winter monsoon.

In summary, similar to ship drifts, the Ekman drifts over the Gulf of Aden undergo a complete reversal in response to the reversing monsoonal winds. However, unlike the ship drifts, the Ekman drifts are unidirectional all over the gulf.

4.2.3 Geostrophic Currents

In the oceans at time scales longer than several days and at spatial scales longer than several kilometers, the balance of forces in the horizontal is between the pressure gradient force and the Coriolis force. This is called "geostrophic balance" or geostrophy. When the flow is geostrophic, forces and accelerations other than the pressure gradient and Coriolis force become negligible . Under geostrophic balance, the pressure gradient forces the water parcel to move from high to low pressure, but Coriolis force moves the parcel off to the right (left) in the northern (southern) hemisphere. In a steady geostrophic state, the water parcel moves exactly perpendicular to the pressure gradient force. The vertical force balance that always goes with geostrophy is hydrostatic balance. The vertical pressure gradient force, that points upwards from high pressure to low pressure, is balanced by gravity, that points downward.

The mathematical expression for the geostrophy is

$$-fv = -\frac{1}{\rho_0}\frac{\partial P}{\partial x} \tag{4.3}$$

$$fu = -\frac{1}{\rho_0}\frac{\partial P}{\partial y} \tag{4.4}$$

and the hydrostatic balance is

$$0 = -\frac{\partial P}{\partial z} - \rho g \tag{4.5}$$

Here f is the Coriolis parameter, u,v are the components of the horizontal velocity, ρ and ρ_0 are the density and a constant reference value respectively, x, y, z denote Cartesian coordinates with z oriented upward, and P is the pressure.

In this study, we have estimated the geostrophic currents using two datasets, a satellite bound altimeter derived sea level anomaly and a climatology of hydrography (1923-2005). The detailed descriptions of the data sets are available in Chapter 2. The motion is assumed to be zero at 1000 m level (level of no motion) for the purpose of geostrophic computation using hydrographic data. The merged altimeter data (TOPEX/Poseidon, ERS-1/2), available in the spatial resolution of 0.3° x 0.3° degrees at weekly intervals for 11 years (1993–2003) is used to construct the monthly climatology of sea level anomaly. The sea level anomaly is then used to compute the geostrophic currents following

$$u = -\frac{g}{f\rho}\frac{\partial \eta}{\partial y} \tag{4.6}$$

$$v = \frac{g}{f\rho}\frac{\partial \eta}{\partial x}, \tag{4.7}$$

To derive the geostrophic currents (relative to 1000 m level) from hydrographic data set, first a monthly climatology of the available hydrographic data (temperature and salinity spanned over a period of 82 years during 1923–2005) was prepared on 0.5° longitude x 0.5° latitude spatial grids as described in Chapter 2. The monthly climatology was then used to derive the geostrophic currents following the procedure detailed in Pond and Pickard [1983].

The surface geostrophic currents derived from both data sets, altimeter SLA and hydrography, are shown in (Figure 4.3). The region west of 45° E is not covered by the hydrography derived geostrophic currents, because the currents are estimated with reference to 1000 m and the region west of 45° E is shallower than 1000 m. Unlike the

ship and Ekman drifts, the geostrophic currents show large spatial variations; often they are dominated by cyclonic and anticyclonic eddies. In Figure 4.3, the locations of these eddies are marked as C (cyclonic) and A (anticyclonic).

The geostrophic currents derived from the hydrographic data and from the altimeter SLA , show similar patterns over the Gulf of Aden. Prior to the establishment of winter, in October, the geostrophic currents derived from both data sets (Figure 4.3j) show the dominance of 3 eddies; an anticyclonic eddy (A1 at 52° E) in the east and two cyclonic eddies (C1 at 48° E and C2 at 45.5° E) inside the gulf. The C1 and C2 eddies are separated by a distance of $\sim$ 150 km in both data sets. In November, the western most eddy C2 disappears and C1 appears further west (47° E) but as a larger eddy covering most of the gulf (Figure 4.3k). The expansion of C1 eddy prompts westward currents along the northern coast and eastward currents along the southern coast. The magnitude of these currents along the northern and southern boundaries are $\sim$ 20–30 cm s^{-1}. The A1 eddy also moves further west (51.5° E) as seen in altimeter SLA, but is not seen clearly in the hydrographic data. As the eddy A1 moves towards the west, another cyclonic eddy C3 appears outside the gulf at 54° E. This eddy is seen in both data sets. The November pattern repeats in December and January except for the apparent shift of eddies C1, A1 and C3. Also, a new anticyclonic eddy (A2) appears in the east, just outside the gulf, between the longitudes 52.5° E and 54.5° E (Figure 4.3l and a). The eddy (A2) is seen in the hydrographic data in December and in the altimeter SLA in January. However, the strength of the currents diminishes ($\sim$ 20 cm s^{-1}) in January than that in November–December. The strength of the geostrophic currents further diminishes in February ($\sim$ 10–15 cm s^{-1}) though the eddies continue to dominate the flow field (Figure 4.3b). All eddies (C1, C3, A1 and A2) seen during November to January continue to exist with less vigour. The eddy pattern dominates the flow field in March–April with weaker geostrophic currents ($\sim$ 10 cm s^{-1}). The C1 eddy seen in March is not seen in April. All other eddies A1, C3 and A2 are seen with a westward shift. Alternate cyclonic and anticyclonic eddies force a

meandering flow pattern in March.

The eddy field strengthens again in May (Figure 4.3e). The altimeter SLA shows three anticyclonic eddies in a row, two inside the gulf (A1 and A3) and one in the east of the gulf (A2). But the hydrographic data shows a cyclonic eddy (C1) inside the gulf in the west in place of A1 in the altimeter SLA.

In June, when the summer monsoon becomes active over the gulf and adjoining north-western Arabian Sea, the eddy fieled also gets strengthened further. An anticyclonic eddy dominates the entire gulf; it appears as a large single eddy in the altimeter SLA derived geostrophy and as two anticyclonic eddies (A1 and A3) in hydrography. Also another anticyclonic eddy (A2) is seen outside the gulf at 54° E in both data sets. The altimeter SLA derived geostrophy also shows a cyclonic eddy extending towards the gulf from the Somali coast, but not clear (C4) in the hydrography due to the absence of data in that region. The geostrophic currents associated with the anticyclonic eddy inside the gulf are towards the east along the northern coast and towards the west along the southern coast.

The anticyclonic eddy (A1) inside the gulf strengthens further in July and the magnitude of associated eastward currents along the northern coast exceeds 50–60 cm s^{-1}. But the size of the eddy reduces than that in June. The cyclonic eddy (C4) extends further north touching the northern coast of the gulf. Due to the presence of this cyclonic eddy, the eastward flows along the northern coast deflect southeastwards when they arrive at the western flank of the cyclonic eddy (Figure 4.3g). The anticyclonic eddy seen outside the gulf strengthens further in both data sets.

In August, the anticyclonic eddy (A1) shrinks further and weakens leading to the weakening of associated geostrophic currents ($\sim$ 40 cm s^{-1}). Also, the cyclonic eddy C4 seen in the east of A1 expands towards the west as well as towards the east along the northern coast. The sea level also drops (by about 10 cm) in the west of A1 in both data sets; but the drop in sea level has not manifested as a cyclonic eddy. The existence of low sea level interspaced with high sea level (A1) manifests as a meandering eastward flow in

Figure 4.3 Geostrophic currents (cm s^{-1}) at surface derived from the monthly climatology of hydrography (left panels) and altimeter derived SLA (right panels). The colour shades on the left panels represents the dynamic topography (dyn cm) (0/1000) and the colour shades on the right panels show the SLA (cm). The basin–wide mean (147 dyn cm) is removed from the dynamic topography field to represent the dynamic topography and SLA in same scale. C(A) denotes cyclonic (anticyclonic) eddy.

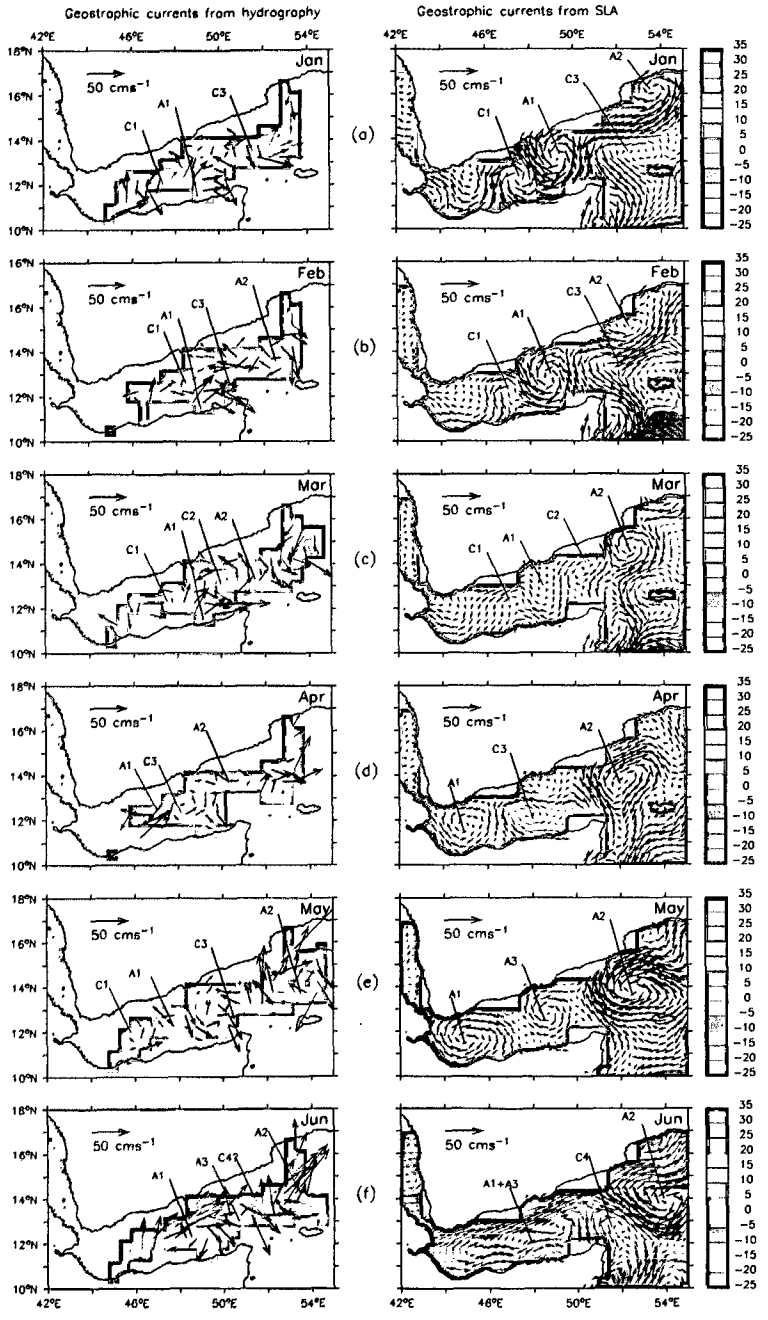

Figure 4.3 (Continued)

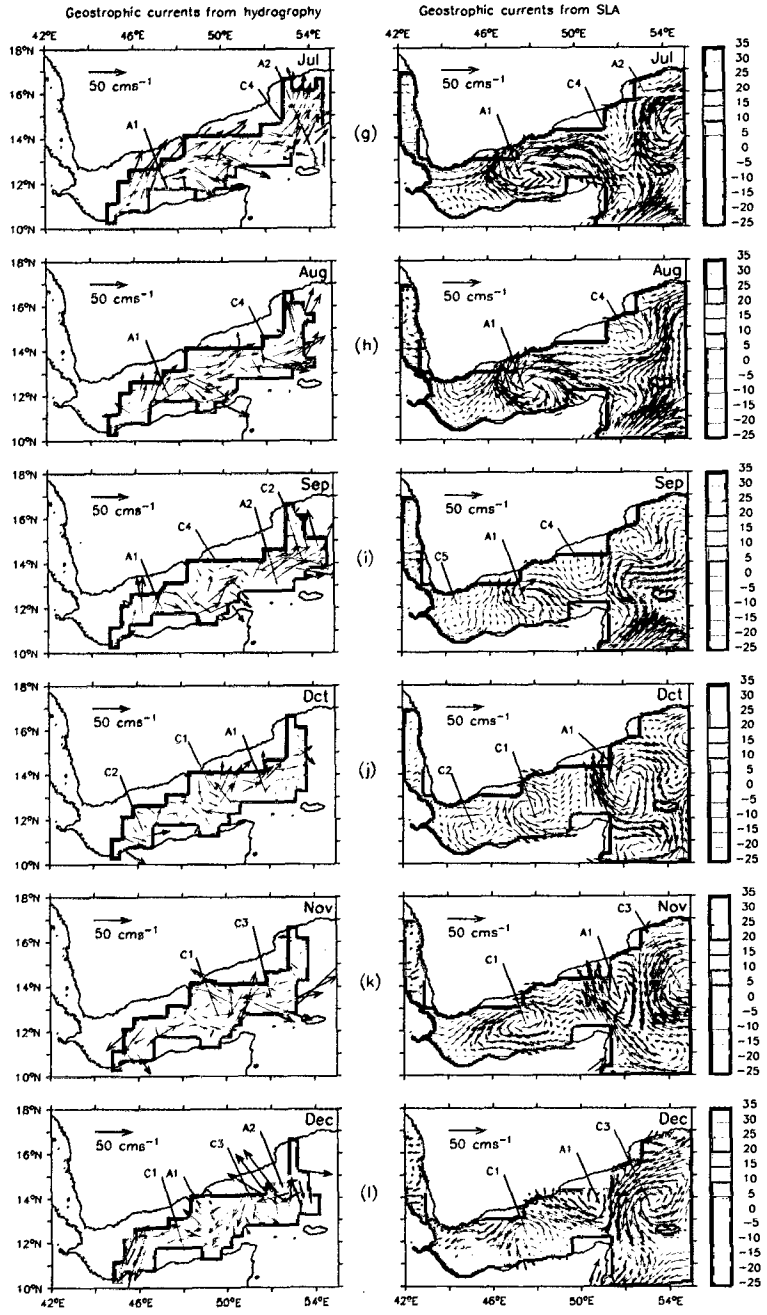

the Gulf of Aden (Figure 4.3h). A similar situation prevails in September also but with weaker geostrophic velocities. The anticyclonic eddy A1, seems to have shifted towards the west from its position at 48° E to 47.5° E. Similarly, the core of the cyclonic eddy, C4 also seems to have shifted towards the west from 52° E to 50.5° E.

In summary, the geostrophic currents in the Gulf of Aden are composed of several cyclonic and anticyclonic eddies and the flow directions along the coasts change depending on the type of eddy that appears in its vicinity. More eddies are seen during winter than in summer, but the geostrophic flows reach their peak in the summer monsoon season in July. The geostrophic currents derived from the altimeter SLA and the hydrography seem to be in good agreement with each other. The type of eddies, their position etc match well in both data sets. The magnitude of geostrophic velocities derived from the altimeter derived SLA, however, cannot be compared with those derived from hydrography because the geostrophic velocities estimated from the hydrographic data are relative to the level of no motion (in this case 1000 m level).

The good match between the geostrophic currents at the surface derived from altimeter derived SLA and hydrography allow us to use either of them to describe the net currents at the surface (geostrophy+Ekman). To derive the net currents at the surface of the Gulf of Aden we chose to use the altimeter SLA derived geostrophic currents and the Ekman drifts presented in 4.2.2. The choice of altimeter SLA derived geostrophic currents over the hydrography derived is made because of its better spatial coverage and resolution.

Similarly, the good match between the geostrophic currents derived from altimeter measured SLA and hydrography gives confidence in using hydrography to describe the geostrophic currents in the deeper layers. Hence, we have used the geostrophic currents derived from hydrography to describe the circulation in the deeper layers.

4.2.4 Net surface currents in the Gulf of Aden

The net flows at the surface of the Gulf of Aden (the sum of Ekman drift and geostrophic current derived from altimeter SLA) are shown in Figure 4.4.

During the transition between summer and winter monsoons, in the month of October, the net surface flows in the gulf are punctuated with three well marked eddies; two cyclonic (C1 and C2) and an anticyclonic (A1) at the entrance to the gulf (Figure 4.4j) as seen in the geostrophic flows (Figure 4.3j). Clearly, during October, the flows are primarily geostrophic all over the gulf with westward flows along the northern boundary and weak eastward flows along the southern boundary (Figure 4.4j). The westward flow continues towards the Red Sea through Bab el Mandab. Near the entrance of the gulf, between C2 and A1, the flows are towards the west contributed by both geostrophy and Ekman drift. The azimuthal velocities in the anticyclonic eddy (A1) are $\sim$ 30–40 cm s^{-1}.

In November when the winter monsoon establishes over the Gulf of Aden and the northwestern Arabian Sea, the eddy C2 disappears and the eddies C1 and A1 appear further west from their October positions. Another cyclonic eddy (C3) appears east of A1 in the northwestern Arabian Sea. Inside the gulf, the strong westward flows get established in the northern part of the gulf due to the strengthening of Ekman drift while the eastward flow along the southern part is weak (Figure 4.4k). The surface flow towards the Red Sea strengthened during this month. In the east, the flows strengthen as northwestward flows along the western flank of A1.

The westward flow inside the gulf strengthens during December and the eddies shrink considerably. The eddy C1 is squeezed towards the south and A1 towards the north (Figure 4.4l) due to the strengthening of westward Ekman drift (Figure 4.2l). The flow towards the Red Sea through the Bab el Mandab also strengthens. The flow entering the gulf from the northwestern Arabian Sea is strong and towards the southwest.

During January and February, as the westward flows continue inside the gulf, the anticyclonic eddy (A1) gets better organised at 49° E. (Figure 4.4a). At the western most

part of the gulf, near the Bab el Mandab, the flows are northwestward towards the Red Sea. In the east, at the entrance to the gulf, under the influence of the anticyclonic eddy, strong westward flows are seen in the northern half and weak southeastward flows are seen in the southern half. Outside the gulf, in the northwestern Arabian Sea, the flow is similar to that in December. Along the Arabian coast another anticyclonic eddy (A2) is seen between 53° E and 55° E.

In March–April, the transition between the winter monsoon and the summer monsoon, the geostrophic currents weaken inside the gulf and the Ekman drifts dominate the westward flows (Figure 4.4c and d). The westward flow towards the Red Sea continues during these months also. The anticyclonic eddy (A1) seen during January–February is not seen in March, but appears as a weakly formed eddy in April. Near the entrance, the northeasterly geostrophic flow is modified by the westward Ekman drift. The anticyclonic eddy (A2) which appeared in January–February near the Arabian coast is well formed and shifts towards the southwest.

The month of May is punctuated by a row of three anticyclonic eddies, A1, A3 and A2. It is not clear whether A3 was a new formation or the manifestation of A2 that moved westward. In that case, the eddy marked as A2 in Figure 4.4e will not be the same eddy as that seen in March–April. At this stage, we will not go into the details of these eddies because Chapter 5 describes them in detail. The flows during this month are eddy centric; eastward flows along the northern coast with a discontinuity at 47.5° E and westward flows along the southern coast with a discontinuity at 48° E. May is the month of the pre–summer monsoon, which means the geostrophic currents dominate with eastward flows along the northern side and westward currents along the southern side of the gulf. In the east, near the entrance, the flows are either northward or northwestward under the influence of anticyclonic eddy (A2). Outside the gulf in the northwestern Arabian Sea the flows have strengthened ($\sim$ 30–40 cm s^{-1}) due to the strengthening of Ekman drift.

In June when the summer monsoon establishes over the Gulf of Aden and the north-

Figure 4.4 Net surface flow (cm s^{-1}) computed as the sum of Ekman drift (Figure 4.2) and geostrophic currents at the surface derived from SLA (Figure 4.3).

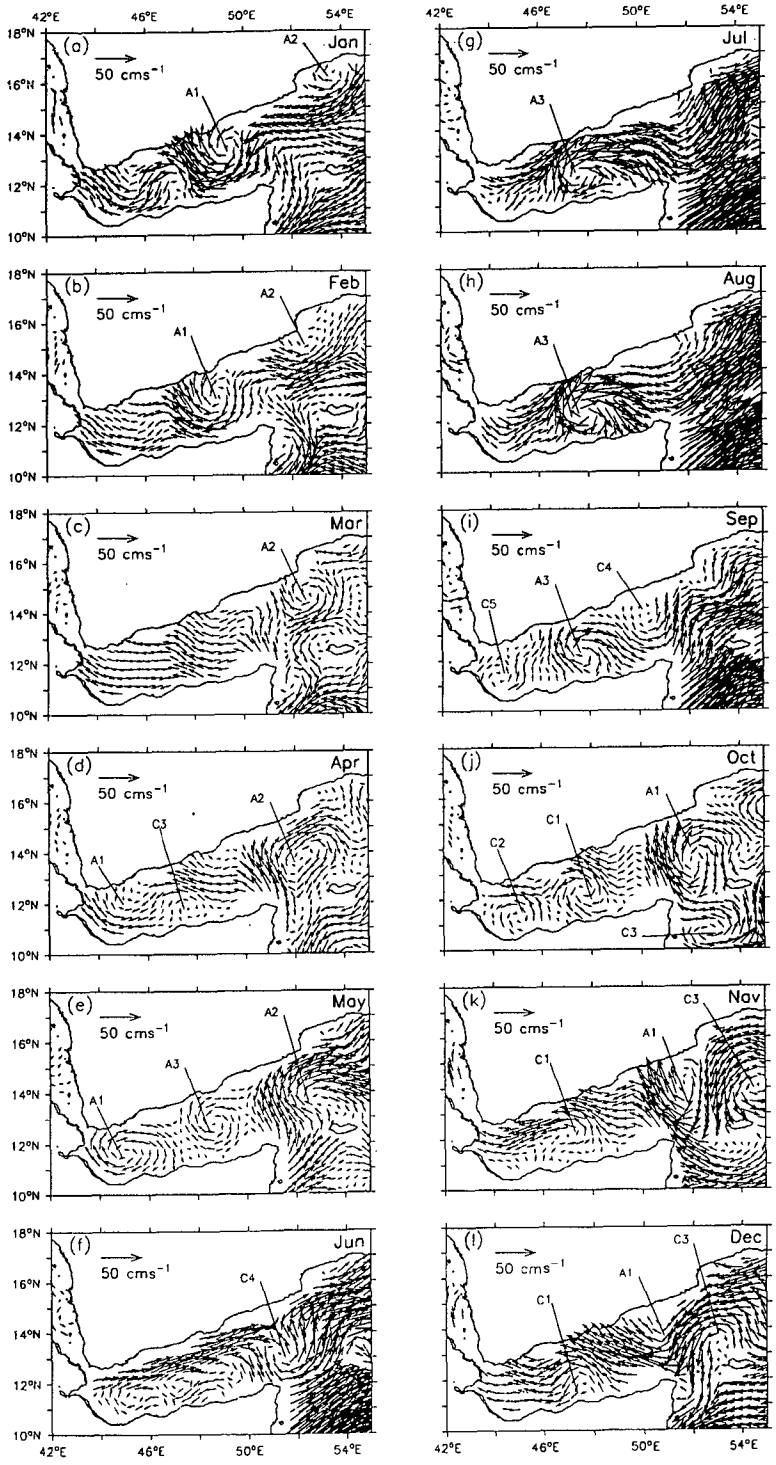

western Arabian Sea, strong eastward (30–40 cm s^{-1}) flows develop in the northern half of the gulf. In the southern half, the westward flows embedded with micro-eddies (not particularly identified) are weak (Figure 4.4f) due to the eastward Ekman drifts (Figure 4.2f) and the weak geostrophic currents (Figure 4.3f). At the entrance of the gulf, a cyclonic eddy (C4) is seen. That seems to be due to the combination of Ekman drift and geostrophy.

During July–August, the summer monsoon strengthens the associated surface flows dominated by the Ekman drift. Over the gulf, by and large, the flows are toward the east, except in the middle where the anticyclonic eddy (A3) generates a westward flow along the southern coast. The azimuthal velocities of A3 are in the range of $\sim$ 40–60 cm s^{-1} (Figure 4.4g and h). In the northwestern Arabian Sea, the northeasterly flows have the magnitude $\sim$ 80 cm s^{-1}.

During September the net surface flows weaken considerably, due to weak Ekman drifts inside the Gulf of Aden. As a result, the geostrophic currents (a row of three eddies C5, A3 and C4) dominate the flows inside the gulf (Figure 4.4i). However, the azimuthal velocities of eddy, A3 are weaker ($\sim$ 30–40 cm s^{-1}) than those in July–August. In the northwestern Arabian Sea, the flows continue in the northeasterly direction (Figure 4.4i) as those in July–August.

In general, during winter, the net flows are towards the west over most of the gulf with cyclonic and anticyclonic eddies embedded in it. This flow structure establishes in October and continues till April, mostly dominated by geostrophy. In May also, the geostrophy dominates the net surface flows because of weak Ekman drifts. During June, at the beginning of the summer monsoon, the flows are eastward in the northern half of the gulf and are westward along the southern half, whereas during the rest of summer monsoon, the flows are eastward all over the gulf.

4.3 Vertical structure of geostrophic currents

As discussed earlier, the geostrophic velocity derived from hydrgraphic data is used to describe the currents at two depth levels, 300 and 600 m. Also described is the vertical structure (from surface to 1000 m) of geostrophic currents across a section in the middle of the Gulf of Aden. For easy comparison, the geostrophic currents at the surface are also shown in Figure 4.5. The two depth levels 300 and 600 m are chosen because the core of Gulf of Aden Intermediate Water flows, more or less, at 300 m level and the core of Red Sea Water flows at around 600 m depth level (see Chapter 3 for a detailed description of water masses in the Gulf of Aden).

During October (Figure 4.5j) the geostrophic currents at 300 m and 600 m are punctuated with three eddies, two cyclonic (C1 and C2) and an anticyclonic similar to those at the surface. The westward flow along the northern side of the gulf and eastward flow along the southern side at 300 and 600 m seem to be similar to that at the surface. The geostrophic currents across the vertical section along the center of the gulf, shown in the bottom panel of Figure 4.5j, also confirm the penetration of eddies up to 1000 m.

In November, the westward flows along the northern side at the surface are repeated at 300 and 600 m. So are the cyclonic eddies C1 and C3 (Figure 4.5k). However, in addition to those two cyclonic eddies an anticyclonic eddy (A1) is also seen in the south central gulf at 300 and 600 m. The vertical section of geostrophic velocities shown in the bottom panel confirms the presence of cyclonic eddies to 1000 m.

In December, the westward currents are strong in the northern half of the gulf, but weaken at 300 and 600 m. However, the signature of the eddies seen at the surface are seen at both levels (Figure 4.5k). The banding structure of geostrophic currents shown in the vertical section (bottom panel) reaches as deep as 1000 m.

During January–March also, there are a row of eddies at the surface as well as in the deeper layers. The anticyclonic eddy, A1, is better developed in January than the cyclonic eddies C1 and C3. The cyclonic eddies are not easily identifiable at 300 and

600 m; they almost got masked in the low dynamic heights covering most of the gulf (Figure 4.5a). However, anticyclonic eddies (A1 and A2) hugging the southern coast are well identifiable at 300 and 600 m levels. Similarly, the band structure of the geostrophic currents, extending all over the water column (bottom panel) suggest the presence of eddies in the deeper layers. Whereas in February and March, the cyclonic eddy (C3) and the anticyclonic eddies (A1 and A2) seen at the surface extend to 600 m depth level. Similarly, the band structure in the vertical section of geostrophic velocities, also extends to about 1000 m depth (Figure 4.5b and c). Though the eddies extend over most of the water column, the geostrophic velocities associated with these eddies are much weaker than that at the surface (about 1/10 only). During both months, in the deeper regions (300 m and 600 m) the eastward flows along the southern side are stronger than the westward flows in the north.

During April, the geostrophic currents are still similar to the previous winter months (Figure 4.5d). They are embedded with a row of eddies in them. At the western part of the gulf, an anticyclonic eddy (A1) is seen only partly along the northern side due to lack of data. The cyclonic eddy (C3) seen in the center of the gulf at the surface, is not seen at 300 and 600 m. Instead another cyclonic eddy (C4) is seen at 300 and 600 m. This cyclonic eddy as well as the other eddies extend to about 900–1000 m depth as seen in the vertical section of geostrophic velocities shown in the bottom panel of Figure 4.5d.

The geostrophic circulation in May is characterized by the presence of three eddies (C1, A1 and C3) inside the gulf and one outside the gulf in the east (A2). The flows in the east are stronger than those in the west. Unlike the previous months, the flows in the north or south are not unidirectional. The flows switch from westward to eastward depending on their proximity to the eddies. The two cyclonic eddies (C1 and C3) seen at the surface are also seen at 300 and 600 m (Figure 4.5e). The anticyclonic eddy A1 sandwiched between the two cyclonic eddies (C1 and C3) also extends to 300 and 600 m depth levels. The anticyclonic eddy (A2) seen outside the gulf, at the surface, also extends to 600 m.

In the vertical section, most of the alternating bands of northward and southward flows extend from the surface to about 800–1000 m. The flows are strong in the upper 400 m.

In June, the summer monsoon establishes over the Gulf of Aden and northwestern Arabian Sea with eastward geostrophic flows all over the gulf (Figure 4.5f). The anticyclonic eddy (A1), that occupies most of the central region of the gulf at the surface, is seen at 300 and 600 m (Figure 4.5f). The anticyclonic eddy (A2) seen outside the gulf, in the east, also extends to 300 as well as 600 m. So does the cyclonic eddy C4.The vertical section of geostrophic velocities shows that the flows are strong in the upper 400 m.

In July, the pattern is similar to that in June; but the eastward flows at the surface as well as in the deeper layers strengthen further. Effectively, the geostrophic currents appear as meandering flows due to the presence of cyclonic and anticyclonic eddies (Figure 4.5g). The anticyclonic eddy (A1) seen at the surface is also seen in the deeper layers (Figure 4.5g). The eddies, C4 and A2 seen outside the gulf in the east are also seen at deeper layers.

The surface circulation pattern during August is also similar to that of July, with eastward flows all over the gulf. However, the geostrophic currents at 300 and 600 m are in the opposite direction to that at the surface (Figure 4.5h). At 300 m and at 600 m, the flows have reversed and are towards the west in the north and eastward in the south. Outside the gulf the cyclonic eddy (C4) seen at the surface extends to the deeper depths, but the weak anticyclonic eddy (A1) seen at the surface does not show up at deeper depths (Figure 4.5h). However, the alternate bands of geostrophic currents seen in the vertical section presented in the bottom panel indicate the effect of eddies in the deeper layers.

The flow structure in September (Figure 4.5i) is also similar to that in August with eastward flows at the surface and westward (eastward) flows on the northern (southern) sides at 300 m and 600 m. The two anticyclonic eddies (A1 and A2) and the cyclonic eddy (C4) seen at the surface are also seen at 300 and 600 m and beyond.

The vertical structure of the circulation in the Gulf of Aden as seen in the geostrophic

Figure 4.5 (a) Geostrophic currents derived from hydrography during January at surface, 300 m and 600 m levels. The colour shades in the upper three panels represent the dynamic topography (dyn. cm) with reference to 1000 m. The geostrophic currents (north–south) across the section, marked with a line in the upper panels, is also shown in the bottom panel. Different colour scales are used to highlight the presence of eddies.

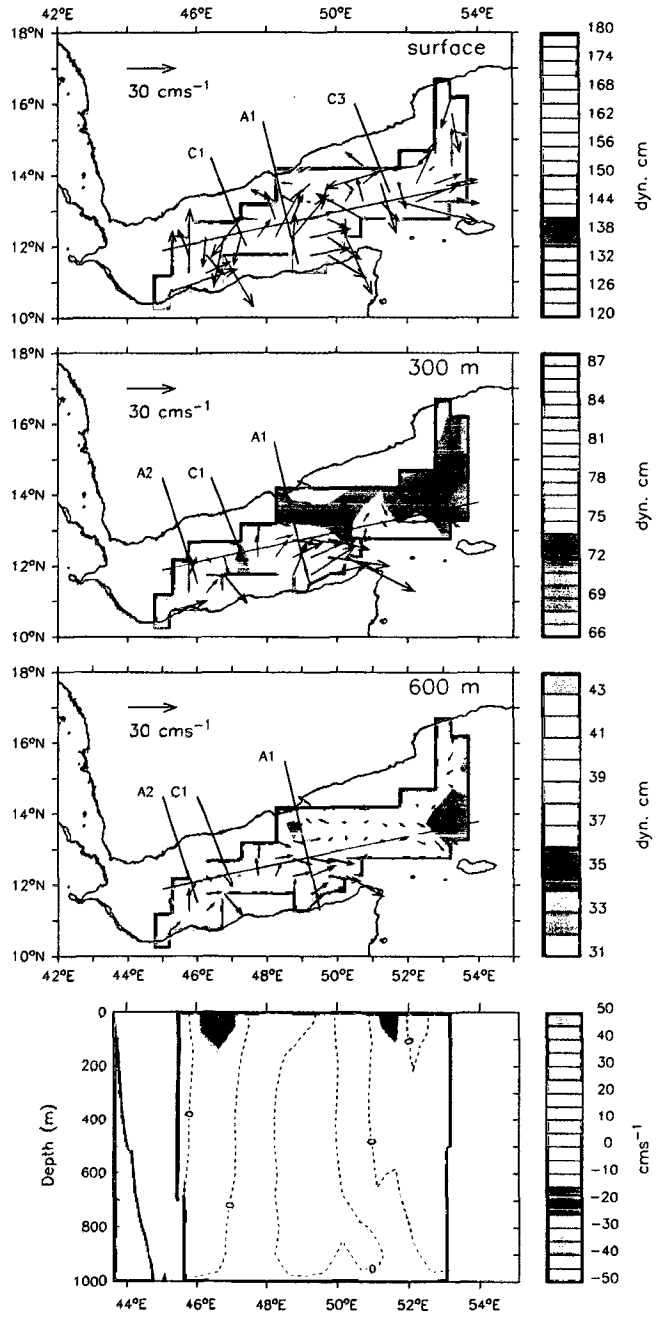

Figure 4.5 (b) Same as for 4.5a, but for the month of February

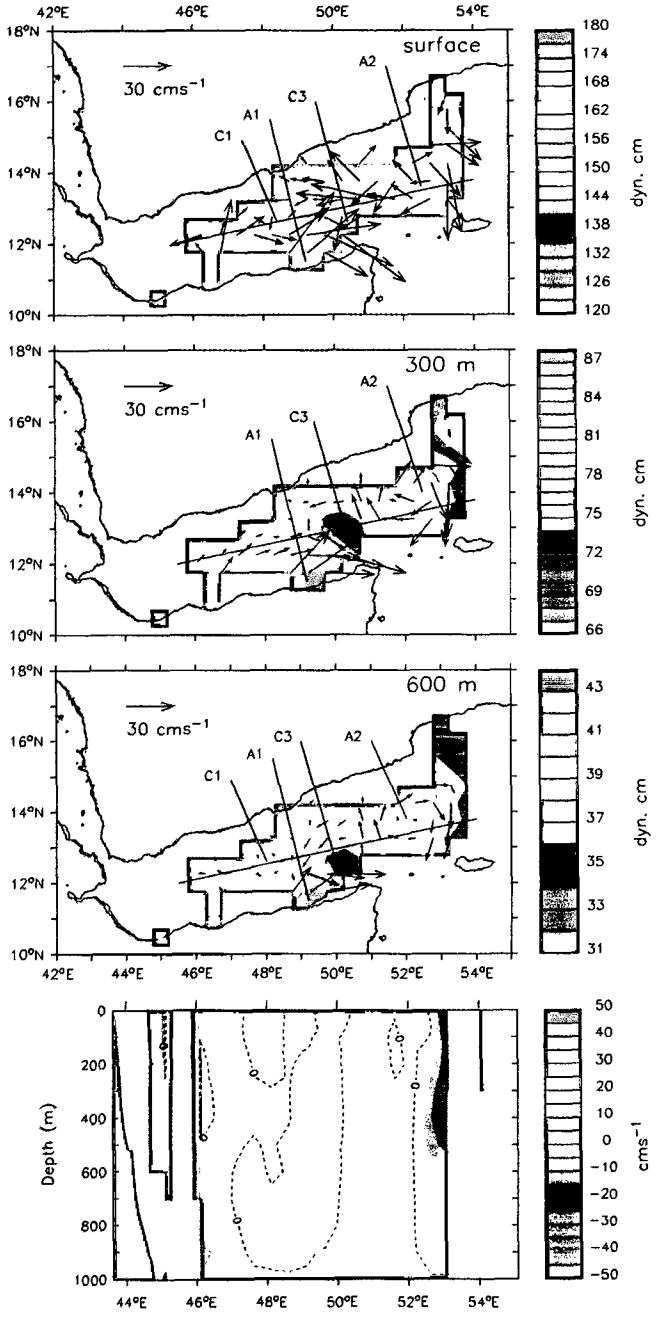

Figure 4.5 (c) Same as for 4.5a, but for the month of March

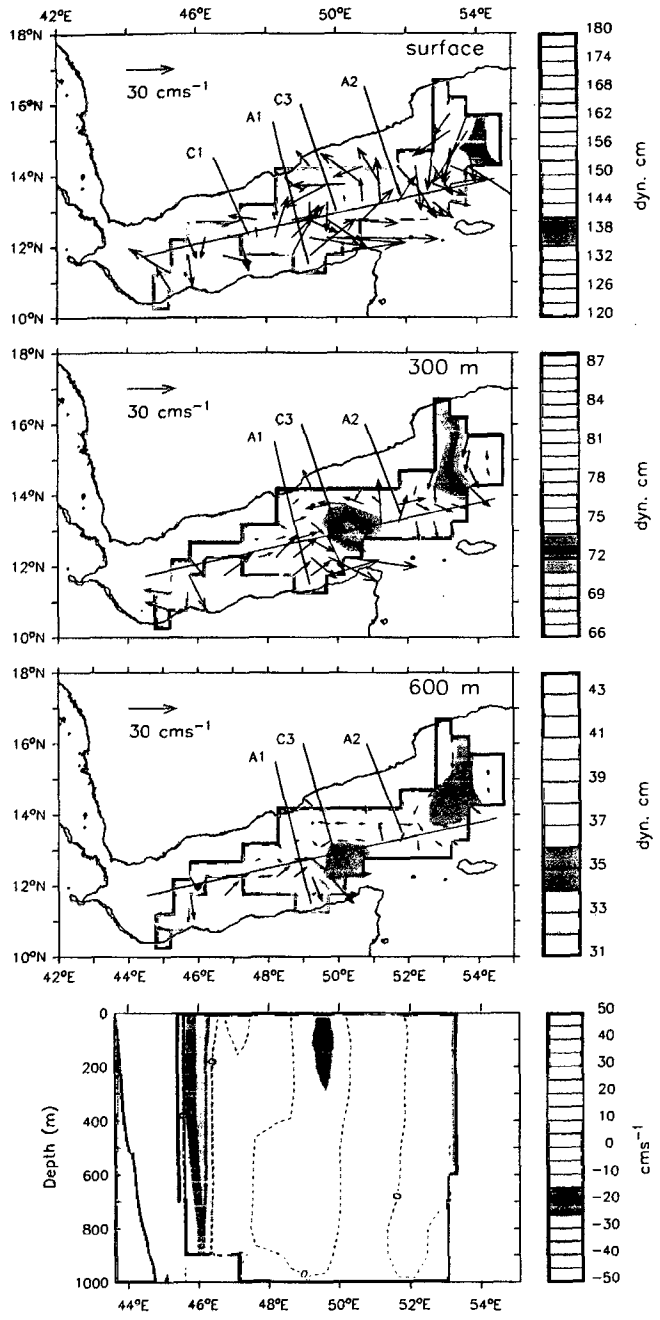

Figure 4.5 (d) Same as for 4.5a, but for the month of April

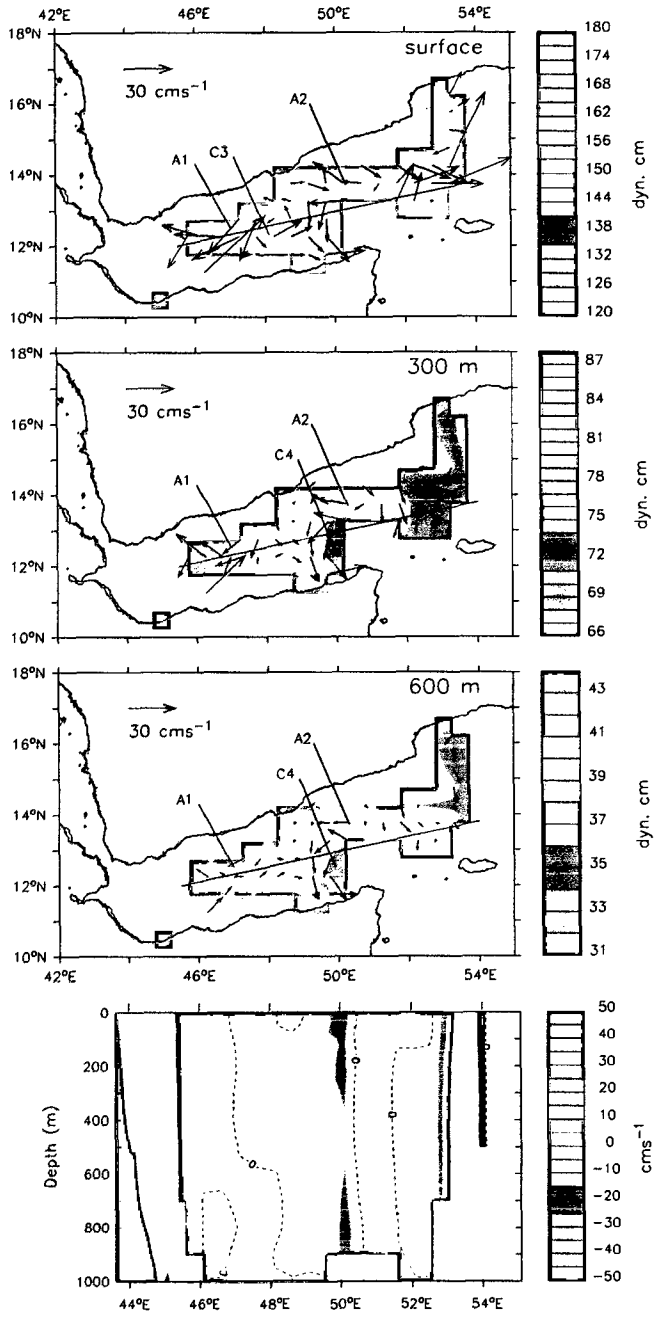

Figure 4.5 (e) Same as for 4.5a, but for the month of May

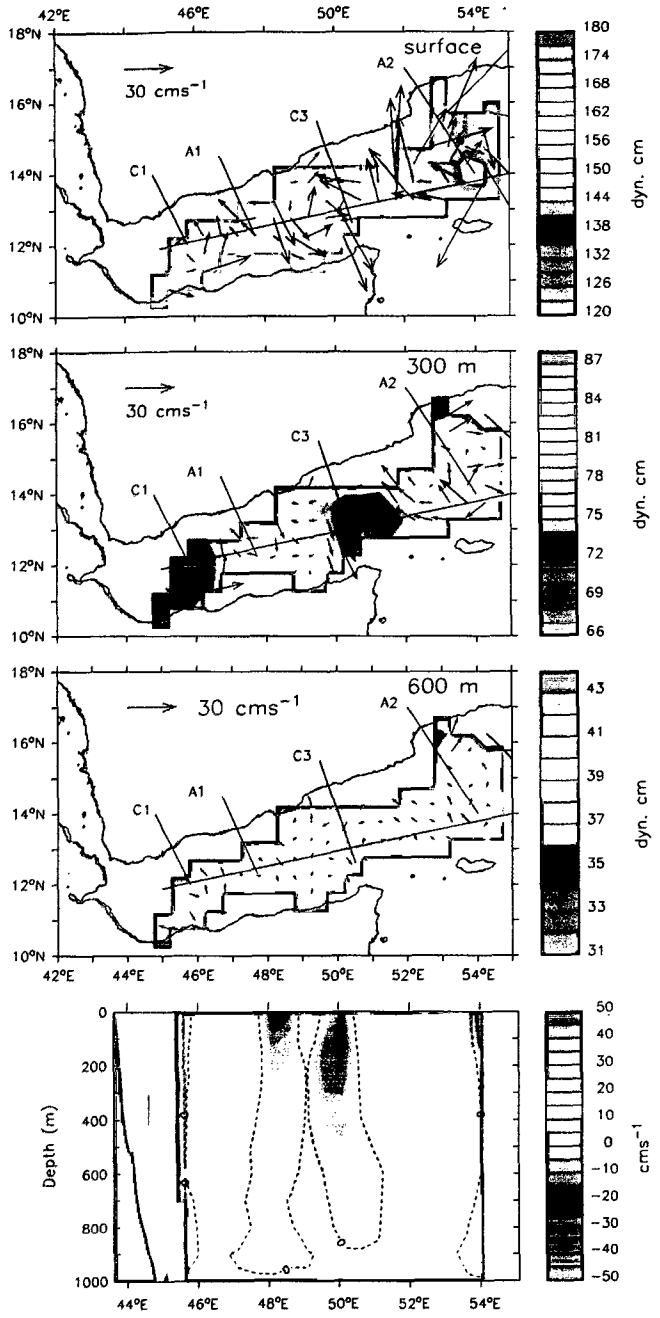

Figure 4.5 (f) Same as for 4.5a, but for the month of June

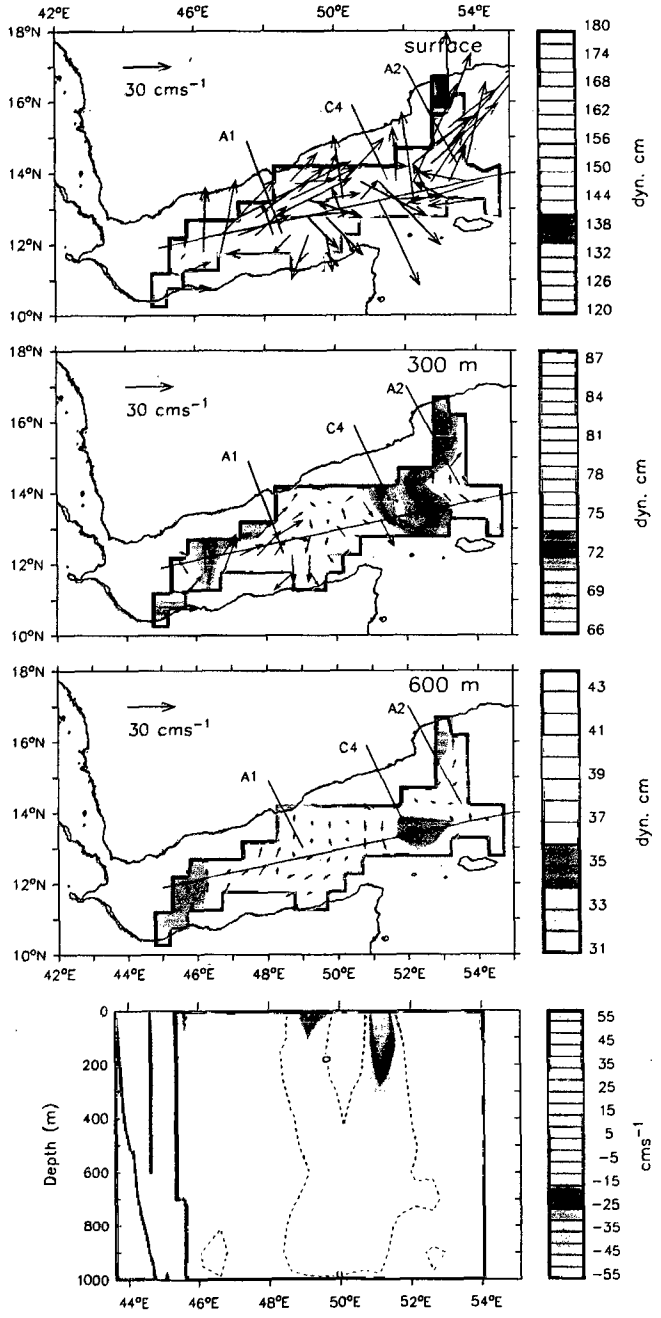

Figure 4.5 (g) Same as for 4.5a, but for the month of July

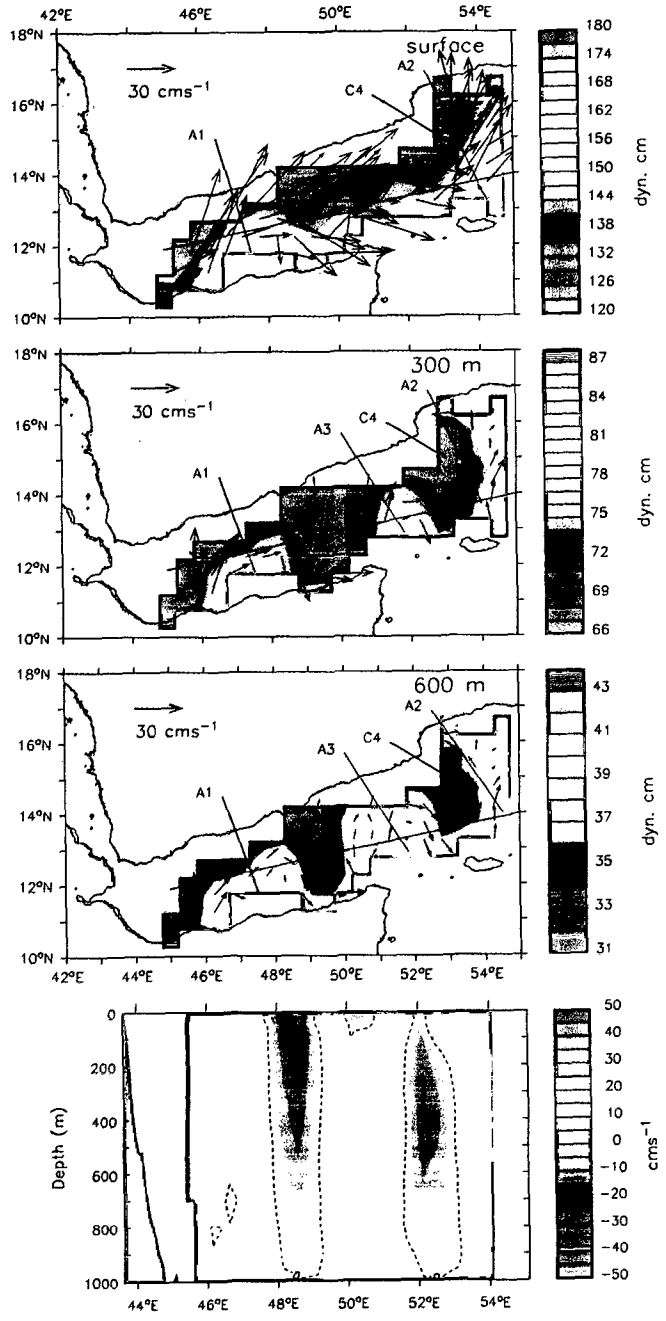

Figure 4.5 (h) Same as for 4.5a, but for the month of August

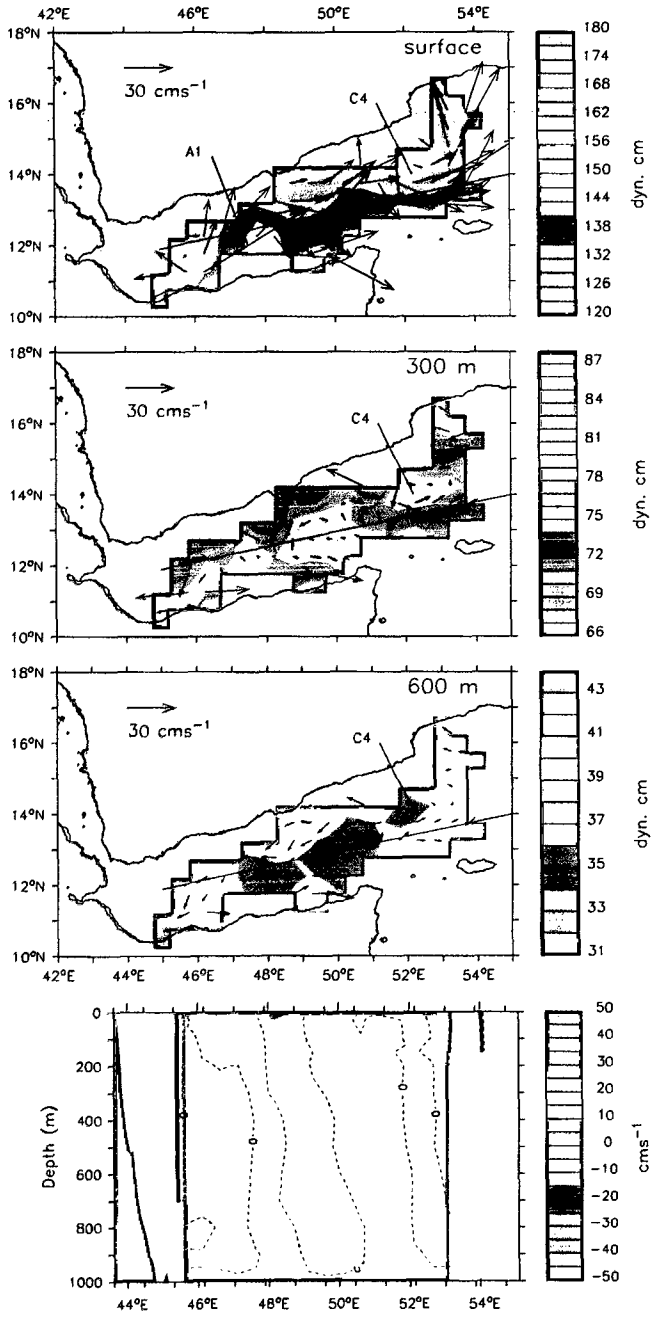

Figure 4.5 (i) Same as for 4.5a, but for the month of September

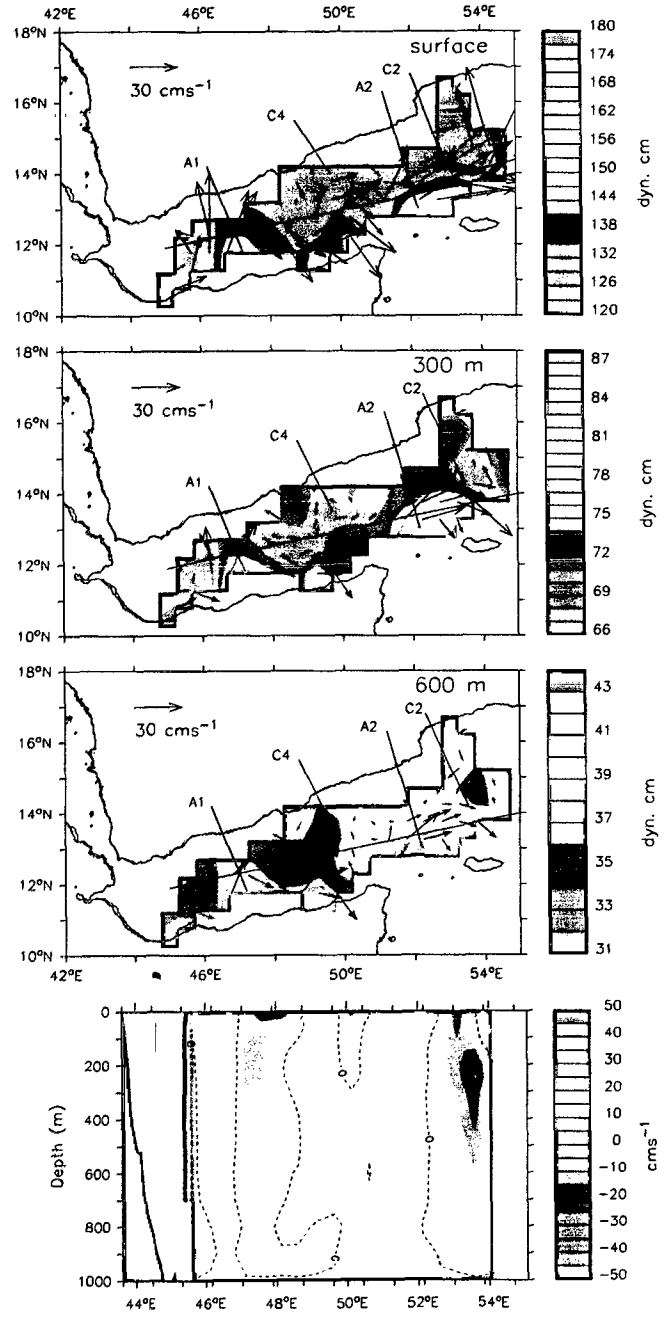

Figure 4.5 (j) Same as for 4.5a, but for the month of October

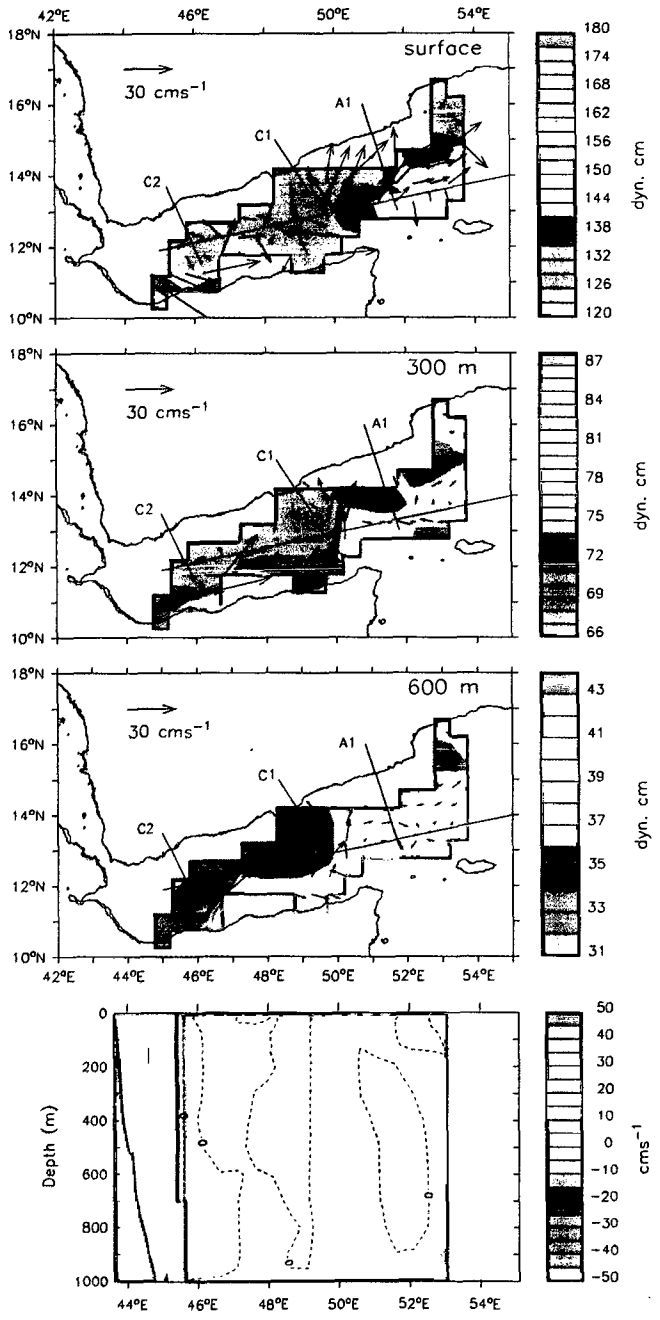

Figure 4.5 (k) Same as for 4.5a, but for the month of November

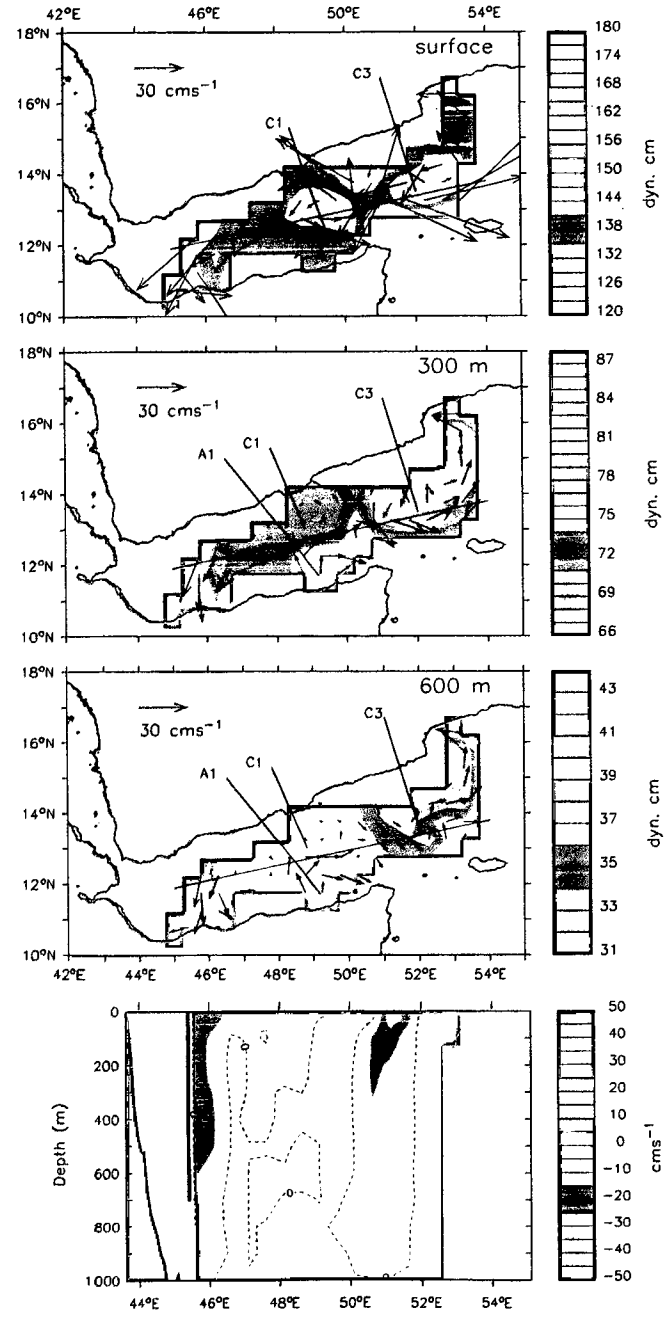

Figure 4.5 (l) Same as for 4.5a, but for the month of December

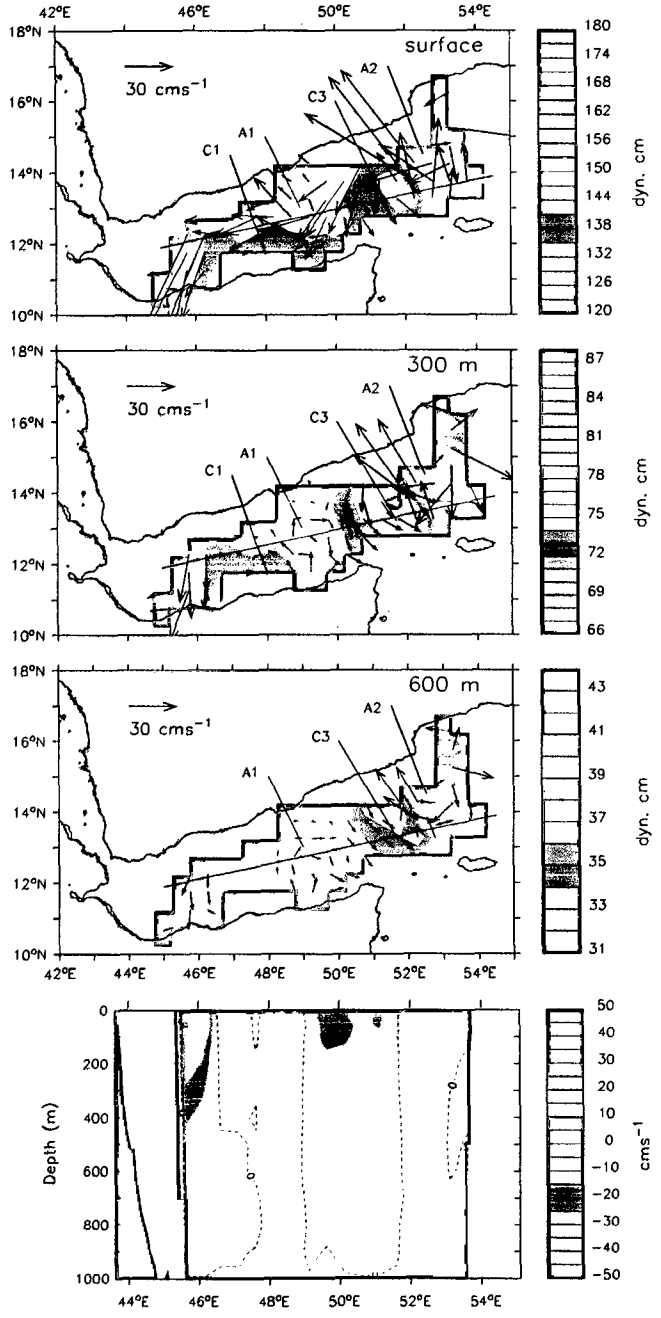

currents derived from hydrographic data are highly influenced by a row of eddies embedded in them. From the analysis, presented here, it is clear that the eddies seen at the surface, in hydrography as well as in the altimeter derived SLA, extend to deeper depths, often to 1000 m. During most of the months, the flows across the water column are unidirectional, except during August-September, when they show a partial reversal on the northern side. Here, the flows are toward the east at the surface and are toward the west at 300 and 600 m. In general, eastward flows exist across the water column during the summer monsoon (June–September) and westward flows exist in the winter monsoon (November–February). The flows during October as well as in March–April resemble the winter pattern. The flow directions during May, however, do not coincide with either the summer or winter monsoon patterns. They are highly cellular under the influence of eddies.

4.4 Interannual variability in the surface currents

Having analyzed the evolution of currents at the surface and in the deeper layers of the Gulf of Aden using the climatology of ship drifts, Ekman drifts, hydrography and altimeter derived SLA, in this section, we present the interannual variability of sea level as a proxy to the variability of geostrophic currents at the surface. For this purpose, the merged altimeter SLA for 11 years during the period 1993 to 2003 are used because that is the only data set available to carry out the analysis of interannual variability. The 11 year long SLA time series is a combination of signals with different time scales. The least resolved periodicity is determined by the repeat period of satellites and the largest resolved periodicity is determined by the length of the series. This implies that this series can resolve signals on the time scales from weeks to a few years (interannual scales).

Several techniques are available to resolve the signals at different periodicities hidden in a time series. Here, we use the wavelets to resolve the variabilities in SLA at different

time scales because that determines the dominant modes of variability and its variability in time. The wavelet technique has wide application in geophysical time series analysis [Foufoula-Georgiou and Kumar, 1995].

To determine the dominant modes of variability in the SLA time series we have used the Morlet wavelet described in Torrence and Compo [1998]. This method allowed us to estimate the wavelet power due to the variability in SLA at different periods ranging from high–frequency (2 weeks) to interannual (5 years) periods. To describe the spatial distribution of the variability in SLA time series, first, we have estimated wavelet power at each grid point of altimeter SLA. Figure 4.6a shows the wavelets at 5 locations, 2 inside the gulf and 3 in the northwestern Arabian Sea adjacent to the gulf. The wavelets significant at 95 and 99% confidence levels are also shown in Figure 4.6b and c. The annual and high–frequency signals were significant inside and outside the gulf, while the interannual signal was not significant inside the gulf (Figure 4.6). These wavelet powers, obtained at each grid point, were averaged over five frequency bands, namely, high-frequency (0.0333-0.00365 cycles per day or periods of 30-274 days), annual (0.00307-000258 cycles per day or 325-388 days) and three interannual bands namely biannual (0.00184–0.00129 cycles per day or 548–776 days), tri-annual (0.00108–0.00091 cycles per day or 922–1097 days) and quad–annual (0.00077–0.00064 cycles per day or 1305–1552 days) in time to represent the spatial variability as shown in Figure 4.7. Essentially, the wavelet power in the high–frequency band represents the magnitude of SLA oscillations at periods less than an year and the wavelet power in the annual band represents the magnitude of SLA oscillations at periods of around 1 year. Similarly, the wavelet power in the interannual band represents the oscillations in SLA at 18 months or more. The spatial variability shown in the middle and right columns of Figure 4.7 represents the averaged wavelet powers significant at 95% and 99% levels respectively.

As expected, the wavelet power in the SLA time series is highest ($> 2^{10}$ cm^2) and significant at 95 as well as 99% confidence levels in the annual band everywhere in the

Figure 4.6 (a) Time-scale representation of the wavelet powers spectrum (log scale) of the time sesies of altimeter derived SLA at the grid points centered at 46° E, 12° N (1), 50° E, 13° N (2), 53° E, 8° N (3), 53° E, 10° N (4), and 53° E, 14° N (5). Morlet wave transform was used to compute the wavelets using 11 years weekly spaced data set. The cone of influence aso is shown (the curved line). Wavelets having periods > 1300 days are not acceptable during any time.

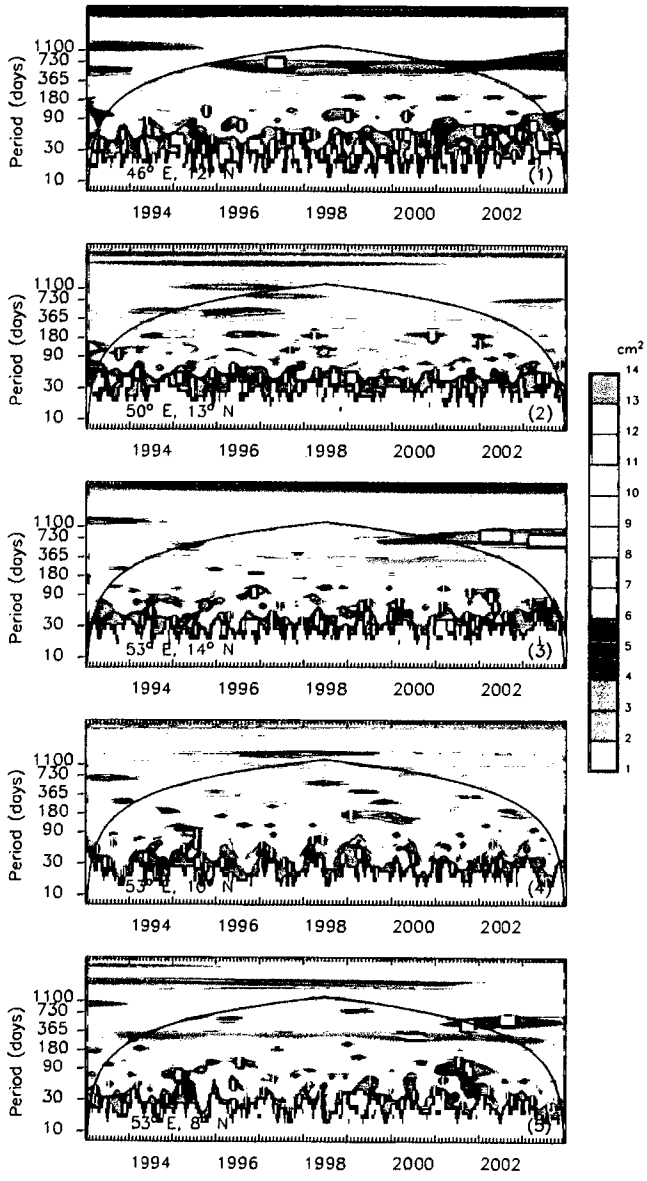

Figure 4.6 (b) same as 4.6a for confidence level at 95%

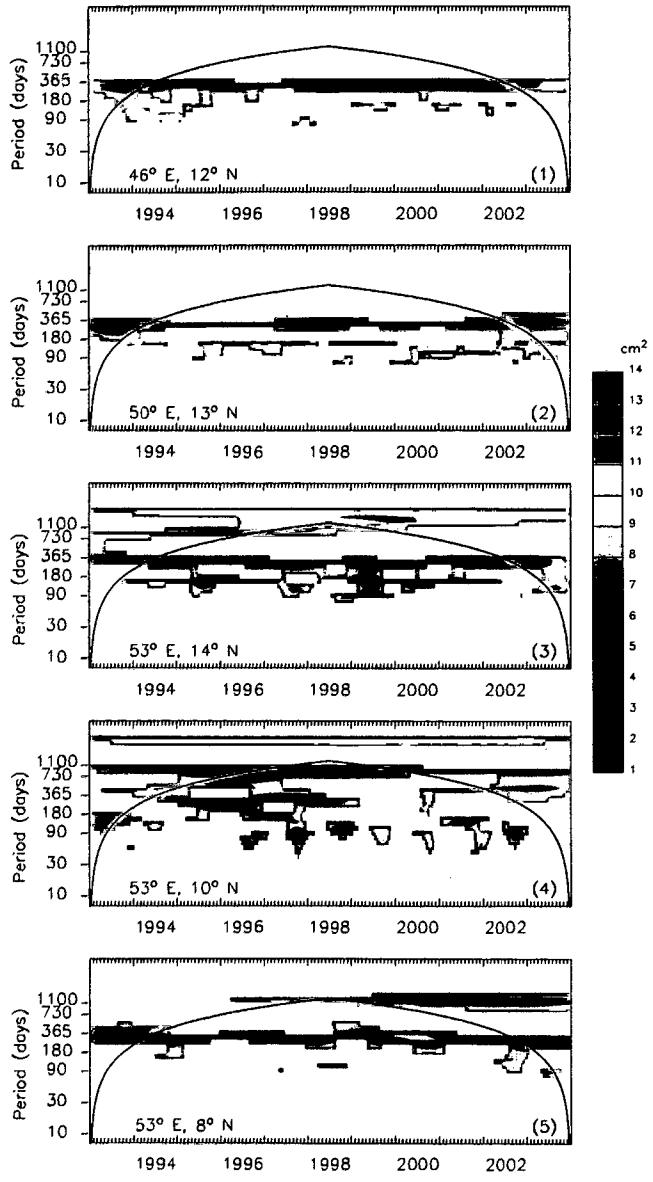

Figure 4.6 (c) same as 4.6a for confidence level at 99%

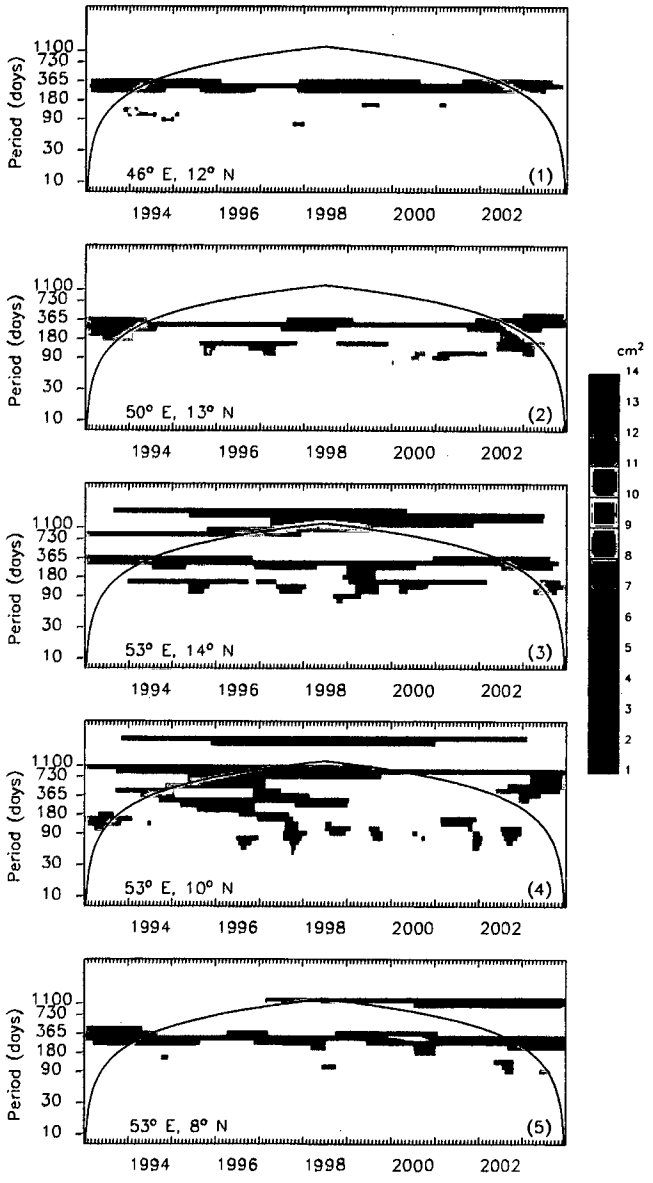

gulf as well as over most of the northwestern Arabian Sea (Figure 4.7). It is highest in the Somali eddy region (2^{13} cm^2), southern Red Sea (2^{12} cm^2) and in the Gulf of Aden (2^{11}–2^{12} cm^2). Comparatively, wavelet powers are higher in the northern half of the Gulf of Aden (2^{12} cm^2) than in the southern half (2^{11} cm^2). The wavelet power in the western most part of gulf (west of 46° E) is also $> 2^{12}$ cm^2. Compared to the wavelet power contained in the annual frequency band, it is lower in the other bands, the high–frequency (30–274 days) and interannual bands (545–1552 days). In the high–frequency band, it is $< 2^7$ cm^2 in the Gulf of Aden and it is $\sim 2^8$ cm^2 in the Somali eddy region and at the entrance to the gulf; it is low (2^6–2^7) in the western gulf (west of 48° E).

The power is least in the Gulf of Aden in all three interannual bands ($< 2^6$ cm^2). Further, it is significant only over small patches in the central gulf at 95 % confidence level in tri–annual bands. However, they are not significant at 99% confidence level (Figure 4.7) inside the gulf in all three interannual bands though they are still significant in the adjoining northwestern Arabian Sea, especially at the entrance to the gulf. This implies that the SLA variability in the Gulf of Aden is insignificant at interannual frequencies. The same will be true in the case of surface geostrophic currents because they are tightly linked to the slope of SLA.

4.5 Discussion

Three major data sets have been used to describe the monthly evolution of currents in the Gulf of Aden. They consisted of a new climatology of hydrography, satellite altimeter derived SLA, and the climatology of ship drifts. The QuikSCAT derived winds were used to estimate the Ekman drifts. The three data sets together with the Ekman drifts were consistent with each other and brought out the salient features of seasonal cycle of circulation in the Gulf of Aden.

The analysis of circulation in the Gulf of Aden presented here not only confirmed

Figure 4.7 Horizontal distribution of the 11 years (1993–2003) averaged wavelet powers spectrum (log scale) of the time sesies of altimeter derived SLA for different bands. Morlet wave transform was used to compute the wavelets using 11 years weekly spaced data set.

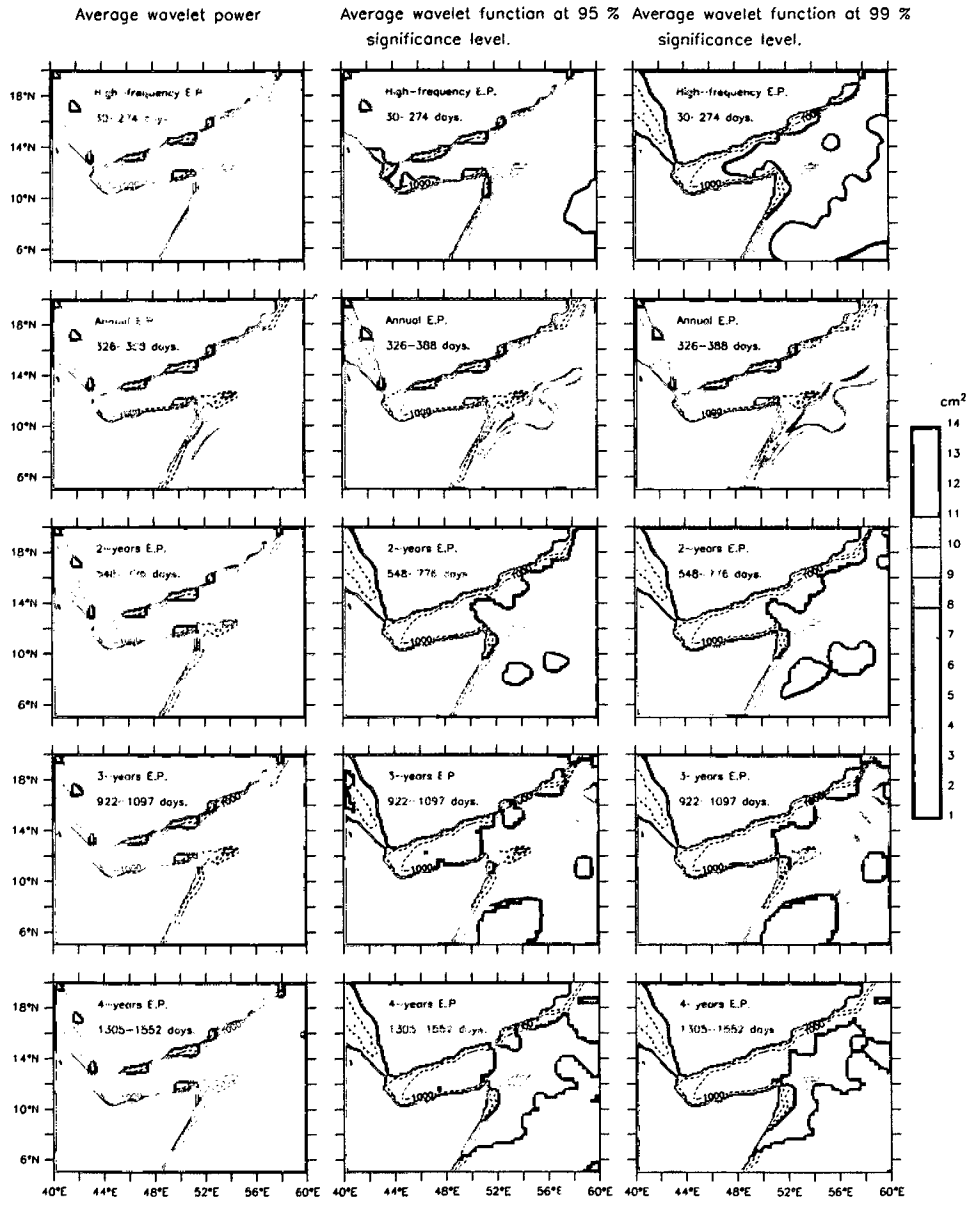

the earlier descriptions on the seasonality of surface currents but also provided new insights. First and foremost is that the currents in the Gulf of Aden are not so simple as thought earlier; they are complicated by the presence of eddies embedded in them. Second, the eddies influenced the flows during all months. Third, the eddies are found only in geostrophic currents and not in Ekman drifts induced by winds and fourth, the eddies act over the entire water column extending from the surface to at least 1000 m.

Due to the presence of eddies, the flow directions in the north often differed from the south. The previous studies [Mohammed and Kolli, 1992; Kolli et al., 1992] that described the circulation in the Gulf of Aden failed to capture the opposite flows in the south because of lack of data from the southern part. The data set used by Mohammed and Kolli [1992] did not extent towards the south; also, it was restricted to just three months (January, May and August). Mohammed and Kolli [1992] and Kolli et al. [1992] presented the circulation for January, May and August based on the dynamic topography (0/500) derived from hydrographic data. During May, they observed weak flows and a clockwise (anticyclonic) cell in the eastern gulf. Our analysis using hydrography and altimeter SLA showed the existence of an anticyclonic cell (A2) in the east and also the two additional cells inside the gulf (Figure 4.3e). During January, they reported an anticlockwise (cyclonic) cell in the central gulf (between 46–50° E). This cell (C1) is seen in our analysis also (Figure 4.3a). But in addition to this cell, our analysis also showed another anticyclonic cell (A1) inside the gulf in both data sets. Mohammed and Kolli [1992] observed that in August, the anticlockwise (cyclonic) cell in the central gulf got replaced with a clockwise (anticyclonic) cell. This is true of our analysis also (Figure 4.3h).

The ship drift data showed the seasonality in the circulation (Figure 4.1) similar to other data sets, but cannot be used to bring out the mesoscale eddies embedded in the flows. Similarly, the Ekman drifts estimated from winds (Figure 4.2) also did not show the presence of eddies in the gulf or adjoining seas. Ekman drifts were towards the west during the winter monsoon (November–March) and towards the east during the summer

monsoon (June–August). The Ekman flows in the month of September appeared to be an exception to the summer monsoon flow pattern; the flows inside the gulf were abysmally weak (Figure 4.2i). The case was similar in May, the transition period between winter and summer monsoons. The Ekman drifts in April as well as in October, the other two transition months, were westward similar to the winter flows. Thus, due to the Ekman drifts, two well defined flow patterns form in the Gulf of Aden; (i) a westward flowing winter pattern and (ii) an eastward flowing summer pattern. The winter pattern started in October and continued till April. Whereas the summer pattern existed only for a short duration of 3 months (June–August). In addition to the generation of well defined flow patterns, the Ekman drifts do not seem to contribute to the generation of eddies in the gulf.

The analysis of geostrophic currents, however, presented the embedded eddies in the flows (Figure 4.3). Several eddies were seen in the geostrophic currents during all the months and they were consistent in the geostrophic currents derived from hydrography and altimeter SLA. As seen in the net surface flows shown in Figure 4.4 the eddies dominated the circulation in the Gulf of Aden over the mean flow. Due to the importance of eddies in the circulation of the Gulf of Aden, a separate chapter (Chapter 5) has been dedicated to further analyse the characteristics of eddies and their origin.

The net flows at the surface in the western gulf are towards the Red Sea during October–April and is at its maximum during November to February. This westward flow would transport water from the Gulf of Aden into the Red Sea. Maillard and Soliman [1986] reported the mean salinity and temperature of this water entering the Red Sea through Bab el Mandab as 36.5 psu and 25 °C. Al Saafani and Shenoi [2004] identified this water with a temperature varying between 27.0 and 28.0 °C and salinity between 36.5 and 37.0 psu during the winter of 1996. The eastward flows in the western end of the gulf in the summer monsoon (June–August) (Figure 4.4g and h) are consistent with the outward flow from the Red Sea in the surface layer [Neumann and McGill, 1962;

Patzert, 1974; Murray and Johns, 1997; Al Saafani and Shenoi, 2004]. Similarly, the westward geostrophic currents in the western end of gulf at 300 and 600 m layers in August–September (Figure 4.5h, i) are consistent with the intrusion of Gulf of Aden water into the Red Sea in the intermediate layers reported by Murray and Johns [1997] and Al Saafani and Shenoi [2004]. Murray and Johns [1997] reported that the summer regime in the Bab el Mandab Strait is dominated by the massive intrusion of cold (19 °C) low salinity (36.0–36.5 psu) water from the Gulf of Aden. They estimated its presence in the water column as high as 70% during July to early September in 1995.

The eddies seen at the surface extend to deeper layers, often to 1000 m or more. Due to the non–availability of direct measurements of currents across the water column, we have to restrict the analysis of vertical structure of currents to the geostrophic currents estimated from hydrography. Our analysis showed a well developed anticyclonic eddy (A1) and a cyclonic eddy (C1) on its west inside the gulf during winter monsoon in the geostrophic currents derived from hydrography and altimeter SLA (Figure 4.3a and b). It reached as deep as 1000 m (Figure 4.5a and b). Bower et al. [2002] found these eddies in the in situ measurements of currents across the water column during February–March 2001. They recorded these eddies at 100, 300 and 600 m and denoted them as A1 and C2 (C1 in our analysis). They also reported another cyclonic eddy, C1, centered at 44.5° E, west of C2. This eddy was not captured in our analysis because the geostrophic currents were estimated with reference to 1000 m depth and the region west of 45° E is shallower than 1000 m. Bower et al. [2002, 2005] have highlighted the importance of these eddies on the spreading rates and pathways of Red Sea water in the Gulf of Aden between 400–800 m.

The annual and high-frequency signals dominate the sea level variability in the Gulf of Aden (Figures 4.6 and 4.7). The SLA variability in the gulf at interannual frequency is minimum and insignificant at 99% confidence level. It is significant at 95% confidence level only over small patches inside the gulf (Figure 4.7). Since the variability in SLA is

related to the geostrophic currents at the surface, it is clear that the interannual variability in the surface geostrophic currents inside the gulf are also insignificant. The geostrophic currents have dominated the net surface flows as seen in Figure 4.4 in the Gulf of Aden. Hence, it would imply that the observed variability (as depicted by the power of wavelets) in the SLA in the five bands depicts the variability of circulation. Based on this argument, we may conclude that the interannual variabilities in the circulation in the Gulf of Aden are lower (and insignificant) than that at annual and higher frequency bands.

Chapter 5

Mesoscale eddies in the Gulf of Aden

5.1 Introduction

Chapter 4 presented the circulation in the gulf of Aden at the surface and in the deeper layers. It was shown that the currents in the Gulf of Aden are not so simple as thought earlier; they are complicated by the presence of eddies embedded in them. Those eddies influenced the flows in all months. The size of those eddies is comparable to the width of the gulf ($\sim$ 250–300 km) (Figure 4.3). They often extend to the deeper layers; at least up to 1000 m (Figure 4.5). Earlier Bower et al. [2002, 2005] described the presence of cyclonic and anticyclonic eddies in the gulf at intermediate depths ($\sim$ 100–600 m) and discussed their role in spreading the Red Sea Water in the gulf. They noted that the azimuthal speed of advecting eddies was as high as 20–30 cm s^{-1}. Based on the water properties in the centre of an anticyclonic eddy, Bower et al. [2002] argued that they are first formed in the Somali Current system and then transported into the gulf. Some of the earlier studies also noted the presence of the eddies in the Gulf of Aden, but did not describe their origin or resident time in the gulf [Piechura and Sobaih, 1986; Nasser, 1992; Awad and Kolli, 1992; Johns et al., 2001]. Recently, Fratantoni et al. [2006] described a series of eddies entering the gulf mostly during the transition between the

summer and winter monsoons. The cyclonic and anticyclonic eddies of approximately 250 km diameter translated towards the west at speeds of 5–8 cm s^{-1}. These eddies entering the gulf from the Arabian Sea are different from the large eddies (the Great Whirl, Southern Gyre, etc.) that develop in the western boundary region during the northern summer (see Schott and McCreary [2001] for a detailed discussion).

Except for Simmons et al. [1988] and Fratantoni et al. [2006], no other study has examined the characteristics of these eddies or their origin. Simmons et al. [1988] related the eddies near the Gulf of Aden to the break up of the upwelling band in late July and early August and the flow from the Great Whirl through the Socotra passage. Fratantoni et al. [2006] argued that a portion of the Somali Current that accelerates northward through the Socotra Passage retroflects sharply and collapses to form discrete anticyclonic current rings, which move westward into the gulf. In particular, they used this mechanism to explain the eddies entering the gulf during the fall inter-monsoon. Similarly, the variability in the Socotra Passage flow was also argued to be the cause of the generation of rings in May during the transition between the winter and summer monsoons. Fratantoni et al. [2006] did not, however, explain the other eddies seen from altimeter derived geostrophic currents; in particular, they did not propose a mechanism for the eddies that moved into the gulf from the interior of the Arabian Sea. Our analysis in Chapter 4 showed that the eddies are exist in the Gulf of Aden round the year. In this chapter[1], we describe the characters of these eddies in detail and investigate the possible reasons for eddy formation in the vicinity of the gulf and their westward movement.

[1]This chapter is based on the paper by **Al Saafani, M. A.**, S. S. C. Shenoi, D. Shankar, M. Aparna, J. Kurian, F. Durand, and P. Vinayachandran. Westward movement of eddies into the Gulf of Aden from the Arabian Sea. *J. Geophys. Res.*,112, C11004, doi:10.1029/2006JC004020, 2007.

5.2 Westward movement of eddies in the gulf

The data used for this analysis are the 11 years (1993-2003) weekly altimeter derived SLA described in Chapter 2.

Figure 5.1 shows the evolution of SLA from June 1999 to April 2000, highlighting the occurrence of cyclonic/anticyclonic eddies in the western Arabian Sea.We chose 1999–2000 as a typical year to demonstrate the westward propagation of eddies in the gulf particularly, during winter. Other years too showed similar westward propagating eddies (see Figure 5.2). Westward movement, however, was not apparent during the summer monsoon, though some eddies were seen in the region in June. During 1999–2000, the anticyclonic eddy seen at 14° N, 53° E on 2 June moved slightly eastward to 14° N, 54° E on 16 June. By 30 June, it had weakened considerably; it disappeared on 28 July. Simultaneously, the large patch of high sea level (SL) seen inside the gulf weakened, broke into two smaller patches (on 30 June), and shrank gradually (in the second half of July), paving the way for a large patch of low SL on 25 August. The large patch of low SL in the gulf continued through September and October and an anticyclonic eddy formed to the east of the gulf at 54° E during the end of the summer monsoon (see the panel for 22 September). This eddy moved westward to 52° E on 20 October, reached the entrance of the gulf at 51° E on 3 November, and moved westward in the gulf during December-1999–January-2000. It arrived at 48° E on 26 January, reached the western end of the gulf on 22 March, and dissipated thereafter. The entry of this anticyclonic eddy into the gulf in December pushed the existing low SL in the gulf towards the west, and the latter manifested as a cyclonic eddy in the western gulf. During February 2000, another anticyclonic eddy manifested at 58° E and propagated into the gulf during March–April. An extended version of Figure 5.1 depicting the evolution of SLA for all the years during 1993 to 2003 is available as an animation at http://www.agu.org/journals/jc/jc0711/2006JC004020/.

The trajectories of eddies shown in Figure 5.2 confirms the westward propagation during all the 11 winters analyzed here, though the tracks of these eddies (cyclonic/anticyclonic)

Figure 5.1 Sequence of altimeter-derived SLA (cm) maps during June 1999 to April 2000, highlighting the presence of cyclonic/anticyclonic eddies inside and outside the Gulf of Aden. The SLA data are from the merged TOPEX/Poseidon and ERS-1/2 data set. The broken contours indicate negative SLA.

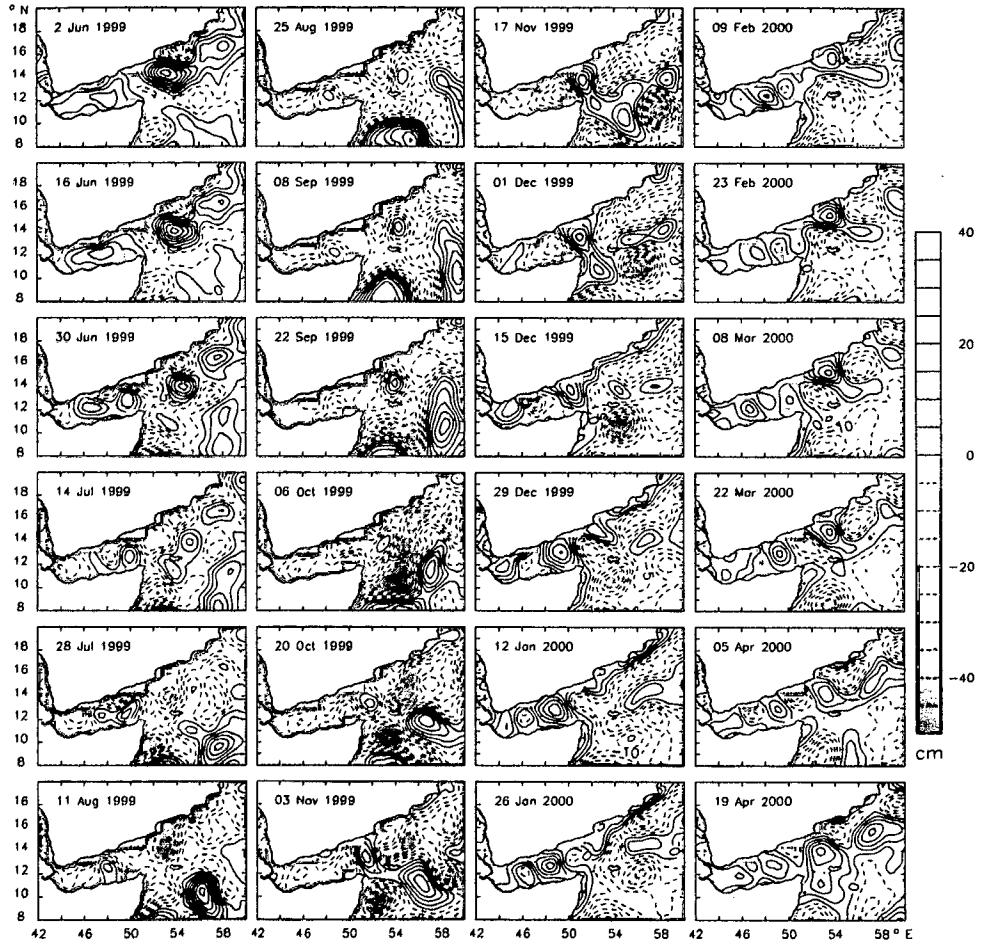

Figure 5.2 The trajectories of eddies entering the Gulf of Aden during 1993–2003. The locations of eddies were derived from the merged TOPEX/Poseidon and ERS-1/2 altimeter SLA data set.

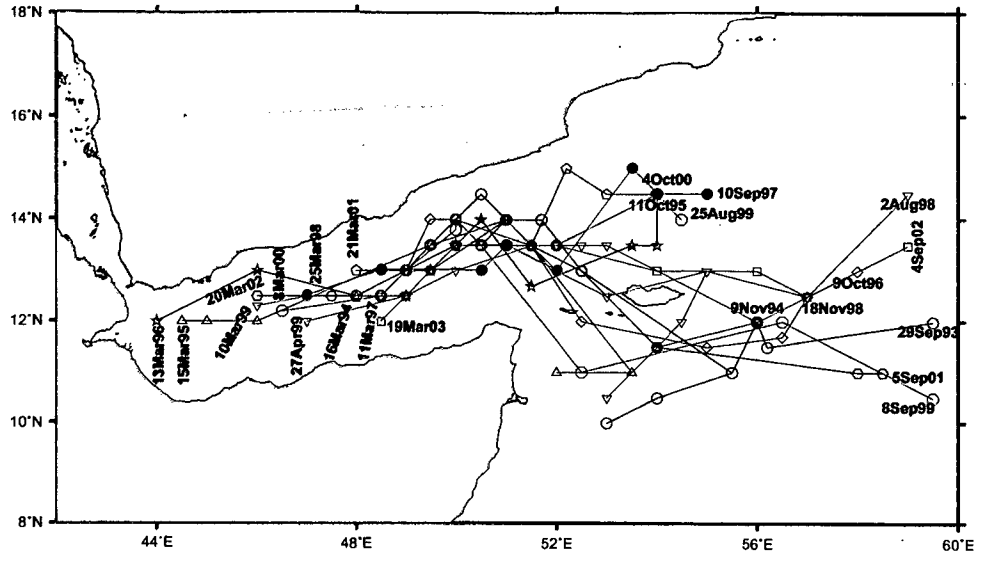

did vary from year to year. Westward propagation was apparent in the SLA maps during winter, but it was absent/weak during the summer monsoon, especially during August–September. During the winter monsoon, the anticyclonic eddies arriving near the Socotra Island from the east propagated directly into the gulf (1995–1996, 1997–1998, 1998–1999, 1999–2000 and 2000–2001) or propagated into the gulf after passing through the Socotra passage (1993–1994, 1994–1995, 1996–1997, 2001–2002, and 2002–2003). In some cases (1997–1998, 1998–1999, and 2002–2003) the eddy that arrived from the east, split into two at Socotra Island before propagating into the gulf; the upper portion propagated directly into the gulf, while the lower portion propagated into the gulf after passing through the Socotra passage. This is seen clearly in the animation available at http://www.agu.org/journals/jc/jc0711/2006JC004020/. Once they entered the gulf, the eddies usually propagated till 46° E and decayed thereafter during March–May. Some eddies, though very few, continued to the western end of the gulf at 44° E (Figure 5.2).

To estimate the westward propagation speed inside the gulf Hovmoller diagram (longitude vs time) of SLA was constructed for the gulf (43° E to 51° E) (Figure 5.3). During the summer monsoon, westward propagation was weak and not discernible except during the summers of 1997, 2000, and 2001. From the slope of the propagating anomalies (Figure 5.3), the propagation speed was estimated to be 6.0–8.5 cm s^{-1}. The maximum azimuthal velocities of the eddies estimated from the geostrophic balance was 50–70 cm s^{-1}. These values are similar to those reported by Fratantoni et al. [2006].

5.3 Mechanisms

We saw that the eddies first appeared outside the gulf in the Arabian Sea and propagated westward to enter the gulf mostly during early winter. This movement continued till March and for some years till May. During summer, no clear westward propagating eddies were discernible in the gulf because of the large patch of low SL that covered the region (Figure 4.3 and 5.1). In the following subsections, we analyse the three basic mechanisms that can cause or favour the generation of westward moving mesoscale eddies in the Gulf of Aden.

5.3.1 Local Ekman pumping

The spatial variation in the wind stress on the sea, i.e., a non–vanishing curl of wind stress, could cause a divergence of the surface layer causing upwelling (positive Ekman pumping) or convergence of the surface layer causing downwelling (negative Ekman pumping). Localised regions of Ekman pumping can then force eddy motions in the ocean. To check whether the eddies and the large patch of low SL were forced by the local wind–stress curl, we have estimated the Ekman pumping velocity (W_e) at the entrance of the gulf following Smith [1968] as follows

Figure 5.3 Time-longitude plot (Hovmoller diagram) of SLA along 12.5° N in the Gulf of Aden (43° E to 51° E). Zero SLA values are contoured.

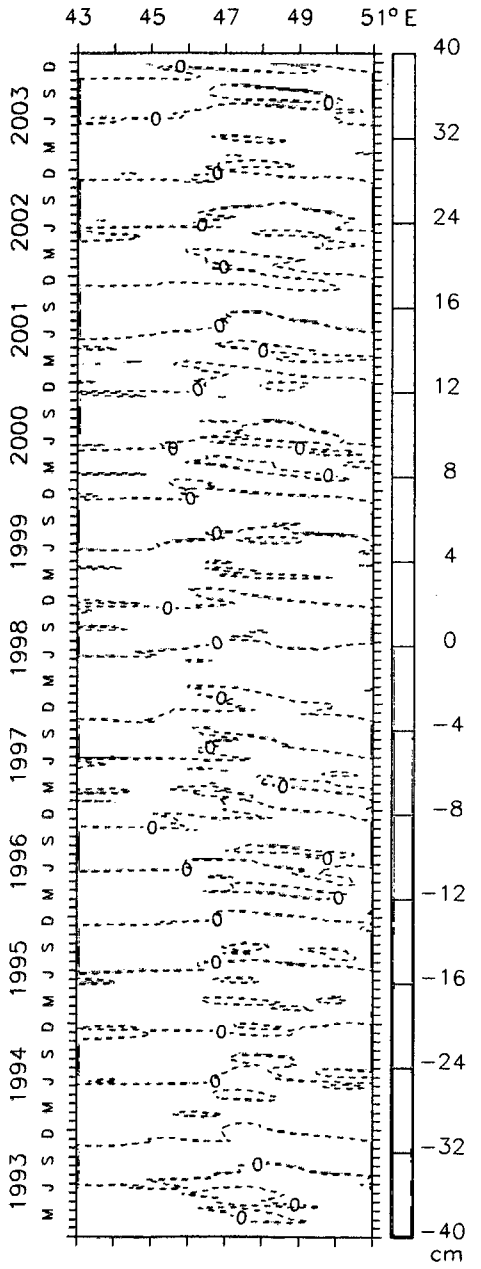

Figure 5.4 Time-latitude plot of SLA and Ekman pumping velocities at the entrance of the Gulf of Aden (along 51.5° E) between the latitudes 11° N and 14.5° N. The shading is for SLA (cm) and the overlaid contours are for Ekman pumping velocities (m day^{-1}); contour interval is 0.5 m day^{-1}. Negative values of Ekman pumping velocities are represented by broken contours.

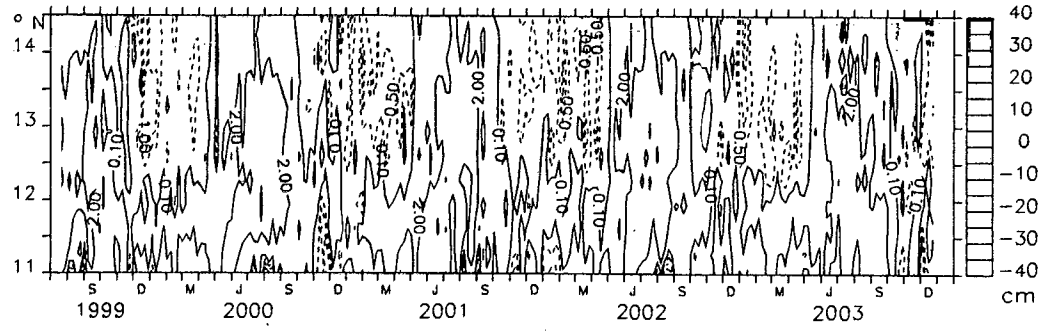

$$W_e = \frac{1}{\rho} curl(\frac{\tau}{f}) = \frac{1}{\rho}\left[\frac{curl(\tau)}{f} + \frac{\tau_x \beta}{f^2}\right] \tag{5.1}$$

where τ is the wind stress, τ_x is the x-component of τ, β is the rate of change of Coriolis parameter (f) with latitude and ρ is the density of sea water.

QuikSCAT wind data (described in Chapter 2) were used to estimate W_e (Figure 5.4). The comparatively strong (2 m day^{-1}) positive W_e was in phase with the negative SLA during June–September for all years (1999–2003) (Figure 5.4). On the contrary, the weak W_e ($\sim$ 0.5 m day^{-1}) was out of phase with the cyclonic/anticyclonic eddies during November–May: for example, during 1999, W_e was positive (negative) when the anticyclonic (cyclonic) eddy appeared in November (December), and it was negative (positive) when the cyclonic (anticyclonic) eddy appeared in March–April (April–May) 2000 (Figure 5.4). Hence, local Ekman pumping cannot be the cause of the eddies entering the gulf during winter, but it can force the low SL during summer.

5.3.2 Westward propagating Rossby waves in the Arabian Sea

The northern Indian Ocean, specially the Arabian Sea adjacent to the Gulf of Aden is known for the westward propagating Rossby waves [McCreary et al., 1993; Shankar and Shetye, 1997]. In the Arabian Sea, the westward propagating Rossby waves were produced either by radiation from the west coast of India in association with poleward propagating coastal Kelvin waves [McCreary et al., 1993; Shankar and Shetye, 1997], or by the forcing due to Ekman pumping over the Arabian Sea (see, for example, [McCreary et al., 1993; Prasad and Ikeda, 2001; Brandt et al., 2002; Shankar et al., 2002]). The Rossby waves or planetary waves arise from the need to conserve the potential vorticity. Rossby waves have been difficult to detect in the oceans because of their small sea surface signature (height variation of order of 10 cm or smaller), slow propagation speeds (of order of 10 cm s^{-1} or less), and long wavelengths (hundreds to thousand km). The advent of satellite altimetry opened a new era for detection of these Rossby waves [Chelton and Schlax, 1996]. Hence, the satellite derived SLA in the Arabian Sea was analysed to understand the propagation of Rossby waves and the associated alternating patches of high/low sea levels or anticyclonic/cyclonic eddies.

A Hovmoller diagram of altimeter derived SLA for the Arabian Sea at 12.5° N (which passes through the center of the gulf) shows the westward propagating highs and lows in the SLA (Figure 5.5a), associated with the westward propagating Rossby waves. The propagations extended from the coast of India (75° E) to the western gulf (47° E). The annual cycle of westward propagating SLA was outstanding, but other periodicities were also evident. The slope of alternating highs and lows was uniform between 75° E and 50° E, but changed abruptly to the west of 50° E. The westward propagating signal took about 250–270 days to travel from the coast of India (75° E) to the gulf (50° E) (Figure 5.5), which implies a speed of $\sim$ 11.7–12.7 cm s^{-1}.

To check whether these speeds match with the theoretical speeds of the westward propagating Rossby waves, we have estimated the phase speeds of the first and second

mode annual baroclinic Rossby waves, by solving an eigenvalue problem that depends only on the local stratification [LeBlond and Mysak, 1978]. The Brunt-Vaisala frequency (stability frequency) ($N^2 = \frac{g}{\overline{\rho}}\frac{\partial \rho}{\partial z}$) profiles used for the vertical mode expansions were estimated from temperature [Stephens et al., 2002] and salinity [Boyer et al., 2002] climatologies for the Arabian Sea, g is the acceleration due to gravity, $\overline{\rho}$ is the mean density of seawater in the water column and ρ is the density of seawater at each depth level.

We followed Shankar et al. [1996] to solve the eigenvalue problem to obtain the phase speed of first and second modes. These modes are the eigenfunctions, $\psi_n(0)$, that satisfy

$$\frac{\partial}{\partial z}\left(\frac{1}{N^2}\frac{\partial \psi_n}{\partial z}\right) = \frac{-1}{c_n^2}\psi_n(z) \tag{5.2}$$

subject to boundary condition

$$\frac{\partial \psi_n}{\partial z}(-D) = \frac{\partial \psi_n}{\partial z}(0) = 0 \tag{5.3}$$

They form an orthogonal set; they are normalized so that

$$\psi_n(0) = 1 \tag{5.4}$$

and are ordered so that their eigenvalue (characteristic speed) c_n decreases monotonically with n. The $n = 0$ eigenfunction is the barotropic mode of the system. The eigenfunctions for $n \geq 1$ are the baroclinic modes, and their eigenvalues are finite. Equations 5.2, 5.3 and 5.4 then imply that $\int_{-D}^{0} \psi_n dz = 0$ for $n \geq 1$ so that horizontal transport relative to the ocean bottom associated with each baroclinic mode vanishes. The phase speed of each mode, c_{rn} were then obtained from the eigenvalues, c_n as

$$c_{rn} = \beta\frac{c_n^2}{f^2} \tag{5.5}$$

At 12.5° N the phase speed of first (c_{r1}) and second (c_{r2}) baroclinic modes work out to be 12.7 cm s^{-1} and 4.1 cm s^{-1} respectively. The estimated theoretical speed of the first–mode Rossby wave is comparable to the speed of westward propagation of SLAs

in Figure 5.5, suggesting that the eddies entering the gulf from the east are associated with westward propagating Rossby waves in the Arabian Sea. The theoretical estimate of the phase speeds of first and second mode Rossby waves are in good agreement with the earlier estimates of Brandt et al. [2002]. They estimated the speeds of first and second mode baroclinic annual Rossby waves at 8° N as 38.0 cm s^{-1} and 14.0 cm s^{-1}; they used the hydrographic data acquired during August 1993. Our estimates for the same modes at 8° N are 31.35 cm s^{-1} and 11.25 cm s^{-1}.

A similar analysis using the average Brunt-Vaisala frequency profile in the gulf yielded a lower Rossby wave phase speed for the first mode owing to a shallower thermocline: the thermocline inside the gulf is $\sim$ 20–50 m shallower than that in the Arabian Sea at 12.5° N latitude (Figure 5.6). The theoretical speed of 7.2 cm s^{-1} is comparable to the SLA propagation speed of $\sim$ 6.0–8.5 cm s^{-1} inside the gulf (Figure 5.3). This decrease in Rossby wave phase speed causes the abrupt change of slope at 50° E in the SLA Hovmoller diagram (Figure 5.5a).

In most of the years, the westward propagating signal was amplified at around 52–60° E. The propagations also showed a discontinuity at this location. The discontinuities were sharp during 1996 and 1998–2001 (Figure 5.5a). To check if this discontinuity occurred at all frequencies, the SLA was partitioned using a low-pass filter (180-days or 26-weeks running mean). The Hovmoller diagram for the low–frequency (high–frequency) part is shown in Figure 5.5b (Figure 5.5c). The Hovmoller diagrams clearly show that both high– and low–frequency Rossby waves propagated from the west coast of India towards the gulf. The high–frequency waves were amplified between 52° E and 60° E while propagating westward (Figure 5.5c). The amplification in this longitude band started around 60° E in September or in early October. No such amplification was apparent in the low–frequency band as the waves propagated westward (Figure 5.5b), but discontinuities were seen in this longitude band at the low frequencies. Hence, we conclude that the amplification seen in Figure 5.5a between 52° E and 60° E was due to high–frequency

waves and the discontinuity was due to low–frequency waves. Both low– and high–frequency waves propagated westward all across the Arabian Sea. Analysis along other latitudes (8 and 10° N) also showed the amplifications and discontinuities west of 60° E (Figure 5.7).

We have seen that there is an abrupt change in Rossby wave speed across the mouth of the gulf owing to a change in thermocline depth (Figure 5.6). The phase speeds estimated above were based on an average stratification for the Arabian Sea and the gulf (at 12.5° N). The thermocline depth, and therefore stratification, in the Arabian Sea changes in both space and time owing to time–dependent monsoonal circulation (see Schott and McCreary [2001]). Hence, to check the role of varying background stratification in modifying the propagation speeds, the phase speeds of first and second baroclinic mode annual Rossby waves along 12.5° N for each month (Figure 5.8) were estimated. The phase speed of the first mode (Figure 5.8a) peaked near 60° E during summer and near the west coast of India during winter (Figure 5.8a). The phase speed of the second mode also peaked between 55–62° E during summer (Figure 5.8b) and near the west coast of India during winter. The summer peak in the western Arabian Sea coincided with the deepest thermocline in the region ($\sim$ 180 m; Figure 5.8c) and the winter peak near the west coast of India with downwelling Rossby waves.

Thus, the stratification and Rossby wave speeds varied considerably in both time and space along 12.5° N in the Arabian Sea. Hence, to check whether the propagating signals, evident at both low and high frequencies in the SLA, are significant, we performed a wavelet analysis on weekly SLA for 11 years along 12.5° N from the west coast of India to the Gulf of Aden (Figure 5.9a). The annual signal was dominant and significant (at 95% confidence level) at all locations from the west coast of India to Gulf of Aden for all years except during 2001–2003 at 55° E.

The high–frequency signals (period less than 180 days) seen in the Hovmoller diagrams (Figure 5.5a and c) were not significant (at 95% confidence level) east of 61° E,

but were significant in the west (Figuree 5.9a). The significant high frequencies included oscillations starting from about 60–80 days, but the most notable frequencies were in the 90–180 days band. The wavelets confirmed the concentration of energy in the high–frequency band seen between 52° E and 58° E in the Hovmoller diagram (Figure 5.5c). In general, the wavelet power spectrum was patchy and the high-frequency wavelets were significant only west of 60° E during September–October, but there was considerable interannual variability: at 55° E, the wavelets were significant in the band around $\sim$ 100–200 days between September 1995 and March 1999 and again between September 2001 and August 2003. The wavelet analysis also showed significant sub–annual signals; an analysis of these frequencies is, however, beyond the scope of this study.

A similar analysis on Ekman pumping, estimated from QuikSCAT winds for 1999–2003, was also performed to check the contribution of local winds to the Rossby waves at 12.5° N. The annual frequency was not significant (at the 90% confidence level) in the east, but was significant west of 60° E (Figure 5.9b). At most locations, the wavelets of Ekman pumping in the high-frequency band ($\sim$ 15 days to $\sim$ 160 days) were significant, but only during the summer monsoon (May–September). Like the high-frequency wavelets of SLA, the high-frequency wavelets of Ekman pumping ($\sim$ 100–160 days) were also most prominent between 52–58° E; the maximum wavelet power was seen at 55° E during 2001–2003, coinciding with the period and location of maximum high-frequency wavelet power in the SLA (Figure 5.9a). From the wavelets of SLA and Ekman pumping, it is clear that the local winds play an insignificant role in generating annual Rossby waves east of 60° E, but they do play a significant role in modulating the waves west of 60° E. The local winds also generate high–frequency Rossby waves in the longitude band 52–58° E. This lack of Rossby wave generation by Ekman pumping east of 60° E implies that the Rossby waves radiating from the eastern boundary (Figure 5.5) are generated by (the mostly remotely forced) coastal Kelvin waves along the Indian west coast [McCreary et al., 1993; Shankar and Shetye, 1997; Nethery and Shankar, 2007]. The wavelet analysis

Figure 5.5 Time–longitude plots (Hovmoller diagram) of (a) observed SLA (cm), (b) the low- frequency (> 180 days) part of SLA (cm), and (c) the high-frequency (< 180 days) part of SLA (cm) along 12.5° N in the Arabian Sea. The 12.5° N latitude was selected because it passes through the center of the Gulf of Aden. Zero SLA values are contoured.

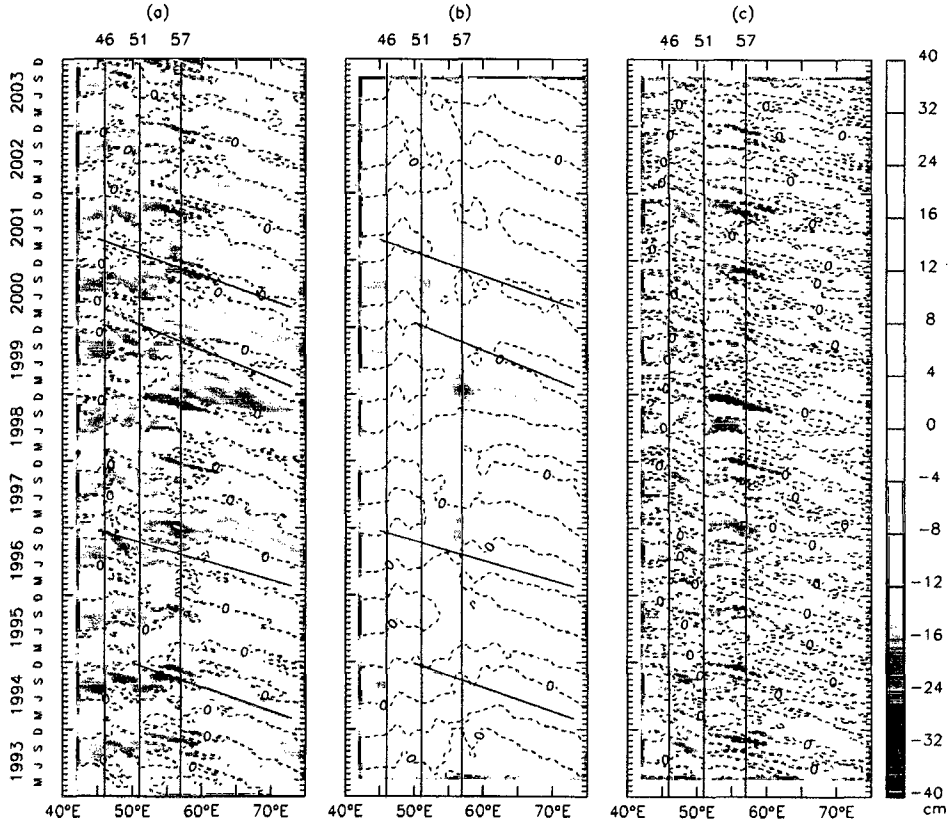

Figure 5.6 Mean temperature profile (°C), estimated from Stephens et al. [2002] along 12.5° N inside the Gulf of Aden (43° E to 51° E) and the Arabian Sea (55° E to 75° E).

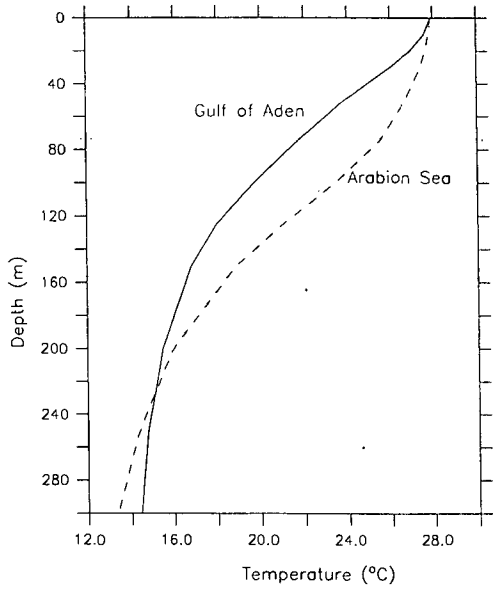

also suggests considerable interannual variability in the local generation of Rossby waves at both low and high frequencies.

5.3.3 Instabilities in western boundary currents

The other sources of cyclonic and anticyclonic eddies that enter the Gulf of Aden are the eddies generated when a part of the Somali current accelerates northward through the Socotra passage [Fratantoni et al., 2006]. Simmons et al. [1988] had noted that when the Findlater Jet, a strong low level jet in the atmosphere associated with the monsoon system over the Arabian Sea [Findlater, 1969], and its associated curl field begin to relax in late July and early August, a broad upwelling band begins to break up into several large eddies in the vicinity of the Gulf of Aden (see their Plate 1). The Great Whirl impinges on the Socotra Island, and the associated flow through the Socotra passage strengthens and continues northward to the Yemen coast, where it turns to the east to flow as a large

Figure 5.7 Time-longitude (Hovmoller diagram) of observed SLA (cm) along (a) 8° N and 10° N latitudes. Zero SLA values are contoured.

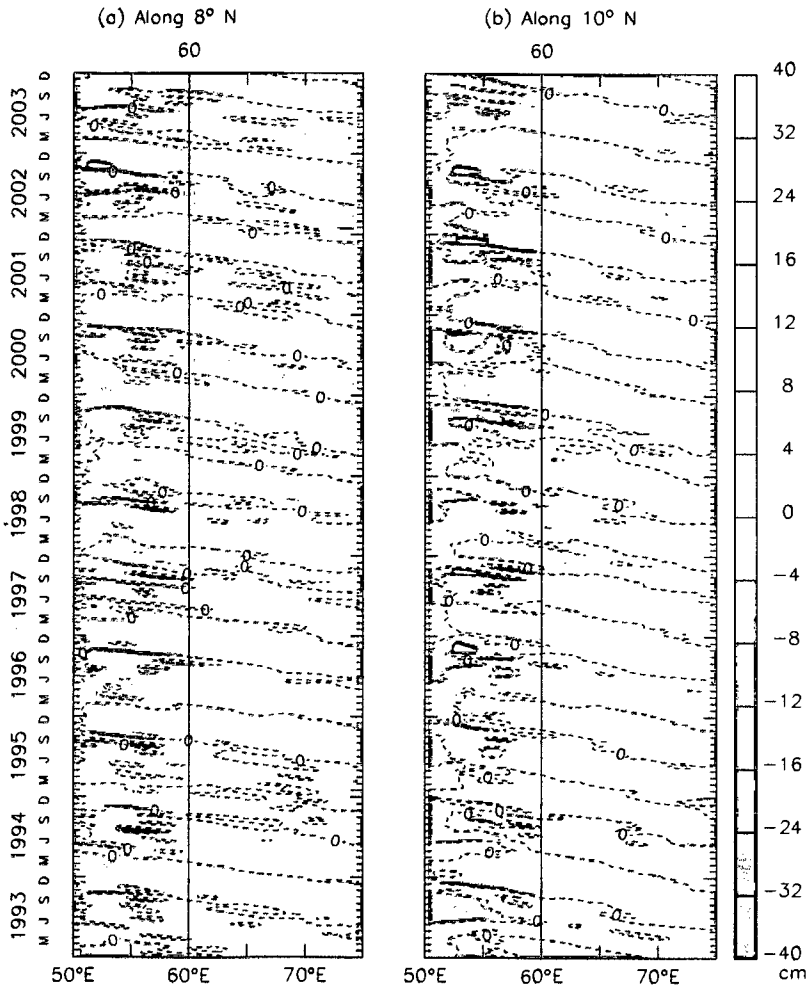

Figure 5.8 Time–longitudes plots (Hovmoller diagram) of (a) the phase speed of the first mode baroclinic Rossby wave (cm s^{-1}) , (b) the phase speed of the second mode baroclinic Rossby wave (cm s^{-1}) , and (c) the depth of 18°C isotherm (indicative of the depth of the thermocline) estimated from [Stephens et al., 2002] along 12.5° N in the Arabian Sea. The two horizontal lines are drawn for January (winter monsoon) and September (summer monsoon), for which a section through this contour plot is shown in (d). The location of Socotra Island is hatched.

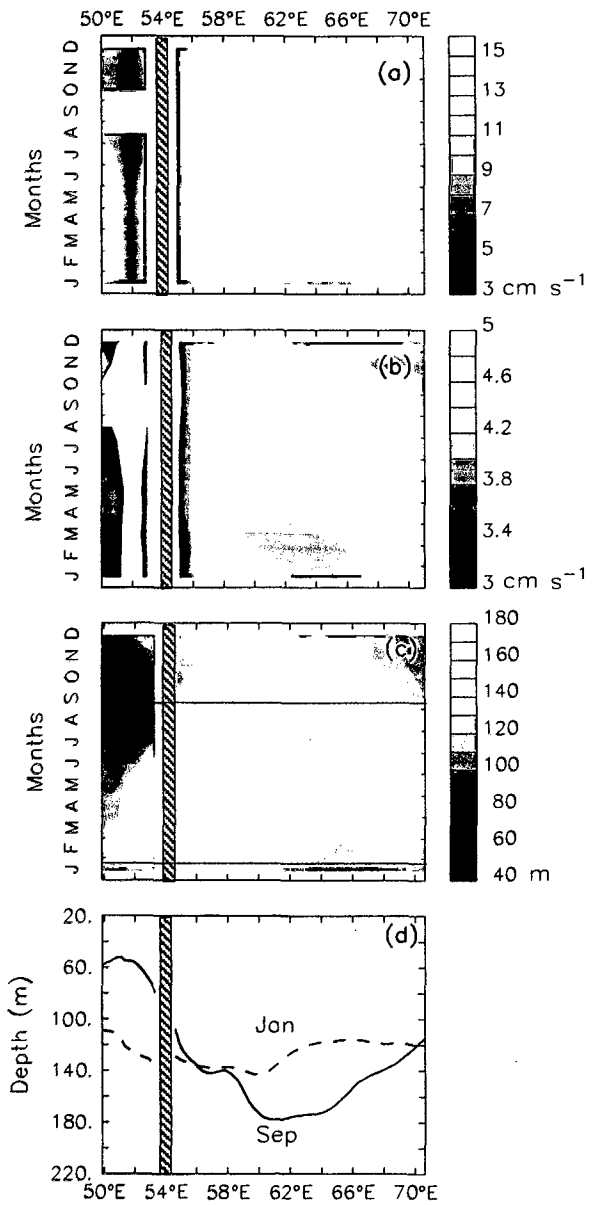

Figure 5.9 (a) Time–scale representation of the wavelet power spectrum of the SLA time series along 12.5° N.

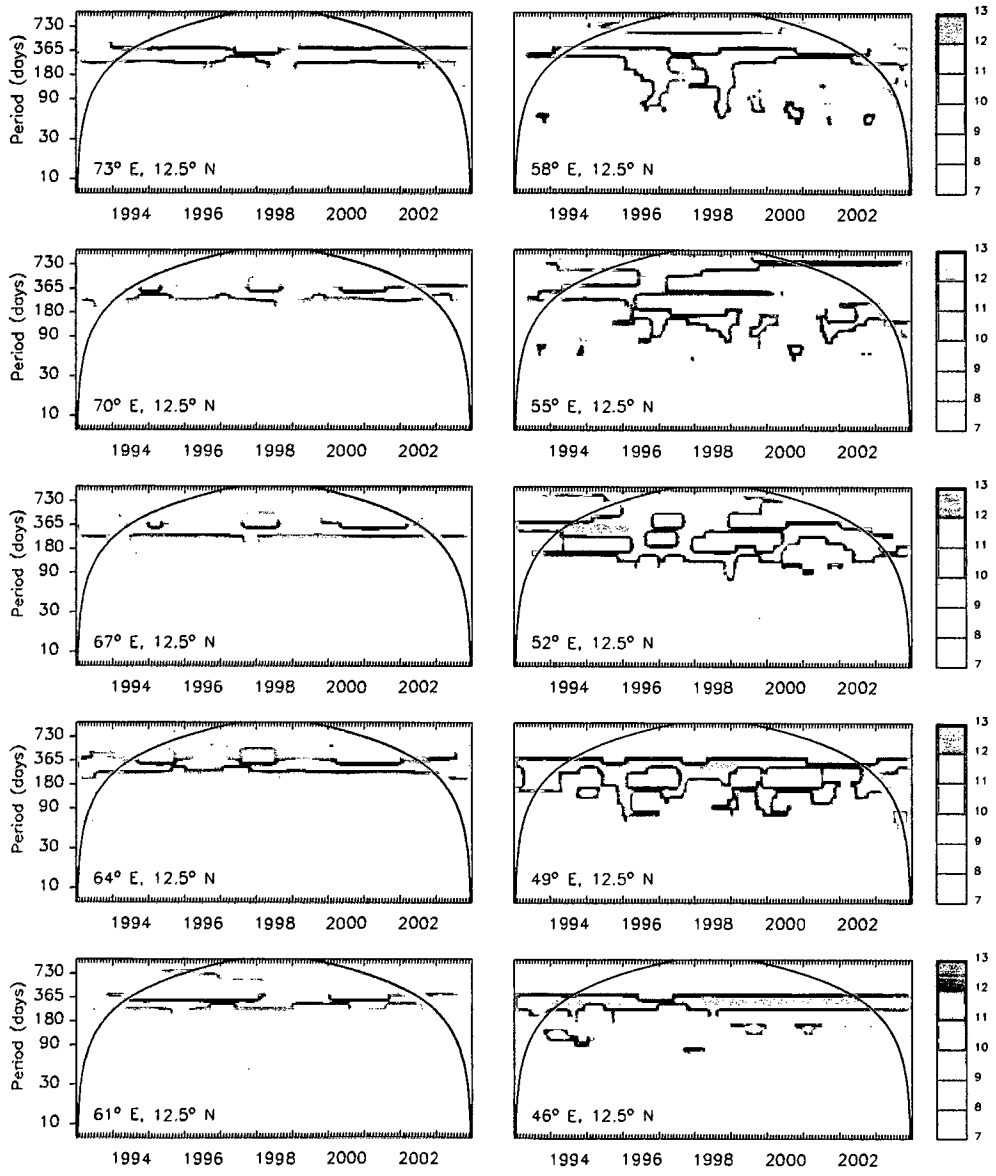

Figure 5.9 (b) Same as 5.9a for Ekman pumping estimated from the QuikSCAT winds for the period 1999 to 2003.

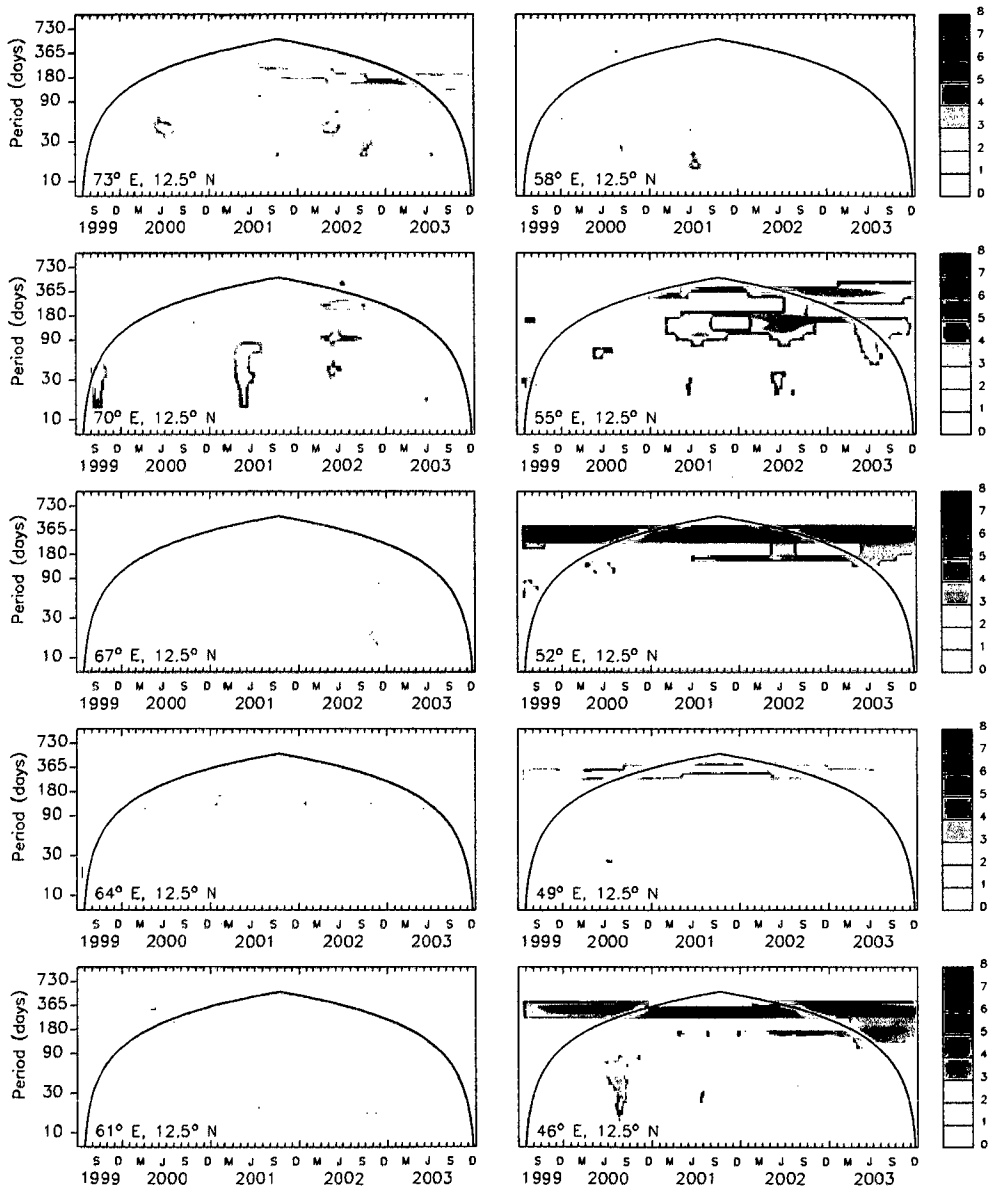

meander. Later in mid-September, the outflow from the Great Whirl causes the formation of Socotra Gyre [Simmons et al., 1988]. This mechanism, in which eddies pinch off from the Somali Current system owing to instabilities, is also active during May [Fratantoni et al., 2006].

To examine the type of instabilities that occur in the flow across the mouth of the gulf, we analysed the energy cycle. The results of an ocean general circulation model (MOM4) simulation for the Indian Ocean [Kurian and Vinayachandran, 2006, 2007] were used to compute the mean and eddy components of energy. The model had a horizontal resolution of $0.25° \times 0.25°$ and had 40 levels in the vertical, with 5–m resolution in the upper 60 m. The model was forced by daily climatology derived from the European Centre for Medium–Range Weather Forecasts (ECMWF) reanalysis (ERA-15) for 1979–1993 [Roske, 2001]. The model, an extensive validation of which was presented by Kurian and Vinayachandran [2007], reproduced (Figure 5.10) the eddies and the westward propagation seen in the observed SLA outside the gulf. Figure 5.10a shows westward propagation of the signal along 12.5° N similar to that seen from altimeter derived SLA (Figure 5.10b). Inside the gulf, however, the model was unable to simulate all the observed features: for example, the model westward propagation was weak during January–May. This limitation of the model, however, should not affect the instability analysis presented here because the analysis was carried out for a box outside the gulf.

Energy budget is presented in the form of a box diagram introduced by Lorenz [1955] showing the energy transfer terms acting upon the various components of the total energy. The mean kinetic energy (MKE), eddy kinetic energy (EKE), mean available potential energy (MPE), eddy potential energy (EPE), and the transfer terms between the energy components were estimated following the formulation used by Boning and Budich [1992]; Vinayachandran and Yamagata [1998] as follows.

The available potential energy per unit mass in a volume element V can be approximated as

$$P = -\frac{1}{2}g\int\int\int \frac{(\rho-\tilde{\rho})^2}{d\tilde{\rho}/dz}dV \tag{5.6}$$

or, using the linear relation between potential density and potential temperature, $\rho = \rho_0(1-\alpha T)$, where $\alpha = 2.5\times 10^{-4}$, the relation is rewritten as

$$P = \frac{1}{2}\alpha g\int\int\int \frac{(T-\tilde{T})^2}{d\tilde{T}/dz}dV \tag{5.7}$$

The reference state, $\tilde{T}(z)$, is obtained from the horizontal average over the time–mean temperature distribution. Neglecting the contribution of vertical velocity w, the kinetic energy per unit mass is given by

$$K = \frac{1}{2}\int\int\int (u^2+v^2)dV \tag{5.8}$$

Separating the actual flow variables into time mean and transient parts, $u = \overline{u}+u'$, $v = \overline{v}+v'$, etc., the time–mean energy of the system may be divided into four components: mean available potential energy

$$MPE = \frac{1}{2}\alpha g\int\int\int \frac{(\overline{T}-\tilde{T})^2}{d\tilde{T}/dz}dV, \tag{5.9}$$

eddy available potential energy

$$EPE = \frac{1}{2}\alpha g\int\int\int \frac{\overline{T'^2}}{d\tilde{T}/dz}dV, \tag{5.10}$$

mean kinetic energy

$$MKE = \frac{1}{2}\int\int\int (\overline{u}^2+\overline{v}^2)dV, \tag{5.11}$$

eddy kinetic energy

$$EKE = \frac{1}{2}\int\int\int (\overline{u'^2+v'^2})dV, \tag{5.12}$$

When integrated over a closed domain, the energy component changes by the work of external forces on the system, that is, wind work (W) and buoyancy work (B), by diffusion (D) and frictional dissipation (F), or by the transfer of energy due to interactions with other components.

Thus the energy transfer (Tr_i), per unit mass, in a closed volume V is given as

$$Tr_1 = \alpha g \int\int\int \overline{w}\overline{T} dV \tag{5.13}$$

$$Tr_2 = \alpha g \int\int\int \frac{\overline{u'T'}\partial\overline{T}/\partial x + \overline{v'T'}\partial\overline{T}/\partial y}{d\tilde{T}/dz} dV \tag{5.14}$$

$$Tr_3 = -\alpha g \int\int\int \overline{w'T'} dV \tag{5.15}$$

$$Tr_4 = -\int\int\int \left\{ \overline{u'u'}\frac{\partial\overline{u}}{\partial x} + \overline{u'v'}\left(\frac{\partial\overline{v}}{\partial x} + \frac{\partial\overline{u}}{\partial y}\right) + \overline{v'v'}\frac{\partial\overline{v}}{\partial y} \right\} dV \tag{5.16}$$

where Tr_1 represents the conversion of mean kinetic to mean potential energy by the work of mean buoyancy force, Tr_2 the conversion of mean to eddy potential energy (baroclinic instability), Tr_3 the conversion from eddy potential to eddy kinetic energy, and Tr_4 the work of the Reynolds stresses against the mean shear (which, if positive, represents barotropic instability).

Complete energy analysis is not attempted because it is beyond the scope of this work. The mean and eddy components were calculated from the daily snapshots of the seventh year of the simulation [Kurian and Vinayachandran, 2006, 2007]. The energy components and their transfer terms (Figure 5.11) were estimated separately for the top 200 m for three periods representing the summer monsoon (June–September), the winter monsoon (November–February), and the transition period between the monsoons (March–May). During the winter monsoon and the transition period, energy was directly transferred from MKE to EKE, implying that the barotropic instabilities were responsible for the generation of the eddy that appears near the gulf. During the summer monsoon, however, energy was transferred not only from MKE to EKE, but also from MPE to EPE and from MKE to MPE, implying that the transfer from the pool of kinetic energy maintained the mean potential energy against the work of the buoyancy forces and that the eddies were generated owing to both barotropic and baroclinic instabilities.

Figure 5.10 Time–longitude plots (Hovmoller diagram) of (a) SLA along 12.5° N from MOM4 Kurian and Vinayachandran [2006, 2007] and (b) altimeter derived SLA along the same latitude.

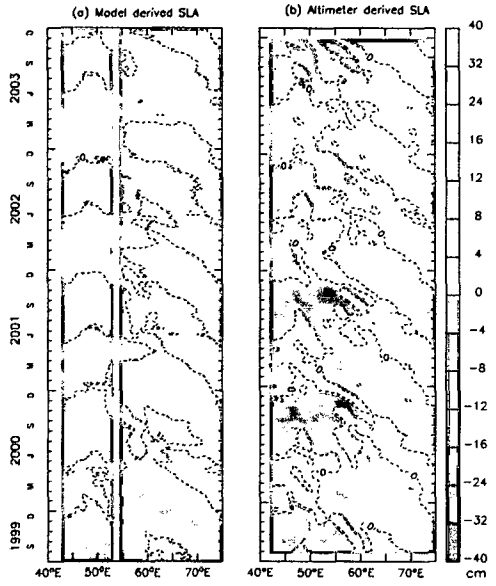

Figure 5.11 Values of the energy components ($cm^2\ s^{-2}$) and transfer terms ($10^{-5}\ cm^2\ s^{-3}$) for a 3° × 3° box outside the gulf (12–15° N, 51–54° E; see inset). A 200-m deep water column was considered for the computation of energy components and transfer terms using the OGCM results of Kurian and Vinayachandran [2006] and Kurian and Vinayachandran [2007]

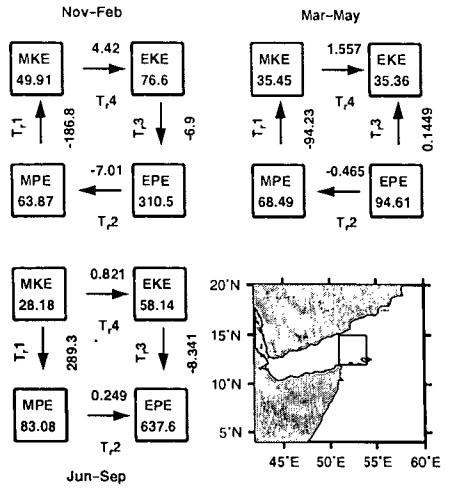

5.4 Discussion

5.4.1 Westward moving eddies in the Gulf of Aden and westward propagating Rossby waves in the Arabian Sea

Westward moving eddies were evident in the Gulf of Aden during November–May (Figures 5.1–5.3) and our analysis showed them to be associated with westward propagating Rossby waves. Westward propagating Rossby waves in the Arabian Sea have also been noted in earlier studies. The Rossby waves in these studies were produced either by radiation from the west coast of India in association with poleward propagating coastal Kelvin waves [McCreary et al., 1993; Shankar and Shetye, 1997], or by the forcing due to Ekman pumping over the Arabian Sea (see, for example, [McCreary et al., 1993; Prasad and Ikeda, 2001; Brandt et al., 2002; Shankar et al., 2002]).

Prasad and Ikeda [2001] noticed an anticyclonic eddy in the vicinity of the gulf and attributed its existence to the arrival of Rossby waves from the interior Arabian Sea, speculating on the southern Arabian Sea high (situated at 5° N between 55–65° E) as the possible source. They did not see the possibility of Rossby waves from the west coast of India reaching the gulf because of the Lakshadweep High (LH), a manifestation of Rossby waves radiated by poleward propagating Kelvin waves [Shankar and Shetye, 1997] in early winter, weakens in March and propagates in a northwestward direction before weakening further and breaking into smaller eddies along the path across the Arabian Sea. Brandt et al. [2002] also felt that the Rossby waves radiated from the LH would not reach the western boundary because those waves would gradually decay during their propagation. Kindle and Arnone [2001], however, did not discount the possibility of remnants of Rossby waves radiating from the west coast of India (specifically the LH) reaching the western boundary of the northern Arabian Sea; the process simulations of Shankar et al. [2002] also support the hypothesis that westward propagating Rossby waves from the Indian west coast propagate all the way across the Arabian Sea. The westward propagations seen in Figure 5.5 confirm this hypothesis, but significant modifications do occur on the way around 52–60° E.

Based on the results of wavelet analysis, we conclude that (i) the annual Rossby waves are significant all over the basin, but the annual Ekman pumping is significant only west of 60° E, (ii) the years 2001–2003 are an exception to the above at 55° E, where the annual wavelets were insignificant, and (iii) the intense high–frequency oscillations ($\sim$ 90–180 days) in SLA correspond to the intense high–frequency ($\sim$ 100–180 days) oscillations in Ekman pumping at 52–58° E (Figure 5.9a, b). This suggests that the westward propagating waves with periods less than $\sim$ 180 days were produced locally (west of 60° E), but with some contribution from the east too. This longitude band (52–60° E) also appears to be special for the low–frequency (annual) westward propagating Rossby waves because they developed a discontinuity at this location (Figure 5.5b). A complete analysis of what

is so special about this longitude band for the Rossby waves is beyond the scope of this study because we basically want to relate the westward propagating mesoscale eddies in the Gulf of Aden and their origin in the westward propagating Rossby waves in the Arabian Sea. Similarly, the effect of reflected shortwave Rossby waves from the western boundary in modulating the westward propagating Rossby waves or their contribution to the eddies in the region is beyond the scope of the study. Nevertheless, in the following section, we list out four possible reasons for this longitude band being so special.

5.4.2 Discontinuity in the low–frequency Rossby waves in the western Arabian Sea

The first possible cause for the collapse of low–frequency waves and the increase in high–frequency waves between 52° E and 60° E could be the higher wind stress in this region during the summer monsoon. The annual wavelets of Ekman pumping, associated with the annual cycle of the monsoon, are significant only west of 60° E (Figure 5.9b). This would force annual Rossby waves, which need not necessarily be in phase with the Rossby waves propagating from the east. Depending on the phase difference between the locally forced SLA response and the Rossby waves from the east, constructive/destructive interference will create a discontinuity [Wang et al., 2001] similar to that noted in Figures 5.5 a and b. Wang et al. [2001] noticed a similar discontinuity in the annual Rossby waves in the interior of the southern Indian Ocean; that discontinuity was caused by constructive/destructive interference between the locally forced response and the Rossby waves propagating from the east.

The high–frequency wavelets of Ekman pumping were energetic in this longitude band between 52° E and 58° E (especially between 52° E and 57° E) during 2001–2003, favouring the local generation of high–frequency Rossby waves (Figure 5.5a and c). The energetic Ekman pumping at 52–57° E during 2001–2003 also coincided with the strong discontinuity in the low–frequency waves (Figure 5.5b). Hence, it is likely that Ekman

pumping, both at low as well as at high–frequency, is involved in the generation of discontinuity in the low–frequency Rossby waves at these longitudes. The exact mechanism through which the high–frequency winds modulated the low–frequency Rossby waves is not clear from this analysis. Experiments with analytical or numerical models forced with different wind patterns is necessary to resolve this issue.

The second possibility is the bottom topography because the region is in the proximity of the, almost, meridionally oriented Carlsberg Ridge in this longitude band. Such topographic features are known to scatter the westward propagating Rossby waves, generated to their east, and change the phase (even up to 180°) across the ridge, thus causing them to break down [Barnier, 1988; Wang and Koblinsky, 1994]. A plot of bottom topography along 12.5° N based on ETOPO2v2 data ([National Geophysical Data Center, 2006], Figure 5.12) shows that the bottom rises by $\sim$ 500–800 m west of 60° E (from $\sim$ 4000 m to $\sim$ 3500–3200 m) owing to the presence of the Carlsberg Ridge. It is unlikely, however, that the topographic scattering was effective in this case because the water column is still deep enough ($>$ 3000 m) for the waves to propagate. This is more so because the propagation speed suggests the dominance of the first baroclinic mode Rossby waves. Also, it is not possible to invoke topography to explain the interannual variability seen in the vicinity of the discontinuity (Figure 5.5a and b) in the low–frequency waves. An exception is near 55° E, where the Socotra Island exists. It is possible that the presence of the island may affect the Rossby waves. The island could also affect the wind field and this possible cause of the high–frequency signal in the Ekman pumping (see Figure 5.9b) needs to be investigated; such an investigation is, however, beyond the scope of this work.

The third possible cause is the spatial structure of the thermocline, which can act, like bottom topography, to scatter the Rossby waves [Wang et al., 2001]. The thermocline, as indicated by the 18 °C isotherm, along 12.5° N latitude first deepens towards the west from 75° E ($\sim$ 40 m) to 60° E ($\sim$ 175 m), and then shoals to $\sim$ 60 m at 50° E (Figure 5.8d) in September, when the high frequency amplifications started west of $\sim$

Figure 5.12 The bottom topography of Arabian Sea based on ETOPO2v2 data [National Geophysical Data Center, 2006] depicting the northeast–south–southeast oriented Carlsberg Ridge. The depth along 12.5° N (the line marked in the upper panel) is shown in the lower panel.

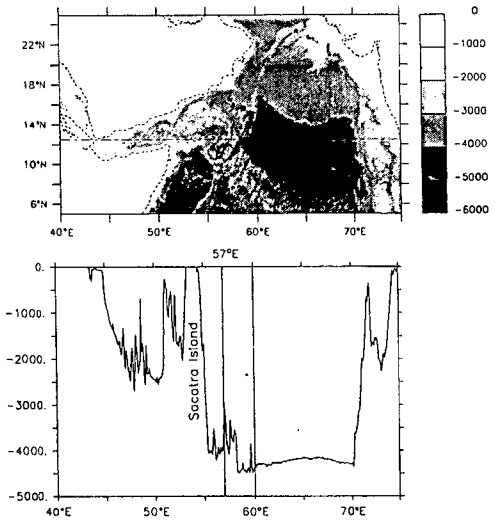

60° E (Figure 5.5c) and the discontinuity started becoming apparent in the low–frequency waves (Figure 5.5b). Most notable is that the slope of the thermocline is steepest between 58° E and 60° E. The east–west thermocline structure in January, however, does not show appreciable variation from 75° E to 50° E.

The fourth possible cause is the anticyclonic Socotra Gyre that exists in the region during August–September (see Figure 36 in Schott and McCreary [2001]). The northeastern boundary of the Socotra Gyre lies in the longitude band 55–57° E. Simmons et al. [1988] stated that a pulse of high sea level propagates westward as a Rossby wave from the interior between 12° N and 14° N, arriving at 57° E in early September and causing intensification of the Socotra eddy. It is possible that the westward propagations are modified by the presence of the Socotra Gyre, which was shown by Shankar and Shetye [1997] to be the result of nonlinear dynamics.

In summary, we conclude that the westward propagating Rossby waves radiated from

the Indian west coast as well as the Rossby waves generated in the interior of the Arabian Sea (52–60° E) contribute to the cyclonic and anticyclonic eddies in the vicinity of the Gulf of Aden. The low–frequency signal (mainly annual signal) shows a discontinuity in the longitudinal band between 52° E and 60° E; its intensity and spatial extent demonstrate considerable interannual variability. Uplifting of the thermocline, local wind stress, and the presence of Socotra Gyre in the vicinity may all contribute to this discontinuity in the annual signal. The westward propagating high–frequency Rossby waves generated locally (west of 60° E) are also a source for westward propagating mesoscale eddies in the Gulf of Aden. They move into the gulf from the east, either directly or through the Socotra Passage. They survive and move westward within the gulf in spite of the frictional effect of the boundaries of the gulf.

The analysis suggests that the eddies entering the gulf from the Arabian Sea owe their existence to more than one mechanism. Local Ekman pumping is important during the summer monsoon (June–September). In May and during the latter half of the summer monsoon (late July to September) and the fall inter–monsoon (October), the dominant mechanism is the generation of eddies by the instabilities in the Somali Current and the large eddies associated with it (Great Whirl and Socotra eddy) [Fratantoni et al., 2006; Simmons et al., 1988]. During the winter monsoon (November–April), the dominant mechanism involves the westward propagating Rossby waves that are generated either in the Arabian Sea by Ekman pumping or along the west coast of India by poleward propagating Kelvin waves. Thus, the westward propagating Rossby waves from the Arabian Sea are more important for the circulation in the gulf over half the year. The multiple eddies and multiple processes that act in this western–boundary region make the case complicated. Numerical experiments with a primitive–equation model capable of separating the processes acting in the region are necessary for understanding details like the mechanisms that caused the discontinuity in the low–frequency waves and the enhancement in the high–frequency waves around 57° E.

Chapter 6

Summary and conclusion

In this thesis we have described the hydrographic structure and the water masses in the Gulf of Aden using the available hydrographic data after applying quality control procedures. Also the circulation in the Gulf of Aden was described at the surface and deeper layers on a monthly basis using different data sets. It has been shown that the currents in the Gulf of Aden are not so simple as thought earlier; they are complicated by the presence of eddies embedded in them. The eddies influenced the flows during all months. The analysis suggests that the eddies entering the gulf from the Arabian Sea owe their existence to more than one mechanism.

The hydrographic structure and the water masses in the Gulf of Aden are presented in Chapter 3. The vertical hydrographic structure of the Gulf of Aden shows four layers, a surface layer, an intermediate low saline layer, a high saline RSW and a bottom layer. The surface layer showed strong seasonal variations in its characteristics. The SST was about 24–25 °C during winter (November–February). It increased to reach a maximum (31 °C) in May. During summer (June–August) the SST decreased along the northern side due to upwelling. The upwelling along the northern side during summer started in the eastern side during June and extended towards the west during July–August. In September, the SST started to rise again to $\sim$ 30 °C. Similarly, the mixed layer depth decreased from $\sim$

80 m during winter to $\sim$ 20 m during summer. The seasonal variation was less in the intermediate low saline layer. It was cooler and more saline during summer as compared to that in winter.

Four water masses were identified using the newly compiled hydrographic data set. Among them, the origin of RSW is well known. The origin of the other three water masses, the GASW, GAIW and GABW were investigated in Chapter 3. As mentioned above, the seasonal as well as the monthly variabilities were highest for the GASW. Though the core density is $\sim$ 1024.10 kg m^{-3}, the lower limit of density varied from 1023.50 kg m^{-3} in winter to 1022.20 kg m^{-3} in summer due to the increase in temperature. The salinity of the core increases towards the west (Figures 3.5 and 3.6). The θ–S-σ_θ structure of this water mass (core θ–S 26.0 °C – 36.0 psu and σ_θ 24.1) is similar to the salinity maximum D of Rochford [1964] and ASHSW described in Shenoi et al. [1993]. As seen in the net surface flows shown in Figure 4.4 the flows during winter are towards the west over most the gulf with cyclonic and anticyclonic eddies embedded in it. This flow structure establishes in October and continues till April, mostly dominated by geostrophy (Figure 4.4). Hence, during winter, a sizable amount of ASHSW from the east enters the Gulf of Aden. Similarly, during the summer monsoon, the flows are eastward all over the gulf with a sizable amount of surface water from the Red Sea entering the gulf from the west (Figure 4.4f, g, h and i). In addition, during both seasons, some water forms locally due to precipitation and evaporation. Hence, it is possible that during winter, the GASW forms as a mixture of locally formed water and ASHSW, while during summer it is a mixture of locally formed water and Red Sea Surface Water.

In the intermediate layers (200–300 m), the GAIW appears as a minimum in the θ–S diagram at σ_θ level 26.5. The salinity of this layer increases westward due to mixing with the high saline RSW. GAIW occupies $\sim$ 9% of the total volume of Gulf of Aden, which is shallower during summer. As shown in Figure 4.5 the GAIW enters the gulf from the east along the northern side during winter and late summer (August–September), whereas dur-

ing June and July the flow at 300 m is eastward similar to that at the surface (Figure 4.5f and g). Our analysis shows that PGW cannot be the source of GAIW (Figure 3.12a). Hence, it is likely that the GAIW enters the gulf either from south through the Somali region or from the east. Three sources have been identified for the low salinity water through the Somali basin in the western Arabian Sea. First, the low salinity water brought into the Somali basin by the northern branch of the South Equatorial Current (SEC). The second possibility is the low salinity Subtropical Subsurface Water (SSW), which originates at the Subtropical Convergence in the southern hemisphere near 40° S. Warren et al. [1966] and Wyrtki [1971] showed that this water penetrates as far as 10° N off East Africa and is partially responsible for the low salinity in the intermediate layer of the northern Somali basin. The third possibility is the Antarctic Intermediate Water (AIW), which forms at the Antarctic Convergence Zone at around 40–50° S, sinks and flows towards the north. Our analysis shows that it is possible that both SSW and AIW contribute to the existence of the salinity minimum in the Gulf of Aden at intermediate levels. The Socotra passage seems to be the main connection between Gulf of Aden and the Somali Basin. The passage also acts as the pathway for the southward migration of RSW.

RSW originated from the Red Sea occupies $\sim$ 35% of the total volume of the Gulf of Aden. On an average, this water mass occupies about 700 m (400–1100 m) thick layer of water column in the gulf, with its core at about 600–800 m (Figure 3.1). The salinity of this water mass decreases towards the east.

The GABW identified in the σ_θ range 27.5 to 27.8 occupies about 38% of the total volume of Gulf of Aden. Since there is no production of bottom water in the Arabian Sea basin it is necessary to transport the bottom water from elsewhere. The AIW could be one of the sources for this water mass. The water of southern origin that enters the Gulf of Aden from the south, through the Somali basin, ultimately mixes with the high saline RSW to produce the GABW with salinity more than 34.80 psu. The mixing of warm RSW with cooler water from the south leaves a wide range of potential temperature

(2–11 °C). The percentage compositions, estimated based on the mixing theory of water masses (Figure 3.10), suggest the presence of ~ 10–20% RSW in the GABW. The bottom water in the western most Gulf of Aden could be the RSW itself.

In Chapter 4, three major data sets have been used to describe the monthly evolution of currents in the Gulf of Aden. The ship drift data showed the seasonality in the circulation (Figure 4.1) similar to other data sets, but cannot be used to bring out the mesoscale eddies embedded in the flows. Similarly, the Ekman drift estimated from winds (Figure 4.2) did not show the presence of eddies in the gulf or adjoining seas. Ekman drifts were towards the west during the winter monsoon (November–March) and towards the east during the summer monsoon (June–August). The Ekman flow in the month of September appeared to be an exception to the summer monsoon flow pattern; the flow inside the gulf was abysmally weak (Figure 4.2i). Similar was the case in May, the transition period between winter and summer monsoons. The Ekman drifts in April as well as in October, the other two transition months, were westward similar to the winter flows. Thus, due to the Ekman drifts , two well defined flow patterns form in the Gulf of Aden; (i) a westward flowing winter pattern and (ii) an eastward flowing summer pattern. The winter pattern started in October and continued till April, whereas the summer pattern existed only for a short duration of 3 months (June–August). In addition to the generation of well defined flow patterns, the Ekman drift does not seem to contribute to the generation of eddies in the gulf.

The analysis of geostrophic currents, however, clearly showed the embedded eddies in the flows (Figure 4.3). Several eddies were seen in the geostrophic currents during all months and they were consistent in the geostrophic currents derived from altimeter SLA. As seen in the net surface flows shown in Figure 4.4, the eddies dominated the circulation in the Gulf of Aden over the mean flow. The eddies seen at the surface extended to deeper layers, often to 1000 m or more.

The net flows at the surface were westward during October–April and were maximum

during November to February. This westward flow would transport water from the Gulf of Aden into the Red Sea. Similarly the eastward flow in the western end of the gulf during the summer monsoon (June–August) (Figure 4.4g and h) is a continuation of the outward flow from the Red Sea in the surface layer. The westward geostrophic currents in the western end of the gulf at 300 and 600 m layers in August–September (Figure 4.5h, i) are consistent with the intrusion of Gulf of Aden water into the Red Sea in the intermediate layers. Earlier reports had also shown that the summer regime in the Bab el Mandab Strait is dominated by the massive intrusion of cold (19 °C), low salinity (36.0–36.5 psu) water from the Gulf of Aden [Murray and Johns, 1997; Al Saafani and Shenoi, 2004].

We presented the analysis of interannual variability of sea level as a proxy to the variability of geostrophic currents at the surface. The annual and high-frequency signals dominate the sea level variability in the Gulf of Aden (Figure 4.6 and 4.7). The SLA variability in the gulf at interannual frequency is minimum and insignificant at 99% confidence level. It is significant at 95% confidence level only over small patches inside the gulf (Figure 4.7). Since the variability in the SLA is related to the geostrophic currents at the surface, it is clear that the interannual variability in the surface geostrophic currents inside the gulf are also insignificant. The geostrophic currents have dominated the net surface flows as seen in Figure 4.4 in the Gulf of Aden. Based on this argument, we conclude that the interannual variabilities in the circulation in the Gulf of Aden are insignificant.

The analysis of circulation in the Gulf of Aden presented here confirmed the earlier descriptions of the seasonality of surface currents and also provided new insights. First and foremost is that the currents in the Gulf of Aden are not so simple as thought earlier; they are complicated by the presence of eddies embedded in them. Secondly, the eddies influenced the flows in all months. Thirdly, the eddies are found only in geostrophic currents and not in Ekman drifts induced by winds and fourthly, the eddies act over the entire water column extending from the surface down to at least 1000 m.

The characteristics of eddies are described in detail in Chapter 5. The possible rea-

sons for the formation of eddies in the vicinity of the gulf and their westward movement were also investigated. Westward moving eddies were evident in the Gulf of Aden during November–May (Figures 5.1– 5.3) and our analysis showed them to be associated with the westward propagating Rossby waves. The westward propagating Rossby waves radiated from the Indian west coast, as well as the Rossby waves generated in the interior of the Arabian Sea (52–60° E), contribute to the cyclonic and anticyclonic eddies in the vicinity of the Gulf of Aden. The low–frequency signal (mainly annual signal) showed a discontinuity in the longitudinal band between 52° E and 60° E; its intensity and spatial extent demonstrated considerable interannual variability. The uplifting of the thermocline, local wind stress, and the presence of Socotra Gyre in the vicinity, all contributed to this discontinuity in the annual signal. The westward propagating high–frequency Rossby waves generated locally (west of 60° E) are also a source for westward propagating mesoscale eddies in the Gulf of Aden. They move into the gulf from the east, either directly or through the Socotra Passage. They survive and move westward within the gulf inspite of the frictional effect of the boundaries of the gulf.

The analysis suggested that the eddies entering the gulf from the Arabian Sea owe their existence to more than one mechanism. Local Ekman pumping was important during the summer monsoon (June–September). In May and during the latter half of the summer monsoon (late July to September) and the fall inter–monsoon (October), the dominant mechanism was the generation of eddies by the instabilities in the Somali Current and the large eddies associated with it (Great Whirl and Socotra eddy) ([Fratantoni et al., 2006; Simmons et al., 1988]). During the winter monsoon (November–April), the dominant mechanism involved the westward propagating Rossby waves generated either in the Arabian Sea by Ekman pumping or along the west coast of India by poleward propagating Kelvin waves. Thus, the westward propagating Rossby waves from the Arabian Sea were more important for the circulation in the gulf over half the year.

Figure 6.1 shows the schematic diagrams summarizing the hydrographic structure and

circulation during winter (January) and summer (July). During January (Figure 6.1a) the distribution of the salinity at the surface is uniform ($\sim$ 36.0 psu) over most of the gulf except for a few patches of higher or lower salinity ($\sim$ 0.1 psu). The surface current during January is towards the west with a cyclonic eddy between 46 to 48° E and an anticyclonic eddy to the east of it along the southern coast of the gulf. The vertical distribution of salinity during this month (Figure 6.1a, bottom panel) shows the four–layer structure in the Gulf of Aden. The GASW occupies the top 100 m of the water column that flows towards the west. The GAIW occupies the layer between 100–500 m in the eastern part of the section and 100–400 m in the west. This layer flows westward along the northern side of the gulf. The salinity of this layer increases towards the west due to the mixing with the high salinity RSW. The RSW layer is seen clearly in this section occupying about 700 m thick layer of the water column, between 400–1100 m, with the salinity decreasing towards the east. The eastward flow of this layer is seen along the southern part of the gulf (Figure 6.1a, bottom panel). GABW is seen below the RSW layer.

During July (Figure 6.1b), the surface salinity along the western and the southern sides of the gulf is > 36.2 psu. Along the northern side of the gulf, lower salinity is seen indicative of upwelling. The flow is eastward over the gulf with an anticyclonic eddy at the center between 46 and 48° E. The four–layer structure seen during January is also seen during this month from the vertical sections (Figure 6.1b, bottom panel) with the GASW occupying only $\sim <$ 50 m along the southern part and $\sim$ 20 m along the northern part of the gulf. This layer flows eastward during this month. The GAIW occupies from 100–400 m; the flow is eastward in this layer also. The RSW show high salinity in the western part of the gulf. The salinity of this layer decreases towards the east as it flows out from the gulf. The anticyclonic eddy seen at the surface extends to the deeper layers, where the isopycnal lines deepen at that location.

In conclusion, this study provides a synthesis of various data sets and describes the structure of hydrography and circulation in the Gulf of Aden diligently. Though we have

attempted to explain the dynamics of the processes within the frame-work of available data, numerical models that can simulate the observations are required to explain the dynamics of unexplained processes.

Figure 6.1 (a) Schematic diagram of the salinity distribution based on the new climatology during winter (January). The top panel represents the horizontal distribution. The vertical sections shown in the lower panel are along the lines AB and BC shown in the upper panel. The vertical (lower panel) distribution of salinity (psu) clearly shows the four–layer structure of the water masses. The flows at surface and at the deeper layer are also shown. The isopycnal lines separating the water masses are also show in the vertical sections.

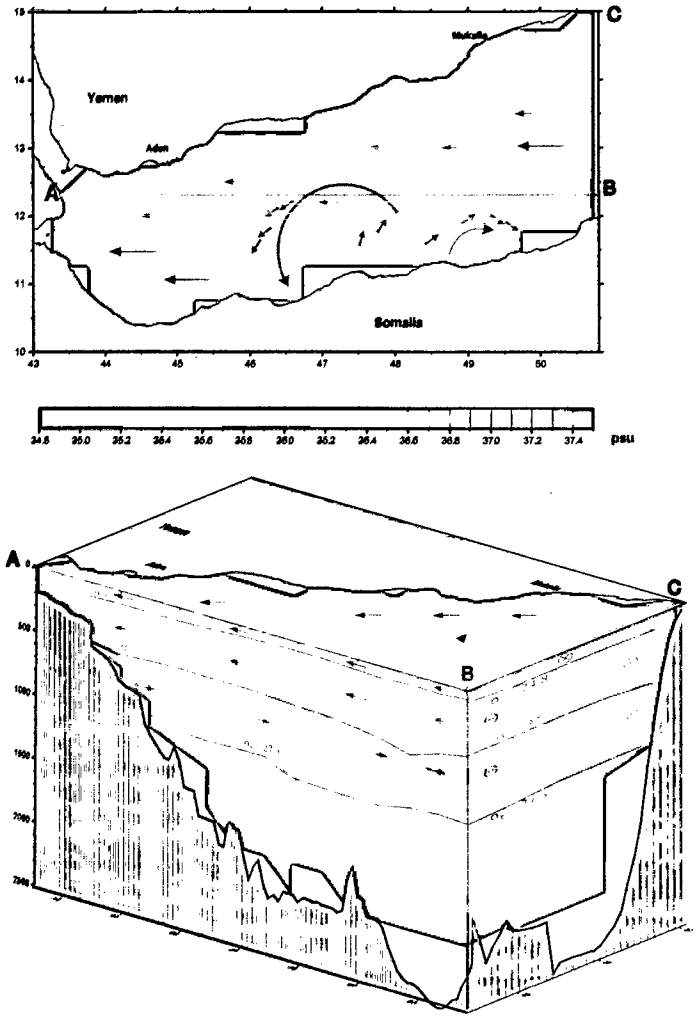

Figure 6.1 (b) Same as for 6.1a for summer (July).

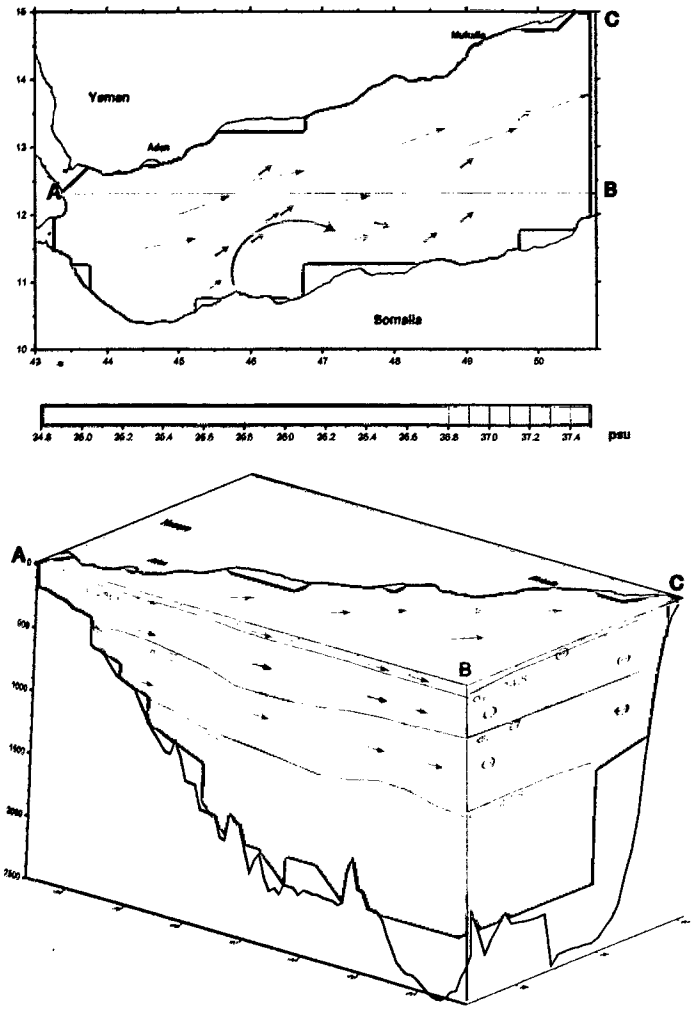

Bibliography

H. Aiki, K. Takahashi, and T. Yamagata. The Red Sea outflow regulated by the Indian monsoon. *Continental Shelf Research*, 26:1448–1468, 2006.

M. A. Al Saafani and S. Shenoi. Seasonal cycle of hydrography in the Bab el Mandab region southern Red Sea. *Proceedings of the Indian Academy of Sciences (Earth and Planetary Sciences)*, 113:269–280, 2004.

M. A. Al Saafani and S. Shenoi. Seasonal and interannual variability of eddy field and surface circulation in the Gulf of Aden. In *Proceeding of the Symposium on 15 years of Progress in Radar Altimetry*. Venice, Italy, 2006.

A. Al Sayed and M. Ghaddaf. Upwelling and fish mortality in the northern Gulf of Aden. *Indian Journal of Marine Sciences*, 22(4):305–307, 1993.

A. Al Sayed and P. Kolli. Seasoonal variation of dessolved oxygen in the northern Gulf of Aden. In *Scientific investigation of the Gulf of Aden*. Marine Science and Resources Research Center, Aden, Republic of Yemen, 1992.

Anonymous. SSALTO/DUACS user hand book. Issue 1, CLS, 2001a.

Anonymous. SeaWinds on QuikSCAT level3 daily, gridded ocean wind vectors, version 1.1. JPL Document D-20335, Jet Propulsion Laboratory, Pasadena, CA. USA, 2001b.

Anonymous. Environmantal Impact Assessment. Environmental Studies Program, Canadian Occidental Petroleum Ltd., Masila, Republic of Yemen, 1993.

Anonymous. Indische Ocean. Oceanografische en Meteorologische. Koninklijk Netherlands Meteorologisch Institut, Oegevens. 2nd ed., 24 charts, 1952.

Anonymous. Climatic study of the Red Sea and Gulf of Aden, Near Coastal Zone. Naval Oceanography Command Detachment, NSTL Station, Bay ST, Louis, MS 39529, September 1982.

J. I. Antonov, S. Levitus, T. P. Boyer, M. E. Conkright, T. O'Brien, C. Stephens, and B. Trotsenko. World Ocean Atlas 1998 Volume 3. Temperature of the Indian Ocean. NOAA Atlas NESDIS 29, 1998.

S. S. Awad and P. Kolli. Upwelling along the northern Gulf of Aden. In *Scientific investigation of the Gulf of Aden*, volume 2, pages 78–110. Marine Science and Resources Research Center, Aden, Republic of Yemen, 1992.

M. A. Baars. Monsoons and pelagic systems. Cruise Reports Netherlands Indian Ocean Programme, National Museum of Natural History, Leiden, 143 pp, 1994.

S. L. Barnes. A technique for maximizing details in numerical map analysis. *Journal of applied Meteorology*, 3:396–409, 1964.

B. Barnier. A numerical study on the influence of mid-Atlantic ridge on nonlinear first mode baroclinic Rossby wave generated by seasonal winds. *Journal of Physical Oceanography*, 18:417–433, 1988.

L. M. Beal and T. K. Chereskin. The volume transport of the Somali Current during the 1995 southwest monsoon. *Deep Sea Research*, 50:2077–2090, 2003.

L. M. Beal, A. Field, and A. L. Gordon. Spreading of Red Sea overflow waters in the Indian Ocean. *Journal of Geophysical Research*, 105:8537–8548, 2000.

R. Boje and M. Tomczak. *Upwelling ecosystems*, volume 1. Springer Verlag, Berlin, 1978.

C. W. Boning and R. G. Budich. Eddy dynamics in a primitive equation model: Sensitivity to horizontal resolution and friction. *Journal of Physical Oceanography*, 22: 361–381, 1992.

W. Bosworth, P. Huchon, and K. McClay. The Red Sea and Gulf of Aden Basins. *Journal of African Earth Sciences*, 43:334–378, 2005.

A. S. Bower, D. H. Hunt, and J. F. Price. Character and dynamics of the Red Sea and Persian Gulf outflows. *Journal of Geophysical Research*, 105:6387–6414, 2000.

A. S. Bower, W. E. Johns, D. M. Fratantoni, and H. Peters. Gulf of Aden eddies and their impact on Red Sea Water. *Geophysical Research Letters*, 29:21, 2025,dio:10.1029/2002GL015342, 2002.

A. S. Bower, W. E. Johns, D. M. Fratantoni, and H. Peters. Equilibration and circulation of Red Sea Outflow Water in the western Gulf of Aden. *Journal of Physical Oceanography*, 35:1963–1985, 2005.

T. P. Boyer and S. Levitus. Quality control and processing of historical temperature, salinity and oxygen data. NOAA Technical Report NESDIS 81, 65 pp, 1994.

T. P. Boyer, S. Levitus, J. Antonov, M. Conkright, T. O'Brien, C. Stephens, and B. Trotsenko. World Ocean Atlas 1998 Volume 6. Salinity of the Indian Ocean. NOAA Atlas NESDIS 32, 1998.

T. P. Boyer, C. Stephens, J. Antonov, M. Conkright, R. A. Locarnini, T. D. O'Brien, and H. E. Garcia. World Ocean Atlas 2001 Volume 2: Salinity. NOAA Atlas NESDIS 50. 176 pp, 2002.

T. P. Boyer, J. Antonov, H. Garcia, D. Johnson, R. Locarnini, A. Mishonov, M. Pitcher, O. Baranova, and I. Smolyar. World Ocean Database 2005, S. Levitus, ed. NOAA Atlas NESDIS 60,U.S. Government Printing Office, Washington, D.C. 176 pp, 2006.

P. Brandt, L. Stramma, F. Schott, J. Fischer, M. Dengler, and D. Quadfasel. Annual Rossby waves in the Arabian Sea from TOPEX/Poseidon altimeter and in situ data. *Deep Sea Research, Part B*, 49:1197–1210, 2002.

J. G. Bruce. Some details of upwelling off the Somali and Arabian Coasts. *Journal of Marine Research*, 32:419–423, 1974.

D. Chelton and M. G. Schlax. Global observations of oceanic Rossby waves. *Science*, 272:234–238, 1996.

J. R. Cochran. The Gulf of Aden: Structure and evolution of a young ocean basin and continental margin. *Journal of Geophysical Research*, 86:263–287, January 1981.

R. I. Currie, A. E. Fisher, and P. H. Hargraves. Arabian Sea upwelling. In B. Zietschel, editor, *The Biology of the Indian Ocean*, pages 1–6. Springer Verlag, Berlin, 1973.

A. N. Cutler and J. C. Swallow. Surface currents of the Indian Ocean (to 25°S, 100°E): Compiled from historical data archived by the Meteorological Office, Bracknell, UK. *Report 187*, Institute of Oceanographic Sciences, Wormley, England, 36 charts, 8 pp, 1984.

J. Dorandeu and P. Y. Le Traon. Effects of global mean atmospheric pressure variations on mean sea level changes from TOPEX/Poseidon. *Journal of Atmospheric and Oceanic Technology*, 16:1279–1283, 1999.

N. Ducet, P. Y. Le Traon, and G. Reverdin. Global high-resolution mapping of ocean circulation from TOPEX/Poseidon and ERS-1 and -2. *Journal of Geophysical Research*, 105(C8):19477–19498, 2000.

S. Dunbar, B. Weiss, B. Stiles, J. Huddleston, P. Callahan, G. Shirtliffe, K. L. Perry, C. Hsu, C. Mears, F. Wentz, and D. Smith. QuikSCAT Science Data product user's manual, version 2.2. JPL Document D-18053, Jet Propulsion Laboratory, Pasadena, CA. USA, 95 pp, 2001.

K. N. Fedorov and S. L. Meshchanov. Structure and propagation of Red Sea Waters in the Gulf of Aden. *Oceanology*, 28(3):279–284, 1988.

J. Findlater. A major low-level air current near the Indian Ocean during the northern summer. *Quarterly Journal of the Royal Meteorological Society*, 95:362–380, 1969.

J. Fischer, F. Schott, and L. Stramma. Currents and transports of the Great Whirl-Socotra Gyre system during the summer monsoon, August 1993. *Journal of Geophysical Research*, 101:3573–3587, 1996.

E. Foufoula-Georgiou and P. Kumar. *Wavelets in Geophysics*. Academic Press, 1995.

D. M. Fratantoni, A. S. Bower, W. E. Johns, and H. Peters. Somali Current rings in the eastern Gulf of Aden. *Journal of Geophysical Research*, 110, 2006.

R. W. Girdler, C. Brown, D. J. M. Noy, and P. Styles. A geophysical survey of the westernmost Gulf of Aden. *Philosophical Transactions of the Royal Society of London. Series A, Mathematical and Physical Sciences*, 298(1434):1–43, August 1980.

S. Hastenrath and L. L. Greischar. The monsoonal current regimes of the tropical Indian Ocean. observed surface flow fields and their geostrophic and wind-driven components. *Journal of Geophysical Research*, 96:12619–12633, 1991.

S. Hellerman and M. Rosenstein. Normal monthly wind stress over the world ocean with error estimates. *Journal of Physical Oceanography*, 13:1093–1104, 1983.

W. E. Johns, G. A. Jacobs, J. Kindle, S. Murray, and M. Carron. Arabian Marginal Seas and Gulfs: Report of a Workshop held at Stennis Space Center May 11-13 1999. University of Miami RSMAS Technical Report No. 2000-01, February 2001.

G. C. Johnson, D. L. Musgrave, B. A. Warren, A. Ffield, and D. B. Olson. Flow of bottom and deep water in the Amirante Passage and Mascarene Basin. *Journal of Geophysical Research*, 103(C13):30973–30984, 1998.

J. G. Kabanova. Primary production of the northern part of the Indian Ocean. *Oceanology*, 8:214–225, 1968.

V. A. Khimitsa. The hydrological structure of the waters of the Gulf of Aden. *Oceanology*, 8:318–322, 1968.

J. C. Kindle and R. A. Arnone. A review of the surface circulation of the northern Arabian Sea. In M. Claereboudt, S. Goddard, H. Al-Oufi, and J. McIlwain, editors, *Proc. 1st International Conference on Fisheries, Aquaculture and Environment in the NW Indian Ocean*, pages 113–122, Sultan Qaboos University, Muscat, Sultanate of Oman, 2001.

P. Kolli, Z. Zubairi, M. Ghaddaf, and P. Koithara. Marine science activities in the Republic of Yemen and future programmes in the Gulf of Aden. Tech. Report, Marine Science and Resources Research Center, 1992.

J. Krey and Babenard. *Phytoplankton production. Atlas of the IIOE.* Inst. Fur Meereskunde, Kiel, Germany, 1976.

J. Kurian and P. N. Vinayachandran. Formation mechanisms of temperature inversions in the southeastern Arabian Sea. *Geophysical Research Letters*, 33:L17611, doi:10.1029/2006GL027280, 2006.

J. Kurian and P. N. Vinayachandran. Mechanisms of formation of Arabian Sea mini

warm pool in a high resolution OGCM. *Journal of Geophysical Research*, 112:C05009, doi:10.1029/2006JC003631, 2007.

P. Y. Le Traon and F. Ogor. ERS-1/2 orbit improvement using TOPEX/Poseidon: the 2 cm challenge. *Journal of Geophysical Research*, 103:8045–8057, 1998.

P. H. LeBlond and L. A. Mysak. *Waves in the Ocean*. Elsevier, Amsterdam, 1978.

S. Levitus. Climatological atlas of the world ocean. *NOAA Professional Paper 13*, 173 pp., U.S. Government Printing Office, Washington D.C., 1982.

S. Levitus and T. P. Boyer. World Ocean Atlas 1994 Volume 4: Temperature. NOAA Atlas NESDIS 4. 129 pp, 1994.

S. Levitus, R. Burgett, and T. P. Boyer. World Ocean Atlas 1994 Volume 3: Salinity. NOAA Atlas NESDIS 3. 111 pp, 1994.

E. N. Lorenz. Available potential energy and maintenance of the general circulation. *Tellus*, 2:157–167, 1955.

C. Maillard and G. Soliman. Hydrography of the Red Sea and exchanges with the Indian Ocean in summer. *Oceanologica Acta*, 9:249–269, 1986.

I. A. Maiyza and E. E. Mohamed. Sea surface temperature anomalies in the northwestern Indian Ocean and its adjacent seas. *Indian Journal of Marine Sciences*, 22:180–187, 1993.

O. I. Mamayev. *Temperature-salinity analysis of the world ocean waters*, volume 1. Elsevier, Amsterdam, 1975.

D. H. Matthews, C. Williams, and A. S. Laughton. Mid-ocean ridge in the mouth of the Gulf of Aden. *Nature*, 215:1052–1053, doi:10.1038/2151052a0, 1967.

J. P. McCreary, P. K. Kundu, and R. L. Molinari. A numerical investigation of the dynamics, thermodynamics and mixed-layer processes in the Indian Ocean. *Progress in Oceanography*, 31:181–244, 1993.

S. Mecking and M. J. Warner. Ventilation of Red Sea Water with respect to chlorofluorocarbons. *Journal of Geophysical Research*, 104:11087–11097, 1999.

E. E. E. Mohamed, S. H. S. El-Din, and A. A. H. Al-Gindy. Dynamic and hydrographic structure in the Red Sea and Gulf of Aden. In *Present and Future of Oceanographic Programs in Developing Countries, Visakhapatnam-India*, pages 78–101. Visakhapatnam-India Andhra-University no. 3 pp. 78-101, 1996.

B. H. Mohammed and P. Kolli. Circulation in the northern Gulf of Aden. In *Scientific investigation of the Gulf of Aden*. Marine Science and Resources Research Center, Aden, Republic of Yemen, 1992.

E. E. E. Mohammed. On the variability, potential energy, potential temperature, salinity and currents in NW Indian Ocean and Gulf of Aden. *Journal of King Abdulaziz University-Marine Science*, 8:47–65, 1997.

R. B. Montgomery. Water characteristics of Atlantic Ocean and of world ocean. *Deep Sea Research*, 5:134–148, 1958.

S. Morcos. Physical and chemical oceanography. In S. A. Morcos and A. Varley, editors, *Red Sea, Gulf of Aden and Suez Canal. A Bibliography on Oceanographic and Marine Environmental Research*, pages pp xvi–xxii. UNESCO, Paris, 1990.

S. Morcos and J. Piechura. From the archives of the John Murray/Mabahiss Expedition: Strong summer cooling of surface water revealed by historic data in Gulf of Aden and Bab el Mandab. In W. Lenz and M. Deacon, editors, *Ocean Sciences: Their History and Relation to Man,Proceeding of the 4th International Congress on the History*

of Oceanography, Hamburg 23–29 September 1987, pages 378–390. Deutsche Hydrographische Zeitschrift, 1990.

J. M. Morrison. Inter-monsoonal changes in the T–S properties of the Near-Surface Waters of the northern Arabian Sea. *Geophysical Research Letters*, 24(21):2553–2556, 1997.

S. P. Murray and W. Johns. Direct observations of seasonal exchange through the Bab el Mandab Strait. *Geophysical Research Letters*, 24(21):2557–2560, 1997.

G. A. Nasser. Seasonal changes in the water characteristics of upper 1000 m in the northern Gulf of Aden. In *Scientific investigation of the Gulf of Aden*, volume 2, pages 51–77. Marine Science and Resources Research Center, Aden Republic of Yemen., 1992.

National Geophysical Data Center. 2-minute Gridded Global Relief Data (ETOPO2v2). Natl. Oceanic. And Atmos. Admin., U.S. Dept. of Commerce, (http://www.ngdc.noaa.gov/mgg/fliers/06mgg01.html), 2006.

D. Nethery and D. Shankar. Vertical propagation of baroclinic Kelvin waves along the west coast of India. *Journal of Earth System Science*, 116(4):331–339, 2007.

A. C. Neumann and D. McGill. Circulation of the Red Sea in early summer. *Deep Sea Research*, 8:223–235, 1962.

T. M. Ozgokman, W. E. Johns, H. Peters, and S. Matt. Turbulent mixing in the Red Sea outflow plume from a high-resolution nonhydrostatic model. *Journal of Physical Oceanography*, 33:1846–1869, 2003.

J. Pattullo, W. Munk, R. Revelle, and E. Strong. The seasonal oscillation of mean sea level. *Journal of Marine Research*, 14:88–156, 1955.

W. C. Patzert. Wind induced reversal in the Red Sea circulation. *Deep Sea Research*, 21:109–121, 1974.

H. Peters and W. E. Johns. Mixing and entrainment in the Red Sea outflow plume. II.Turbulence characteristics. *Journal of Physical Oceanography*, 35:584–600, 2005.

H. Peters, W. E. Johns, A. S. Bower, and D. M. Fratantoni. Mixing and entrainment in the Red Sea outflow plume. I. Plume structure. *Journal of Physical Oceanography*, 35: 569–583, 2005.

J. Piechura and O. A. G. Sobaih. Oceanographic conditions of the Gulf of Aden. In *Scientific investigation of the Gulf of Aden Series A Oceanography,2*, pages 1–26. Marine Science and Resources Research Center, Aden Republic of Yemen, 1986.

S. Pond and G. L. Pickard. *Introduction to dynamical oceanography*. Pergamon Press, second edition, 1983.

T. G. Prasad and M. Ikeda. Spring evolution of Arabian Sea High in the Indian Ocean. *Journal of Geophysical Research*, 106:31085–31098, 2001.

D. W. Privett. Monthly charts of evaporation from the northern Indian Ocean, including the Red Sea and Persian Gulf. *Quarterly Journal of the Royal Meteorological Society*, 85(366):424–428, 1959.

D. Quadfasel and F. A. Schott. Water-mass distribution at intermediate layers off the Somali Coast during the onset of the southwest monsoon 1979. *Journal of Physical Oceanography*, 12:1358–1372, 1982.

D. Quadfasel and F. A. Schott. Southward subsurface flow below the Somali Current. *Journal of Geophysical Research*, 88:5973–5979, 1983.

D. Quadfasel, J. Fischer, F. A. Schott, and L. Stramma. Deep water exchange through the Owen Fracture Zone in the Arabian Sea. *Geophysical Research Letters*, 24:2805–2808, 1997.

R. A. Ray. A global ocean tide model from TOPEX/Poseidon altimetry, GOT99.2. NASA Tech. Memo. NASA/TM-1999-209478, Goddard Space Flight Center, NASA Greenbelt, MD, USA, 55 pp, 1999.

D. J. Rochford. Salinity maxima in the upper 1000 meters of the north Indian Ocean. *Australian Journal of Marine and Freshwater Research*, 15:1–24, 1964.

F. Roske. An atlas of surface fluxes based on the ECMWF Re-Analysis a climatological dataset to force global ocean general circulation models. Tech. Report, 323, Max-Planck-Inst. Fur Meteorol., Hamburg, Germany, 2001.

S. Sandven. Coastal oceanography of the Arabian Sea. Data processing and interpretation. part-I text, 39-pp and part II 70 figures. Cruise Reports Netherlands Indian Ocean Programme, University of Bergen, Norway, 109 pp, 1979.

G. Savidge, H. J. Lennon, and A. D. Matthews. A shore based survey of upwelling along the coast of Dhofar region, southern Oman. *Continental Shelf Research*, 10:259–275, 1990.

J. B. Scarborough. *Numerical Mathematical Analysis, 6th Ed.* Oxford and IBH, Calcutta, India, 1966.

F. Schott. Monsoon response of the Somali Current and associated upwelling. *Progress in Oceanography*, 12:357–381, 1983.

F. A. Schott and J. Fischer. Winter monsoon circulation of the northern Arabian Sea and Somali Current. *Journal of Geophysical Research*, 105:6359–6376, 2000.

F. A. Schott and J. P. McCreary. The monsoon circulation of the Indian Ocean. *Progress in Oceanography*, 51:1–123, 2001.

V. V. Seriy and V. A. Khimitsa. The hydrography and chemistry of the Gulf of Aden and the Arabian Sea. *Okeanologiya*, 3:994–1003, 1963.

D. Shankar and S. R. Shetye. On the dynamics of the Lakshadweep high and low in the southeastern Arabian Sea. *Journal of Geophysical Research*, 102:12551–12562, 1997.

D. Shankar, J. P. McCreary, W. Han, and S. R. Shetye. Dynamics of the East India Coastal Current. 1. Analytic solutions forced by interior Ekman pumping and local alongshore winds. *Journal of Geophysical Research*, 101:13975–13991, 1996.

D. Shankar, P. N. Vinayachandran, and A. S. Unnikrishnan. The monsoon currents in the north Indian Ocean. *Progress in Oceanography*, 52:63–120, 2002.

S. S. C. Shenoi, R. Shetye, A. D. Gouveia, and G. S. Micheal. Salinity extrema in the Arabian Sea. In V. Ittickkot and R. R. Nair, editors, *Monsoon Biogeochemistry*, pages 37–49. Mitt Geol. Palaont. Inst. Univ. Hamburg, Humburg, Germany, 1993.

S. R. Shetye and A. D. Gouveia. Coastal circulation in the north Indian Ocean. Coastal segment (14,S–W). In A. R. Robinson and K. H. Brink, editors, *The Sea*, volume 11, pages 523–556. John Wiley and Sons, Inc, 1998.

M. Siddall, D. Smeed, S. Matthiesen, and E. Rohling. Modelling the seasonal cycle of the exchange flow in Bab El Mandab (Red Sea). *Deep Sea Research*, 49(9):1551–1569, 2002.

R. C. Simmons, M. E. Luther, J. J. O'Brien, and D. M. Legler. Verification of a numerical ocean model of the Arabian Sea. *Journal of Geophysical Research*, 93(12): 15437–15453, 1988.

R. L. Smith. Upwelling. *Oceanography and Marine Biology: An Annual Review*, 6: 11–46, 1968.

O. A. G. Sobaih. Basic meteorological conditions in the Gulf of Aden. In *Scientific investigation of the Gulf of Aden, 1(3)*. Marine Science and Resources Research Center, Aden, Republic of Yemen, 1986.

C. Stephens, J. Antonov, T. P. Boyer, M. Conkright, R. A. Locarnini, T. D. O'Brien, and H. E. Garcia. World Ocean Atlas 2001, Volume 1: Temperature. NOAA Atlas NESDIS 49. 176 pp, 2002.

J. Stirn, R. Edwards, J. Pichura, M. Savich, M. Ghaddaf, M. Fadel, F. Mutlag, O. A. G. Sobaif, A. Al-Sayed, A. Shaer, and Z. Zubairi. Oceanographic conditions, pelagic productivity and living resources in the Gulf of Aden. In *Workshop on Regional Co-operation in Marine Science in the Central Indian Ocean and Adjacent Seas and Gulfs*, page 225 pp. IOC/UNESCO Report No. 37, 1985.

J. C. Swallow. Some aspects of the physical oceanography of the Indian Ocean. *Deep Sea Research*, 31:639–650, 1984.

J. C. Swallow, R. L. Molinari, J. G. Bruce, O. B. Brown, and R. H. Evans. Development of near-surface flow pattern and water mass distribution in the Somali Basin in response to the southwest monsoon of 1979. *Journal of Physical Oceanography*, 13:1398–1415, 1983.

P. Tchernia. *Descriptive regional oceanography*, volume 3. Pergamon Marine Series, Pergamon, Oxford, UK., 1980.

M. J. Tomczak. A multi–parameter extension of temperature/salinity diagram techniques for the analysis of non-isopycnal mixing. *Progress in Oceanography*, 10(3):173–192, 1981a.

M. J. Tomczak. Non-isopycnal mixing in the frontal zone of South and North Atlantic Central Water off North-West Africa. *Progress in Oceanography*, 10(3):147–171, 1981b.

C. Torrence and G. P. Compo. A practical guide to wavelet analysis. *Bulletin of the American Meteorological Society*, 79:61–78, 1998.

P. N. Vinayachandran and T. Yamagata. Monsoon response of the sea around Sri Lanka: generation of thermal domes and anticyclonic vortices. *Journal of Physical Oceanography*, 28:1946–1960, 1998.

D. L. Volkov. Interannual variability of the altimetry-derived eddy field and surface circulation in the extratropical north Atlantic Ocean in 1993–2001. *Journal of Physical Oceanography*, 35:405–426, 2005.

L. Wang and J. Koblinsky. Influence of mid-ocean ridge on Rossby waves. *Journal of Geophysical Research*, 99:25143–25153, 1994.

L. Wang, J. Koblinsky, and S. Howden. Annual Rossby wave in the southern Indian Ocean. Why does it "appear" to break down in the middle ocean? *Journal of Physical Oceanography*, 31:54–74, 2001.

B. A. Warren, H. Stommel, and J. C. Swallow. Water masses and pattern of flow in the Somali Basin during the southwest monsoon of 1964. *Deep Sea Research*, 5:108–109, 1966.

S. D. Woodruff, S. Lubker, K. Wolter, S. Worley, and J. Elms. Comprehensive Ocean-Atmosphere Data Set (COADS) release 1a: 1980-92. *Earth System Monitor*, 4:1–8, 1993.

W. S. Wooster, M. B. Schafer, and M. K. Robinson. *Atlas of the Arabian Sea for fishery oceanography*, volume 1. University of California, IMR, La Jolla, California, 1967.

K. Wyrtki. *Oceanographic Atlas of the International Indian Ocean Expedition.* NSF, Washington, D. C., 1971.